The Role of the Complement System in Associative Learning and Risk for Schizophrenia

A thesis presented for the degree of

Doctor of Philosophy

By

Jack Timothy Reddaway

January 2022

Acknowledgements

This work is an accomplishment reliant on the contribution and unwavering support provided by supervisors, colleagues, friends, and family.

The project was supervised by Dr. Kerrie Thomas, Professor Jeremy Hall, and Professor Paul Morgan, to whom I extend my heartfelt gratitude. Throughout the project they have provided countless ideas, support and motivation for my research and developed me as a scientist.

Further thanks must be extended to Peter Richardson, Dr. Nicholas Clifton and Dr. Matthew Smith who contributed tirelessly to the machine learning experiments presented herein. I must also acknowledge the contributions made my colleagues and friends Dr. Niels Haan, Dr. Anna Moon and Dr. Laura Westacott who aided in the optimisation of experimental protocols and always were available as 'sounding boards' for ideas and experimental design.

Additionally, thank you Dr. Timothy Wells for his patience and support whilst I completed writing this thesis during my post-doctoral position in his research group.

I also must use this opportunity to thank Professor Jonathan Liftshitz and Dr. Jenna Ziebell for first introducing me to the world of research and whose advice and guidance I have drawn upon ever since.

I would also like to express my gratitude to my friends who have that have met during my studies but in particular I must say a particular thank you to: Bethany Shaw, Edward Portal, Dr. Owen Moon, Peter Henley and Roanne Hynes without

whom my time in Cardiff would have been rather dull. Finally thank you to my family who have supported me and my endeavours without question.

This work was funded by studentship generously provided by the Hodge Foundation, to whom I am eternally grateful.

Abstract

Schizophrenia and post-traumatic stress disorder are neuropsychiatric disorders which in part are characterised by impairments in the acquisition and updating of associative memories. Recent genome-wide association studies involving thousands of individuals, have revealed an association between the risk for schizophrenia and genetic variations in the complement system, in particular the genes *C4* and *CSMD1*. However, the reason why aberrances in the complement system increases an individual's risk for schizophrenia remains unclear. One hypothesis to explain the link between the complement system and schizophrenia is that the complement system drives the adult synaptic plasticity that underlies the recall and extinction of associative memories. In neural development and neurodegenerative diseases, the complement system facilitates synaptic pruning and remodelling. Establishing whether complement mediated plasticity occurs in adulthood and the precise mechanisms by which it occurs, could explain the origins of the associative learning deficits seen in schizophrenia and post-traumatic stress disorder, whilst opening a new avenue for the development or repurposing of drugs to treat these disorders.

The experiments in this thesis investigated the relationship between two phases of associative learning: retrieval and extinction, with the changes in the neuroimmune environment in brain regions activated during these phases of learning. We first identified differential activation of hippocampal, pre-frontal cortical and thalamic subregions following contextual fear memory retrieval and extinction, by measuring the protein levels of three immediate early genes: Arc, cFOS and

zif268 (Chapter 3). We also reported a decrease in expression of complement system receptor C3aR in the CA1 subregion of the hippocampus following the retrieval of a contextual fear memory (Chapter 4). Following this, we examined whether there were changes in microglial activation following retrieval and extinction which required the development of a novel pipeline to assess morphology across thousands of microglia, in a rapid and non-biased manner (Chapter 5). The successful development of said morphological analysis pipeline revealed decreased microglial activity in the dentate gyrus of the hippocampus following fear memory retrieval when compared to extinction (Chapter 6). These results combine to further our understanding of the role of the neuroimmune system in adult synaptic plasticity and pave the way for future experiments to examine the effects of modulating microglial and complement system activities upon the phases of associative learning.

Abbreviations, acronyms and shorthands

3D – three dimensional

A – adenine

ACC – anterior cingulate

AD – Alzheimer's disease

ADP – adenosine diphosphate

Akt – serine-threonine protein kinase

AMP – adenosine monophosphate

AMPA – α-amino-3-hydroxy-5-methyl-4-isoazolepropionic acid

ANN – artificial neural network

ANOVA – analysis of variance

Arc – activity-regulated cytoskeleton-associated protein

Arp2/3 – actin related protein 2/3

ATP – adenosine triphosphate

AUC – area under curve

Bad – Bcl-2-asscoiated death promoter

Bax – Bcl-2 associated X protein

BBB – blood brain barrier

BCE – before the common era

Bcl-2 – B-cell lymphoma 2

BDNF – brain-derived neurotrophic factor

BF – brightfield

BID – BH3 interacting-domain death agonist

BLA – basolateral amygdala

BNST – bed nucleus of the stria terminalis

BrdU – 5-bromo-2’-deoxyuridine

βSpIVΣ5 – βIV-spectrin

bZIP – basic leucine zipper

C - cytosine

C1-INH – C1-inhibitor

C1q – complement component 1q

C1r – complement component 1r

C1s – complement component 1s

C2 – complement component 2

C3 – complement component 3

C4 – complement component 4

C5 – complement component 5

C6 – complement component 6

C7 – complement component 7

C8 – complement component 8

C9 – complement component 9

C3aR – C3a receptor

C5aR – C5a receptor

C5L2 – C5a-like receptor 2

CA1/2/3 – cornu ammonis

CaMKIIβ – Ca^{2+}/calmodulin-dependent protein kinase IIβ

caret – classification and regression training

CBP – CREB-binding protein

CD – cluster of differentiation

CEA – central nucleus of the amygdala

CEl – central lateral amygdala

CEm – central medial amygdala

CFB – complement factor B

CFD – complement factor D

CFH – complement factor H

CL11 – collectin 11

CN – central nucleus

CNS – central nervous system

CFL1 – cofilin 1

cPLA2 – cytosolic phospholipase A2

CR – conditioned response

CR2 – complement receptor 2

CR3 – complement receptor 3

CREB – cAMP response element-binding protein

CRP – C-reactive protein

CS – conditioned stimulus

CSMD1 – CUB and Sushi multiple domains 1

CSV – comma-separated values

CX3CL1 - chemokine (C-X3-C motif) ligand 1

CX3CR1 – CX3C chemokine receptor 1

CZI – Carl Zeiss image

DAB – 3, 3’-diaminobenzidine

DAG – diacylglycerol

DAMP – damage associated molecular pattern

DAPI – 4’,6-diamidino-2-phenylindode

dLGN – dorsolateral geniculate nucleus

DNA – deoxyribonucleic acid

DNM2 – dynamin-2

DSM – diagnostic and statistical manual of mental disorders

E. coli – Escherichia coli

ECM – extracellular matrix

Egr1 – early growth response 1

Elk-1 – E26 transformation-specific like-1 protein

eIF4AIII – eukaryotic initiation factor 4A-III

Endo3 – endophilin 3

ERK1/2 – extracellular signal-regulated kinase 1/2

E# - embryonic day #

Fc domain – fragment crystallizable region

FIJI – Fiji is just image-J

FMRP – fragile X mental retardation protein

G – guanine

GB – gigabyte

GBM – gradient boosting algorithm

GFAP – glial fibrillary acidic protein

GL – granular layer

GLM – generalised linear model

GKAP – guanylate kinase-associated protein

GM – grey matter

GPCR – G-protein coupled receptor

HMGB1 – high mobility group box 1

IBA1 – ionised calcium-binding adapter molecule 1

ICAM1 – intracellular adhesion molecule 1

ICD – international classification of disease

IFN – interferon

IgM – immunoglobulin M

IHC – immunohistochemistry

IL – interleukin

IL1ra – interleukin 1 receptor antagonist

IQ – intelligence quotient

JAK – Janus kinase

JNK – c-JUN N-terminal kinase

KO – knockout

Krox-24 – Krüppel box-24

LAL – Limulus amoebocyte lysate

LPS – lipopolysaccharide

LTD – long-term depression

LTP – long-term potentiation

MAC – membrane attack complex

MAL – myelin and lymphocyte protein

MAPK – mitogen-activated protein kinase

MASP – mannan-binding lectin serine protease

MATLAB – matrix laboratory

MBL – mannose binding lectin

Mef2 – myocyte enhancer factor-2

MEK1/2 – mitogen-activated protein kinase kinase 1/2

mGluR – metabotropic glutamate receptor

ML – molecular layer

MMP-9 – matrix metalloprotease

mRNA – messenger ribonucleic acid

mRNP – messenger ribonucleoprotein

MS – multiple sclerosis

MYD88 – myeloid differentiation primary response 88

NADPH – nicotinamide adenine dinucleotide phosphate (reduced)

NDS – normal donkey serum

NFAT – nuclear factor of activated T-cells

NGF1A – nerve growth factor-induced protein A

NMDA - N-methyl-D-aspartate

NMDAR – NMDA receptor

OCT – optimal cutting temperature

P15 – post-natal day 15

p24 – precursor 24

p300 – histone acetyltransferase p300

PAMP – pathogen associated molecular pattern

PAX3 – paired box protein 3

PBS – phosphate-buffered saline

PCA – principal component analysis

PFA – paraformaldehyde

PGE2 – prostaglandin E_2

PKC – protein kinase C

PML – promyelocytic leukaemia protein

PP2A – protein phosphatase 2

Poly I:C – polyinosinic:polycytidylic acid

PRM – pattern recognition molecule

PSD95 – postsynaptic density protein 95

PTSD – post-traumatic stress disorder

PTX3 – pentraxin 3

px – pixel

RE – nucleus reuniens

RF – random forest

RGC – retinal ganglion cell

ROC – receiver operating characteristic

ROI – region of interest

SERPING1 – serpin family member G member 1

sIL6R – soluble IL-6 receptor

SSL – self-supervised learning

STAT3 – signal transducer and activator of transcription 3

SVM – support vector machine

SZ - schizophrenia

T – thymine

TBI – traumatic brain injury

TC – temporal cortex TCC – terminal complement complex

TCF – ternary complex factor

TIFF – tag image file format

Tip60 – Tat interactive protein 60

TIS8 – tetradecanoyl phorbol acetate induced sequence 8

TLR – toll-like receptor

TNF – tumour necrosis factor

TNFR – tumour necrosis factor receptor

tPA – tissue plasminogen activator

TRAP – targeted recombination in active population

TSPO – translocator protein

US – unconditioned stimulus

v/v – volume per volume

VC – visual cortex

VCAM1 – vascular cell adhesion molecule 1

VIF – variance inflation vector

WM – white matter

WNV – West Nile virus

WT – wildtype

zif268 – zinc finger protein 268

Contents

List of Figures

Chapter 1

Chapter 2

Chapter 3

Chapter 4

List of Tables

Chapter 6

List of Equations

Chapter 1: General Introduction

1.1 Associative learning

The antecedents of associative theory can be traced back to ancient Greece and the work of Aristotle (384-322 B.C.E) whose law of contiguity stated: “the experience or recall of one object will elicit of things that were originally experienced along with the object” (Olson and Hergenhahn, 2011). Aristotle’s ideas on the nature of memory were developed by the British empiricists John Locke and David Hume in the 17th and 18th centuries, with Hume proposing: “perceptions (impressions) determine trains of thought (succession of ideas)” and “there are no ideas in the mind that were not first given in experience” (Hume, 1978). However, the basis of modern-day practical investigations into associative learning lies with the experiments of Ivan Pavlov in the 19th century. Based upon his observations in these ground-breaking experiments, Pavlov established the behavioural paradigm of classical conditioning, in which an association is formed between an unconditioned stimulus (US) and a conditioned stimulus (CS). This association is displayed when exposure to the CS in the absence of the US elicits a conditioned response (CR). In the case of Pavlov’s experiments in dogs, the US was a bell ringing, the CS the presentation of food and the CR was salivation (Frolov, 1937). In dogs and other species, additional US/CS pairings include context/footshock, tone/footshock or light/puff of air to the eye (Curzon, Rustay and Browman, 2009). Since Pavlov’s discovery of classical conditioning, his work has remained at the core of modern psychology and forms the basis of learning theory in educational psychology and

behavioural therapies such as systematic desensitisation (Tracy, Britton and Steinmetz, 2001; Michael Dougher, 2004; Olson and Ramirez, 2020).

Deficits in associative learning are included in diagnostic criteria (both ICV-11 and DSM-5) for several psychiatric disorders, most notably schizophrenia (SZ) (American Psychiatric Association, 2013). Early pioneers of psychiatry Heinrich Schüle and Eugen Bleuler, described conditions with SZ-like symptoms as dementia praecox, highlighting the severe cognitive deficits they were observing in young patients “wrecked on the cliffs of puberty” (McNally, 2013). Eugen Bleuler went so far as to describe the disorder’s core deficit as a “loosening of associations” (Peralta and Cuesta, 2011). In spite of these early observations, the general public predominantly associates SZ with hallucinations and delusions, potentially in part due to inaccurate portrayals in the media and sensationalising by journalists (Knifton and Quinn, 2008; Owen, 2012). However, in reality these symptoms represent only one aspect of the disorder. Symptoms such as hallucinations and delusions are grouped into the category of positive symptoms, i.e., patients have gained something that neurotypical individuals do not exhibit. SZ patients also exhibit traits from two other categories: negative and cognitive. Negative symptoms represent something lost, that a neurotypical person has but an individual with SZ does not have and includes symptoms such as affective flattening (unchanging and unresponsive facial expression), alogia (poverty of speech), anhedonia (inability to feel or express pleasure) and avolition (lack of motivation). Cognitive symptoms of SZ are perhaps the most poorly understood aspect of the disorder, but have a dramatic impact upon a patient’s quality of life. They include, but are not limited to, lower intelligence quotient (IQ), impaired working memory and deficits in associative learning (Gold,

1997; Caspi, 2003; Bowie and Harvey, 2006; Diwadkar, Flaugher, Jones, Zalányi, Ujfalussy, Keshavan and Érdi, 2008). Table 1.1 provides more details on the sequela of SZ. Multiple studies have confirmed the association of SZ and associative learning deficits, including the work of Hofer et al., (2001), where SZ patients failed to correctly associate a puff of air to the eye with a change in light colour, whereas neurotypical controls were able to make the association (Hall, Romaniuk, Andrew M McIntosh, *et al.*, 2009). Current treatments for SZ such as chlorpromazine and haloperidol exclusively target the positive symptoms of the disorder (Patel *et al.*, 2014). Some trials have shown moderate efficacy for adjunctive agents to treat negative symptoms however, researchers suggest this may be improved by patient stratification (Correll and Schooler, 2020). Despite the large body of evidence supported by patient demand, there is an unmet clinical need for therapies to address SZ's cognitive symptoms (Moghaddam, 2004).

Positive	Negative	Cognitive
Hallucinations	**Avolition** – lack of motivation to do tasks	**Working memory dysfunction** – difficulties in the ability to maintain and manipulate informative stimuli
Delusions	**Anhedonia** – inability to feel pleasure	**Impaired attention**
Thought insertion – belief that ones thoughts are not their own	**Social withdrawal**	**Associative learning deficits** – inability to form appropriate associations between two stimuli
Thought broadcasting – belief that ones thoughts can be heard by others	**Alogia** – poverty of speech	**Poor executive functioning** – difficulty forming a conceptual framework to understand ambiguous stimuli
Hebephrenia – disorganised speech	**Affective flattening** – unresponsive facial expression	**Lower IQ**
	Apathy	
	Aprosodia – avoidance of eye contact	

Table 1.1 – Breakdowns of the three symptomatic categories presented by individuals with schizophrenia. Adapted from Andreasen (1982), Andreasen et. al. (1991), Bowie et. al. (2006) and Crow (2018).

Post-traumatic stress disorder (PTSD), like SZ, is another psychiatric disorder where impaired associative learning is thought to be implicated. However, in the case of PTSD, issues with associative learning are thought to be driving the disease's aetiology rather than as a symptom, as is the case with SZ. PTSD is a fear-based disorder wherein patients after experiencing or witnessing a fear inducing event, such as sexual assault, war, or road traffic accident, have a strong emotional association of locations, smells, sounds, people, or objects with the trauma. This means that if the individual is reexposed to these otherwise innocuous stimuli, they experience flashbacks and intrusive memories related to the adverse event (Bryant, 2019). These inappropriate associations have drastic implications on a person's life including crippling dissociative episodes, anxiety, and hyperarousal. The persistence of these associations despite the lack of the original adverse stimulus, may be explained by a failure of extinction learning, an aspect of associative learning wherein associative memories are 'overruled' by a new more salient (stronger) associative memory containing updated information about the pairing of a US and CS (Lambert and McLaughlin, 2019). By better understanding the neural and molecular mechanisms underlying associative learning and in particular extinction learning, there is a capacity for both pharmacological and psychiatric strategies (potentially a combination of the two) used to treat PTSD to be developed/improved. An example of this can be seen in the work of Difede et al., (2014) where oral administration of a N-methyl-D-aspartate (NMDA) partial receptor antagonist (D-cycloserine); commonly employed in clinical trials as a cognitive enhancer, was successfully used to augment NMDA receptor (NMDAR) mediated synaptic plasticity

and improve fearful associative memory extinction using virtual reality driven exposure therapy.

1.1.1 Contextual fear conditioning

Contextual fear conditioning (CFC) is a single or multiple trial learning paradigm commonly used to induce learned fear in rodents. In CFC, the CS is the static environmental cues associated with an aversive event opposed to a discrete CS like a tone. CFC represents a quick, reproducible, and long-lasting method to study the molecular mechanisms driving associative learning and its associated processes (LeDoux, 2003). During CFC, a particular context (the chamber the subject is placed in) is paired with an aversive fear inducing footshock. Following the acquisition of the contextual fear memory (CFM), presentation of the context to the subject in the absence of a footshock still elicits a fearful freezing response (CR) in a process termed retrieval. Prolonged or repeated presentation of the context along with no footshock elicits a graduated reduction in the CR and freezing returns to near pre-shock levels. It is important however, to note that this CFM extinction does not represent a loss of the original CFM. Instead, a new more salient memory is formed: that the context is not associated with a fearful stimulus. The fearful association and accompanying CR can be reinstated with US reminder, which in a previously unconditioned animal would not be sufficient for the acquisition of a CFM a process termed reacquisition. The original fear association can also re-emerge after an extended period of following the extinction event (spontaneous recovery) or following reexposure to the conditioned stimulus in within a novel context (renewal) (Bouton, 2004; Myers and Davis, 2007; Dickinson, 2012; Orsini and Maren, 2012; Tovote, Fadok and Lüthi, 2015).

1.1.2 Neural and cellular mechanisms of contextual fear conditioning

The amygdala is the neural hub of fear conditioning; information from the hippocampus, perirhinal cortex and thalamus regarding the CS arrives in the frontotemporal subregion via glutamatergic neurons. Like other brain regions, the amygdala can be subdivided into several subregions termed nuclei, with the basolateral amygdala (BLA) and central nucleus of the amygdala (CEA) being the nuclei most involved in facilitating fear learning. The BLA consists predominantly of glutamatergic spiny projection neurons and a smaller population of GABAergic interneurons. Conversely, the CEA is mostly comprised of GABAergic medium spiney neurons which project to the hypothalamus and bed nucleus of the stria terminalis (BNST) brain regions, where activity is associated with the presentation of fear anxiety-like behaviours (Sah *et al.*, 2003; Choi *et al.*, 2007; Keifer *et al.*, 2015a). Studies involving both pharmacological and lesion driven inhibition of the amygdala highlight its essential role in the induction of fear and anxiety. Individuals who have undergone temporal lobectomies or experienced ischemia localised to temporal lobes, exhibit ‘psychic blindness’ characterised by a lack of response to stimuli that would normally elicit fear and anxiety (Terzian and Ore, 1955; Davis, 1997). Likewise, electrical stimulation of amygdala elicits fear-like behaviours and feelings of anxiety and apprehension. Regarding the acquisition of a CS-US association during fear conditioning, evidence presented by Aggleton (2000) and LeDoux (2003) implicates the BLA as the site where the association is formed. In fear conditioning paradigm where a tone is paired with a footshock, conditioning increased the magnitude of evoked auditory responses in the BLA driven by synaptic plasticity in the region (Tsvetkov *et al.*, 2002; Keifer *et al.*, 2015b; Tovote, Fadok and Lüthi,

2015). Furthermore, optogenetic induced long-term depression (LTD) of inputs into the BLA from the auditory cortex is sufficient to inactivate the memory of the association between the tone and shock (Nabavi *et al.*, 2014). Extinction learning as discussed previously, is the process by which a new associative memory is formed with updated information regarding a US. Crucially however, it does not replace the association but is just more salient. As with the acquisition of associative memories, the BLA facilitates extinction learning, a switch in the balance between fear and extinction neurons is driven by NMDAR-dependent plasticity and remodelling of inhibitory circuits and synapses (Falls, Miserendino and Davis, 1992; Mao, Hsiao and Gean, 2006; Heldt and Ressler, 2007; Lin, Mao and Gean, 2009). Recent research has also begun to shine a spotlight on the CEA and it is now considered to play an essential role in the acquisition and expression of conditioned fear, rather than just being a passive relay station for information from the BLA to regions involved in the presentation of fear responses. Within the lateral central amygdala (CEl); a subdivision of the CEA, *in vivo* electrophysiological experiments have revealed that post-conditioning, and driven by synaptic plasticity, two distinct populations of inhibitory neurons emerge ‘on’ and ‘off’. The population of ‘on’ cells drives the activation of outputs from the medial central amygdala (CEm, another subdivision of the CEA) and thus the expression of fear. In contrast, the ‘off’ population of neurons identifiable through their expression of protein kinase Cδ (PKC), inhibits the expression of conditioned fear through promoting inhibitory currents in CEm projections (Ciocchi *et al.*, 2010; Haubensak *et al.*, 2010; Knobloch *et al.*, 2012) (Figure 1.1).

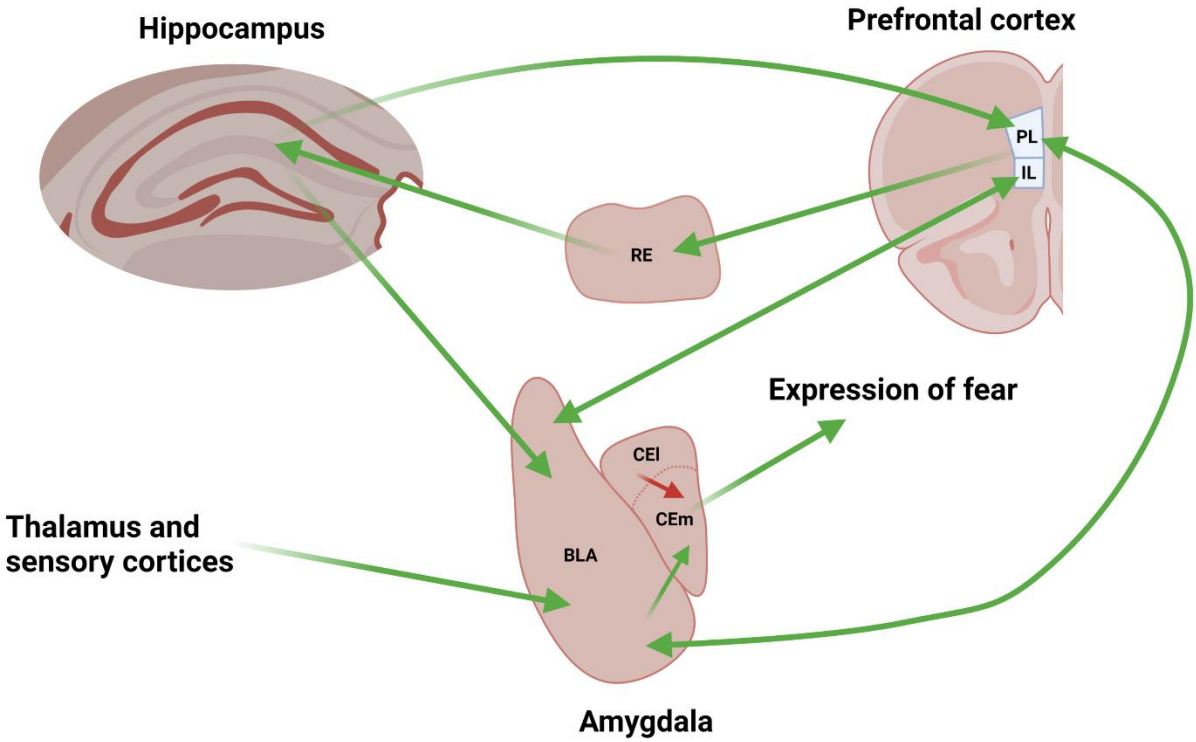

Figure 1.1 – The network of connections between the amygdala, hippocampus, medial prefrontal cortex and the nucleus reuniens (RE) responsible for the fear learning and its expression. Green arrows denote excitatory projections, red arrows represent inhibitory projections and double ended arrows indicate bidirectional excitatory projections. BLA (basolateral amygdala), CEl (central lateral amygdala), CEm (central medial amygdala), PL (prelimbic cortex) and IL (infralimbic cortex). Adapted from Tovote et. al. (2015) and Careaga et. al. (2016).

The hippocampus, like the amygdala, is in the temporal lobe and consists of two C-shaped interlocking layers: the granular cell layer of the dentate gyrus (DG) and the pyramidal cell layer, which is divided into the cornu ammonis 1 (CA1), CA2 and CA3 subfields (Gottlieb and Cowan, 1973). The DG can be subdivided into the molecular layer (ML), granular layer (GL) and hilus (Treves *et al.*, 2008) (Figure 1.2). Hippocampal neurons are predominantly glutamatergic excitatory pyramidal cells complimented with a small population of inhibitory GABAergic neurons (West and Gundersen, 1990). The subregions of the hippocampus are connected in a network termed the 'trisynaptic loop'. In the main, information enters the DG via projections from the entorhinal cortex, which then projects along its mossy fibres into the CA3 (Basu and Siegelbaum, 2015). The Schaffer collateral axons in the CA3 project into the CA1 to complete the 'trisyaptic loop' (Stepan, Dine and Eder, 2015). This 'loop' however is not unidirectional as was once believed; the mossy fibres connecting the DG and CA3 are bidirectional and projections from the cortex also innervate the CA1 and CA3 (Figure 1.3) (Knierim, 2015; Botterill *et al.*, 2021). The hippocampus plays an essential role in the regulation of the neuroendocrine stress response, learning and memory (Maren, 2001; Kim and Cho, 2020). Additionally, the DG is one of the two brain regions (alongside the olfactory bulb) where adult neurogenesis has been detected. However, unlike the amygdala, the role of the hippocampus in conditioned fear memory appears not to be so straightforward, with some authors proposing that it might not be required at all. They point to experiments where hippocampal inactivation does not affect subjects' acquisition of associative memories such as tone-shock pairings (Jarrard, 1995; Jonathan C Gewirtz, McNish and Davis, 2000; Zaben *et al.*, 2017; Toda *et al.*, 2019). The same authors also critique lesion

experiments, saying that they do not only target the hippocampus but also inadvertently damage cortical structures, meaning the effects upon fear learning they observe are difficult to attribute to one specific brain region (Kim and Jung, 2006). However, putting controversy aside, when considering CFC where more complex associations are required between the US and CS, the hippocampus unquestionably plays an essential role (Kim and Jung, 2006b). Lesions to the hippocampus before conditioning prevents acquisition of a CFM. Furthermore, lesions administered 24 hours post-conditioning also inhibit the CR to the context (Jarrard, 1995b; S Maren, Aharonov and Fanselow, 1997; Anagnostaras, Maren and Fanselow, 1999). The CA1 is also essential for the retrieval of CFMs at recent timepoints, evidenced by functional tract tracing of hippocampal neurons and their input onto the somas and dendrites of active neurons in the amygdala (Knapska *et al.*, 2012). Early evidence based upon lesions to the hippocampus had no effect upon CFM extinction as described by Wilson, Brooks and Bouton (1995). However, these researchers did note that said lesions prevented the reinstatement fear memory following an extinction paradigm, suggesting that the hippocampus is specifically required for forming context-US associations only, not for encoding other information about the context (Jonathan C Gewirtz, McNish and Davis, 2000). Plasticity within the hippocampus appears to be vital for contextual associative learning. Mice lacking NMDAR (essential for long-term potentiation: LTP) in solely CA1 pyramidal neurons have impaired CFM acquisition (Huerta *et al.*, 2000). Furthermore, mice with impaired hippocampal LTP, due to either the loss of cAMP response element binding protein (CREB) (α and δ isoforms) or PKCγ, experience mild deficits in contextual learning (Bourtchuladze *et al.*, 1994). Brain derived neurotrophic factor (BDNF); a

protein essential for synaptic modulation, neural plasticity, and induction of LTP, is increased in expression (messenger ribonucleic acid: mRNA) 24 hours post-CFC in the CA1 (Hall, Thomas and Everitt, 2000; Yang *et al.*, 2020). BDNF heterozygous knockout mice display impaired conditioned freezing, which can be rescued by the administration of recombinant human BDNF protein into the hippocampus via a cannula (Liu *et al.*, 2004; Kim and Jung, 2006).

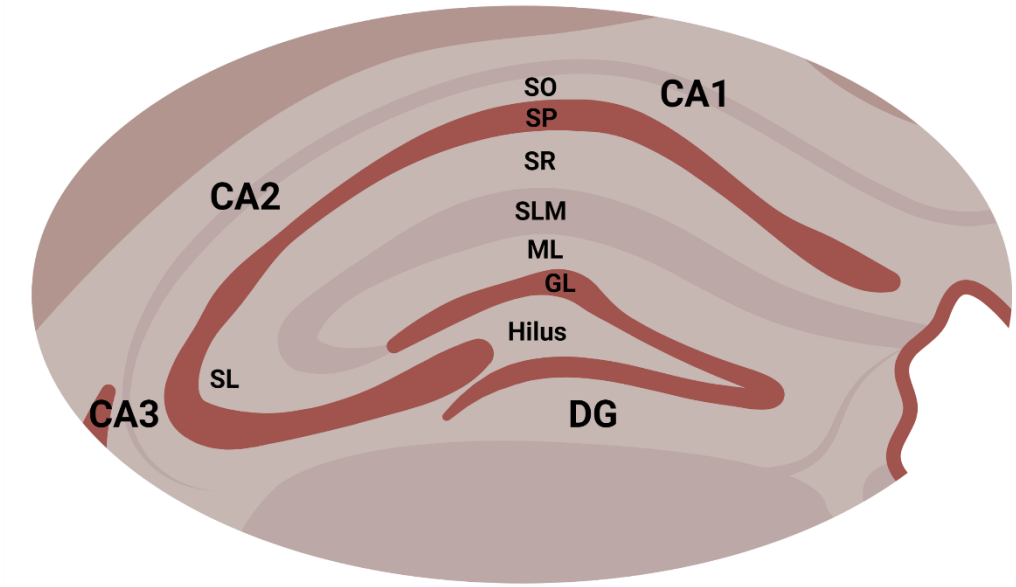

Figure 1.2 – The cytoarchitecture of the dorsal hippocampus with all subregions and strata annotated. CA (cornum ammonis), DG (dentate gyrus), GL (granular layer), ML (molecular layer), SL (stratum lucidum), SLM (stratum lucunosum-moleculare), SO (stratum oriens) and SP (stratum pyramidale).

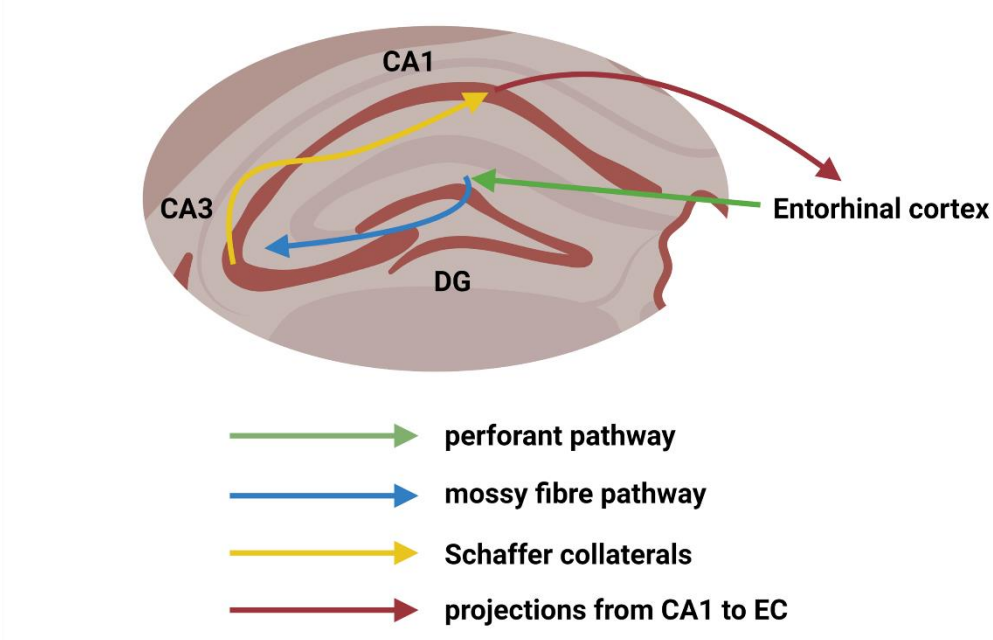

Figure 1.3 – The trisynaptic loop of the hippocampus. Excitatory inputs of the perforant pathway originating from the second layer of the entorhinal cortex (EC) innervate the granule layer of the DG. Mossy fibre projections from the granule cells transmit information to the pyramidal cells of the CA3, which in turn projection to the pyramidal cells of the CA1 along the Schaffer collaterals. Projections from the CA1 innervate layers five and six of the EC. Adapted from Basu et. al. (2015) and Stepan et. al. (2015).

The rodent medial pre-frontal cortex (mPFC) is a subdivision of the frontal lobe which itself comprises of three distinct regions: the anterior cingulate (ACC), prelimbic (PL) and infralimbic (IL) cortices (Heidbreder and Groenewegen, 2003). Neurons in these regions are laminarly arranged into six layers all with different densities, sizes, and heterogeneities of their neurons. Inputs from other brain regions innervate layer I, which contains no neuronal cell bodies but does contain apical projections from neurons in layers II and III (Miller, Pinto and Simons, 2001; Muralidhar, Wang and Markram, 2014) (Figure 1.4). Akin to the hippocampus, most (~90%) neurons in the mPFC are pyramidal and excitatory with the remainder (~10%) being GABAergic interneurons. The GABAergic population can be subdivided into fast-spiking parvalbumin interneurons, which modulate glutamatergic output from pyramidal neurons and the somatostatin interneurons that control the information pyramidal neurons in layers II and III neurons receive (Kvitsiani *et al.*, 2013) (Figure 1.4). Projections from the PL cortex enter the BLA where the excitatory signals they provide are thought to modulate the expression of fear (Brinley-Reed, Mascagni and McDonald, 1995). The communication between the PL and BLA is bidirectional, with neurons associated with the expression of fear memory in the BLA specifically targeting the PL cortex. Conversely, BLA neurons associated with the extinction of a fear memory project into the IL cortex, with the relative differences in neural activity between these two pathways controlling the level of CR (Senn *et al.*, 2014). Both the PL and IL cortices also receive input from the CA1 subregion of the hippocampus. These projections are thought to be essential for the integration of contextual of information with the signalling received from the amygdala (Swanson, 1981; Hoover and Vertes, 2007; Giustino and Maren, 2015).

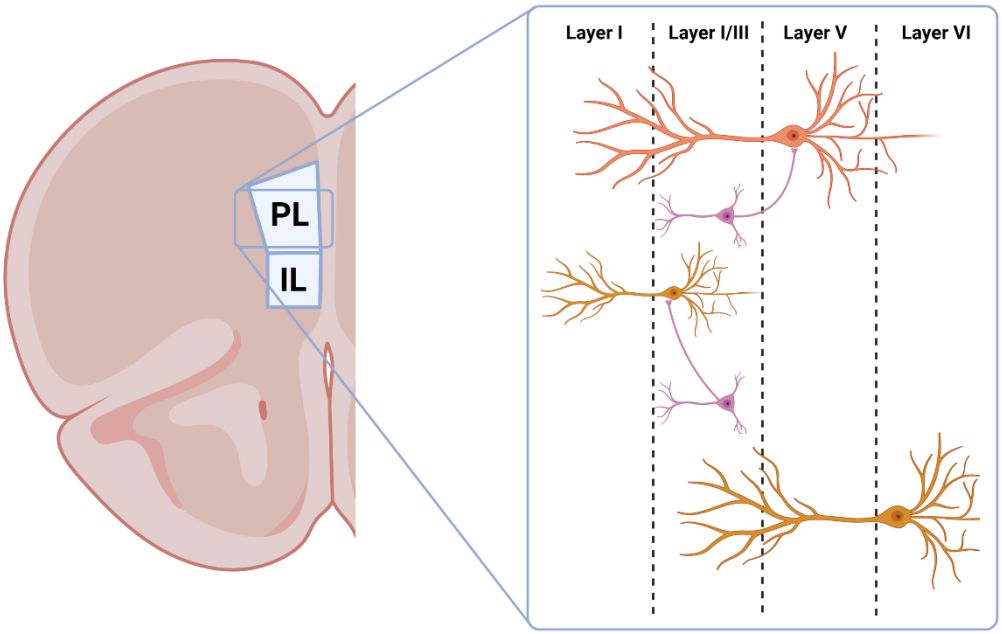

Figure 1.4 – The cytoarchitecture of the laminar organisation of the prelimbic (PL) and infralimbic (IL) subregions of the mPFC (medial prefrontal cortex). Layers, starting with I closest to midline and layer VI closest to the forceps minor of the corpus callosum contain both excitatory pyramidal neurons (orange) and regulatory GABAergic parvalbumin interneurons (pink). Adapted from Xu et. al. (2019).

No projections exist which travel directly from the mPFC to the hippocampus, instead projections from the mPFC innervate a small region of the thalamus, the nucleus reuniens (RE) (Figure 1.1). Pharmacological inactivation of RE with muscimol inhibits the acquisition of contextual fear memories (Karthik R. Ramanathan *et al.*, 2018). Furthermore, inactivation of the RE during reexposure of a fear associated context increases expression of learned fear and prevents its extinction (Karthik R Ramanathan *et al.*, 2018). Evidence of the IL cortex's role in facilitating fear memory extinction is seen in experiments showing pyramidal neurons in the subregion in NMDAR-dependent manner change their synapses during extinction training (Milad and Quirk, 2002; Burgos-Robles *et al.*, 2007). However, historically there have been mixed reports on the role of the IL in the expression of extinction learning arising from studies utilising lesions to the mPFC, leading researchers to summarise that the role of the IL cortex in extinction memory acquisition and retrieval is dependent on the specific fear conditioning paradigm being employed (Chang and Maren, 2010; Giustino and Maren, 2015). However, the rise of optogenetic techniques has provided categorical proof of the IL in the acquisition of extinction memories. Optogenetics employs light sensitive ion channels; cation-conducting channelrhodopsins (excitation) and anion-conducting channelrhodopsins (inhibition), and delivery of light via an optic fibre placed in a specific brain region to modulate neuronal activity (Joshi, Rubart and Zhu, 2020). Optogenetic inhibition of neurons in the IL was shown to impair the acquisition of extinction memories and optogenetic stimulation of the IL can promote 'relapse' after extinction of a fear memory (Do-Monte *et al.*, 2015; Kim *et al.*, 2016). Multiple pharmacological and microstimulation studies have provided evidence in support of

PL cortex's role in the expression of learned fear. Administration of an inhibitor of neural activity (tetrodotoxin) to the PL has no effect upon CFM acquisition, but does reduce the CR upon reexposure to the fear associated context (Corcoran and Quirk, 2007). Microstimulation of the mPFC with an electrode placed in the PL cortex increased the expression of learned fear and prevented extinction, whereas the placement of the electrode in the IL cortex did the exact opposite (decreased the expression of learned fear and promoted fear memory extinction). This experiment reinforces the hypothesis that the PL and IL cortices are diametrically opposed, with activation of PL driving expression of fear memories and activation of the IL promoting their extinction (Vidal-Gonzalez et al., 2006; Giustino and Maren, 2015).

1.2 The neuroimmune environment

1.2.1 Microglia

The central nervous system (CNS) is populated with tissue specific macrophages termed microglia that comprise 10-15% of cells in the adult brain (Li and Barres, 2018; Morimoto and Nakajima, 2019). Early in development (5.5 weeks gestation in humans, E8 in rodents), primitive macrophages from a pool in the yolk sac colonise the embryonic brain (Thion, Ginhoux and Garel, 2018). Upon maturation of the blood brain barrier (BBB), microglia are confined to the CNS under healthy conditions and self-renew throughout adulthood (Daneman and Prat, 2015; Lenz and Nelson, 2018). Following traumatic injuries and the late stages of neurogenerative diseases, the BBB becomes ‘leaky’ and peripheral macrophages can enter the CNS (Minagar and Alexander, 2003; Alluri *et al.*, 2015; Zenaro, Piacentino and Constantin, 2017). Microglia exhibit very slow turnover, meaning events (injury, disease, and/or stress) that affect developing or mature microglia can have long lasting effects upon their function (Jenna M Ziebell *et al.*, 2017). Microglia are unevenly distributed throughout the brain, with concentrated populations located in the hippocampus, basal ganglia, and substantia nigra (Rivest, 2009). Microglial transcriptomes are sculpted by the subregions they reside in, meaning microglia in the hippocampus, for example, are phenotypically distinct from those found in the cerebral cortex, amygdala, or cerebellum (Tan, Yuan and Tian, 2020). This heterogeneity of microglia highlights their functional pluralism (roles include but are not limited to: phagocytosis, maintenance of homeostasis, promotion of repair and synaptic pruning) and may explain the varying sensitivities of different regions to the same physical, chemical, and psychological stimuli (Kim *et al.*, 2000).

Traditionally microglia in the healthy adult brain have been termed ‘resting’ which is a misnomer. Microglia in a healthy adult brain actively patrol their territories surveying their local environment for pathogens, apoptotic/necrotic cells, neurofibrillary tangles, amyloid plaques, and deoxyribonucleic acid (DNA) fragments (Nimmerjahn, Kirchhoff and Helmchen, 2005a; Bolmont *et al.*, 2008; Ohm *et al.*, 2021). Additionally, microglia in the healthy brain actively participate in CNS homeostasis, support of neurotransmission, facilitating synaptic pruning, LTP and LTD, neuronal maintenance and regulation of neurogenesis (Rosa C Paolicelli *et al.*, 2011; Frost and Schafer, 2016; Salter and Stevens, 2017; Weinhard *et al.*, 2018a). Microglia upon recognition of a damaged or pathogen associated molecular pattern or detection of a disturbance in the CNS homeostasis via their arrays of trans-membrane receptors become ‘activated’. Following their activation microglia synthesise and release inflammatory cytokines and migrate following chemotactic gradients to sites on injury and damage (Thameem Dheen, Kaur and Ling, 2007; Bachiller *et al.*, 2018). Traditionally, activated microglia are characterised as having either a M1 or M2 phenotype matching the nomenclature used to classify T helper cells in the peripheral immune system (Fernando O. Martinez and Gordon, 2014; Tang and Le, 2016). Adoption of the M1 phenotype is driven by exogenous pathogen associated molecular patterns such as lipopolysaccharide (LPS) and endogenous pro-inflammatory cytokines tumour necrosis factor (TNF) and interferon-γ (IFNγ). Functionally the M1 phenotype is considered pro-inflammatory, releasing pro-inflammatory cytokines (interleukin-1β: IL1β, TNF and IL6), actively phagocytising cells (and cell debris) and generating reactive oxygen species. Conversely, M2 microglia are described as anti-inflammatory and are involved in the resolution of the

immune response, releasing anti-inflammatory cytokines such as IL10 and interleukin 1 receptor antagonist (IL1ra) to promote tissue repair and wound healing. Adoption of the M2 phenotype is triggered by cytokines IL4, IL10 and IL13 (Lee, 2019; Orecchioni *et al.*, 2019). The M1 and M2 paradigm has been challenged as being reductive, overly simplistic and that the processes underlying microglial activation is too complex to be summarised with a binary classification model (Fernando O Martinez and Gordon, 2014). To address these issues, a new model has been proposed with activated microglia lying on a spectrum, where traditional M1 and M2 phenotypes represent the two extremes. However, even this model is now being challenged with M2 phenotype being subdivided into M2a, M2b, M2c and M2d ‘subphenotypes’, each with their own unique set of markers and functions (Rőszer, 2015) (Figure 1.5).

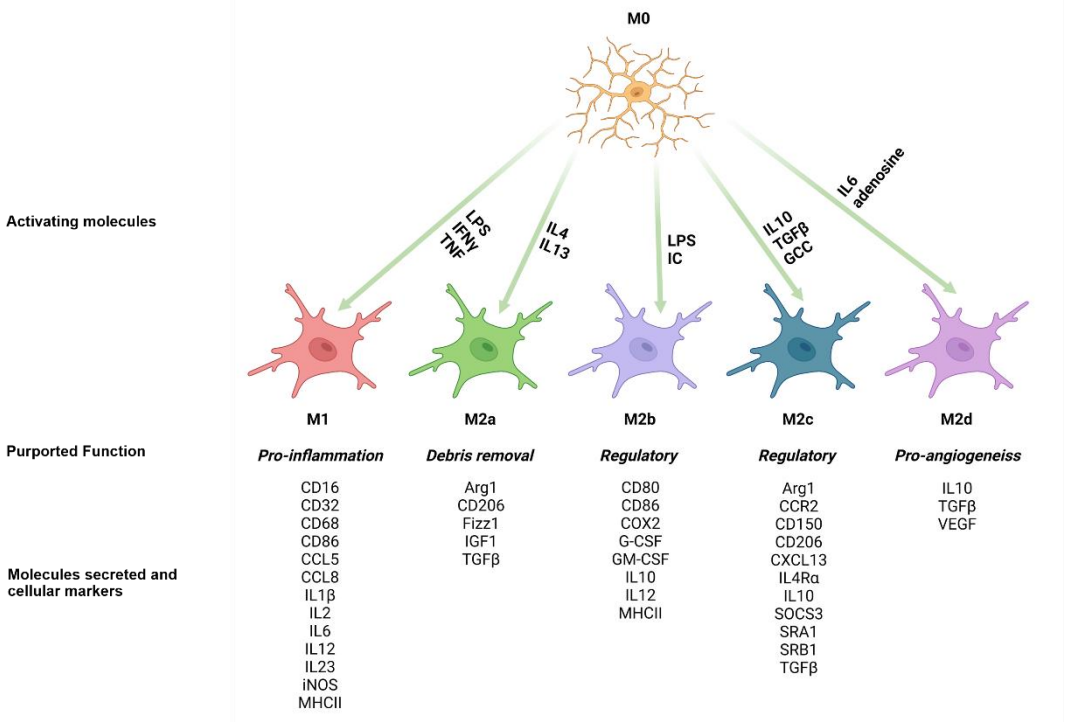

Figure 1.5 – The M1/M2 paradigm of macrophage/microglial activation. M0 or 'resting' cells are activated following interactions with a range molecules. M0 microglia stimulated with LPS (lipopolysaccharide), IFNγ (interferon-γ) and TNF (tumour necrosis factor) adopt a pro-inflammatory M1 phenotype expressing and secreting CD16 (cluster of differentiation 16), CD32, CD32, CD68, CD86, CCL5 (C-C motif) ligand-5, CCL8, IL1β (interleukin-1β), IL2, IL6, IL12, IL23, iNOS (inducible nitric oxide synthase) and MHCII (major histocompatibility complex II). M0 stimulated with IL4 and/or IL13 become cellular debris engulfing M2a microglia which are defined though their expression of Arg1 (arginase 1), CD206, Fizz1 (found in inflammatory zone-1), IGF1 (insulin-like growth factor) and TGFβ (transforming growth factor-1). Microglia adopt a M2b phenotype when stimulated by LPS and immune complexes. M2b cells regulatory anti-inflammatory roles in the inflamed brain and are identified by their expression of CD80, CD86, COX2 (cyclooxygenase-2), G-CSF (granulocyte colony stimulating factor), GM-CSF (granulocyte-macrophage stimulating factor), IL10, IL12 and MHCII. M2c cells are also anti-inflammatory regulators of immune activation induced by M0 stimulation with IL10, TGFβ and GCC (glucocorticoids). Markers of the M2c phenotype include: Arg1, CCR2 (chemokine receptor type 2), CD150, CD206, CXCL13 (chemokine ligand-13), IL4Rα (interleukin-4 receptor alpha), IL10, SOCS3 (suppressor of cytokine signalling-3), SRA1 (steroid receptor RNA activator-1), SRB1 (scavenger receptor class B type 1) and TGFβ. The M2d class of cells are pro-angiogenic induced by stimulation by IL6 and adenosine. The M2d phenotype is characterised by expression of IL10, TGFβ and VEGF (vascular endothelial growth factor). Adapted from Nakagawa, et. al. (2014), Rószer (2015), Franco et. al. (2015), Zhnag et. al. (2018) and Benedetto et. al. (2019).

Inter-microglial interactions and communication between microglia and other cells of the CNS (neurons and astrocytes) utilise the same array of signalling molecules as the peripheral immune system. Small molecules including chemokines, interferons, interleukins, and tumour necrosis factors, grouped under the broad term cytokines, comprise the backbone of immune signalling. Chemokines are divided into four sub-families based upon the number and spacing of cytokine residues: CXC, CC, CX3C and XC, all acting via G-protein coupled receptors direct immune cells to sites of damage and injury (Moser, 2004; Moser and Willimann, 2004; Hughes and Nibbs, 2018). Interferons are grouped into three classes (type I, II and III) and were classically defined as antiviral cytokines. In the CNS, interferon expression is essential for mounting an effective response to viral infection and coordinating immunomodulation (Paul et al., 2007; Owens et al., 2014). Interleukins are characterised as being either pro- or anti-inflammatory, which upon binding to type 1 or 2 cognate receptors, control immune cell activation, maturation, and proliferation (Cuneo and Autieri, 2009; Akdis *et al.*, 2011). Tumour necrosis factors are synthesised as transmembrane proteins which, when cleaved, become signalling molecules capable of promoting inflammation, apoptosis, and immune cell activation (Tracey and Cerami, 1994; Baud and Karin, 2001).

Several other classes of signalling molecule are utilised by microglia in addition to cytokines. Anaphylatoxins (C3a and C5a) produced by the complement system (described in Chapter 1.3) induce the release of pro-inflammatory cytokines and modulation of immune response. Fatty acid-based signalling molecules prostaglandins produced during the metabolism of arachidonic acid by cyclooxygenases, promote and regulate immune activation (Scher and Pillinger,

2009; Ricciotti and FitzGerald, 2011; Aoki and Narumiya, 2012). Neurotransmitters histamine and serotonin both can act as modulators of the immune system. Histamine via histamine receptor 1 is pro-inflammatory and immunomodulatory (Branco *et al.*, 2018). Likewise, serotonin also regulates immune response and acts as a chemoattractant (Eugen-Olsen *et al.*, 1997; Herr, Bode and Duerschmied, 2017).

Microglial morphology is determined by their cytoskeletal structure, comprised of three structural elements: microfilaments; consisting of polymerised units of globular actin, microtubules formed from tubulin polymerisation, and intermediate filaments; a large superfamily of cell specific proteins (Etienne-Manneville, 2004). Actin dynamics are the primary driver of changes in microglial morphology (Franco-Bocanegra *et al.*, 2019). A single layer of actin filaments (termed the cell cortex) covers the inner leaflet of the plasma membrane, and a network of actin filaments fills the cytoplasm. Actin networks require branching, which is tightly controlled by the actin related protein 2/3 (Arp2/3) complex, which, with a supply of adenosine triphosphate (ATP), binds to the “mother” filament and initiates the formation of a subfilament (Mullins, 2000; Rouiller *et al.*, 2008). Arp2/3’s ability to promote filament branching is regulated in microglia by coronins, which blocks its attachment to filamentous actin (Humphries *et al.*, 2002; Ahmed *et al.*, 2007; Liu *et al.*, 2011). Filamentous structures created by actin branching can rearrange into three different forms of cytoskeletal protein actin projection: lamellipodia, filopodia and uropods. Lamellipodia are very thin projections of the plasma membrane containing a two-dimensional mesh of densely packed actin just under the leading edge of the cell. Small spikes, formed by bundles of actin parallel to the lamellipodia extending

beyond the leading edge, are termed filopodia. Uropods comprised of actin and actomyosin protrude from the hind of the cell body and enables the cell to push forward in the direction of the leading edge (Gupton and Gertler, 2007; Lai *et al.*, 2008; Blanchoin *et al.*, 2014; Hind, Vincent and Huttenlocher, 2016). Cross-linking proteins interact with branched actin networks to enable microglia to control their morphologies; these proteins bridge together filaments allowing them to coordinate the formation of complex structures that dictate the shape of the entire cell. The cross-linking protein ionised calcium-binding adapter molecule 1 (IBA1) exclusive to microglia promotes actin bundling and supports the formation of multiple lamellipodia and filopodia required for microglia to achieve their array of different morphologies (Bartles, 2000; Ohsawa *et al.*, 2000, 2004). IBA1 expression increases post-microglial activation, reflecting its role in facilitating the gross cytoskeletal rearrangements that accompanies microglial stimulation (Ito *et al.*, 2001; Lee *et al.*, 2017). Cofilin 1 (CFL1) is a widely distributed actin-binding protein that promotes filament severing. Immortalised microglia deficient in CFL1 display have severe deficits in microglial morphology and subsequent response to LPS-induced activation (Alhadidi and Shah, 2018).

After over a century of study, the morphological phenotypes of microglia are well classified into four distinct groups: ramified, activated, amoeboid and rod (Sierra, Paolicelli and Kettenmann, 2019). Most microglia in the healthy adult brain adopt a ramified morphology with small somas, long processes and complex branches surveying a relatively large area in the search for signs of infections or neuronal distress (Glenn *et al.*, 1992). Upon detection of an aversive stimuli the cytoskeleton rearranges driving microglia to adopt an activated morphology, during this transition

microglia adopt an intermediate morphology termed hyper-ramified or bushy (Ziebell, Adelson and Lifshitz, 2015; Fernández-Arjona *et al.*, 2017). Activated microglia are characterised by their reduced process number, larger somas and thicker processes compared to the ramified morphological phenotype (Tynan *et al.*, 2010; Ziebell, Adelson and Lifshitz, 2015; Savage, Carrier and Tremblay, 2019). This morphological phenotype is indicative of activated microglia no longer looking for signalling molecules associated with damaged neurons or pathogens, but also the production of inflammatory cytokines, phagocytosing of cellular debris and/or migrating to sites of injury (Li *et al.*, 2007; Lynch, 2009). Following prolonged immunological activation along with axonal severance, active microglia retract their processes entirely, resulting in a round amoeboid-like cell that is classed as being fully active and thus indistinguishable at least morphologically from infiltrating peripheral macrophages (Giulian and Baker, 1986; Parakalan *et al.*, 2012; Jurga, Paleczna and Kuter, 2020a). Activated microglia can also adopt one final morphology; where the somas are very skinny, and processes are highly polarised meaning the cells resemble rods. Rod microglia align with damaged neuron post-injury and appear to facilitate either their repair or further breakdown (Taylor *et al.*, 2014; Holloway *et al.*, 2019; Giordano *et al.*, 2021) (Figure 1.6). Given the well-established literature on microglial morphology and its relation to function, researchers often use assessments of microglial morphology as a proxy for assessing the functional state of microglial in the brain during development, disease post-injury or following behavioural paradigms (Tynan *et al.*, 2010; Morrison *et al.*, 2017; Cengiz *et al.*, 2019; Paasila *et al.*, 2019).

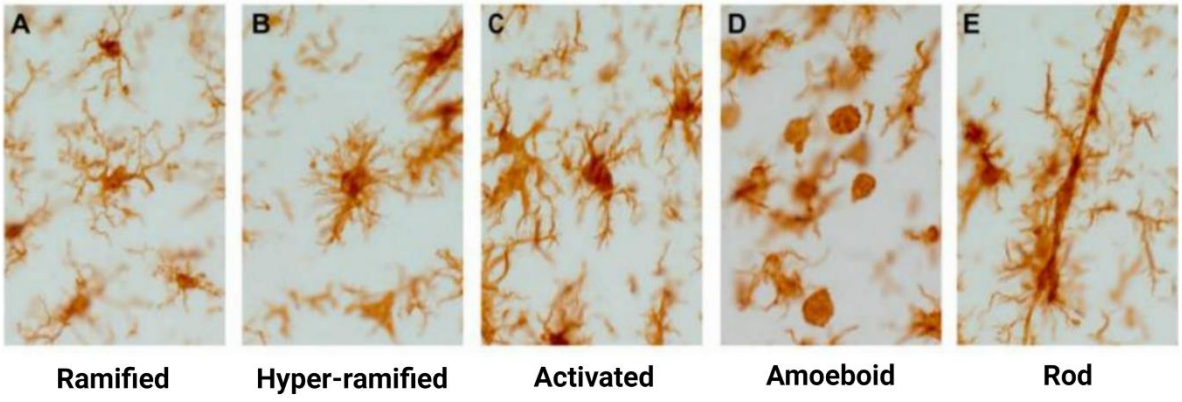

Figure 1.6 – Representative images of microglia obtained from the rat cortex by Ziebell et. al. (2015). **A.** Ramified 'surveying' microglia characterised by their long complex processes and small somas. **B.** Hyper-ramified 'bushy' microglia and intermediate morphology between ramified and activated, in which microglia have retracted and begun to thicken their processes. **C.** Activated microglia processes have further retracted and decreased in number, somas also appear larger and rounder. **D.** Amoeboid microglia lack any processes and are morphologically indistinguishable from blood-borne macrophages. **E.** Rod-shaped microglia adopt a highly polarised morphology characterised by their long thin somas and long extended processes. Adapted from Ziebell et. al. (2015).

1.2.2 Microglia and synaptic and structural plasticity

The role of microglia in the CNS is not limited to responding to infection and injury. The same biological mechanisms that allow microglia to sample their environment for signs of neuronal damage and repair neuronal circuitry, are also essential for the modelling of synaptic circuitry in the developmental and adult brain. In development, the supernumerary neurons and synapses require pruning and 'fine tuning' facilitated by microglia, to establish mature and functional circuits. The murine visual cortex at four weeks of age has been well characterised as a site of microglial driven circuit reorganisation and during this developmental phase, virtually all microglia in the visual cortex that are in a highly motile state, contact axonal terminals, dendritic spines and the synaptic cleft (Tremblay, Lowery and Majewska, 2010). These regular contacts between microglia are in turn associated with increased growth and elimination of dendritic spines. Furthermore, if mice receive no excitatory input into the visual cortex (i.e. they are left in the dark), microglial motility in the region and the number of contacts made with neurons is reduced, suggesting this developmental plasticity is driven by neuronal activity, which the microglia can 'sense' (Tremblay, Lowery and Majewska, 2010). In the developing murine CA1 at P15, microglia engulf axonal terminals and dendritic spines, evidenced by the colocalization of CX3C chemokine receptor 1 (CX3CR1) (a microglial marker) and postsynaptic density protein 95 (PSD95) (a synaptic marker) immunoreactivity. This developmental pruning was shown to be driven by neurons upregulating the chemokine fractalkine chemokine (C-X3-C motif) ligand 1 (CX3CL1), the ligand for the microglial specific receptor CX3CR1; indeed, mice lacking this receptor have transiently higher dendritic spine densities on CA1 pyramidal neurons compared to

wildtype (WT) littermates (Rosa C. Paolicelli *et al.*, 2011). The transient nature of the loss of synaptic pruning observed in these CX3CL1 knockouts (KOs) indicates that there is more than one 'find me-eat me' signalling pathway used by microglia for circuit refinement in the developing brain (Mody *et al.*, 2001; Ransohoff and Stevens, 2011).

In the mature adult brain, microglia are constantly surveying their microenvironment, extending and retracting their processes, allowing them to make frequent but brief contacts with synapses (Wake *et al.*, 2009). Studying microglial driven plasticity in the adult brain has proven difficult as unlike during the CNS' developmental window, adult pruning and plasticity is thought to be small in scale and localised to specific subregions of the hippocampus and cortex. Nevertheless, a body of evidence has emerged to support the hypothesis of microglia interacting with 'healthy' neurons and mediating synaptic plasticity in the adult brain (Wake, Andrew J Moorhouse, *et al.*, 2013). Hippocampal slices treated with glutamate induces increased microglial contacts with neuronal somata; this observation was dependent upon NMDA signalling (and not AMPA/kainite signalling) driving the release of ATP from active neurons which is detected by microglial purigenic receptors such as P2Y12 (Eyo *et al.*, 2014). Conversely, another study utilising tetanic stimulation of the Schaffer collateral pathway to induce LTP; a of form adult synaptic plasticity, in the CA1 observed no microglial chemotaxis towards neurons in the CA1 (Wu and Zhuo, 2008; Kruijssen and Wierenga, 2019). Microglial control of synaptic plasticity is not entirely dependent upon their direct interaction with neurons The extracellular matrix (ECM) is a highly dynamic three-dimensional structure providing structural and biochemical support to cells, which has emerged as a driver of neuronal

structural plasticity (Berardi, Pizzorusso and Maffei, 2004; Dityatev and Fellin, 2008). Specifically, ECM components matrix metalloprotease-9 (MMP-9) and tissue-plasminogen activator (tPA) facilitate dendritic spine enlargement, increases in synaptic strength and synaptic plasticity (Baranes *et al.*, 1998; Wang *et al.*, 2008). Evidence suggests that microglial interact with these ECM proteins and drive the ECM's modification in response to local synaptic activity (Tremblay, Lowery and Majewska, 2010b; Nguyen *et al.*, 2020a). Recently Nguyen et al., (2020) showed that in the hippocampus experience-dependent synapse remodelling is driven by changes in the ECM mediated by a IL33 signalling axis between microglial (expressing IL33 receptor) and neurons (releasing IL33). Cytokines such as IL1β, IL6 and TNFα; which microglia are a potential source of, are required for normal hippocampal LTP (Prieto and Cotman, 2017; Bourgognon and Cavanagh, 2020). TNFα specifically appears to be the driving force behind a process termed synaptic scaling. Synaptic scaling a form of heteroassociative (non-Hebbian) plasticity is the mechanism by which neurons, following activity dependent potentiation or depression adjust the weight of all their synapses to balance its overall excitability and prevent excitotoxicity induced neurodegeneration and maintain a network's ability to retain and store information (Turriggiano, 2008; Chistiakova *et al.*, 2015; Chater and Goda, 2021). Synaptic scaling requires changes in the ratio of AMPA (α-amino-3-hydroxy-5-methyl-4-isoazolepropionic acid) receptors to NMDA receptors with the direction of change depending upon whether a synapse is being strengthened or weakened. In the hippocampus TNFα signalling increases the ratio whereas conversely, in the striatum TNFα signalling decreases the ratio, suggesting that the precise mechanisms of cytokine and therefore microglial dependent circuit

modification, may vary in a region dependent manner (Stellwagen *et al.*, 2005; Stellwagen and Malenka, 2006; Rogers *et al.*, 2011a; Lewitus *et al.*, 2014; Wu *et al.*, 2015).

1.3 The complement system

The complement system is a biologically ancient facet of the immune system found in jawed vertebrates, jawless fish, non-vertebrates and deuterostomes, which recognises molecular patterns to trigger inflammatory and anti-pathogen pathways (Nonaka and Yoshizaki, 2004). A functional complement system is required for the detection, clearance, and resolution of infection and/or injury, but also plays a pivotal role in development and homeostasis (Dunkelberger and Song, 2010). Activation of the complement system occurs via the classical and lectin pathways with both pathways' activity being amplified by the alternative pathway. The three pathways converge on complement component 3 (C3) which is cleaved generating anaphylatoxins (C3a and C5a) and biologically active peptides before culminating with the induction of the terminal pathway (Figure 1.7).

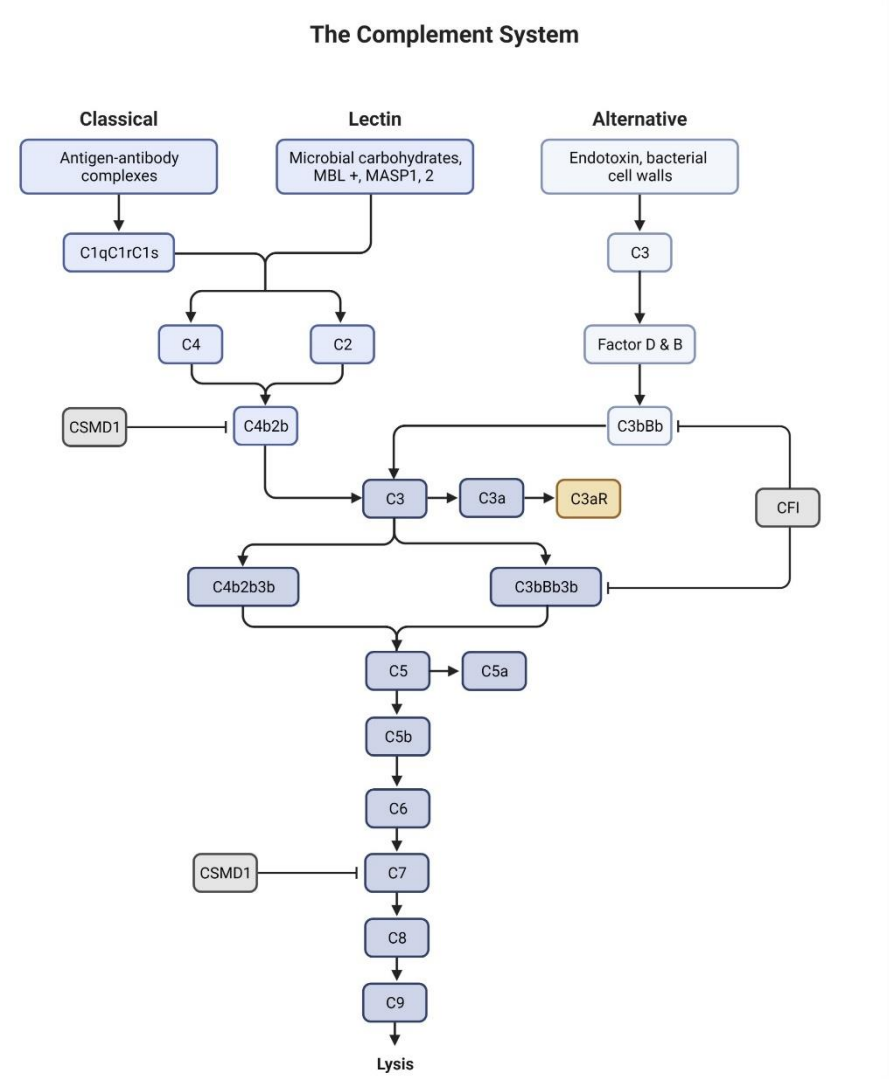

Figure 1.7 – Simplified schematic of the complement system in the CNS. Detection of a ligand by C1q triggers C1 complex mediated the cleavage of C4 and C2 which generates the C4b2b complex. The C4b2b complex cleaves C3 generating C3a and C3b fragments (classical and lectin pathway). C3 can also be cleaved by the C3bBb generated by the spontaneous hydrolysis of C3 (alterative pathway). C3a an anaphylatoxin binds to its cognate receptor C3aR. The C3b fragment forms a complex with either C4b2b or C3bBb to form a C5 convertase. The C5 convertase cleaves C5 into C5a and b, the later of which associates in sequence with C6, C7, C8 and multiple units of C9. This final complex termed the membrane attack complex and is inserted in cell membranes.

1.3.1 Complement system activation

The classical pathway is initiated by the Ca^{2+} dependent C1 enzyme complex. C1 (or $C1qr^2s^2$) is comprised of two copies of the proteases C1r and C1s along with the C1q trimer containing A, B and C subunits. C1q is a pattern recognition molecule able to identify and bind: fragment crystallizable region (Fc domain) of IgG/M, Aβ oligomers, LPS, C-reactive protein (CRP), prion protein, DNA, lipid A and pentraxin 3 (PTX3) (Idusogie *et al.*, 2000; Kojouharova, Reid and Gadjeva, 2010; Mortensen *et al.*, 2017a). Following C1q interacting with an antagonist, the two C1r units in C1 autoactivate and convert the proenzyme C1s into a fully active highly specific serine protease. The activity of the C1 complex is regulated by serpin family member G member 1 (SERPING1), a member of the serpin superfamily of protease inhibitors. SERPING1, also referred to as C1-inhibitor (C1-INH), inactivates the proteolytic activity of both C1r and C1s preventing the progression of complement system activation (Mortensen et al., 2017; Almitairi et al., 2018).

The lectin pathway begins with homotrimeric oligomers of pattern recognition molecules (PRMs): mannose binding lectin (MBL), collectin 11 (CL11) and ficolin 1-3 interacting with D-mannose, L-fucose or N-acetylglucosamine, sugars predominately found on the surface of pathogens and apoptotic/necrotic cells (Degn *et al.*, 2012; Heja *et al.*, 2012). Upon binding a sugar PRMs induce the autoactivation of the serine protease mannan-binding lectin serine protease-1 (MASP-1), which in turn activates an additional protease MASP-2. Like the C1 complex, MASP activation is tightly regulated by SERPING1 (Gulati *et al.*, 2002).

1.3.2 The complement cascade

The activated serine proteases generated by the classical and lectin pathways cleave C2 and C4 generating the complement fragments C4b and C2a, which combine to yield C4bC2a, a C3 convertase which promotes the cleavage of C3 into C3a and C3b. C3b joins with the C4bC2a complex producing a C5 convertase (C4bC2aC3b), which cleaves C5 to produce C5a and C5b. C5b initiates the formation of membrane attack complex (MAC) or terminal complement complex (TCC). The MAC comprises C5b, C6, C7, C8 and a varying number of C9 subunits. Its formation requires the association of C5b with C6, enabling C6 to attach to a membrane, C5b then recruits sequentially C7 and the membrane inserting C8 protein. C8 is necessary for the complex to associate with the first C9 molecule which facilitates polymerisation with additional units of C9 to form a pore in the membrane (Tegla *et al.*, 2011). The pore formed has a functional diameter between 1-11 nm allowing for the free exchange of intra- and extracellular ions (Nesargikar, Spiller and Chavez, 2012). 'Termination' of cells (including neurons) requires the insertion of multiple MACs into the membrane facilitating: the efflux of adenine nucleotides (ATP, adenosine diphosphate: ADP, and adenosine monophosphate: AMP), an increase in intracellular Ca^{2+} concentration, the loss of mitochondrial membrane potential and caspase mediated cleavage of BH3 interacting-domain death agonist (BID) (Papadimitriou, Carney and Shin, 1991; Papadimitriou *et al.*, 1994; Ziporen *et al.*, 2009).

1.3.3 Sub-lytic MAC concentrations

Insertion of MAC numbers that are not sufficient for lysis are termed sub-lytic but still are able to exert an effect upon targeted cells. Sub-lytic MAC doses can induce cell

proliferation through the activation of cytosolic phospholipase A2 (cPLA2), (extracellular signal-regulated kinase 1 (ERK1), Ras, mitogen-activated protein kinases (MAPKs) and inhibitory G-proteins, along with the phosphorylation of Janus kinase-1 (JAK1) and signal transducer and activator of transcription 3 (STAT3) (Niculescu *et al.*, 1997; Niculescu and Rus, 1999; Dashiell, Rus and Koski, 2000). Additionally, sub-lytic MAC prevents apoptosis via the inhibition of caspases-3, promotion of Bcl-2-associated death promoter (Bad) phosphorylation (via PI3K/Akt signalling) and increases the expression of B-cell lymphoma 2 (Bcl-2) and CFLAR (Soane *et al.*, 1999, 2001; Cudrici *et al.*, 2008). Finally, the exchange of ions through sub-lytic doses of MACs and subsequent fluctuation in membrane, potentially alters the physical properties of the cell. MAC insertion into a platelet's plasma membrane increases their surface area and aids the clotting of blood at a wound (Markiewski *et al.*, 2007). Before complete MAC assembly some of the precursory complexes have their own independent functions. Both C5b-7 and C5b-8 complexes can generate fatty acid signalling molecules: ceramide and diacylglycerol (DAG) from the plasma membrane of B-lymphocytes (Niculescu *et al.*, 1993). Ceramide promotes BID cleavage and protein phosphatase 2 (PP2A) activation which together increase the Bax:Bcl-2 ratio resulting in caspase activation and finally apoptosis (Taha *et al.*, 2006). DAG activates members of the PKC family, who modulate a range of processes including migration, survival, and proliferation of cells (Taha *et al.*, 2006).

1.3.4 The alternative pathway

The generation of the C3 convertase (C4bC2a) by the activation of classical and lectins pathways alone is insufficient to evoke responses able to mitigate the effects of infection and/or injury; a complement system amplifier is necessary. The

alternative pathway meets this requirement for amplification and is responsible for up to 80% of total C5a and C5b produced by immunoglobulin M (IgM) induced complement activation (Harboe et al., 2004). The pathway is antigen independent, instead it is constantly 'ticking over' through the spontaneous hydrolysis and conformational rearrangement of C3 into C3(H_2O). The addition of a water molecule shifts a thioester bond in C3 giving it a C3b-like stable platform domain which can bind and facilitate the cleavage of complement factor B (CFB) by CFB forming the C3 convertase (C3(H_2O)Bb) (Xu and Chen, 2016). In a healthy multicellular environment, complement factor H (CFH) competes for CFB's binding site, inhibiting C3(H_2O)Bb formation and in turn preventing uncontrolled propagation of the complement system in the absence of an antigen. However, C3b generated by activation of the classical and lectin pathways also provides a platform for CFB cleavage and subsequent formation of the C3 convertase: C3bBb. This formation of an additional CFB cleaver overpowers the inhibitory effects of CFH and enables both C3(H_2O)Bb and C3bBb to propagate complement activation and its effector functions (Müller-Eberhard and Schreiber, 1980; Pangburn and Müller-Eberhard, 1984).

1.3.5 The anaphylatoxins

Proteases and the MAC are not the only proteins of functional significance generated by complement activation. The anaphylatoxins C3a and C5a, produced by the cleavage of C3 and C5 respectively, induce inflammatory and apoptotic signalling cascades via their homologous G-protein coupled receptors (GPCRs): C3a receptor (C3aR), C5a receptor (C5aR) and C5a-like receptor (C5L2) (Ricklin *et al.*, 2010; Woodruff, Nandakumar and Tedesco, 2011). The anaphylatoxins and their catabolites C3aDesArg and C5aDesArg upon binding to their cognate receptors,

activate the PKC/p47, PI3K/Akt, mitogen-activated protein kinase kinase 1/2 (MEK1/2) and ERK1/2 signalling axes (Guo and Ward, 2005; Sarma and Ward, 2012). These axes work synergistically inducing an inflammatory cascade driving: the production of reactive oxygen species (O^{2-} and H_2O_2) by nicotinamide adenine dinucleotide phosphate (reduced) (NADPH) oxidase, increased cell adhesion, induction of phagocytosis, immune cell recruitment, modulation of apoptosis, release of granule-based enzymes, cytokine production (particularly those under the control of NF-κB) and histamine secretion (Guo and Ward, 2005; Woodruff, Nandakumar and Tedesco, 2011). C5aR and toll-like receptors (TLRs) 2, 4 and 9 exhibit synergistic and antagonistic relationships via the adaptor protein myeloid differentiation primary response 88 (MyD88) and kinases MAPK, ERK1/2 and c-JUN N-terminal kinase (JNK) (Woodruff *et al.*, 2010). C5L2 is a secondary C5a receptor, which due to its lack of a coupled G-protein, has been proposed as decoy receptor whose sole purpose is to sequester and control the activity of C5a or modulate C5aR through a β-arrestin dependent mechanism (Woodruff, Nandakumar and Tedesco, 2011). Other studies, however, have provided evidence of C5L2 signalling regulating anti-inflammatory processes. C5L2 deficiency increases pro-inflammatory cytokine IL1β expression, reduces cell survival and induces septic shock post-LPS administration. In addition, C5L2 like C5aR has been identified as a potential TLR co-receptor who together upregulate the expression of pro-inflammatory high mobility group box 1 (HMGB1) (Hajishengallis and Lambris, 2010).

1.4 Complement in the CNS

1.4.1 Complement expression in the CNS

Components of the complement system in the CNS are synthesised by macroglia (astrocytes and oligodendrocytes). Early research utilising primary cultures of murine astrocytes and human astrocytes-derived tumour cell lines, showed their capability to express components of the classical, alternative, and terminal complement pathways (Lévi-Strauss and Mallat, 1987; Veerhuis, Nielsen and Tenner, 2011). Subsequent analysis has also demonstrated microglial expression of many of the same components as astrocytes, with the notable exception of terminal pathway proteins (Woodruff *et al.*, 2010). However, whilst both astrocytes and microglia can express many of the same complement system components, the degree to which the two cell type populations contribute to local levels of secreted protein has been highlighted by subsequent studies. For instance, both Lampert-Etchells *et. al.,* (1993) and Veerhuis et al., (1999) noted that in the brains of patients with Alzheimer's disease (AD), microglia are the primary source of C1q (Mathys *et al.*, 2019). Complement expression in the CNS is not solely a glial affair, neurons are also capable of producing complement system components. Neurons, particularly pyramidal neurons from AD brains, show expression of C1-INH and other regulators of the complement system such as CD59 (Veerhuis *et al.*, 1998; Pedersen *et al.*, 2007). Neurons from AD brains and other neurodegenerative diseases such as motor neurone disease, exhibit expression of many complement system components from the classical, alternative, and terminal pathways (Shen *et al.*, 1997; Thomas *et al.*, 2000; Lobsiger, Boillée and Cleveland, 2007; Pedersen *et al.*, 2007; M. Sta *et al.*, 2011). Neuronal expression of complement components is

not limited to disease states; during development, C1q expression is induced in neurons in a TGFβ dependent manner (Bialas and Stevens, 2013). The functional relevance of the differential contributions of cell types in the brain to the milieu of secreted complement components in the neuropil is yet to be determined, particularly outside of the setting of disease and/or development (Magdalon *et al.*, 2020; Schartz and Tenner, 2020). However, the ability of neurons to produce C1q themselves may provide a mechanism by which 'weak' synapses target themselves for pruning and how 'strong' synapses promote the elimination of neighbouring synapses (Veerhuis et al., 1999). Table 1.2 provides a comprehensive summary of cell type specific expression of complement system components in the CNS.

Complement system component	Neurons	Astrocytes	Microglia	Oligodendrocytes
C1-INH		✓	✓	
C1q	✓	✓	✓	
C1qR		✓	✓	
C1s		✓	✓	
C1r		✓	✓	
C2	✓	✓	✓	
C3	✓	✓	✓	
C3aR		✓	✓	
C4	✓	✓	✓	✓
C5	✓	✓		
C5aR1	✓	✓	✓	
C6	✓	✓		
C7	✓	✓		
C8	✓	✓		
C9	✓	✓		
CD40			✓	
CD46		✓		
CD55	✓			
CD59		✓	✓	
CFB		✓		
CFD		✓		
CFH		✓		
CFI		✓		
clusterin		✓		
CR1		✓	✓	
CR2		✓		
CR3			✓	
CR4			✓	
DAF		✓		

Table 1.2 – Summary of the complement genes expressed by the four major cell types in the CNS based upon data from human and animal models of neurodegenerative disease, injury and development. C1-INH (C1-inhibitor), C1qR (C1q receptor), C3aR (C3a receptor), C5aR1 (C5a receptor-1), CD (cluster of differentiation), CF (complement factor), CR (complement receptor) and DAF (decay-accelerating factor). 'Ticks' denote expression of the complement gene in the corresponding tissue. Adapted from Veerhuis et. al. (2011) and Schartz et. al. (2020).

1.4.2 Functions of the complement system in the CNS

The complement system's function to recognise, coordinate immune response to, and eliminate whole cells or cellular debris is not limited to response to injury or infection. A body of evidence has built up highlighting complement's role in nervous system development, CNS homeostasis and controlling behaviour (Rahpeymai *et al.*, 2006; Moriyama *et al.*, 2011; Alexander H Stephan, Barres and Stevens, 2012; Ducruet *et al.*, 2012; Coulthard *et al.*, 2018; Westacott *et al.*, 2022). Evidence highlighting complement's role in developmental synaptic pruning comes from work examining the establishment of the ipsilateral and contralateral layers of the dorsolateral geniculate nucleus (dLGN) thalamic subregions. Each dLGN (one per hemisphere) receives input from the retinal ganglion cells (RGCs) emanating from both the ipsilateral and contralateral eyes. In adulthood RGC synapses in the dLGN are separated based upon their origin, however at birth this dichotomy is not present. The separation of these inputs into distinct layers is dependent upon synaptic pruning driven by the complement system. Mice lacking complement components C1q, C3 or complement receptor 3 (CR3) exhibit failed separation and decreased engulfment of retinogeniculate synapses by microglia (Stevens *et al.*, 2007a; Schafer *et al.*, 2012; Tyler and Boulanger, 2012) (Figure 1.8). Trimming of a mouse's whiskers induces synaptic loss via pruning in the sensory barrel fields of the cortex (Lee *et al.*, 2009) . In a recent study from Györffy et al., (2018) following whisker trimming C1q was predominantly associated with pre-synaptic (synaptophysin positive) terminals, but also post-synaptic (PSD95 positive) boutons indicating a role of the complement system being the driving force behind their microglial mediated pruning and engulfment. In support of this isolation of C1qA tagged and non-tagged

synapses, followed by proteomic and pathway analysis identified an enrichment in proteins associated with pruning and apoptosis in the C1qA tagged group. Downstream of C1q, C3 and its cleavage products appear to be at the heart of complement mediated circuit organisation/reorganisation in the CNS. C3a/C3aR signalling has been shown however, to regulate neural plasticity and proliferation. Studies examining both healthy and injured brains, have found C3a to regulate adult hippocampal neurogenesis, neural progenitor migration, and functional recovery following an experimental model of murine ischemia (Shinjyo *et al.*, 2009; Stokowska *et al.*, 2017; Wadhwa *et al.*, 2019). The faster and sustained recovery of post-ischaemia following C3a administration is attributed to an increase in synaptogenesis and axonal plasticity promoting the restoration of damaged neural circuits (Stokowska *et al.*, 2017). C3aR, the cognate receptor for C3a, regulates the appearance of depressive-like behaviours and the infiltration of peripheral macrophages into the mPFC following a chronic unpredictable stress induced mouse model of depression. In this model, increasing levels of C3 expression in the mPFC via a stereotaxic injection of a C3 lentivirus induced depressive-like behaviours. Whereas knocking out C3 or C3aR prevented increases in depressive-like behaviours post-chronic unpredictable stress. Furthermore, C3aR KO prevents the increases in vascular cell adhesion molecule 1 (VCAM1), intracellular adhesion molecule 1 (ICAM1) and IL1β which normally accompany chronic stress, suggesting that the C3a/C3aR signalling axis controls the expression of pro-inflammatory mediators of depressive behaviours (Crider *et al.*, 2018). C3aR is also, via through an as yet undetermined mechanism, been implicated in the control of anxiety-like behaviours. Mice lacking C3aR displayed an increase in unconditioned innate

anxiety. This behavioural phenotype observed, interestingly does not appear to be dependent upon C3a/C3aR, as knocking out C3 expression is not anxiogenic like C3aR KOs. The authors suggested that interactions of C3aR with alternative ligands such as TLQP-21 (non-acronymic) a cleavage product of neuropeptide precursor protein VGF (non-acronymic), may instead be responsible for mediating anxiety-like behaviours and has previously been shown to rapidly increase synaptic activity in CA1 neurons (Alder et al., 2003; Pozo-Rodrigálvarez et al., 2021; Westacott et al., 2022). Curiously C3 KO mice did display a behavioural phenotype not seen in C3aR KOs, an increase in conditioned learned fear. These findings suggest that C3's other cleavage product C3b/iC3b binding its cognate receptor CR3, regulates conditioned fear potentially through its ability to modulate synaptic plasticity (Westacott *et al.*, 2022). Previously the iC3b/CR3 signalling axis has been shown to be necessary for microglial engulfment of synaptic elements. It has been proposed that iC3b selectively 'tags' weak synapses by covalently binding to their cell surfaces, attracting microglia expressing CR3 and thus facilitating phagocytosis or trogocytosis (Schafer et al., 2012; Weinhard et al., 2018; Druart and le Magueresse, 2019; Jensen et al., 2021).

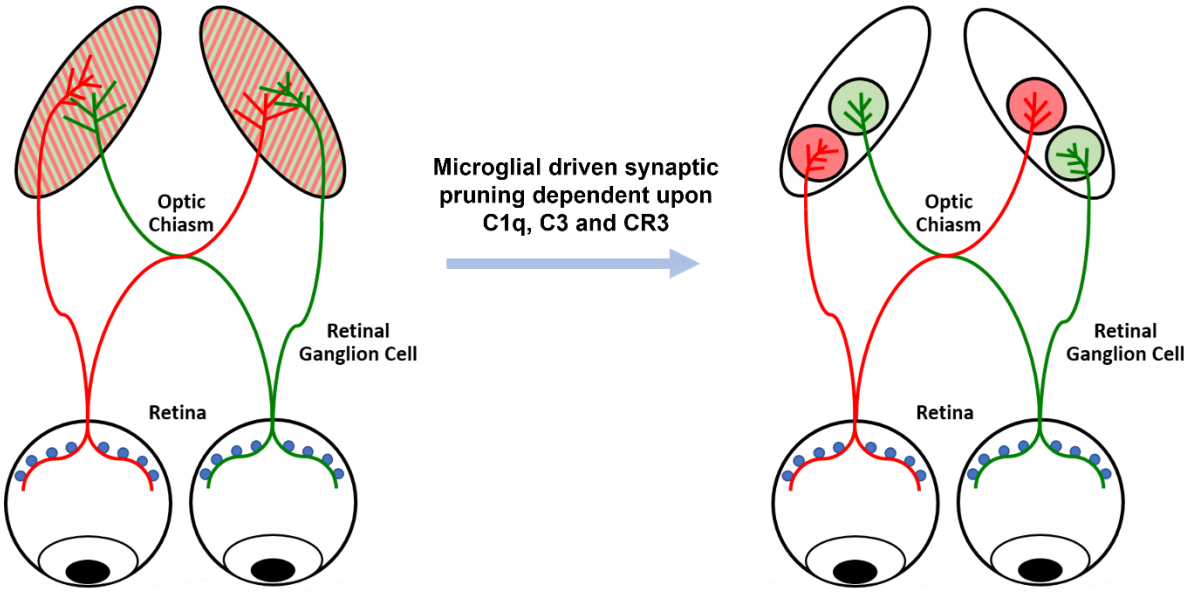

Figure 1.8 – Simplified schematic of microglial dependent circuit refinement in the developing dLGN (dorsolateral geniculate nucleus). At P5 (post-natal day five) contralateral and ipsilateral eye retinal ganglion cell inputs innervate the dLGN and compete for territory. By P8 (post-natal day eight) inputs from the two eyes have established non-overlapping eye specific territories in the dLGN. Separation of input is dependent upon microglial engulfment facilitated by the proteins of the complement system: C1q, C3 and CR3 (complement receptor 3). Adapted from Schafer et. al. (2012).

1.4.3 Complement dysfunction in SZ

The complement system is implicated in a variety of diseases and disorders of the CNS. In the case of diseases such as traumatic brain injury (TBI), ischemic stroke and West Nile virus (WNV) infection, complement system activation drives inflammation and subsequent tissue repair through the induction of apoptosis and regulating pro- and anti-inflammatory cytokine release (Schäfer *et al.*, 2000; Storini *et al.*, 2005; Vasek *et al.*, 2016a; Xiao *et al.*, 2016; Roselli *et al.*, 2018). However, the introduction of large cohort GWASes has implicated members of the complement system in the aetiology and genetic risk of neurodevelopmental and neurodegenerative disorders (Crehan, Hardy and Pocock, 2012; Sekar *et al.*, 2016; Ruiz-Martínez *et al.*, 2017).

A large GWAS examining 39,989 cases and 113,075 control identified 108 loci with genome-wide significant association with an increased risk of developing SZ (Ripke *et al.*, 2014). The strongest association was located within the MHC locus on chromosome 6. The gene encoding C4 is contained within MHC locus and following analysis by Sekar et al., (2016) a CNV in C4's two alleles A and B was shown to confer increased risk of developing SZ. Specifically, an increased burden of the C4A allele was associated with a greater risk of SZ. Higher expression of C4A was also noted in the brains of SZ patients compared to healthy controls. C4A has a different binding affinity than C4B, preferring amine to hydroxyl groups which may alter complement's ability to prune synapses during development and adulthood. In addition, a SNP within CUB and Sushi multiple domains 1 (CSMD1); a promoter of C3b/C4b degradation and inhibitor of the MAC, whose expression is highly enriched

in the CNS, has also be shown to confer an increased risk of developing SZ (Ripke et. al., 2011; Escudero-Esparza et al., 2013; Steen et al., 2013).

The complement system's role in synaptic pruning may hold the key to its implication in pathogenesis of neuropsychiatric disorders such as SZ. An increased burden of C4A or defective CSMD1 mediated inhibition of complement activity could impair synaptic pruning during CNS development, neurogenesis, and synaptic plasticity, deficits in which are associated with the aetiology of SZ. Abnormal developmental synaptic pruning is a hallmark of SZ, large longitudinal studies have highlighted significant losses of grey matter in SZ patients compared to healthy controls. Grey matter (GM) reduction driven by synaptic pruning is essential for adolescent brain development allowing the white matter (WM) to expand and facilitate higher brain functions (Stokes, 2015). The loss of GM volume in the frontal lobes of people with SZ is not due to the loss of whole neurons, but instead a decrease in neuropil and a number of processes resulting in a reduction in overall neuronal volume. During development of the murine PFC the number of spines in the PFC increases from precursor 24 (p24) to p50, however during this same time microglial association with spines and glutamatergic elements also increases, reflecting the engagement of synaptic pruning machinery to remove supernumerary cortical processes (Mallya *et al.*, 2019). Extended or dysregulated synaptic pruning during adolescence therefore could contribute to the severe loss of GM in the frontal lobe of SZ patients (Andreasen *et al.*, 2011).

Neuronal wiring driven by deficits in adult neurogenesis have been proposed as the mechanism underlying the 4-8% loss in hippocampal volume and impaired hippocampal activation exhibited by individuals with SZ (Reif *et al.*, 2007). Microglia's

ability to regulate neurogenesis and the integration of new-born neurons into existing circuitry depends upon synaptic pruning machinery, therefore the aberrant neurogenesis seen in SZ patients may be driven by deficits in the complement system driven synaptic pruning. Associative learning deficits associated with SZ can also be attributed to this atrophy of the hippocampus, but additionally more subtle alterations to the synaptic plasticity required for the formation, retrieval and updating of associative memories could also contribute to the sequela of SZ.

1.5 Experimental plan

Cells of the brain's neuroimmune system, particularly microglia, are critical to the normal development of neuronal circuits and are capable of modulating said circuits throughout an individual's life, particularly in brain regions exhibiting high degrees of plasticity, such as the hippocampus. The complement system appears to play a key mechanistic role in facilitating microglial driven neural plasticity and therefore any alterations to this tightly regulated facet of the innate immune system could allow for the manifestation of symptoms associated with mental health disorders such as SZ.

In this thesis I investigate whether the complement system and microglial activation plays a role during contextual fear conditioning and contextual fear memory (CFM) extinction. My aims were as follows:

- Identify the differential activation of mPFC, hippocampal and thalamic subregions in extinction versus retrieval of contextual fear memories.
- Explore the expression of complement associated genes in subregions of the mPFC and hippocampus in contextual fear learning and

memory, in order to confirm and expand upon the findings of Scholz et. al., (2016).

- Develop a high throughput method analysing low-grade microglial activation in immunohistochemical brain sections.
- Observe whether contextual fear learning and memory is paired with complimentary changes in the extent of microglial activation in the subregions of the mPFC, hippocampus and thalamus.

Chapter 2: Materials and Methods

2.1 Animals

2.1.1 Animal husbandry

Adult male Lister Hooded rats (300-500g, Charles River UK Limited, Essex, UK) were housed in pairs or trios in standard cages (38 cm [width] x 56 cm [length] x 22 cm [height]) lined with wood shavings and bedding material. A carboard biotunnel was provided as a source of basic enrichment. Cages were held in a room maintained at 19-21^{o}C and 45-60% humidity on a reversed 14:10 hour light-dark cycle. Animals were supplied with water and food (standard rat chow, RM1(P), Special Services Diet, Essex) ad libitum. Upon arrival from suppliers, animals were given a minimum of 14 days in their home cages before being used in experiments. All procedures were conducted in accordance with local Cardiff University Ethical Committee approval and the UK Animals (Scientific Procedures) Act 1986, under UK Home office licenses PPL 30/3135 and PIL I52FB2EB9.

2.1.2 Behaviour

2.1.2.1 Contextual fear conditioning and extinction

2.1.2.1.1 Apparatus

All sessions occurred in two standard modular fear conditioning chambers for rats (interior dimensions: 31 cm [length] x 24 cm [width] x 21 cm [height]), with aluminium side walls and clear polycarbonate rear and door (Med Associates Inc., Vermont, USA). The interior of the chambers consisted of a grid (containing 19 equally spaced bars) raised 1.6 cm above an aluminium floor that can deliver a

scrambled footshock (0.5mA). Delivery of shock was controlled by a Stand-alone Aversive Stimulator/Scrambler (Med Associates Inc., Vermont, USA). Test chambers were placed in a medium-density fibreboard (MDF) sound dampening cubicle (56 cm [length] x 56 [width] x 36 cm [height]) (Med Associates Inc., Vermont USA). Footage of subjects in chambers was captured using an infrared digital camera (JSP Electronics Limited Co., Guangdong, China) positioned at the top of the dampening cube centred above the middle of the chamber and recorded using Numeriscope (ViewPoint, Ain, France) for subsequent offline analysis.

2.1.2.1.2 Conditioning protocol

Animals were individually transported from the home cages in the holding room to the testing room in a large opaque box and placed into individual test chambers. Rats were free to explore the chambers for two minutes before receiving a single 0.5mA scrambled foot shock (US) lasting two seconds. Following foot shock, subjects were left in the chamber for a further minute before being returned to the home cages. Conditioning took place over the course of a day, with subjects assigned to the same behavioural group dispersed throughout the day (Figure 2.1).

The conditioned cohort were subsequently randomly split into three groups: recall, extinction and no recall. 48 hours after their conditioning day rats in the first two groups were transported using the same method described previously and returned to the testing chamber (CS). Animals in the recall group were reexposed to the context with no footshock (no US) for two minutes. Two-minute reexposure elicits the retrieval of the CFM wherein rats ‘remember’ the context’s association with the footshock and freeze as a result. Additionally, according to some researchers, two-minute reexposure is also sufficient to induce memory reconsolidation (Lee, Everitt

and Thomas, 2004a; Curzon, Rustay and Browman, 2009; Yamada *et al.*, 2009; Cassini *et al.*, 2017). Rats in the extinction group remained in the chamber in the absence of footshock for ten minutes; a protocol which previously has been shown to initiate the extinction of a CFM. CFM extinction occurs when a new, more salient association is made with the context that it is safe and no longer warrants a fearful response upon reexposure (J. L. C. Lee, Milton and Everitt, 2006; Bronwyn M Graham and Milad, 2016; Cassini *et al.*, 2017). Subjects' return to the chambers was matched to the time when they were conditioned two days prior. Rats assigned to the control group received conditioning on day one but were never returned to the testing chamber. On the day animals in the other two groups were reexposed, control animals remained in their home cages and were sacrificed throughout the day at time points matching when they had been conditioned 48 hours previously (Figure 2.1).

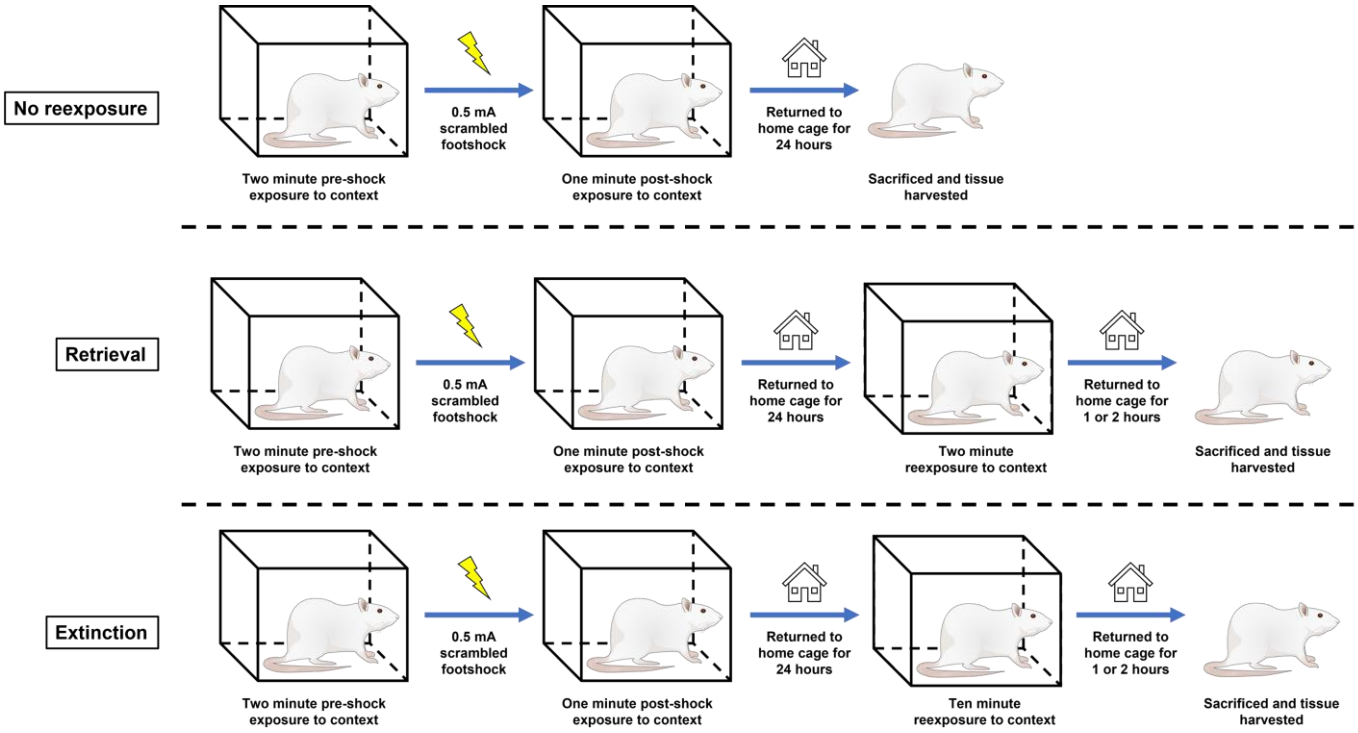

Figure 2.1 Schematic of the behavioural paradigms employed to generate the three behavioural groups used in all contextual fear conditioning experiments. All rats received were exposed to the context for two minutes before receiving a single scrambled 0.5 mA footshock for two seconds. Following the shock all rats remained in the context for one minute before being returned to their home cages. Subjects in the retrieval and extinction groups were reexposed to the context 24 hours later, with rats in the retrieval group being reexposed for two minutes and those in the extinction group being reexposed for ten minutes. Animals in the no reexposure group remained in their home cages for 24 hours and did not return to the context.

2.1.2.1.3 Analysis

Freezing behaviour was used as an index of rats' fear and was defined as the cessation of movement excluding respiration for more than one second (Curzon, Rustay and Browman, 2009). Recordings of rats in the testing chamber were scored for freezing behaviour once every five seconds. All video recordings were renamed according to a unique key and those from rats that underwent the extinction paradigm were divided into two-minute-long segments to blind the scorer to the rats' groups and the stage of the CFC protocol the video was from. The number of freezing events were recorded from each session the animal was in the chamber, with pre- and post-US freezing being recorded separately during the fear conditioning session. Percentage freezing was calculated for each animal in each two-minute bin and then averaged within each behavioural group.

2.1.2.1.4 Statistics

Percentage freezing from CFC experiments was compared across experimental groups using a multivariate general linear model with Mauchly's Test of Sphericity in IBM® SPSS® Statistics (Version 26.0.0.0, IBM, New York, USA). If Mauchly's test was significant, then a Greenhouse-Geiser correction was applied.

2.1.3 Perfusion

Brains were fixed with 4% paraformaldehyde (PFA) by transcardial perfusion under anaesthesia to preserve tissue rapidly and uniformly in a life-like state (Gage, Kipke and Shain, 2012). Briefly, rats received an intraperitoneal injection of pentobarbital (200 mg/ml Euthatal, Boehringer Ingelheim Animal Health, Surrey, UK) and left in a holding cage until a surgical plane of anaesthesia was achieved. A lateral incision was made through the integument and abdominal wall beneath the rib

cage to expose the diaphragm. Cuts to the diaphragm and rib cage opened the pleural cavity and the heart was isolated from the sternum and connective tissue. A perfusion needle was inserted into the ascending aorta via the left ventricle and clamped with a haemostat near the point of entry. A further incision was made to open the right atrium. Using a perfusion pump, ice cold 0.1 M phosphate-buffered saline (PBS) (flowrate: 13-20 ml/min) was flushed through the needle to exsanguinate the rat. Following this, the perfusate was switched to ice cold 4% PFA in 0.1M PBS (flowrate: 20 ml/min) and allowed to flow until the liver cleared and fixation tremors had ceased (approximately 15-20 min, 300-400 ml 4% PFA per animal). Perfused rats were decapitated and whole brains rapidly dissected. Brains were immersed in a volume of 4% PFA at least ten times the volume of the brain itself (approximately 10 ml) for 24 hours at 4^{o}C. Post-fixed brains were washed with 0.1 M PBS and transferred to 30% sucrose for cryoprotection. Complete sucrose infiltration into the brains took between 2-6 days and was marked by the brains sinking to the bottom of their containers. Following cryoprotection, brains were placed vertically into custom cylindrical moulds (1.5 cm [diameter], 5.3 cm^3 [volume]), covered with optimal cutting temperature (OCT) compound (Scigen, California, USA), frozen on dry ice, moulds removed and stored at -80^{o}C until required.

2.1.4 Brain dissection

2.1.4.1 Gross dissection of mPFC and hippocampus

For RT-qPCR experiments rats were sacrificed via a rising concentration of CO_2 in a Semi-Automatic Home Cage Culling Unit (Clinipath Equipment Limited, East Yorkshire, UK). After death had been confirmed by the absence of hind limb withdrawal reflex , rats were decapitated, the brains removed before gross dissection

of mPFC and hippocampus. Dissected brain regions were stored at -80^{o}C until needed.

2.1.4.2 Micro-dissection of mPFC and hippocampal subregions

Rats for use in experiments requiring micro dissected regions of the mPFC and hippocampus, were sacrificed using a rising concentration of CO_2 in a Semi-Automatic Home Cage Culling Unit (Clinipath Equipment Limited, East Yorkshire, UK). After death had been confirmed by the appearance of pale extremities, rats were decapitated and the whole brains were collected, and flash frozen on dry ice. Dissected brains were stored at -80^{o}C until needed.

Frozen brains were placed into a Rodent Coronal Brain Matrix (Rat 175-300 g, RBMS-300C, World Precision Instruments, Hertfordshire, UK) precooled to 4^{o}C. Cold feather razor blades (Agar Scientific Ltd, Essex, UK) were placed using coordinates obtained from (Paxinos and Watson, 2006) from the most rostral appearance of the forceps (Bregma 5.16 mm) to the genu of the corpus callosum (Bregma 2.52 mm) in one-millimetre increments, producing three coronal brain slices containing the prefrontal cortex. Slices were transferred to SuperFrost Plus microscope slides (VWR International, Pennsylvania, USA) and flash frozen on a metal cold block placed in dry ice. Locations where blades were placed are presented in Figure 2.2. Using a Precision Brain Punch (Ted Pella Inc., California, USA) and the Palkovits punch technique, tissue punches (1 mm [diameter], 0.79 mm^3 [volume]) were taken from the PL and IL cortices of the mPFC (Palkovits, 1973). The forceps minor corpus callosum was used as a landmark to correctly position the punches to be taken from the PL and IL cortices. 1 mm thick slices containing the dorsal hippocampus were also taken from Bregma -2.76 mm to

Bregma -4.36 mm, mounted and frozen as described previously. These slices were used to collect tissue punches from the CA1, CA3 and DG hippocampal subregions. Punches from all regions were immediately frozen on dry ice before use in further experiments. Locations of all punches taken are detailed in Figure 2.3.

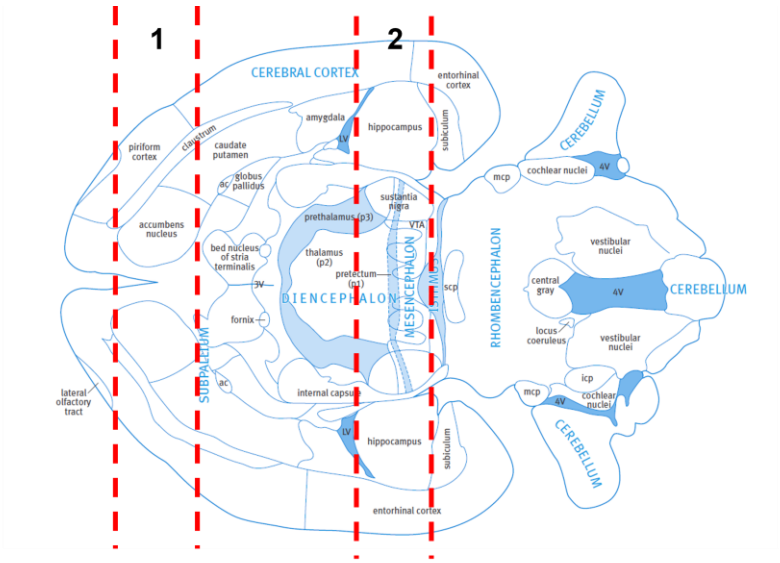

Figure 2.2 Position of feather blades used to produce coronal brain sections from which one millimetre diameter punches were taken for RNA purification and subsequent cDNA synthesis for RT-qPCR. Red lines denote start and points of feather blade placement, with blades being placed every millimetre between the two points. 1 denotes the area from which sections covering the mPFC were collected. 2 denotes the area from which sections covering hippocampus were collected. Adapted from Paxinos, 2009.

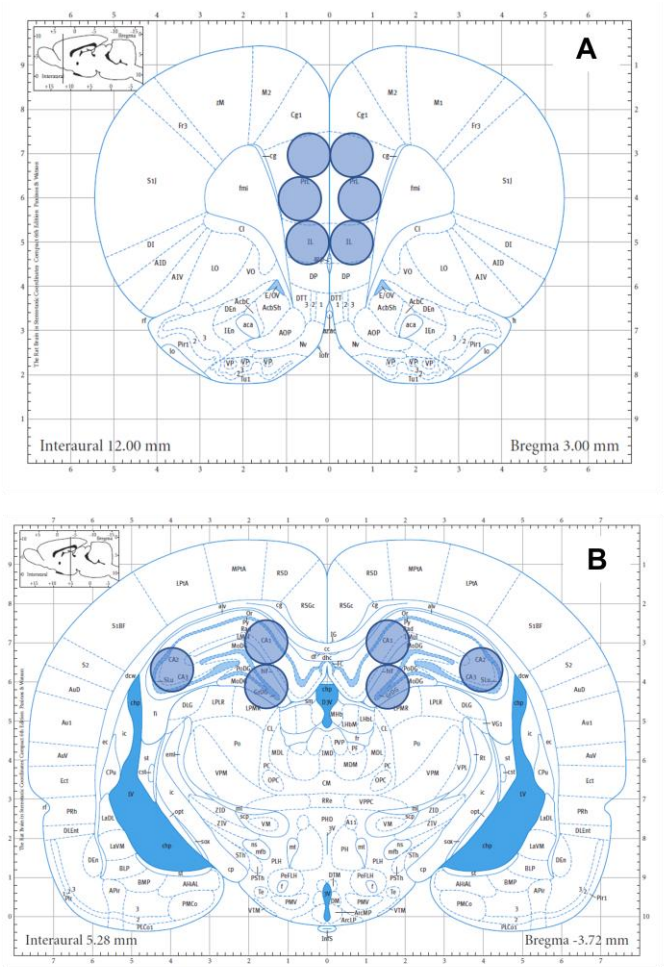

Figure 2.3 A. Locations of 1 mm diameter punches taken from 0.5 mm coronal sections to isolate the prelimbic cortex (PL) and infralimbic cortex (IL) from the prefrontal cortex (PFC) from which RNA was extracted for use in RT-qPCR experiments. **B.** Location of punches taken isolate hippocampal subfields: CA1, CA3 and dentate gyrus (DG) from which RNA was extracted for use in RT-qPCR experiments. Adapted from Paxinos, 2009.

2.1.5 Lipopolysaccharide solution and injection

Five-month-old Lister Hooded rats (300-500g, Charles River UK Limited, Essex, UK) received intraperitoneal injections of LPS-EB (Escherichia coli 0111:B4, activity confirmed with Limulus amoebocyte lysate (LAL) assay, InvivoGen, California, USA), a large lipoglycan found in the outer membrane of Gram-negative bacteria, which induces a substantial immune response in rodents (Raetz and Whitfield, 2002). LPS(E. col 0111:B4, InvivoGen, California, USA) was dissolved in 0.1 M PBS (pH 7.4) to 5 mg/ml and administered in a single bolus (0.1 mg/kg) intraperitoneally. Control animals received a single IP injection of 0.1 M PBS (5 ml/kg). Following injection rats were returned to their home cages.

For investigations of microglial cytorachitecture, LPS and vehicle-injected rats were sacrificed using an overdose of pentobarbital (200 mg/kg, Euthatal, Boehringer Ingelheim Animal Health, Surrey, UK) administered via intraperitoneal injection 24 hours after LPS challenge.

2.1.5.1 LAL Assay

LAL assays are used to confirm the efficacy of endotoxins such as LPS. The assay consists of treating an aqueous extract of amoebocytes from Limulus polyphemus (Atlantic horseshoe crab) with an endotoxin. Endotoxicity of LPS is confirmed through its induction of amoebocyte clotting which is observable to the naked eye (Cooper, Hochstein and Seligmann, 1972). Before being used in animal experiments, LPS was tested for endotoxicity with a LAL assay. LPS was reconstituted from stock using endotoxin free water to a concentration of 5 mg/ml. 100 µl of LPS solution was added to 100 µl Limulus amoebocyte lysate (Lonza Group, Basel, Switzerland), vortexed and heated at 37°C for 60 minutes. After

incubation, tubes were inverted 180°, a clot was deemed to have formed if the solution remained in the base of the tube (Booth, 1986).

2.3 Molecular Techniques

2.3.1 RT-qPCR.

2.3.1.1 RNA extraction (tissue)

RNA extraction was performed using a RNeasy kit (QIAGEN, Limburg, Netherlands) with the manufacturer's protocol being followed with no deviations or alterations. Tissue (2-7 mg of punched tissue or 20-30 mg of grossly dissected tissue) was removed from storage at -80^{o}C, thawed on wet ice and placed into lysing matrix D tubes (MP Biomedical, California, USA) containing Lysis Buffer RLT (QIAGEN, Limburg, Netherlands) and β-mercaptoethanol (Bio-Rad Laboratories Inc., California, USA) at a concentration of 1% (volume of β-mercaptoethanol per volume of buffer RLT). Tissue was homogenised using a Precellys 24 (Berten Instruments, Somme, France) at 5000 rpm for 5 seconds (Microcentrifuge 5418, Eppendorf, Hertfordshire, UK). Samples were centrifuged for 3 minutes at 14,000 rpm (5 cm rotor size); the resulting supernatant was retained and centrifuged again (14,000 rpm, 3 min) retaining both the pellet and supernatant. The pellet was resuspended through tube inversion in lysis buffer and centrifuged (14,000 rpm, 3 min) and the supernatant retained. Supernatants were pooled, mixed with an equal volume of 70% ethanol to precipitate and desalt the DNA and RNA and then added to RNeasy spin columns (QIAGEN, Limburg, Netherlands). Columns were centrifuged (10,000 rpm, 30 sec) and the flow discarded before being washed with Buffer RW1 (QIAGEN, Limburg, Netherlands). Flow through was discarded again, columns

underwent two Buffer RPE (QIAGEN, Limburg, Netherlands) washes and centrifuged for an extended period (10,000 rpm, 5 min) to thoroughly dry out their beds. Columns were transferred to a fresh collection tube and spun dry (15,000 rpm, 1 min) to eliminate any Buffer RPE carryover. 30 µl of RNase-free water (QIAGEN, Limburg, Netherlands) was added to the bed and columns centrifuged (10,000 rpm, 1 min) to elute nucleic acid. Eluate was collected in a fresh tube, immediately flash frozen on dry ice and stored at -80^{o}C.

2.3.1.2 RNA quality analysis

A DS-11 series spectrophotometer (DeNovix Inc., Delaware, USA) was calibrated using nuclease-free water (Ambion Inc., Texas, USA) before the RNA concentration and integrity of samples defrosted on wet ice were measured (Equation 2.1). Concentrations between 20 and 10,000 ng/µl were deemed acceptable for use in RT-qPCR experiments (Mazzolini, Chia and Sieger, 2018). In addition, the ratio of absorbance at wavelengths 260 nm and 280 nm (A260/A280) was used to assess nucleic acid purity and the absence of protein contamination. Samples with A260/A280 values of ~2.0 ± 0.1 were classed as being of sufficient quality for use in further experiments (Wilfinger, Mackey and Chomczynski, 1997).

$$Transmission\ (T) = I/I_0$$

$$Absorbance\ (A) = log(T)$$

$$Concentration = A/(L\ x\ \varepsilon)$$

Equation 2.1 – Equations used to calculate RNA concentration using a spectrophotometer. Where I is the light that exits the sample, I_0 is the light that enters the sample, L is the optical path length and ε is the sample specific extinction coefficient.

2.3.1.3 DNase treatment

Samples underwent treatment to remove any contamination with genomic DNA. Eluted nucleic acids were incubated at 37ºC for 30 minutes with TURBO™ DNase (Thermo-Fisher, Massachusetts, USA). The reaction was stopped with the addition of DNase inactivation reagent (Thermo-Fisher, Massachusetts, USA), incubation for 5 minutes at room temperature and centrifugation (13,000 rpm, 1 min) to collect the RNA. Purified RNA was diluted with nuclease-free water to a final concentration of 10 ng/ul.

2.3.1.4 cDNA synthesis

RNA was converted to cDNA by incubating 20 µl of 10 ng/ul RNA to cDNA EcoDry Premix Random Hexamers (Takara Bio Inc., Shiga, Japan) at 42ºC for 60 minutes using a dry block T100 thermocycler (Bio-Rad Laboratories, California, USA). The reaction was stopped with a 10 min 72ºC incubation, and the cDNA produced was diluted with 300 µl of nuclease-free water. Diluted cDNA was stored at -80ºC until required for RT-qPCR experiments.

2.3.1.5 Primer design

FASTA mRNA sequences for genes of interest were obtained from the NCBI gene database (https://www.ncbi.nlm.nih.gov/gene, NCBI, Maryland, USA). Using the Primer-BLAST webtool (https://www.ncbi.nlm.nih.gov/tools/primer-blast, NCBI, Maryland, USA) candidate forward and reverse probes were identified and filtered by five criteria: product size between 50 and 150 bp, GC content between 40-60%, primer length between 18 and 22 bp, span an exon-exon junction and a 3’ end with a G-C bond. Pairs of probes, which met these criteria had their homology confirmed using a Nucleotide-BLAST webtool (https://www.blast.ncbi.nlm.nih.gov/Blast.cgi,

NCBI, Maryland, USA). Lyophilised probes were obtained from Sigma-Aldrich (Dorset, UK), rehydrated using nuclease-free water to produce a 100 µM stock solution and stored at -20^{o}C.

2.3.1.6 Primer validation and efficiency

Aliquots of probe stocks were diluted with nuclease-free water to 5 µM which were used as working solutions during all RT-qPCR experiments. The efficacy and single amplicon specificity of each primer pair was assessed by running RT-qPCR on cDNA using a range of different forward and reverse probe concentrations: 0.17, 0.33 and 0.42 µM. 7.5 µl of SensiFAST® SYBR Hi-ROX master mix (Bioline, London, UK), 1.5 µl of forward and reverse primers were diluted with the appropriate volume of nuclease-free water and 5 µl of cDNA were loaded into 96 well plates.

Plates were run on StepOnePlus thermocyler (Thermo-Fisher, Massachusetts, USA) beginning with an initialisation step of 95^{o}C for 10 minutes to heat activate the master mix's DNA polymerases, followed by 45 cycles of denaturation (95^{o}C, 15 seconds) and annealing (60^{o}C, 1 minute). Runs ended with a melt curve stage during which samples were cooled to 55^{o}C before the temperature was incrementally increased (1^{o}C steps) to 95^{o}C where it was held for 15 seconds. Fluorescent intensity of intercalated SYBR Green dye was normalised using signal from a passive reference dye (ROX) to generate a delta Rn value for each cycle of the reaction. The resulting plot of delta Rn value against cycle number is used determine the cycle number at which set a threshold delta Rn value was reached (Ct). cycle Primer efficacy was determined by selecting probes that produced Ct values of 10-35 and with no signal in the no template control (H_2O). The lowest probe concentration that produced a useable Ct value was used in all further

experiments. Single amplicon specificity of primers was established by the presence a single peak with no shoulders in the melt curve.

Efficiency of all working primers was determined by comparing Ct values across a cDNA 1:10 dilution series (seven different concentrations) with each dilution run in triplicate. Ct values from each dilution point were plotted against log10(cDNA concentration) to which a straight line ($R^2 > 0.99$) was fitted. This gradient was used to calculate the percentage efficiency of the primers (Equation 2.2). Primers with efficiencies between ~90 and 110% were deemed valid and suitable for use in further experiments (Sint, Raso and Traugott, 2012). Details of all validated primers are detailed in Table 2.1.

$$primer\ effciency = 10^{(\frac{-1}{m}-1)}$$

Equation 2.2 – Equation used to calculate primer efficiency, where *m* is the gradient of a line fitted to a plot of average Ct against $\log_{10}$ of primer concentration.

Target	Forward	Reverse	Probe concentration (µM)	Efficiency (%)
Arc	AGTGCTCTGGCGAGTAGTC	CAGTGGCAGTGGCAAGTG	0.17	94.93
C1qA	GAGGCAGGAACATCATGGAGACC	GCAGACATCTTCAGCCACTGT	0.17	104.54
C3	CGTGCTGATCGAGGATGGTT	ACTTCCCCACTAGGGCTTCT	0.17	106.34
C3aR	CGGCTGGACCAGATAGGATT	CCATTGCTCAGTCAAGAGCAC	0.33	95.26
CSMD1	ATGGTCTCTGGAGCGGATCT	CCACTGTGTCCCTGTAGCTG	0.33	92.32
SDHA	GCTCTTTCCTACCCGCTCAC	GTGTCATAGAAATGCCATCTCCAG	0.10	95.43
UbC	CTTTGTGAAGACCCTGAC	CCTTCTGGATGTTGTAGTC	0.10	98.70

Table 2.1 – Summary of primers and their associated concentrations and efficiencies used in RT-qPCR experiments. SDHA and UbC were used as housekeeping genes.

2.3.1.7 RT-qPCR

96-well plates were loaded with master mix, primers and cDNA as previously described. Samples loaded were run in triplicate and all plates included primers for two housekeeping genes (SDHA and UbC) and an NTC for all primers used (Kozera and Rapacz, 2013). RT-qPCR was run as before: initiation (95^{o}C, 10 min), amplification (45 cycles of denaturation [95^{o}C, 15 seconds] and annealing [60^{o}C, 1 minute]) and melt curve (55-95^{o}C).

2.3.1.8 Analysis

The comparative Ct method ($2^{-\Delta\Delta Ct}$ method) was used to calculate fold changes in gene expression from Ct values generated by RT-qPCR experiments (Livak and Schmittgen, 2001) (Equation 2.3). A well's Ct values were eliminated if within each triplicate there was variance greater than 0.5 cycles before the geometric mean was calculated. The geometric mean was also calculated for both housekeeping genes for each cDNA sample. Genes of interest's Ct values were normalised by subtracting the housekeeping gene average Ct from the corresponding gene of interest's Ct value (ΔCt = gene of interest Ct – housekeeping gene average Ct). ΔΔCt values were calculated by averaging (geometric mean) the ΔCt's from subjects in the control group from each animal's ΔCt. Data was analysed using one-way analysis of variance (ANOVA) using Prism 8 (GraphPad, California, USA).

$$\Delta Ct_{(sample)} = Ct_{(gene\ of\ interest)} - Ct_{(average\ of\ HK)}$$

$$\Delta\Delta Ct = \Delta Ct_{(control)} - \Delta Ct_{(other\ experimental\ group)}$$

$$Fold\ change = 2^{-\Delta\Delta Ct} = \frac{1}{2^{\Delta\Delta Ct}}$$

Equation 2.3 – Equations used to calculate fold change from Ct (cycle threshold) values generated by RT-qPCR experiments using primers targeting a gene of interest and two HKs (house keeping genes).

2.3.2 Immunohistochemistry

2.3.2.1 Sectioning of brains

Perfused brains were removed from -80^{o}C and placed in a pre-cooled (-20^{o}C) CM1860 UV cryostat (Leica Microsystems, Buckinghamshire, UK) for one hour. Brains were mounted on 30 mm cryostat chucks using OCT and left to fully harden (~ five minutes) before sectioning commenced. Brains were sectioned coronally at 40 µm thickness from the rostral appearance of the forceps (Bregma +5.16 mm) to the genu of the corpus callosum (Bregma +2.52 mm) to capture slices containing the mPFC. Sections were placed in a 1/12 series into 0.1 M PBS in a 12-well plate (six sections per well). A second series of 40 µm sections were taken from Bregma -1.44 mm to Bregma -4.36 mm covering the hippocampus, nucleus reuniens and amygdala, which were stored in a separate 12-well plate in 0.1 M PBS (six sections per well). Plates were sealed with Parafilm (Amcor plc., Bristol, UK) and stored at 4^{o}C until needed.

2.3.2.2 Immunohistochemical staining

Free floating sections were washed with 0.1 M PBS for five minutes with agitation three times. Tissue was blocked with agitation for two hours at room temperature, to prevent non-specific binding of antibodies, using 500 µl of blocking solution containing 1/10 normal donkey serum (NDS) (Thermo-Fisher, Massachusetts, USA), 1% volume per volume (v/v) Triton X-100 (Bio-Rad Laboratories, California, USA) in 0.1 M PBS. Primary antibodies (detailed in Table 2.2) were diluted with blocking solution to their optimised concentrations (see Chapters 3, 5 and 6 for details) using 0.1 M PBS containing 1/500 NDS and 0.1% v/v Triton X-100. Sections were incubated with diluted primary antibodies for 24 hours at

4°C on a seesaw rocker. Sections were washed three times in 0.1 M PBS containing 1/500 NDS and 0.01% v/v Triton X-100 with agitation. Tissue was incubated under agitation for two hours at room temperature with appropriate secondary antibodies (1/1000, Alexa Fluor 488 polyclonal antibody, A-11094, Thermo-Fisher, Massachusetts, USA) at a concentration of 1/1000 diluted with 0.1 M PBS containing 1/500 NDS and 0.01% v/v Triton X-100. Unbound secondary antibodies were removed with three 0.1 M PBS washes with agitation. The penultimate wash also included 4',6-diamidino-2-phenylindode (DAPI) (0.1 ng/ml, 62248, Thermo-Fisher, Massachusetts, USA). Sections were mounted on SuperFrost Plus™ Adhesion Slides (Thermo-Fisher, Massachusetts, USA) and coverslipped with Mowiol mounting medium and Superwhite glass coverslips (Landon LaboQuip, London, UK). Slides with mounted sections were stored at 4°C in opaque slide boxes until required.

Target	Host species	Working concentration	Supplier	Product Number
Arc	Rabbit	1/1000	Synaptic Systems, Lower Saxony, Germany	156 003
cFOS	Rabbit	1/1000	Merck Group, Hesse, Germany	ABE457
IBA1	Rabbit	1/1000	FUJIFILM Wako, Tokyo, Japan	019-1974
Zif268/EGR1	Rabbit	1/1000	Cell Signalling Technology, Massachusetts, USA	4153

Table 2.2 – Details of primary antibodies used in IHC experiments.

2.3.2.3 Analysis (neuronal density measurement)

To quantify nuclear staining of activity-regulated cytoskeleton-associated protein (Arc), cFOS and zinc finger protein 268 (zif268) one in twelve sections containing the mPFC or hippocampus/RE were stained per animal. Whole sections were imaged at 20x magnification on an epifluorescent upright Leica DM6000 B microscope system (Leica Microsystems, Buckinghamshire, UK) using the mosaic addon in Leica Application Suite X (Leica Microsystems, Buckinghamshire, UK) and images stored for offline analysis. Using the Fiji distribution of ImageJ (https://imagej.nih.gov/ij/download.html, NIH, Maryland, USA), mosaic images converted to TIFFs were opened and region of interest outlines were added manually. The hippocampi were divided into the CA1, CA3, GL, ML and hilus and the mPFC into PL and IL cortices. The RE was traced in its entirety. Images were converted to 8-bit and globally auto-thresholded (v1.16.5) to retain only the top 1% signal. Using the automatic particle counting function with constraints of a particle size: 40-infinity and circularity: 0.00-1.00, the number of positive nuclei in each region of interest was automatically counted. The area of each region of interest was calculated enabling the number of positive nuclei per unit area to be calculated. Measurements for each subregion represents the average of six individual subregions from each animal. IEG expression per unit area was averaged within each behavioural group, with said averages being compared between groups using one-way ANOVA followed by multiple comparisons in Prism 8 (GraphPad, California, USA).

2.3.2.4 Analysis (microglial morphology)

2.3.2.4.1 Image acquisition

20X images a containing a region or subregion of interest (CA1, CA3, DG, IL, PL and RE) obtained using a ZEISS Axio Scan.Z1 Slidescanner (Carl Zeiss AG, Baden-Württemberg, Germany) and ZEISS ZEN imaging software (v3.1 blue edition) collecting tiled images every 1 µm along the z-axis were collected from colabelled sections stained for IBA1 (microglia) and DAPI (all cellular nuclei).

2.3.2.4.2 Image processing

Carl Zeiss image (CZI) image data files output during image acquisition were converted into single BigTIFF images from only the 488 nm channel; corresponding to the secondary used for the IBA1 primary antibodies, for each subregion. Using a custom ImageJ script (Appendix 1) BigTIFFs were converted to 8-bit and divided into 500 x 500 px squares. The script utilises the Bio-Formats v6.5.1 plugin (University of Dundee and Open Microscopy Environment, Dundee, UK) to enable ImageJ to open the BigTIFF file type. The script calculates the number of whole squares (size set by user) that fit within the image. The first square is placed at coordinates 0,0 the image is cropped to this square, converted to 8-bit, and saved as a TIFF. The original image is then reopened, the square shifted to 500 px along the x-axis and the image cropped again, a process that is repeated until the extreme of the x-axis is reached. The incremental cropping of the image is repeated down the y-axis until the entire image has been captured within these 500 x 500 px squares. When saved, images retain the original files names with the addition of a unique numerical identifier.

2.3.2.4.3 Morphometric analysis using 3DMorph

3DMorph image analysis software was obtained from GitHub (https://github.com/ElisaYork/3DMorph) running in MATLAB R2019b (MathWorks, California, USA) and was used as the basis for all morphometric analyses. An unedited version of the 3D-Morph release was used to generate a parameters file for use in automated analyses. The parameters file contains limits on the maximum and minimum size of microglia and instructions to not analyse cells that touch the image border. Large scale and timely generation of microglial morphometrics required the 3DMorph script to be run on Cardiff University's high-performance computing cluster Hawk. The 12,736 cores of Hawk allow the morphological analysis of ~50,000 microglia to be completed in four hours compared to over a month on a standard four-core desktop PC. For this to occur 3D-Morph was adapted to run in a UNIX environment. This involved the removal of all graphical user interfaces, the introduction of a try loop to the program getting 'stuck' on error generating files and adapting the (comma-separated value) CSV data files output from each image (https://github.com/NiCl2/Morph3D). A custom script running in RStudio (v1.4.1103, RStudio PBC, Massachusetts, USA) was also developed to combine the individual CSV files output by 3DMorph and make subsequent analysis easier (Appendix 2).

Analysis of microglial morphology by 3DMorph generates seven morphological parameters from each microglia: cell volume, cell territory, number of branch points, number of endpoints, average process length, minimum process length, maximum process length and ramification index. Cell volume is the total volume of the cell including the soma and all processes. Cell territory is the volume in space the cell is in contact with and thus able to survey. Number of branch points

is the number point where a new process emerges from either the soma or another process of the cell. Number of endpoints is the count of terminal points on a cell's processes. Average process length is the mean length of primary, secondary and tertiary processes. Minimum process length is the shortest length of uninterrupted process emanating from the cell. Maximum process length is longest length of uninterrupted process emanating from the cell. Ramification index is the ratio between cell territory and cell volume and is regularly used within the literature as a metric of microglial activation, with a higher ramification index reflecting a lower degree of activation (York *et al.*, 2018a). In Prism 8 (GraphPad, California, USA) t-tests and one-way ANOVAs were used to compare the raw morphometric parameters output by 3DMorph.

2.3.2.4.4 Machine learning

Microglial morphological data from LPS and PBS treated rats was used to develop a binary classification predictive model of microglial activation in RStudio (v1.4.1103, RStudio PBC, Massachusetts, USA). Specifics of the model and its development are detailed in Chapter 5.2 and 5.3. Briefly, a binary classification machine learning algorithm was trained using a model dataset comprised of morphometrics from activated and non-activated microglia. This model was used in subsequent analysis to assign activation status to the population with a heterogenous mix of microglial activation statuses. Provided in the subsequent sections are lay descriptions of the models and metrics employed during model development.

2.3.2.4.4.1 Data Transformation

2.3.2.4.4.1.1 Yeo-Johnson transformation

Yeo-Johnson transformation is a method of transformation from the Box-Cox family that does not require input values to be positive, commonly used in machine learning to normalise data distribution. The Yeo-Johnson transformation law is provided in Equation 2.4.

$$\Psi(\lambda, y) = \begin{cases} ((y+1)^{\lambda} - 1/\lambda & if\ \lambda \neq 0, y \geq 0 \\ \log(y+1) & if\ \lambda = 0, y \geq 0 \\ -[(-y+1)^{2-\lambda} - 1)]/(2-\lambda) & if\ \lambda \neq 2, y < 0 \\ -\log(-y+1) & if\ \lambda = 2, y < 0 \end{cases}$$

Equation 2.4 – Yeo-Johnson transformation law. Where *y* is a list of positive and/or negative numbers, *λ* is any real number. Adapted from Weisberg, 2001.

2.3.2.4.4.1.2 Centring and scaling

Centring and scaling are both pre-processing tools used to standardise numerical datasets. Centring involves subtracting the mean parameter value of from each individual data point resulting in a new mean of zero. Scaling multiplies parameters by their standard deviations to standardise the range of features with a dataset. Pre-processing data with scaling is essential for data being used to train support vector machines (SVMs) (van den Berg *et al.*, 2006; Gromski *et al.*, 2015).

2.3.2.4.4.2 Data quality control

2.3.2.4.4.2.1 Variance inflation factor

Variance inflation factor (VIF) is a measure of multicollinearity for each parameter in a regression analysis. Multicollinearity is when one variable a multiple regression model can be linearly predicted from other variables with a high degree of accuracy. A high VIF represents a substantial degree of accuracy and therefore colinearity. VIFs are calculated by subtracting the R^2 value (from regressing a parameter against every other parameter in the model) from one and finding the reciprocal of this sum (Marcoulides and Raykov, 2019) (Equation 2.5).

$$VIF_i = \frac{1}{1 - R_i^2}$$

Equation 2.5 – Equation used to calculate VIFs, where *i* denotes parameter, R_i^2 is the coefficient of determination.

2.3.2.4.4.2.2 Principal component analysis

Principal component analysis (PCA) can be employed in exploratory data analysis to reduce dimensionality in a dataset, whilst still preserving as much information as possible. Before PCA ,input data must be standardised using z-scores, to ensure parameters have comparable scales and prevent those with larger ranges dominating ones with smaller ranges. A standardised dataset can undergo covariance matrix computation to examine correlations between parameters. A positive covariance between two parameters indicates they are correlated, whereas a negative covariance denotes an inverse correlation. From the covariance matrix eigenvectors and eigenvalues are computed to calculate the principal components of the dataset. Principal components are new uncorrelated linear combinations of existing parameters; a dataset containing five parameters will produce five principal components. The first principal component contains the maximum possible information to account for the maximal amount of variance in the dataset. The first principal component is constructed by fitting a line to a scatter plot of the dataset that maximises the average of squared distances from the projected points to the origin. Subsequent principal components: holding increasingly less information, are constructed by fitting a line perpendicular to the first principal component and account for the next highest amount of variance (Jolliffe and Cadima, 2016; Wu *et al.*, 2018).

2.3.2.4.4.2.3 ROC curve and AUC

Receiver operating characteristic (ROC) curve summarises a binary classifier’s predictive ability by plotting true positive rate against false positive rate across all classification thresholds. The area under the ROC curve or AUC is a

performance metric used to determine the ability of a classification model to distinguish between two classes. A high AUC (close to one) is produced by a model that can accurately place subjects into the correct classes (Hajian-Tilaki, 2013).

2.3.2.4.4.2.4 Sensitivity and specificity

Sensitivity and specificity are two metrics used to evaluate classification models. Both are calculated from confusion matrices generated during the testing stage of model development (Equation 2.6). Sensitivity or the true positive rate is a measure of the positive cases identified correctly by a model. Specificity or the true negative rate is a measure of the negative cases identified correctly by a model (Lalkhen and McCluskey, 2008).

$$\text{Sensitivity} = \frac{\text{True Positives}}{\text{True Positives} + \text{False Negatives}}$$

$$\text{Specificity} = \frac{\text{True Negatives}}{\text{True Negatives} + \text{False Negatives}}$$

Equation 2.6 – Equations used to calculate model performance metrics sensitivity and specificity.

2.3.2.4.4.3 Machine learning models

Five different approaches were used to develop a machine model for microglial classification. The five models were selected in consultation with Dr. Matthew Smith (Psychological Medicine & Clinical Neurosciences, School of Medicine, Cardiff University, UK) and due to being the most used models intended to answer binary classification questions.

2.3.2.4.4.3.1 GLM

General linear models (GLMs) serve as an extension to linear regression models and aim to provide a linear model that can deal with real world problems. Linear models assume that input features follow Gaussian distribution, meaning that categoric input features are not compatible. GLMs enable non-Gaussian outcomes to be included in a linear model by linking weighted sums of features with the mean of assumed distribution. The assumed distribution is chosen based upon the type of predictive model being developed and selected from the exponential-family of distributions which includes: Bernoulli, binomial and Poisson distributions (Bono, Alarcón and Blanca, 2021).

2.3.2.4.4.8 GBM

Gradient boosting algorithms (GBMs) gather multiple weak decision trees (flowchart where each node represents a component in an eventual decision/prediction) into a strong ensemble model in a gradual, additive, and sequential manner. A GBM begins with an initial tree where all parameters are given equal weighting, which is then evaluated based upon a loss function calculated using gradient descent. From the first tree, a second is grown from the weighted data and predictions assessed using a loss function. A third tree is made to predict residuals

from the 2-tree model and the model quality assessed again. Additional trees are planted (number controlled by *tune length*) each trying to solve classification errors in the previous tree. The final model with all trees is the weighted sum of the predictions made by all previous trees (Natekin and Knoll, 2013).

2.3.2.4.4.9 SVM

Support vector machines (SVMs) are employed in classification and regression problems. SVMs are capable of handling mixed datasets containing continuous and categorical input parameters. SVM fits in an iterative manner a hyperplane in multidimensional space, which produces maximal separation between classes. Positioning of the maximal marginal hyperplane is driven by data points close to the hyperplane termed support vectors. In situations where a linear hyperplane cannot separate classes, a kernel trick (a weighting function enabling linear learning algorithms to learn a nonlinear function) is employed to transform the data into a higher dimensional space to which a linear hyperplane can be fitted. The kernel selected for transformation is tailored to the problem at hand. The RBF kernel is commonly used in SVMs solving classification problems, it allows for mapping an input space with infinite dimensional space (Mahesh, 2020).

2.3.2.4.4.10 RF

Random forest (RF) models are employed in classification and regression problems. Employing ensemble learning methods in a RF model means multiple independent decision trees are generated, each tree producing its own prediction on how the subject should be classified. The prediction receiving the highest number of ‘votes’ from each decision tree is selected as the model’s ‘answer’. The use of multiple trees prevents the generation of a model which contains more parameters

than can be justified by the data (effectively including ‘noise’ as a parameter for a predictive algorithm), a phenomenon termed overfitting. An overfitting model produces excellent predictions for the training dataset however, when applied to an experimental dataset it may fail to make reliable predictions (Segal, 2004; Tarca *et al.*, 2007).

Chapter 3

3.1 Introduction

3.3.1 Immediate early genes

Synaptic activity is intricately linked to the IEG expression in neurons. IEG expression is rapid as their transcription requires no new protein synthesis and are characterised as the “gateway to the genomic response” (Pérez-Cadahía, Drobic and Davie, 2011). Hundreds of IEGs have been identified in the CNS with *Arc*, *cFOS*, *cJun*, *Homer1a* and *zif268* (early growth response 1: *Egr1*) being IEGs that are particularly important for long-term, memory and plasticity processes (Herdegen and Leah, 1998; Lerch *et al.*, 2014). Most of these IEGs are DNA binding transcription factors; however, this is not universally true. Some, like *Arc*, are found within the nucleus and the dendritic compartment including synaptic spines (Peebles *et al.*, 2010; Gallo *et al.*, 2018).

Arc is a highly conserved protein exclusive to vertebrates and predominantly expressed in the dendrites and postsynaptic compartments of glutamatergic neurons (Lyford *et al.*, 1995; Husi *et al.*, 2000; Irie *et al.*, 2000; Fujimoto *et al.*, 2004; Moga *et al.*, 2004; Rodríguez *et al.*, 2005; Bloomer, VanDongen and VanDongen, 2007). Under baseline conditions, *Arc* has very low levels of expression (Rao *et al.*, 2006). Like other IEGs, *Arc’s* expression is induced by increases in neuronal activity and its onset of expression; five minutes post-stimulation, it is rapid even when compared to other immediate early genes (Guzowski *et al.*, 1999; Ramírez-Amaya *et al.*, 2005). Activation of metabotropic glutamate receptors (mGluR1s), NMDARs, muscarinic acetylcholine receptors and TrkB, translate neural activity into an increase in Arc

expression using the ERK cascade to transduce the activating signal to Arc's transcription factors early growth response 1 (*Elk-1*) (a ternary complex factor: TCF), myelin and lymphocyte protein (*MAL*) and myocyte enhancer factor-2 (*Mef2*) (Steward and Worley, 2001; Ying *et al.*, 2002; Teber *et al.*, 2004; Posern and Treisman, 2006; Rao *et al.*, 2006; Zaromytidou, Miralles and Treisman, 2006; Waung *et al.*, 2008; Kawashima *et al.*, 2009; Pintchovski *et al.*, 2009). *Arc* expression is also dependent upon rises in intracellular calcium from either extracellular influx (via NMDARs) or release from intracellular stores (triggered by BDNF and cAMP signalling) (Carmichael and Henley, 2018). Following its transcription, Arc mRNA is actively transported along dendrites to post-synaptic compartments in a ribonucleoprotein complex with the eukaryotic initiation factor 4A-III (eIF4AIII), fragile X mental retardation protein (FMRP), kinesin motor complex, messenger ribonucleoprotein (mRNP) and Pur-alpha (Guzowski *et al.*, 1999; Kanai, Dohmae and Hirokawa, 2004; Rao *et al.*, 2006). The transcript's Arc's association with eIF4AIII targets it for non-sense mediated decay and means its half-life is less than an hour (Rao *et al.*, 2006; Giorgi *et al.*, 2007). Arc mRNA translation within neuronal spines is regulated by NMDAR stimulation, further linking neuronal activity to the increases in the presence of Arc in the dendrites and post-synaptic densities (Yin, Edelman and Vanderklish, 2002; Bloomer, VanDongen and VanDongen, 2008). The mature Arc protein associates with many binding partners at the synapses, including machinery mediating AMPA receptor endocytosis (Endo3: endophilin 3 and dynamin-2: DNM2), actin, Ca^{2+}/calmodulin-dependent protein kinase IIβ (CaMKIIβ), guanylate kinase-associated protein (GKAP), presenilin 1 and PSD95 (Chowdhury *et al.*, 2006; Rial Verde *et al.*, 2006; Wu *et al.*, 2011; Myrum *et al.*, 2015). These

interactors at the synapse enable Arc to regulate the processes of LTP and LTD; examples of Hebbian plasticity, but also regulate homeostatic plasticity (related to network excitability) (Shepherd *et al.*, 2006). For example, Arc's regulation of actin is essential for synapse structure and remodelling, a function linked with plasticity, learning and memory (Nikolaienko *et al.*, 2018; Zhang and Bramham, 2021). In addition to its functions at the synapse, an emerging body of evidence suggests that some Arc protein is present in the nucleus and interacts with several nuclear proteins including βIV-spectrin (βSpIVΣ5), Tat interactive protein 60 (Tip60) and promyelocytic leukaemia protein (PML) (Bloomer, VanDongen and VanDongen, 2007; Wee *et al.*, 2014). Functionally nuclear Arc is required for the increases in GluA1 and AMPA receptors associated with LTP and LTD (Korb *et al.*, 2013).

cFOS is an IEG encoding the protein Fos (Morgan and Curran, 1986). Its expression is intrinsically linked to neuronal activity via calcium influx facilitated by glutamatergic NMDARs and L-type voltage-sensitive calcium channels (Ghosh *et al.*, 1994; Chaudhuri *et al.*, 2000). Blockade of NMDARs inhibits *cFOS* expression and conversely, cortical electrical stimulation induces an increase in *cFOS* expression (Berretta, Robertson and Graybiel, 1992; Liste *et al.*, 1995). Downstream of calcium influx, *cFOS* expression is predominantly regulated by the MAPK pathway which requires sustained neural activity and the high increase of calcium associated with this (Chaudhuri *et al.*, 2000; Deisseroth *et al.*, 2003). MAPK phosphorylates and activates transcription factors CREB and Elk-1 (Lyons and West, 2011). Post-translation, Fos proteins in the nucleus arrange into heterodimers with other members of the AP-1 family of transcription factors such as cJun (providing multiplicity of regulator control) to form the basic leucine zipper (bZIP) transcription

factor AP-1 (Chiu *et al.*, 1988). AP-1 is subsequently activated through phosphorylation by ERK and JNK, then binds to TGACTCA DNA sequences (Schulman, 2013). AP-1 regulates a large range of genes including those associated with cell proliferation, cell differentiation and the immune system (Herrlich, 2001; Karin and Chang, 2001; van Dam and Castellazzi, 2001; Schonthaler, Guinea-Viniegra and Wagner, 2011; Wang *et al.*, 2013). Under baseline conditions, *cFOS* has low constitutive expression due to the active repression of *cFOS'* promoter and the negative feedback loop of the Fos protein upon its own expression. Following the induction of neuronal activity, through a behavioural paradigm or administration of a neuro-stimulatory compound such as cocaine *cFOS*, expression rapidly increases (Lucibello *et al.*, 1989; Morgan and Curran, 1991; Lyons and West, 2011; Schonthaler, Guinea-Viniegra and Wagner, 2011; Ames and Lim, 2012). Repeated or sustained exposure to a stimulus can in fact reduce *cFOS* signal due to the complex interaction of multiple stimuli upon the regulatory pathways surrounding *cFOS* (Wang *et al.*, 2014; Chung, 2015).

Zif268 (also known as *Egr1,* nerve growth factor-induced protein A (*NGF1A*), Krüppel box-24: *Krox-24* and tetradecanoyl phorbol acetate induced sequence 8: *TIS8*) is another IEG that, like cFOS, is a transcription factor with a rapid increase in expression following neural activity (Jeffrey, 1987; Cheval *et al.*, 2012; Veyrac *et al.*, 2014; Duclot and Kabbaj, 2017). *Zif268* is ubiquitously expressed throughout the adult CNS, but absent in embryonic stages, and has high basal expression in the amygdala, hippocampus (predominantly the CA1), neocortex and thalamus (Beckmann and Wilce, 1997). *Zif268* expression is strongly correlated with NMDA receptor, AMPA receptor and L-type voltage-sensitive calcium channel activity

(Murphy, Worley and Baraban, 1991; Wang, Daunais and McGinty, 1994; Beckmann and Wilce, 1997). Activation of these receptors and calcium influx triggers the phosphorylation of the transcription factor Elk-1 by the MAPK/ERK, JNK and p38MAPK pathways. Phosphorylated Elk-1, NF-κB-p65, p53 and *zif268* itself promotes the expression of *zif268*. *Zif268* protein undergoes several post-translational modifications through phosphorylation; by Akt, casein kinase II and PKC, acetylation by the p300/CBP complex and ubiquitination by paired box protein 3 (PAX3)-FOX01. Zif268 regulates the expression of genes associated with synaptic plasticity and/or memory. A study of hippocampal cells over-expressing *zif268* identified 153 candidate genes regulated by zif268. The gene ontology terms associated with these differentially regulated gene following *zif268* over-expression include: synapse formation, immune response, major histocompatibility complex, vesicle trafficking and pre-synaptic function (James, Conway and Morris, 2005). Out of the 153 genes identified, 151 had reduced expression in response to zif268, suggesting that it acts predominantly as transcriptional repressor (Veyrac *et al.*, 2014). This transcriptional regulation is performed by zif268 acting alone or in complex with other transcription factors including cFos, c-Jun, nuclear factor of activated T-cells (NFAT), NF-κB (Cogswell, Mayo and Baldwin, 1997; Levkovitz and Baraban, 2002; Decker, 2003; Wieland *et al.*, 2005; Cheval *et al.*, 2012).

3.1.2 Immediate early genes as makers of post-retrieval and post-extinction regional activation

Given their rapid onset of expression, IEGs have long been used as markers of neuronal activation. Quantifying changes in their expression and protein level using in-situ hybridisation and immunohistochemistry (IHC) respectively, can be a

brain region specific measure of neuronal activity (Hoffman, Smith and Verbalis, 1993). In the case of behavioural paradigms such as CFC, specific brain regions are engaged after the retrieval and extinction of fear memories. Several studies have employed the quantification of IEG expression and protein to determine the brain regions and sub-regions engaged during these memory processes. Understanding where and when IEG are expressed throughout the brain enable researchers to target subregions and timepoints in future experiments, whether they are investigating the mechanisms behind CFC consolidation, retrieval and extinction processes, or administering agonists/antagonists to modulate memory processes.

Experiments by Hall et al., (2001) investigated, using in situ hybridisation, the expression of Zif268 mRNA in the hippocampi and amygdalae of adult rats 90 minutes after the retrieval (two days post-conditioning, eight-minute reexposure) of a CFM. Analysis of autoradiograms produced from these in situ experiments revealed an increase in *zif268* expression in the CA1, but not the DG subregions of the hippocampus following the retrieval of a CFM. In subregions of the amygdala, increases in *zif268* expression were observed in the BA, LA and CeN but not the AB (Hall, Thomas and Everitt, 2001). Another study looking at *zif268* expression in a single-trial CFC paradigm revealed, using in situ hybridisation, increases in its expression in the LA, supporting Hall et. al. (2001) findings, and also the IL, AC and OFC following the retrieval (one day post-conditioning, five-minute reexposure, brains collected 30 minutes post-retrieval) of a CFM (Chakraborty *et al.*, 2016). Thomas et al., (2002) also identified increased expression of zif268 in the AC and PL with CFM recall (three days post-conditioning, eight-minute reexposure). An increase in *zif268* expression following the recall (one day post-conditioning, two-minute

reexposure, brains collected 90 minutes post-reexposure) of a CFM were observed in IHC experiments performed Frankland et al., (2004) in the CA1. However, no changes compared to a no reexposure control were observed post-recall in the AC, IL, PL, visual cortex (VC) and temporal (TC). In further support of ***zif268's*** association with activity following CFM retrieval, work from Lee et al., (2004) used inhibitory oligodeoxynucleotides targeting *zif268* infused into the dorsal hippocampus, which resulted in reduced freezing of rats upon their return to the context compared to control; showing that *zif268* expression is necessary for the maintenance of the CFM after retrieval, but also plays a possible role in CFM restabilisation. This proposed role of *zif268* was confirmed by Trent et al., (2015), whose targeted knock down of the IEG resulted in a non-recoverable retrograde amnesia termed reconsolidation blockade. A summary of changes in *zif268* expression observed with CFM retrieval and extinction can be found in Table 3.1.

	Subregion	Direction of change	Reference
Recall	CA1	↑	Hall et. al., 2001 Frankland et. al., 2004 Kirtley et. al., 2010
	CA3	No change	Kirtley et. al., 2010
	DG	No change ↑	Hall et. al., 2001, Kirtley et. al., 2010 Besnard et. al., 2014
	PL	↑ No change	Chakraborty et. al., 2001, Thomas et. al., 2002 Frankland et. al., 2004
	IL	↑ No change	Chakraborty et. al., 2001 Frankland et. al., 2004
Extinction	CA1	↑	Kirtley et. al., 2010
	PL	↑	Herry et. al., 2004
	IL	↑	Herry et. al., 2004

Table 3.1 – Tabular summary of changes observed in zif268 expression following CFM recall found within the literature..

Identification of brain regions associated with CFC using IEG expression has not solely been driven by studies using *zif268* as a marker of activity. As discussed previously, *cFOS*, like *zif268*, can be used as a marker of neural activity and thus identify regions associated with the retrieval and extinction of a CFM. In mice, distinct patterns of cFOS expression were observed using IHC following retrieval (one day post-conditioning, two-minute reexposure, brains collected 90 minutes post-reexposure), primarily with increases in the CA1 and DG. Additionally, in the same mice, researchers also looked at another IEG's expression and observed a positive correlation between the expression profiles of *cFOS* and *zif268*, indicating that IEGs are largely expressed in overlapping neuronal populations (Stone *et al.*, 2011; Trent *et al.*, 2015). (Frankland *et al.*, 2004), whose work looking at zif268 protein levels post-retrieval (one day post-conditioning, two-minute reexposure, brains collected 90 minutes post-reexposure) of a CFM was discussed above, also examined *cFOS* in the same mice. The *cFOS* expression pattern observed was akin to that of *zif268*, only being elevated in the CA1 post-recall and being no different compared to a no reexposure control in other brain regions (AC, IL, PL, TC and VC). Another study, looking at *cFOS* levels using IHC following CFM retrieval (four weeks post-conditioning, three-minute reexposure, brains were collected 90 minutes post-reexposure), revealed increases in its expression in cortical structures (AC, PL, IL and RSP), RE (thalamic subregion), amygdalar structures (CEA and BLA) and ventral CA3 (hippocampal subregion) compared to mice not re-exposed to the context (Silva, Burns and Gräff, 2019). Furthermore, the emerging use of viral targeted recombination in active population (TRAP) strategies have fostered a deeper understanding of *cFOS'* expression profile during CFC. Chemotactic

administration of TRAP vectors has enabled the chemogenetic inhibition of neurons expressing *cFOS* in a subregion specific manner. Inhibition of *cFOS* positive neurons in the PL cortex immediately before reexposure to the context was shown to supresses CFM retrieval (Silva, Burns and Gräff, 2019). A summary of changes in *cFOS* expression observed with CFM retrieval and extinction can be found in Table 3.2.

	Subregion	Direction of change	Reference
Recall	Hippocampus	↑	Huff et. al., 2006
	CA1	↑	Wheeler et. al., 2013 Frankland et. al., 2004 Strekalova et. al., 2003
	CA3	↑	Silva et. al., 2018
	DG	↑	Wheeler et. al., 2013 Besnard et. al., 2014
	PL	No change ↑	Frankland et. al., 2004, Wheeler et. al., 2013 Silva et. al., 2018
	IL	No change ↑	Frankland et. al., 2004, Wheeler et. al., 2013 Silva et. al., 2018
Extinction	CA1	↑	Silva et. al., 2018
	CA3	↑	Silva et. al., 2018
	PL	↑	Silva et. al., 2018, Herry et. al., 2004
	IL	No change	Herry et. al., 2004
	RE	↑	Silva et. al., 2018

Table 3.2 – Tabular summary of changes observed in cFOS expression following CFM recall and extinction found within the literature.

Arc has also been used to identify brain regions associated with CFC. Work from (Trent *et al.*, 2015) showed an increase in *Arc* expression following the retrieval (two days post-conditioning, two-minute reexposure, brains collected 30 minutes post-reexposure) of a CFM in the CA1 of the hippocampus, which is concordant with the findings of Zhang et al., (2005) who also observed increases in the CA3 and amygdala post-retrieval. Hudgins & Otto, (2019) also mapped *Arc* protein expression in the hippocampus, finding an increase in its expression in the ventral CA1 following reexposure to the conditioned context (one day post-conditioning, two-minute reexposure, brains collected 60 minutes post-reexposure). In the BLA, (Nakayama *et al.*, 2016) found, with their IHC experiments, increased *Arc* expression two- and twelve-hours post-acquisition of the CFM. Additionally, when these animals were returned to the conditioned context (one day post-conditioning, five-minute reexposure), Arc levels increased again at the two- and twelve-hour time points. A summary of changes in *Arc* expression observed with CFM retrieval and extinction can be found in Table 3.3.

	Subregion	Direction of change	Reference
Recall	Hippocampus	↑	Huff et. al., 2006
	CA1	No change ↑	Barnes et. al., 2008, Trent et. al., 2017, Zelikowsky et. al., 2014 Hudgins et. al. 2019
	CA3	↑	Zhang et. al., 2005
	DG	↑	Besnard et. al., 2014
	PL	↑	Zelikowsky et. al., 2014
	IL	No change	Zelikowsky et. al., 2014
Extinction	CA1	↓	Barnes et. al., 2008, Trent et. al., 2017

Table 3.3 – Tabular summary of changes observed in Arc expression following CFM recall and extinction found within the literature.

As we have seen in the studies presented above, *Arc*, *cFOS* and *zif268* are well documented markers of neuronal activity and have been used to map which brain regions are engaged/required for CFM retrieval and the facilitation of CFM extinction. However, one of the major limitations of these previous experiments is that retrieval and extinction are rarely examined within the same cohort of animals, making direct comparison of the brain regions engaged during these learning/memory events difficult. The experiments in this chapter used IHC staining for the IEGs: Arc, cFOS and zif268, to map neural activity following the retrieval or extinction of a CFM. Regions of interest were targeted for IEG quantification based upon prior evidence of IEG expressional changes at the mRNA or protein level and studies using chemical/mechanical inhibition of brain regions. Such studies include those discussed previously (Chapter 3.1.2, summarised Tables 3.1 and 3.2), which showed increases in *cFOS*, z*if268* and *Arc* in multiple different hippocampal, cortical and thalamic subregions. Chemical inhibition experiments such as those performed by (Ramanathan and Maren, 2019) showed the integral role of RE in the acquisition and expression of an extinction CFM. Rats infused with muscimol (selective $GABA_A$ agonist) into a cannulated RE continued to freeze in the response to the context, whilst animals infused with saline returned to near pre-shock levels of freezing at the same time points. Likewise, studies utilising neurotoxic lesions in specific brain regions support the findings of investigations using IEG expression to map brain regions necessary for the retrieval and extinction of CFMs. For example, lesions in the BLA of rats impairs the acquisition of CFMs; subjects still acquire the memory however, they require additional training to do so (Maren, 1999). To quantify the expression of IEGs in the CNS post-retrieval and -extinction, a cohort of 17 male

adult rats underwent CFC, some of which were returned to the context 48 hours later for either two (retrieval) or ten minutes (extinction). Two different methods of analysing the fear-associated freezing behaviour used in the literature were trialled to select the method that provides the best representation of animals' freezing behaviour. Brains collected one-hour post-reexposure from these animals were immunohistochemically stained for *cFOS*, *zif268* or *Arc*. Sections were imaged and ROIs (PL, IL, CA1, CA3, hilus, GL, ML, and RE) extracted from them. All ROIs were selected based upon previous evidence indicating that the regions they are contained within (mPFC, hippocampus, amygdala, and thalamus) are implicated in CFM retrieval and/or extinction. Unlike other studies, the experiments in this chapter compared recall and extinction within the same cohort of animals across a wide range of brain regions, which provided a detailed analysis of the non-discriminatory and differential engagement of subregions following the retrieval and extinction of a CFM.

3.2 Materials and methods

3.2.1 Animals, contextual fear conditioning and extinction

17 adult male Lister Hooded rats were housed in pairs or trios with ad libitum access to food and water as previously described on a reverse day/night schedule. As previously described, (2.1.2.1), all subjects underwent CFC and received a single scrambled 0.5mA foot shock (US) for two seconds in a novel context (CS). 48 hours later six rats were returned to the context for two minutes to elicit the recall of the fear memory (2 min Recall group) and six rats were re-exposed to the context for ten minutes to induce the extinction of the fear memory (10 min Recall group). One-hour post-reexposure, rats were sacrificed with an intraperitoneal injection of pentobarbital (200 mg/ml Euthatal, Boehringer Ingelheim Animal Health, Surrey, UK) and left in a holding cage until cessation of heartbeat. Five subjects were not re-exposed to the context (No Recall Group) and were sacrificed on the same day as animals in the other two groups.

Freezing behaviour was used as the index of rat's fear and was defined as the cessation of movement excluding respiration for more than one second (Curzon, Rustay and Browman, 2009). Rats' freezing was assessed every five seconds with the scorer blinded to timepoint and behavioural group and reported as percentage freezing.

3.2.2 Perfusion

Following sacrifice, animals underwent transcardial perfusion with 0.1 M PBS followed by ice cold 4% PFA in 0.1 M PBS (flowrate: 20 ml/min) and allowed to flow until the liver cleared and fixation tremors had ceased (approximately 15-20 min,

300-400 ml 4% PFA per animal) (Gage, Kipke and Shain, 2012). Perfused rats were decapitated and whole brains removed and stored in 4% PFA for 24 hrs at 4^{o}C. Post-fixed brains were washed with 0.1 M PBS and transferred to 30% sucrose in 0.1 M PBS for cryoprotection. Cryoprotected brains were embedded in OCT compound (Scigen, California, USA), frozen on dry ice and stored at -80^{o}C until required.

3.2.3 Tissue sectioning

Imbedded brains were mounted on 30 mm cryostat chucks with OCT compound and coronally sectioned at a thickness of 40 µm. Sections through the mPFC (containing PL and IL cortices) were collected from the rostral appearance of the forceps (Bregma +5.16 mm, Paxinos & Watson, 2006) to the genu of the corpus callosum (Bregma +2.52 mm). An additional series of sections were collected from Bregma -1.44 mm to Bregma -4.36 mm spanning the hippocampus, nucleus reuniens and amygdala. Sections from the two 1/12 series were stored in separate 12-well plates containing 0.1 M PBS and at 4^{o}C until required.

3.2.4 Immunohistochemical staining

A complete set of sections from each of the two series collected during sectioning (mPFC series: six sections, hippocampal series: six sections) were removed from storage in PBS for each animal. Sections were placed in a new 12-well plate and washed for five minutes under agitation in fresh 0.1 M PBS, three times. 500 µl of blocking solution (1/10 NDS, Thermo-Fisher, Massachusetts, USA, 1% v/v Triton X-100, Bio-Rad Laboratories, California, USA, in 0.1 M PBS) was added to each well and agitated at room temperature for two hours. Following blocking, sections were incubated with primary antibodies with specificity for

epitopes of Arc (1/1000, 156 003, Rabbit, Synaptic Systems, Lowe Saxony, Germany), cFOS (1/1000, ABE457, Merck Group, Hesse, Germany) or zif268 (1/1000, 4153, Cell Signalling Technology, Massachusetts, USA) (Table 2.2), diluted with 0.1 M PBS containing 1/500 NDS and 0.01% v/v Triton X-100, for 24 hours on a seesaw rocker at 4 ^{o}C. After incubation with primary antibodies, sections were incubated with the appropriate Alexa Fluor 488 anti-mouse or rabbit secondary antibodies (1/1000, Alexa Fluor 488 polyclonal antibody, A-11094, Thermo-Fisher, Massachusetts, USA) diluted with 0.1 M PBS containing 1/500 NDS and 0.01% v/v Triton X-100, for two hours with agitation at room temperature. Unbound secondary antibodies were washed away with three 0.1 M PBS washes, the second wash also contained DAPI (0.1 ng/ml, 62248, Thermo-Fisher, Massachusetts, USA). Tissue was mounted on SuperFrost Plus™ Adhesion Slides (Thermo-Fisher, Massachusetts, USA) and coverslipped with Mowiol mounting medium and Superwhite glass coverslips (Landon LaboQuip, London, UK). Slides with mounted sections were stored at 4^{o}C in opaque slide boxes until required.

3.2.5 Photomicrograph acquisition

All 20x magnification mosaic photomicrographs used for subsequent analysis were obtained with an epifluorescent upright Leica DM6000 B microscope system (Leica Microsystems, Buckinghamshire, UK) and its proprietary software Leica Application Suite X (LAS X, Leica Microsystems, Buckinghamshire, UK). From sections covering the mPFC a ROI was drawn within LAS X that encompassed the PL and IL cortices from each hemisphere (based upon the anatomy laid out in Paxinos and Watson, 2005) and imaged as a mosaic by the software. For sections

containing the hippocampus and RE, a mosaic image covering the entire section was collected.

3.2.6 Counting immunopositive nuclei

Arc, cFOS or zif268 immunopositive nuclei were quantified in mPFC (IL and PL) and hippocampal (CA1, CA3, hilus, GL and ML) subregions and the RE. Mosaic images were converted into TIFFs using the Fiji distribution of ImageJ (https://imagej.nih.gov/ij/download.html, NIH, Maryland, USA). ROIs (PL, IL, CA1, CA3, hilus, GL, ML and RE) were manually traced for each image, before being converted to 8-bit and auto-thresholded (v1.16.5) retaining the upper 1% of total signal. Remaining particles were quantified using the automated counting function (particle size: 40-infinity, circularity: 0.00-1.00). After measuring the area of each ROI within ImageJ, the total number of particles across the total area assessed were calculated for each subregion and averaged within each behavioural group.

3.2.7 Statistics

Percentage freezing from CFC experiments was compared across experimental groups using a multivariate repeated-measures general linear model with Mauchly's Test of Sphericity in IBM® SPSS® Statistics (Version 26.0.0.0, IBM, New York, USA). If Mauchly's test was significant, then a Greenhouse-Geiser correction was applied.

Particle densities per unit area from each ROI were compared across experimental groups using one-way ANOVAs followed by multiple comparisons in Prism 8 (GraphPad, California, USA).

3.3 Results

3.3.1 Rats show contextual fear conditioning and extinction of fear memory

Foot shock (US) induced the normal rodent fear response (Figure 3.1). Before the delivery of a US, rats exhibited normal exploratory behaviour and spent the majority of their time moving around the box or grooming. Post-US, subjects displayed little to no exploratory behaviour or grooming; instead they displayed high levels of freezing behaviour for the majority of the one minute they remained in the box, $F_{(1,15)} = 627.699$, $p < 0.0001$, repeated-measures ANOVA. Rats reexposed to the context 48-hours later exhibited greater conditioned freezing behaviour than they did before receiving the shock, $F_{(1,11)} = 107.545$, $p < 0.0001$, repeated-measures ANOVA. Animals in the extinction groups had lower freezing behaviour following ten minute reexposure to the context compared to the first two minutes of reexposure, $F_{(1,5)} = 81.814$, $p < 0.0001$, repeated-measures ANOVA (Figure 3.1B).

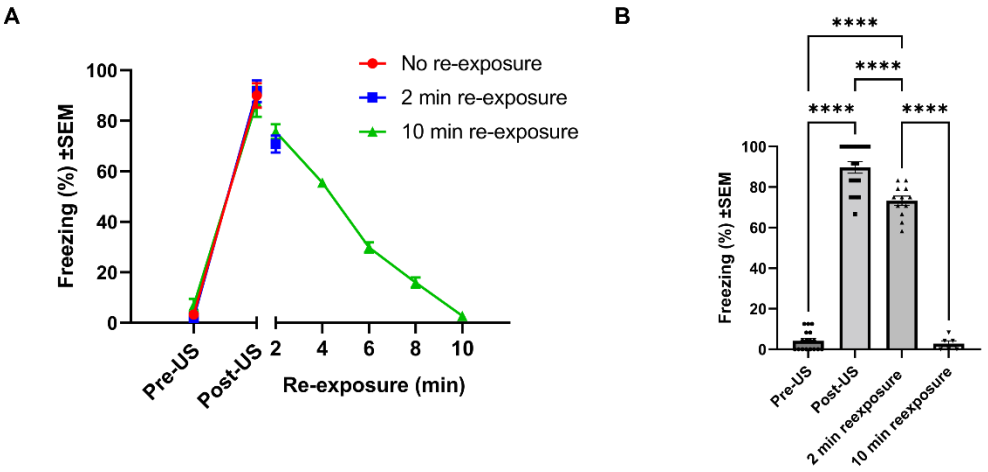

Figure 3.1 – The retrieval and extinction of a contextual fear memories in rat. Subjects froze immediately following a single unconditioned shock in the context. 48 hours post-initial shock rats returned to the context froze initially. Freezing behaviour returned to pre-shock levels after 10 minutes re-exposure to the context. Panel B combines percentage freezing for all three experimental groups, the same changes were observed if each group was analysed separately (Appendix 4). **** denotes p <0.0001.

3.3.2 Method of analysing freezing behaviour does not alter overall trends in freezing behaviour

All data presented in Figure 3.2 was generated by sampling, whether the animal was freezing every five seconds and calculating the percentage of time frozen. Before this method was selected for quantifying freezing behaviour, it was compared, using a trial dataset, to another which is also commonly used in the literature: measuring the total time spent frozen (Scholz *et al.*, 2016). Both methods showed the same trend in freezing behaviour, peaking immediately following the shock, being present after reexposure, before returning to pre-shock levels after a ten-minute reexposure to the context (Figure 3.2). Whilst the same trend in freezing behaviour was seen with the two methods, sampling every five seconds results in the assessment of higher levels of freezing compared to measuring the total time spent frozen; the portion of time spent freezing was higher immediately following the shock, $F_{(1,96)} = 7.168$. $p < 0.01$, ANOVA. However, sampling every five seconds reduced variance and proved to be a more practical method overall. Therefore, it was selected as the method to quantify freezing in all future experiments.

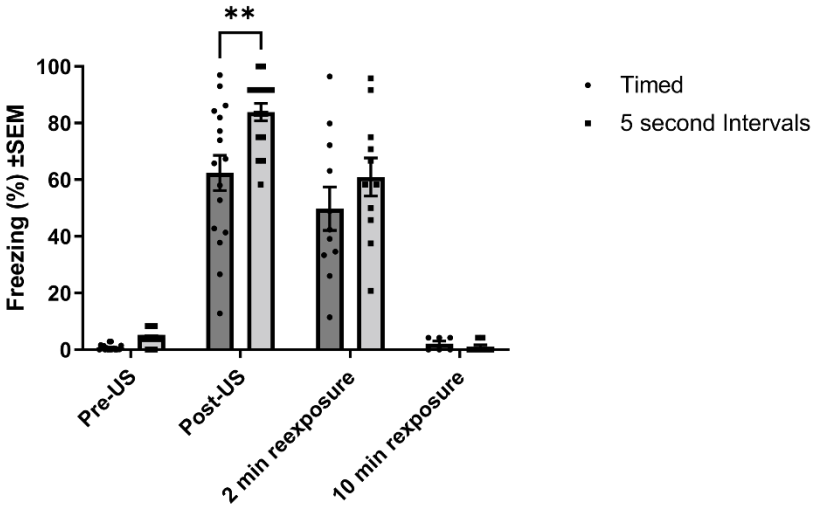

Figure 3.2 – Evaluation of two methods for assessing rats' freezing behaviour. The two methods of assessing freezing; timed and five second intervals, both produce the same overall profiles of freezing behaviour. The to methods both showed increased freezing levels post-US, which was still present post-return to the context, however sustained reexposure to the context resulted in a return to pre-shock levels of freezing. However, measuring freezing in five minute intervals produces high percentage freezing value than calculating freezing percentage by timing total freezing ** denotes $p < 0.01$.

3.3.2 Arc

3.3.2.1 mPFC

No changes in the number of Arc positive nuclei were observed between groups in the PL or IL cortices of the mPFC (Figure 3.4, Table 3.4). Representative images of *Arc* immunopositivity in the mPFC are provided in Figure 3.3.

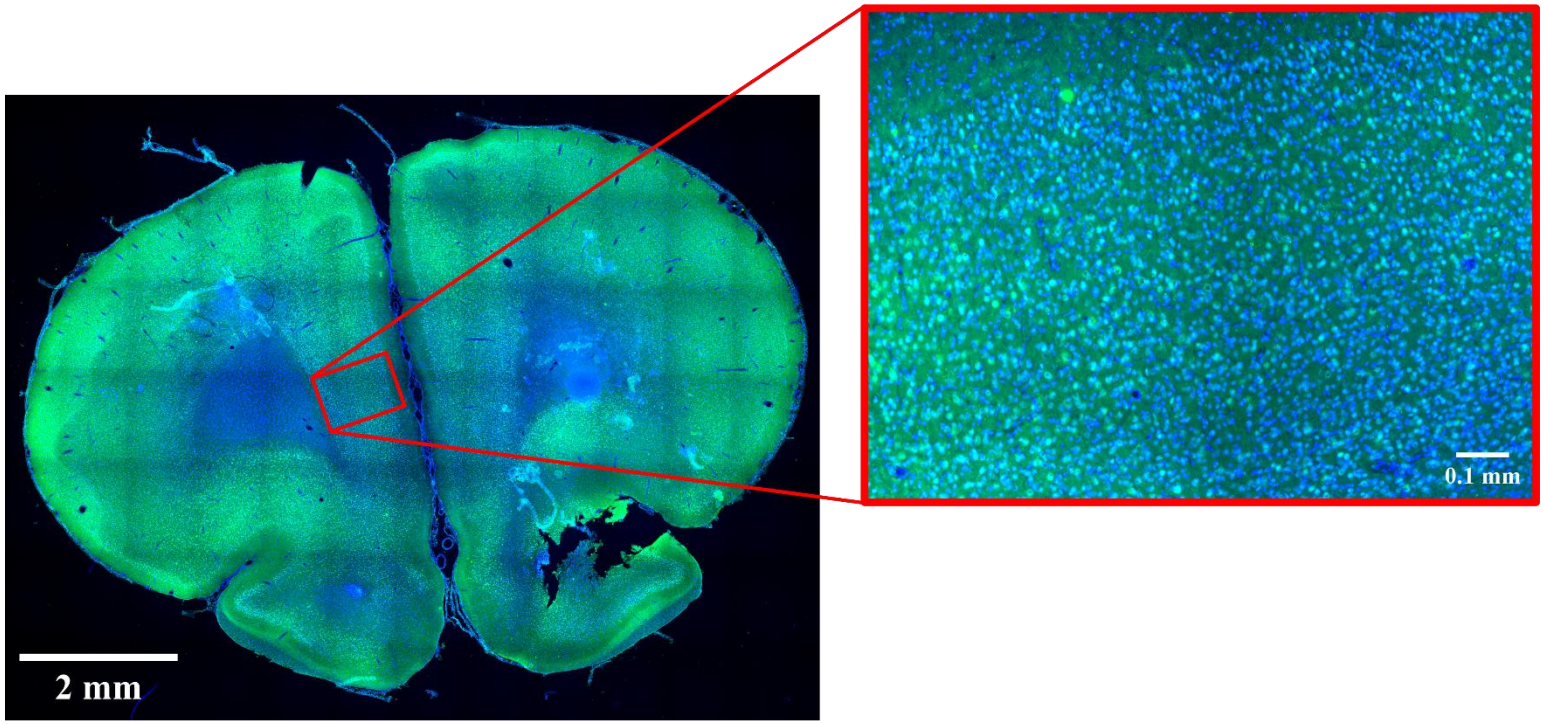

Figure 3.3 – Representative image of Arc IHC staining in the mPFC used in the analysis of its expression following CFM retrieval and extinction. Representative images of Arc negative controls are provided in Appendix 6.

	DF	F value	P value	NR vs 2 min	NR vs 10 min	2 min vs 10 min
CA1	2,14	0.7994	0.0501	N/A	N/A	N/A
CA3	2,14	1.340	0.420	N/A	N/A	N/A
GL	2,14	0.7695	0.3079	N/A	N/A	N/A
Hilus	2,14	0.7945	0.6030	N/A	N/A	N/A
IL	2,13	0.9596	0.9982	N/A	N/A	N/A
ML	2,14	2.825	0.0029	No difference	0.0046	0.0099
PL	2,14	2.016	0.6871	N/A	N/A	N/A
RE	2,14	0.5356	0.6012	N/A	N/A	N/A

Table 3.4 – Tabular summary of changes observed in Arc expression following CFM recall and extinction from IHC experiments.

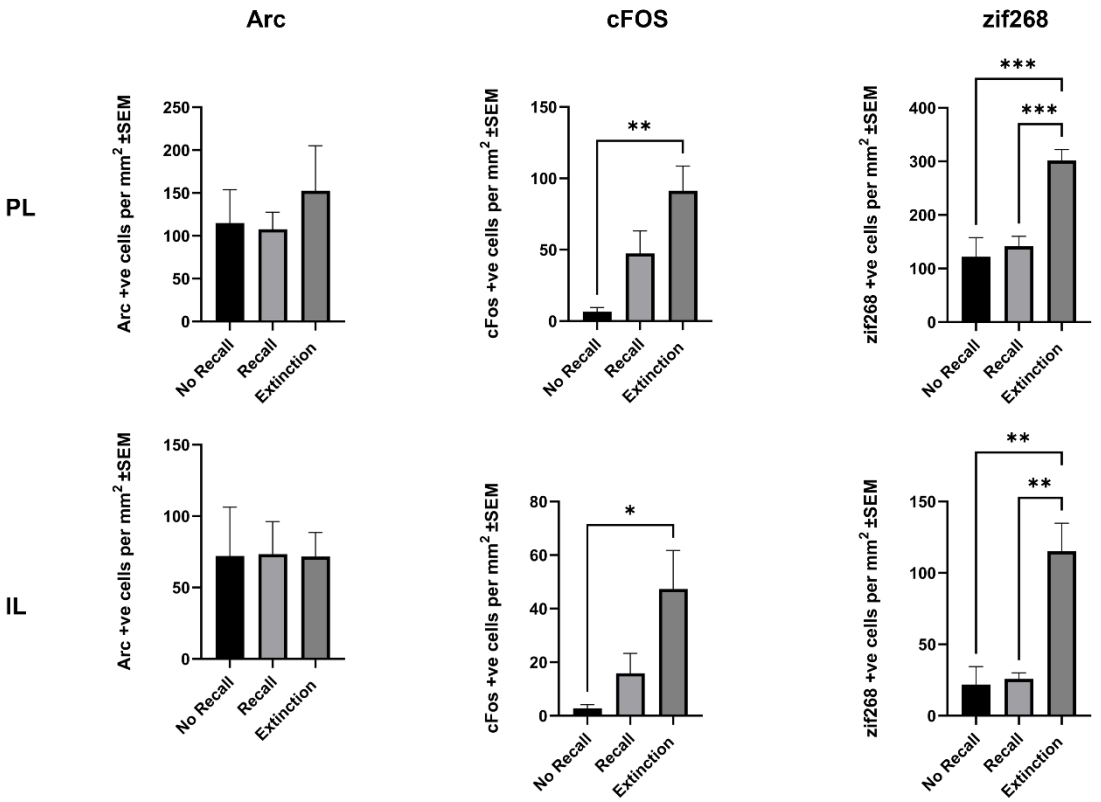

Figure 3.4 – Arc, cFOS and zif268 protein levels in the mPFC subregions PL and IL 1 hour following the retrieval and extinction of a CFM. The expression of cFOS increased in both subregions following extinction compared to a no reexposure control. Similarly the expression of zif268 increased following extinction compared to recall and non-reexposed animals. * denotes $p < 0.05$. ** denotes $p < 0.01$.

3.3.2.2 Hippocampus

A difference in the number of Arc positive nuclei in the ML of the hippocampus was observed between groups $F_{(2, 14)} = 2.825$, $p = 0.0029$, ANOVA. Multiple comparisons revealed a decrease in positive nuclei following ten-minute (Extinction) reexposure compared to two minute (Recall, $p = 0.0099$) and no reexposure (No Recall, $p = 0.0046$). No difference was observed between the no reexposure and recall groups. No changes in the number of Arc positive nuclei were observed between groups in the CA1, CA3, GL or Hilus hippocampal subregions (Figure 3.5, Table 3.4).

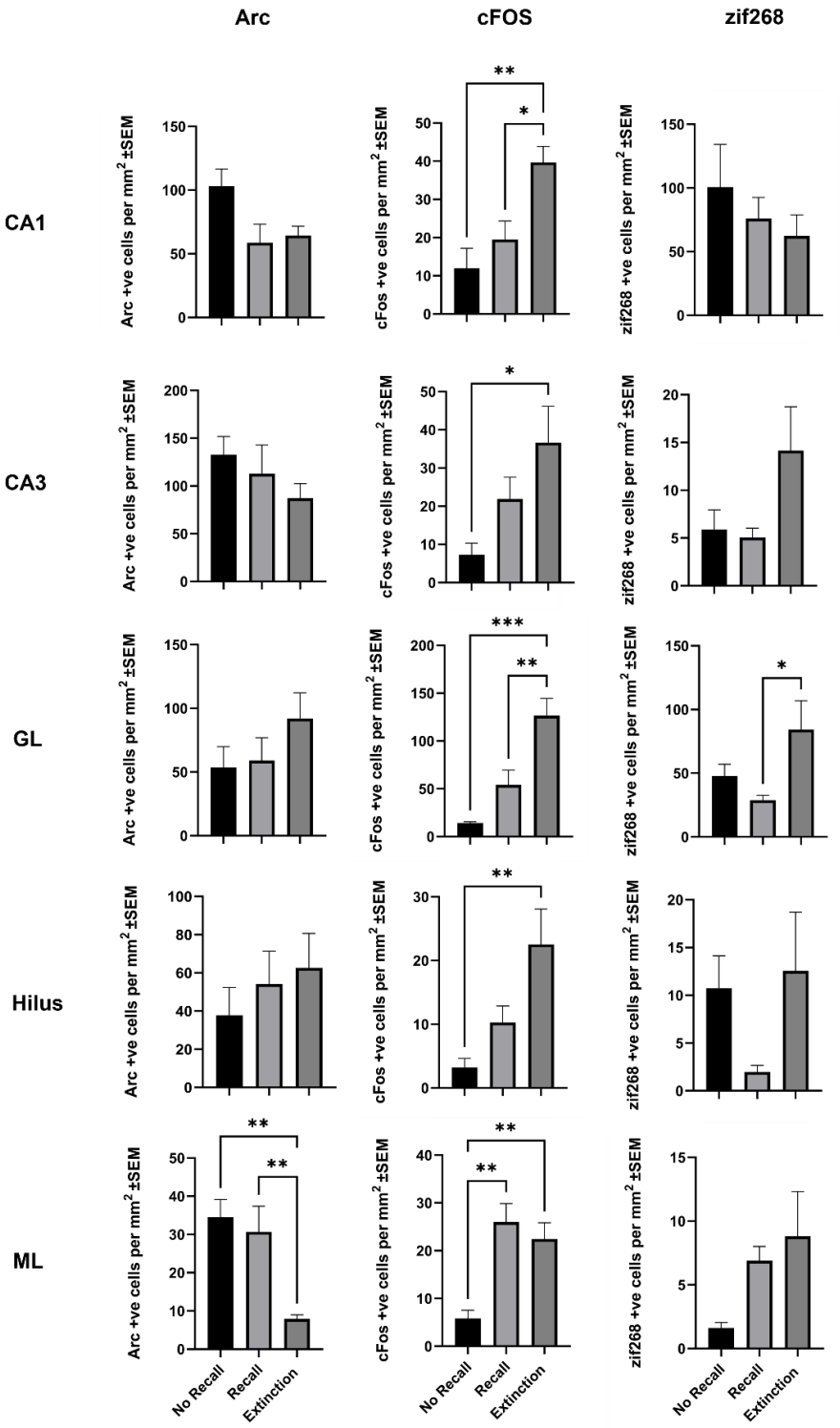

Figure 3.5 – Arc, cFOS and zif268 protein levels in the hippocampal subregions: CA1, CA3, GL, Hilus and ML were quantified 1 hour after the retrieval and extinction of a CFM. The expression of Arc decreased in the ML following the extinction of a CFM compared to rats not reexposed to the context and those reexposed for two minutes. cFOS expression was increased following extinction in the CA1, GL, Hilus and ML compared to no reexposure control. The expression of zif268 only increased in the Hilus following extinction compared to animals that underwent a two minute reexposure to the context. Additionally cFOS expression was increased in the ML following the retrieval of a CFM compared to control. * denotes $p < 0.05$. ** denotes $p < 0.01$. *** denotes $p < 0.001$.

3.3.2.3 RE

No changes in the number of Arc positive nuclei were observed between groups in the RE (Figure 3.6, Table 3.4).

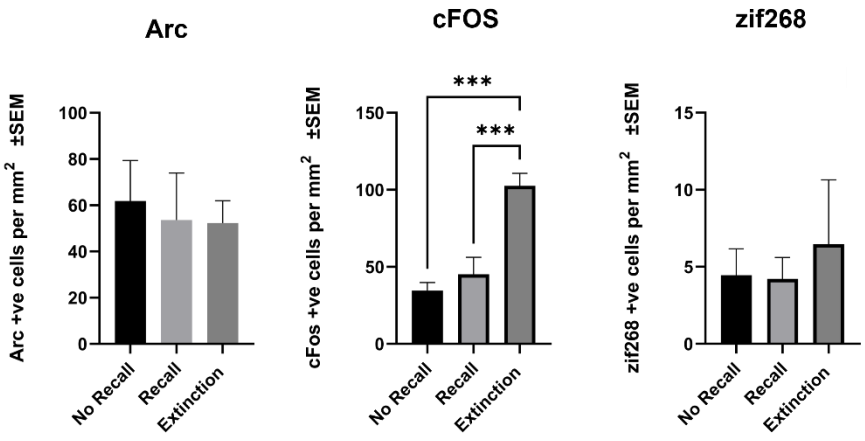

Figure 3.6 – Arc, cFOS and zif268 protein levels in the RE; a thalamic subregion, 1 hour after the retrieval and extinction of a CFM. The extinction of a CFM increased the expression of cFOS in RE compared to rats not reexposed to the context and those reexposed for two minutes. *** denotes $p < 0.0001$.

3.3.3 cFOS

3.3.3.1 mPFC

Differences in the number of cFOS positive nuclei in the PL and IL cortices of the mPFC were observed between groups ($F_{(2,14)}$ = 4.514, p = 0.0043, ANOVA and $F_{(2,13)}$ = 3.452, p = 0.0321, ANOVA respectively). Multiple comparisons revealed an increase in positive nuclei following ten-minute reexposure (Extinction) compared to no reexposure (No Recall) in both regions of interest (PL: p = 0.0032, IL: p = 0.0365). No additional differences were observed in either PL or IL cortices (Figure 3.4, Table 3.5). Representative images of *cFOS* immunopositivity in the mPFC are provided in Figure 3.7.

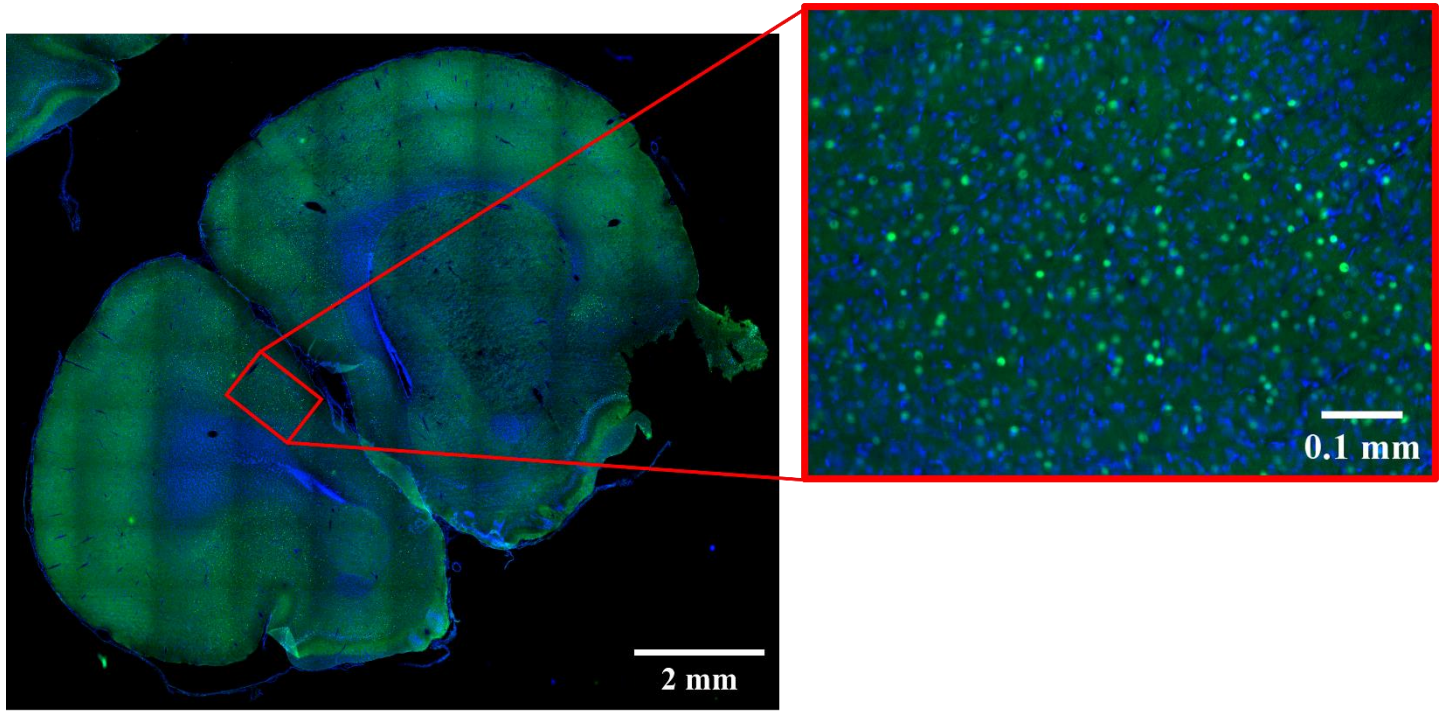

Figure 3.7 – Representative image of cFOS IHC staining in the mPFC used in the analysis of its expression following CFM retrieval and extinction. Representative images of cFOS negative controls are provided in Appendix 7.

	DF	F value	P value	NR vs 2 min	NR vs 10 min	2 min vs 10 min
CA1	2,14	0.2593	0.0029	No difference	0.0031	0.0199
CA3	2,14	0.7095	0.0357	No difference	0.0285	No difference
GL	2,14	2.311	0.0003	No difference	0.0003	0.0075
Hilus	2,14	3.269	0.0108	No difference	0.0094	No difference
IL	2,13	3.452	0.0321	No difference	0.0365	No difference
ML	2,14	0.8272	0.0019	0.0020	0.0088	No difference
PL	2,14	4.514	0.0043	No difference	0.0032	No difference
RE	2,14	0.3607	0.0002	No difference	0.0003	0.0009

Table 3.5 – Tabular summary of changes observed in cFOS expression following CFM recall and extinction from IHC experiments.

3.3.3.2 Hippocampus

Differences in the number of cFOS positive nuclei in the CA1, CA3, GL, Hilus and ML were observed between groups: $F_{(2,14)} = 0.2593$, $p = 0.0029$, ANOVA, $F_{(2,14)} = 0.3517$, $p = 0.0357$, ANOVA, $F_{(2,14)} = 2.311$, $p = 0.0003$, ANOVA, $F_{(2,14)} = 3.269$, $p = 0.0108$, ANOVA, $F_{(2,14)} = 0.8272$, $p = 0.0019$, ANOVA respectively. Multiple comparisons revealed an increase in positive nuclei following ten-minute reexposure (Extinction) compared to two-minute reexposure (Recall) and no reexposure (No Recall) in the CA1 ($p = 0.0199$ and $p = 0.0031$ respectively) and GL ($p = 0.0075$ and $p = 0.0003$ respectively). Multiple comparisons also revealed an increase in the number of positive nuclei following two- (Recall) and ten-minute (Extinction) reexposure compared to no reexposure (No Recall) in the ML ($p = 0.0020$ and $p = 0.0088$ respectively). Additionally, multiple comparisons showed an increase in the number of positive nuclei following ten-minute reexposure compared to no reexposure in the CA3 ($p = 0.285$) and Hilus ($p = 0.0094$). No additional differences were observed between groups in any other hippocampal subregions (Figure 3.5, Table 3.5).

3.3.3.3 RE

A difference in the number of cFOS positive nuclei was observed in the RE between groups $F_{(2,14)} = 0.3607$, $p = 0.0002$, ANOVA. Multiple comparisons revealed an increase in the number of positive nuclei following ten-minute reexposure (Extinction) compared to the two-minute reexposure (Recall) and no reexposure (No Recall) groups ($p = 0.0003$ and 0.0009 respectively, Figure 3.6, Table 3.5.

3.3.4 Zif268

3.3.4.1 mPFC

Differences in the number of zif268 positive nuclei were observed between groups in both the PL and IL cortices of the mPFC ($F_{(2,14)}$ = 1.326, p = 0.0002, ANOVA and $F_{(2,13)}$ = 1.512, p = 0.0005, ANOVA respectively). Multiple comparisons revealed an increase in the number of positive nuclei following ten-minute reexposure (Extinction) compared to the two-minute reexposure (Recall, PL: p = 0.0008, IL: p = 0.0011) and no reexposure (No Recall) groups (PL: p = 0.0004, IL: p = 0.0019). No additional differences were observed in mPFC subregions between groups (Figure 3.6, Table 3.6). Representative images of zif268 immunopositivity in the mpFC are provided in Figure 3.8.

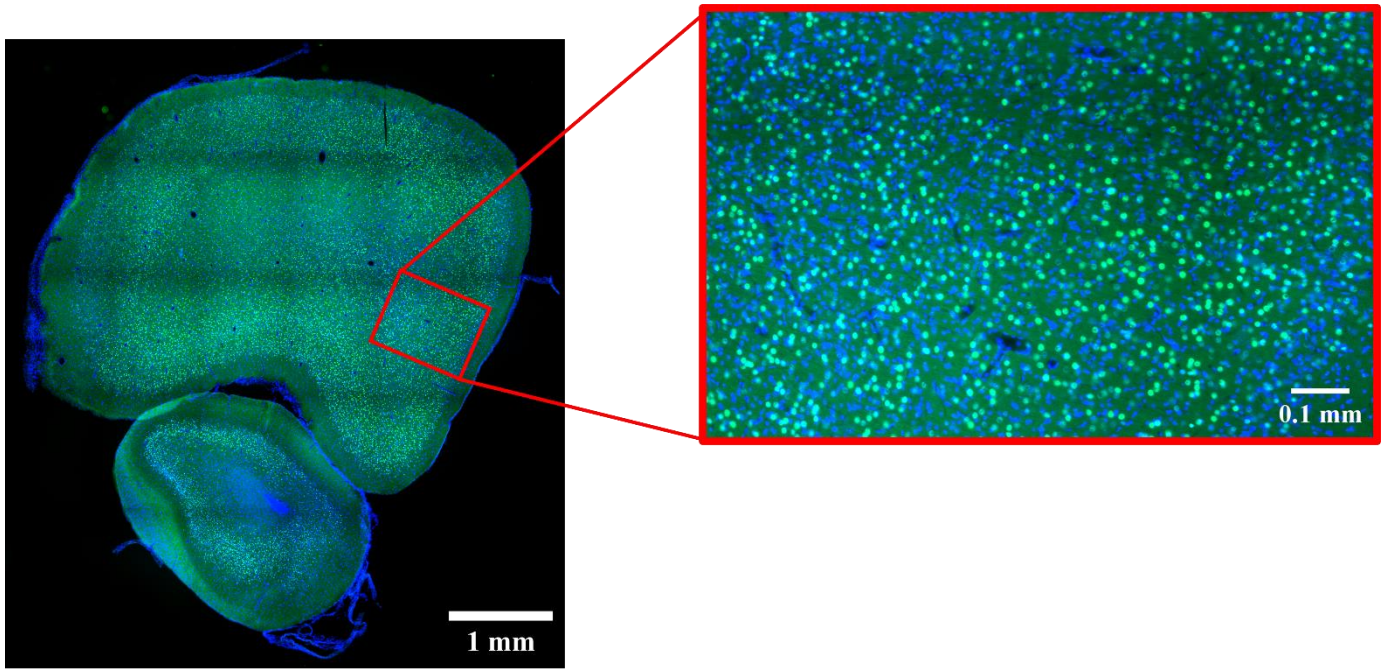

Figure 3.8 – Representative image of zif268 IHC staining in the mPFC used in the analysis of its expression following CFM retrieval and extinction. Representative images of zif268 negative controls are provided in Appendix 8.

	DF	F value	P value	NR vs 2 min	NR vs 10 min	2 min vs 10 min
CA1	2,14	0.7382	0.5030	N/A	N/A	N/A
CA3	2,14	0.1820	0.0944	N/A	N/A	N/A
GL	2,14	3.840	0.0482	No difference	No difference	0.0417
Hilus	2,14	1.739	0.1829	N/A	N/A	N/A
IL	2,13	1.512	0.0005	No difference	0.0019	0.0011
ML	2,14	2.538	0.1147	N/A	N/A	N/A
PL	2,14	1.326	0.0002	No difference	0.0004	0.0008
RE	2,12	0.4539	0.8526	N/A	N/A	N/A

Table 3.6 – Tabular summary of changes observed in zif268 expression following CFM recall and extinction from IHC experiments.

3.3.4.2 Hippocampus

A difference in the number of zif268 positive nuclei was observed between groups in the GL subregion of the hippocampus ($F_{(2,14)} = 3.840$, $p = 0.0482$, ANOVA). Multiple comparisons revealed a decrease in the number of positive nuclei following two-minute reexposure (Recall) compared to ten-minute reexposure (Extinction, $p = 0.0417$). No further differences were observed between groups in any other hippocampal subregions (Figure 3.5, Table 3.6).

3.3.4.3 RE

No difference in the number of zif268 positive nuclei was observed between groups in the RE: $F_{(2,12)} = 0.4539$, $p = 0.8526$, ANOVA (Figure 3.6, Table 3.6).

3.4 Discussion

The experiments in this chapter successfully implemented a CFC behavioural paradigm. Conditioned rats froze in response to a single scrambled foot shock. Rats returned to the context froze initially, but if they remained in the context for an extended period (ten minutes), they returned to baseline (pre-shock) levels of movement: evidence of successful CFM extinction. Two methods of analysing rats' freezing behaviour were compared to select an appropriate method for use in all further CFC video analysis. The two methods compared (sampling in five second bins and measuring time spent frozen), produced the same trends in freezing behaviour between the different stages of the CFC paradigm (acquisition, recall and extinction). Sampling freezing every five seconds was selected for use in all subsequent analysis. Whilst continuous sampling does not materially affect the scores with a high level of CR, it results in higher variance and is more time consuming. Furthermore, sampling in five- or ten-second bins has a long and established history and is well validated, so was selected as the method to assess freezing behaviour in all future experiments in this thesis (Anagnostaras, 2010). After establishing that rats had successfully gone through the CFC paradigm, and those in the two-minute and ten-minute reexposure groups behaved as expected based upon previous data from our group, brains from these animals were sectioned and stained for IEGs: Arc, cFOS and zif268 (Barnes and Thomas, 2008; Clifton, Thomas and Hall, 2018). Analysis of IEG expression in brain regions associated with CFC (mPFC: PL and IL, hippocampus: CA1, CA3, hilus and GL, ML, and thalamus: RE) revealed region specific changes in their expression linked to the retrieval and/or extinction of a CFM, summarised in Tables 3.4, 3.5 and 3.6).

3.4.1 Subjects exhibited the recall and/or extinction of contextual fear memory

Rats displayed contextual fear conditioning. After being placed in a novel context (CS, conditioning chamber) rats display normal exploratory behaviour as is expected of a healthy rat in an unfamiliar environment. Upon receipt of single foot shock (US) rats immediately began ceasing movement (aside from respiratory movement) which is an established fear associated behaviour termed freezing (Anagnostaras, 2010). Returning to the same context (CS) 48 hours later elicited freezing behaviour again in the rats, albeit to a slightly lesser extent than seen immediately post-foot shock. This indicates that the rats had acquired a CR to the context driven by the acquisition; during their training 48 hours earlier, of a fearful associative memory which paired the CS with the US (Maren, Phan and Liberzon, 2013). Rats reexposed to the context for an extended period (ten minutes) presented an incremental attenuation of their freezing response. This return to normal exploratory movement/grooming by rats who remained in the context for ten minutes, reflects animals acquiring a new memory that the context is no longer associated with a fearful stimulus (Bouton, 2004). This new association is given greater salience than the previous fearful association. The results of these CFC experiments are completely in line with existing literature from both other groups within our lab group and the wider scientific (Scholz *et al.*, 2016) .

3.4.2 Comparing methods to analyse freezing behaviour

Within the existing CFC literature discussed above, there is a clear discordance in how fear associated freezing behaviour of rats is quantified. The two methods primarily used to sample freezing behaviour are: sampling a rat's behaviour every five seconds (giving it a binary score of movement or no movement), and

measuring the exact amount of time spent freezing. Comparing the two methods, using a subset of data generated from the behavioural experiments in this chapter, revealed that the two methods produce the same pattern of freezing behaviour in our CFC paradigm that was expected based upon the existing literature (Lee, Everitt and Thomas, 2004b; Barnes and Thomas, 2008; Maren, Phan and Liberzon, 2013). Rats had little to no freezing pre-shock, very high levels of freezing immediately post-shock, then froze initially upon reexposure to the context, the level of which gradually reduced the longer they remained in the context. However, sampling freezing behaviour in five-second bins tended to overestimate (only at high levels of CR) the amount of freezing compared to timing the freezing. Sampling freezing, despite the apparent overestimation at high levels of CR, was selected as the preferred method as it can detect changes in freezing behaviour in a sufficiently powered experiment in a timely and cost-effective manner. Furthermore, continuous non-automated methods of analysing freezing behaviour may be more open to subjective errors (due to fatigue or distraction) and bias, which increase variance.

3.4.3 IEGs revealed the activation of distinct brain regions following the retrieval and extinction of a CFM

Across hippocampal, pre-frontal cortical and thalamic subregions, CFM associated processes were correlated with changes in the expression of three IEGs: *Arc*, *cFos* and *zif268*, at a time point of one-hour post-reexposure to the context (Table 3.7). All but one of the changes were increases compared to rats not re-exposed to the context, with only *Arc* expression in the ML decreasing compared to both no reexposure and two-minutes reexposure groups. Additionally, the majority of changes in IEG expression accompanied the extinction of the CFM (ten-minute

reexposure), with the only change in IEG expression following the retrieval of a CFM being seen with *cFOS* in the ML of the hippocampus, with a comparable increase also being observed in the extinction group.

	Recall	Extinction
Arc		↓ ML
cFOS	↑ ML	↑ CA1, CA3, GL, Hilus, IL, ML and PL
zif268		↑ IL and PL

Table 3.7 – Summary of changes observed in IEG expression (Arc, cFOs and zif268) following CFM retrieval and/or extinction in comparison to rats not reexposed to the context.

The expression of *zif268* and *cFOS* in the mPFC appears coordinated post-CFM extinction, with increases in both being observed in the PL and IL cortices. Previously, Silva et al., (2019) have reported similar increases in cFOS protein levels in the PL cortex following CFM extinction. However, did they not observe the increase in cFOS protein in the IL post-extinction that is shown here. The discordance between our results and those of Silva et al., (2019) may have arisen due to inter species differences between mice and rats or due to us employing different paradigms for inducing CFM extinction. In their experiments Silva et al., 2019 induced extinction by reexposing mice to the context with twice daily three-minute sessions for four days, compared to our single day one session ten-minute reexposure. Therefore, the difference in subregion engagement between experiments may have arisen due to the use of divergent behavioural paradigms, with the IL being engaged in the single reexposure extinction but not during the use of repeated short reexposures to induce CFM extinction. The increase in cFOS-positive neurons in the PL post-extinction is the opposite pattern than what would typically be expected due to the region's well documented in fear generating pathways. However, as our experiments do not distinguish between excitatory and inhibitory neurons the increase in neural activity observed could be due to activation of pathways in the PL which inhibit the expression fear (facilitate extinction) (Brinley-Reed, Mascagni and McDonald, 1995). In addition to the increases cFOS expression, we also observed complimentary increases in zif268 protein in the PL and IL cortices post-extinction. This finding may represent a previously unknown role of zif268 in the mPFC during extinction. This result is not particularly surprising as cFOS and zif268 are often expressed in overlapping populations of neurons, and

pathway analyses show that the functional outcomes of their expression are highly concordant (Guzowski *et al.*, 2001; Filipkowski, Knapska and Kaczmarek, 2006).

Our experiments found no change in the expression of any IEGs in either the PL or IL cortices following the retrieval of a CFM, a finding which, in regard to cFOS, is at odds with the findings of Silva et al., 2019 who showed increases in cFOS protein in the PL and IL cortices following remote fear memory retrieval paradigm and a three-minute reexposure time. This discordance may reflect that the engram is latent or weak at this point after conditioning (recent memory), and therefore less likely to induce neural activity (indicated by cFOS expression) compared to stronger/mature fear memory engrams present after consolidation four weeks later (remote memory) (Kitamura *et al.*, 2017). The lack of changes following recent memory retrieval is supported by the work of Frankland et al., (2004) who, despite measuring mRNA levels, not protein, showed, like our experiments, no change in cFOS expression in the mPFC in animals reexposed to the context for two-minutes. Frankland et al., (2004) also, as with the experiments in this chapter, examined *zif268* mRNA expression in the same paradigm and like our experiments showed zif268 levels did not change in the PL and IL cortices following the retrieval of a CFM. However, conflicting reports of zif268's role in facilitating CFM retrieval come from Chakraborty et al., (2016) who identified an increase in *zif268* mRNA in the IL cortex post-retrieval. However, unlike the experiments in this chapter and those of Frankland et al., (2004) Chakraborty et al., (2016) employed a retrieval paradigm which used a five-minute reexposure unlike our our two-minute one. Therefore, this discrepancy may have arisen due the two different recall conditions promoting either fear memory destabilisation and restabilisation , both of which are processes that

rely upon protein synthesis but may engage different transcriptional programmes (Knapska and Maren, 2009; Vaverková, Milton and Merlo, 2020).

Despite the apparent coordination of zif268 and cFOS expression in the mPFC post-extinction, the same cannot be said for the hippocampus. Increases in cFOS expression was observed in the CA1, CA3, GL, Hilus and ML. The increase in expression of cFOS in the CA1 we observed supports the findings of Silva et al., (2019), who saw a similar increase in cFOS expression post-extinction. This may reflect that prolonged reexposure (i.e., over two-minutes) to context in absence of the US induces the reactivation of the original associative memory/engram that is necessary for the formation of the extinction memory/engram, but also the engagement of a new neuronal population in the formation of the CS- no US engrams (Khalaf *et al.*, 2018; Lacagnina *et al.*, 2019). Furthermore, Silva et al., (2019) also reported similar increases in the CA3 following CFM extinction, but also showed an increase following CFM retrieval, something that we did not observe in our experiments. The reason for this divergence in cFOS profiles in the CA3 post-retrieval is unclear. It could be because our experiment is underpowered (G*Power analysis estimates a group size of 22 is required for a small effect size: f = 0.4), as a trend towards increased cFOS expression was observed, but did not meet the threshold for significance. Alternatively, rather than the two-minute reexposure group producing fear memory restabilisation as expected, nothing is induced as reported by (Vaverková, Milton and Merlo, 2020). Additionally, the gap between CFM acquisition and context reexposure used by Silva et al., (2019) (four weeks) was far longer than the 48 hours used in our experiments, meaning they were investigating remote fear memories, rather than recent ones as we did. Remote memories are

traditionally thought to have undergone consolidation with some groups saying they even become independent of the hippocampus (Hall, Thomas and Everitt, 2001; Thomas, Hall and Everitt, 2002; Kitamura *et al.*, 2017).

The multi-subregion spanning induction of cFOS expression seen in the hippocampus following exposure to the CFM extinction paradigm was not accompanied by complimentary increases in expression of other IEGs. A singular increase in zif268 expression was observed in the GL of DG following ten-minute reexposure however, this was only in comparison to rats reexposed to the context for two minutes, and not in rats which received no reexposure. These findings suggests that zif268 plays a subregion specific role in the DG during extinction. No other studies have reported a similar finding. However, this may be because their focus is often on the CA1 and if the IEG expression is measured in the DG, it is taken as a whole and not split into its constituent parts (GL, Hilus and ML). Our findings are also at odds with data found in the literature. Hall et al., (2001) reported an increase in zif268 mRNA in the CA1 post-eight-minute reexposure and Frankland et al., (2004) observed an increase in zif268 protein in the CA1 post-two-minute reexposure. There is no clear explanation for why we did not observe a similar increase of zif268 in our experiments however, it could be due to differences in experimental paradigms. Hall et al., (2001) looked at zif268 expression at a similar time point post-reexposure to our experiments, measured mRNA rather than protein. Therefore, the lack of concordance between our observations could be explained by a temporal disconnect between mRNA and protein levels, with expression of the protein being seen later than one-hour post-reexposure. Furthermore, we may have selected the wrong timepoint post-reexposure and missed the optimal window to measure

changes in zif268 expression. In order to address this issue, future experiments could include a series of sections stained for zif268 obtained from brains collected at different timepoints post-reexposure (i.e. 30 minutes, 1 hour and 2 hours. Whilst our experiments and those of Frankland et al., (2004) both examined protein, we did not report the same increase in the CA1 following a two-minute reexposure to the context. However, Frankland et al., (2004) employed a CFC paradigm during which subjects received five-foot shocks with one-minute intervals between them, opposed to our single shock, suggesting that the severity of the footshock received may alter the strength of the acquired CFM and thus alter neuronal activity following its reactivation during reexposure to the context (Baldi, 2004).

As with zif268, the data we have presented looking at Arc protein levels in the hippocampus, is at odds with what is reported in the current literature. We observed no changes in Arc expression following the retrieval or extinction of a CFM in any hippocampal subregions. Work from Trent et al., (2015) and Hudgins & Otto, (2019) suggests that Arc expression increases following a two-minute reexposure to the context. Whilst Hudgins & Otto's, (2019) experiments used a different CFC paradigm to our experiments (rats received pre-exposure to the context and received seven-foot shocks), Trent et al., (2015) used an identical one, but measured *Arc* mRNA and not protein levels as we did. In fact, in their follow up paper Trent et al., (2017) identified no change in Arc protein expression following CFM retrieval; a finding supported by the work of Barnes & Thomas, (2008) who reported no change in Arc protein levels at four- and six-hours post-retrieval. These findings suggest that there is a disconnect between Arc mRNA expression and its translation and the subsequent synthesis of Arc protein, which may arise due to the well documented

spatial-temporal control of Arc with it being transcribed in the soma before being transported to dendrites to be translated (Barnes and Thomas, 2008). However, Barnes & Thomas, (2008) and Trent et al., (2017), whilst seeing no changes in Arc protein following CFM recall, reported decreased Arc expression following CFM extinction at the six-hour timepoint post-reexposure, thus suggesting, as with zif268, we may have missed the optimal time-point to observe changes in Arc protein levels following CFM extinction.

The RE is a thalamic nucleus that acts as an interconnecting bridge between the mPFC, hippocampus and amygdala (Karthik R Ramanathan *et al.*, 2018). Projections from the hippocampus innervate the PL cortex however, a returning direct connection (PL neurons innervating the hippocampus) does not exist. The RE acts as a hub and facilities the PL to hippocampal communication and therefore is likely to be an essential brain region for facilitating CFM retrieval and extinction (Dolleman-van der Weel *et al.*, 2019; Ramanathan and Maren, 2019) (Figure 1.1). Several studies have shown lesions or inhibition of the RE to impair the extinction of CFMs, confirming its purported role in the acquisition of new memories that compete with the existing fear memory facilitating CFM extinction (Ramanathan and Maren, 2019). Data from our experiments examining IEG expression in the RE following the extinction of a CFM, support these findings. The increase in cFOS positive cells in the RE post-CFM extinction seen in our experiments indicates that neurons located in the RE are actively engaged during extinction, but not following retrieval; a pattern that is very similar to our observations in both the mPFC and hippocampus. However, this increase was not accompanied with increases in the expression of Arc or zif268, perhaps reflecting that the RE is merely acting as a ‘junction box’ between

the mPFC and hippocampus, which requires the transmission of signals, but not neuronal and synaptic reorganisation driven by IEGs associated with plasticity such as Arc and zif268 (Korb *et al.*, 2013; Duclot and Kabbaj, 2017). However, just because we have not seen evidence of plasticity in the RE does not mean it is not occurring. There are several other IEGs associated with plasticity such as BDNF whose expression could be measured in the RE in future experiments (Cunha, 2010; Lu, Nagappan and Lu, 2014).

Taken together, the results of our IEG experiments have broadly confirmed the findings of other groups; that the mPFC, hippocampus and RE are activated during the extinction of a CFM. Contrary to what the literature suggests, we saw little evidence of the same regions being activated during CFM retrieval. As discussed previously, the reasons for the lack of concordance between our results and the literature may have arisen due to methodological differences in the CFC paradigms used or what is actually being measured (mRNA or protein). Additionally, the increases in regional activation seen after extinction versus retrieval may be because they are larger and thus more easily seen in an underpowered experiment (there are trends towards expected increases in the hippocampus and mPFC following retrieval). The difference in size of said changes between extinction and retrieval may be associated with the activation of two (versus one) non-overlapping neuronal ensembles in the hippocampus and mPFC following ten-minute reexposure (Lacagnina *et al.*, 2019). However, despite its time-point and power-driven issues aside, what our experiments have achieved is that unlike previous investigations, we have examined multiple IEGs, across multiple brain regions following two distinct CFC associated processes (retrieval and extinction) in the same cohort of rats. This

allowed us to directly compare expression between regions and IEGs, confident that the effects we measured were due to physiological mechanisms rather than slight alterations in methodological approach or inter/intra-species differences.

Whilst IEG experiments were primarily focussed on identifying subregions actively engaged during CFM retrieval and extinction in order to target them for analysis in subsequent experiments (Chapters 4 and 6), the results we have presented portray a very interesting picture by themselves. The discordance between our findings and those found in the literature highlight the unique patterns of IEG induction seen in brain regions associated with CFM retrieval, with variations in behavioural paradigms and tissue harvest time points apparently having drastic effects upon the observed expression of IEGs and where said expression is localised. Future experiments could be designed to investigate IEG expression in a new cohort of animals; all subjected to the same basic CFC paradigm, where expression is mapped across different time points to see the full profile of IEG expression. Whilst feasible, these experiments would require extremely large numbers of animals especially if both mRNA and protein levels are to be quantified. Additionally, by looking at IEGs across multiple timepoints post-reexposure, these experiments are less likely to miss the time windows of IEG expression, which may have happened with Arc and zif268 in the experiments presented in this chapter. Furthermore, counting the number of positive nuclei to assess IEG expression, whilst sufficient to meet the aims of this chapter does not quantify IEG protein levels in neurons. The quantification of both IEG mRNA and protein is desirable as it could help unlock whether the apparent disconnect, between mRNA levels reported in the literature and protein levels (measured by both ourselves and other groups), is due

to an actual biological mechanism or is purely the result of comparing experiments from different research groups using inconsistent ways of modelling foot shock dependant CFC.

3.5 Conclusions

The experiments in this chapter assessed whether the CFC paradigm selected for use in all subsequent experiments produced the behavioural outcomes we desired (i.e., CFM retrieval and extinction) and that the method of assessing freezing behaviour (sampling freezing in five second bins) was appropriate. Subsequently, the expression of IEGs was assessed across the hippocampus, mPFC and RE at the protein level using IHC. These experiments revealed that one-hour post-undergoing our CFM extinction inducing paradigm, the hippocampus (CA1, CA3, GL, Hilus and ML), mPFC (PL and IL) and RE are engaged, as evidenced by increases in the number of cells expressing IEGs cFOS and/or zif268. Conversely, very limited activation of the neurons in the same regions was seen following the retrieval of a CFM.

Chapter 4: Expression of complement associated genes following the retrieval and extinction of a contextual fear memory

4.1 Introduction

Facets of the neuroimmune system including the complement system have been proposed as facilitators of not only the synaptic pruning associated with development and diseases of the CNS, but also the homeostatic modulation of synapses and their function required for the acquisition and updating of memories (Marin and Kipnis, 2013; Scholz *et al.*, 2016; Tchessalova, Posillico and Tronson, 2018; Brucato and Benjamin, 2020; Sakai, 2020; Posillico, 2021). Genetic alterations in components of the complement system have been identified in the aetiology of psychiatric disorders, where deficits in associative learning and memory extinction are observed in patients (Mayilyan, Weinberger and Sim, 2008; Hovhannisyan *et al.*, 2010; Woo *et al.*, 2020). The experiments presented in this chapter investigated whether changes in the expression of complement system associated genes accompany the region-specific changes in neural activity following CFM recall and extinction identified in Chapter 3.

The brain regions associated with fear memory processes have been identified (hippocampus, mPFC and amygdala) and lesions to these areas have been shown to induce fear conditioning deficits (LeDoux *et al.*, 1990; Phillips and LeDoux, 1994; Stephen Maren, Aharonov and Fanselow, 1997). However, the changes occurring at a cellular level in these sub-regions driving the presentation of these CFC associated behaviours have not been fully elucidated. Retrieval of memory by reexposure to a context (CS) can initiate at least two forms of mnemonic

processes: restabilisation and destabilisation. Restabilisation is the process whereby retrieved or reactivated labile memory is re-estabilised and over repeated reexposures events becomes resistant to change (Auchter *et al.*, 2017). On the other hand, destabilisation (extinction) is the process during which a new contextual memory is formed, that the CS is no longer associated with the US following prolonged and/or repeated reexposure to the CS with no aversive stimuli present (Myers and Davis, 2007b; Bronwyn M. Graham and Milad, 2016). These two processes permit flexibility in behavioural responses to changing experiences/circumstances and represent an adaptive advantage to the individual (Izquierdo, Furini and Myskiw, 2016). Maladaptive fear memories underlie prevalent psychiatric disorders including SZ and PTSD, promoting their destabilisation and enhancing their extinction and therefore offer a therapeutic strategy to treat said disorders (Wessa and Flor, 2007; Holt *et al.*, 2009, 2012; Milad *et al.*, 2009; Gill, Miller and Grace, 2018). Both fear memory retrieval and extinction are plasticity and protein-synthesis dependent processes, however it is unknown to what extent the molecular/ plasticity/cellular processes overlap/diverge.

Exploratory studies have identified several pathways/systems that could underlie the retrieval and/or extinction of a CFM. (Scholz *et al.*, 2016) examined transcriptomic changes in the CA1 following a behavioural paradigm which induced the recall or extinction of a contextual fear memory using a rat genome array covering 28,000 genes. The study used adult male Lister Hooded rats that received a three-minute conditioning session (two minutes pre-shock and one-minute post-shock), during which they received a single scrambled foot shock. 48 hours post-conditioning, rats were reexposed to the context for two minutes (recall group) or ten

minutes (extinction group). A third group of rats were not returned to the context and were used as the comparator group. Freezing behaviour in all animals was scored to confirm that the animals retrieved and/or extinguished the contextual fear memory. Animals were sacrificed (rising CO_2) two hours post-reexposure and tissue from the CA1 collected. RNA isolated from gathered tissue was hybridised to microarray probes. Analysis of microarray data from this experiment highlighted hundreds of genes differentially regulated by the recall or extinction of a contextual fear memory. Enrichment analysis of differentially regulated genes in the recall group revealed ontology clusters around multiple immune system related terms (Table 4.1). Immune system related genes contained within these clusters are detailed in Table 4.2. However, of particular interest is the range of complement system associated genes enriched following retrieval. Complement associated genes identified included the classical pathway initiator C1qA, the central complement protein C3, the anaphylatoxin receptor C3aR as having decreased expression and complement inhibitors CFI and Serping1 both exhibited increased expression (Figure 4.1). This wide range of complement associated genes exhibiting changes in expression accompanying fear memory retrieval, indicates that the complement system could have a key role in the maintenance of fear memory responses following recall of a contextual fear memory. The processes to maintain said fear memories have been proposed as being simply facilitating the restabilisation of the labialised CFM (Haubrich *et al.*, 2015). However, others have made the alternative argument that the complement system's involvement in fear memory maintenance could be through its inhibition of extinction, rather than promoting fear memory restabilisation (Trent *et al.*, 2017). This potential link between associative learning and the complement

system is plausible. Synaptic plasticity and synaptogenesis underly the neuronal flexibility required for associative learning (Poirazi and Mel, 2001; Maren, 2005; Mozzachiodi and Byrne, 2010). For instance, in the dorsal CA1 and cingulate cortex there are increases in spine density following associative memory formation, increases that are reversed in extinction (Leuner, Falduto and Shors, 2003; Restivo *et al.*, 2009; Vetere *et al.*, 2011; Garín-Aguilar *et al.*, 2012; Bender *et al.*, 2018). A similar increase in spine density and subsequent reversal with extinction also occurs in the auditory cortex with cued fear conditioning (Lai, Adler and Gan, 2018). Interestingly, auditory cued conditioning results in decreased spines in frontal association areas that are reversed by extinction (Lai, Franke and Gan, 2012). This difference in polarity likely reflects the specific contribution of the frontal association area to fear behaviour/learning. Overall, there is a pattern of increased spine density in fear memory circuits that correlate with conditioned fear responses, which are reversed in extinction. These changes in spine density associated with fear learning and extinction could be facilitated in part by the activity or reduced activity of the complement system (Alexander H. Stephan, Barres and Stevens, 2012; Han *et al.*, 2015; Györffy *et al.*, 2018; Stein and Zito, 2019; Scholl, Rule and Hennig, 2021). An intact complement system is required for normal developmental pruning of supernumerary synapses in the dLGN (Stevens *et al.*, 2007b; Schafer *et al.*, 2012). Complement's integral role in the phagocytosis of damaged cells and restoration of circuitry following either physical or ischaemic injury, again highlights its ability to modulate and alter neural connectivity (Gorsuch *et al.*, 2012; Hammad, Westacott and Zaben, 2018; Galloway *et al.*, 2019).

Ontology Cluster	Number of Ontology Terms	Number of unique genes
Response to bacterium	6	17
Response to stress	4	14
Inflammatory response	3	35
Positive immune system regulation	3	13
Immune system development	3	13
Immune-cell motion	13	27
Cytokine activity	3	10

Table 4.1 – Tabular summary of ontology clusters contained with the differentially expressed genes identified by Scholz et. al. (2016) following the retrieval of a contextual fear memory.

Gene	Gene ID	Expression p-value	Direction of Change
IL1RN	60582	< 0.001	↑
CD86	56822	< 0.001	↑
CD46	29333	< 0.001	↑
CXCL13	498335	< 0.001	↑
CFI	79126	< 0.001	↑
CD74	25599	< 0.01	↑
CCL3	25542	< 0.01	↑
CCL4	116637	< 0.01	↑
C3aR	84007	< 0.01	↓
IL6	24498	< 0.01	↑
IL1β	24494	< 0.01	↑
IL4	287287	< 0.01	↓
C3	24232	< 0.05	↓
Serping1	295703	< 0.05	↑
C1qA	298566	< 0.05	↓

Table 4.2 – Tabular summary of the neuroimmune system associated genes contained within the differentially expressed genes identified by Scholz et. al. (2016) following the retrieval of a contextual fear memory.

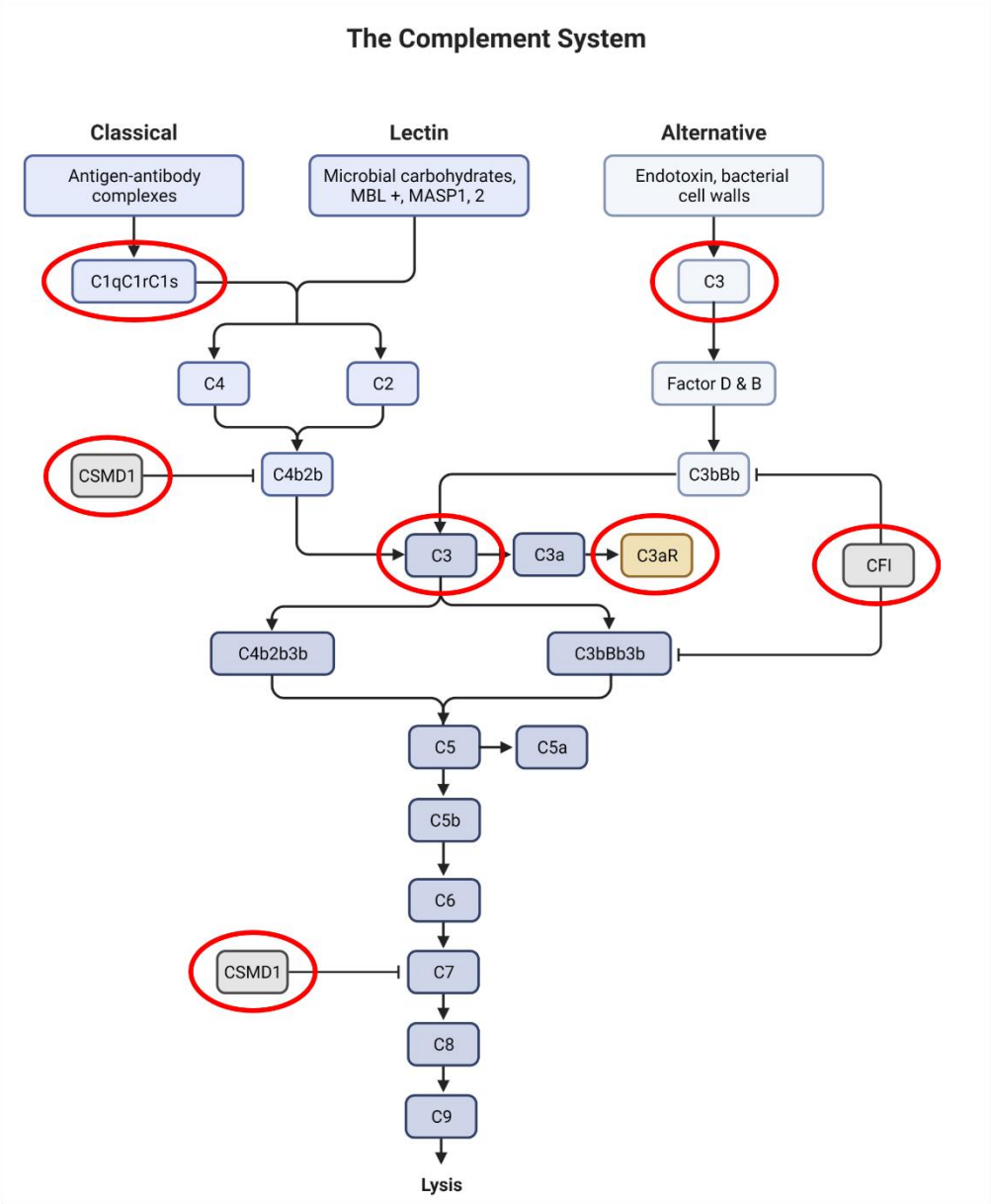

Figure 4.1 – Simplified schematic of the complement system. Red circles indicate complement associated genes identified by Scholz et. al. (2016) as being differentially expressed during the retrieval of a CFM.

Microglia, the primary source of the major complement proteins in the CNS, are not uniformly distributed throughout the brain and instead, regions such as the hippocampus and substantia nigra contain numerous densely packed microglia (Lawson *et al.*, 1990). The high concentration of microglia in the hippocampus, a region deeply engrained within the mechanisms underlying associative learning, is of interest (Jonathan C. Gewirtz, McNish and Davis, 2000; Kim and Cho, 2020). It has been proposed that microglial enrichment in the hippocampus is reflective of the role microglia play in facilitating the numerous functions of the region such as neurogenesis in adulthood (microglial provide trophic support) and hippocampal LTP (Grabert *et al.*, 2016; Milior *et al.*, 2016; Toda *et al.*, 2019b). Furthermore, the idea that the high number of microglia in the hippocampus are present to drive the complement dependent synaptic pruning which underlies hippocampal dependent learning, is a tantalising prospect. Additionally, the subgranular zone of the DG is a site of adult neurogenesis, a process by which new neurons are produced by neural stem cells in a healthy adult (Moreno-Jiménez *et al.*, 2019). The concentration of microglia in the hippocampus are actively involved in controlling the survival, and directing the migration, of new-born neurons from the subgranular zone and some evidence suggests this process is dependent upon the complement system (Mathieu *et al.*, 2005; Therien, 2005; Diaz-Aparicio *et al.*, 2020). Adult neurogenesis has also been linked with associative learning. The acquisition of an associative memory increases adult neurogenesis and the newly born neurons respond upon reexposure to the previously learned experience, suggesting that these new neurons are functionally integrated into hippocampal circuitry required for the retrieval and/or expression of the learned memory (Kee *et al.*, 2007; Trouche *et al.*, 2009; Anderson

et al., 2011). This body of evidence may suggest that microglia in the hippocampus during the acquisition and/or recall of associative memories are not only driving the pruning and plasticity of existing neural circuitry, but also modulating the survival of new neurons and facilitating their integration into hippocampal networks.

To generate the original differential expression analysis associated with recall and with extinction, two different experimental protocols were used, which may confound the comparison of altered gene expression following CFM retrieval with extinction (Scholz *et al.*, 2016). We therefore investigated the expression of complement system components: *C1qA*, *C3* and *C3aR* identified by Scholz et al., (2016) following the retrieval of a CFM under conditions that are associated with recall (two-minute reexposure) and extinction (ten-minute reexposure), compared to a no reexposure control to permit a more direct comparison. *CSMD1*; a purported CNS specific complement inhibitor, that has been implicated in the aetiology of SZ, was also included in our experiments to investigate its potential role in associative learning (Steen *et al.*, 2013; Liu *et al.*, 2019). In addition, micro-punching a novel refinement for tissue acquisition in RT-qPCR experiments was developed and validated, to extend the analysis of Scholz et al., (2016) to spatially restricted regions of the fear memory and extinction circuits: in the hippocamps (CA1, CA3 and DG) and mPFC (IL and PL)

4.2 Methods

4.2.1 Animals

28 adult male Lister Hooded rats were housed in pairs or trios with ad libitum access to food and water, on a reversed light-dark schedule as previously described. All subjects underwent the CFC paradigm presented in Chapter 2.1.2.1. Animals were placed individually into conditioning chambers and allowed to explore freely. Following two minutes in the chamber, the rats received a single scrambled foot shock (US, 0.5 mA for 2 seconds) and left in the novel context (CS) for a further minute before being returned to the 'home cage'. 48 hours later, ten rats were reexposed to the context for two minutes to elicit the recall of the fear memory and eight rats were reexposed to the context for ten minutes to facilitate the extinction of the fear memory, before being returned to the 'home cage'. Behaviour in conditioning chambers was digitally recorded for later offline analysis. Two hours post-exposure, the rats were sacrificed using a rising concentration of CO_2. Ten subjects assigned to the no reexposure group were not reexposed to the context and were sacrificed on the same day as animals in the two- and ten-minute reexposure groups. Brains were collected post-mortem, flash frozen on dry ice and stored at -80^{o}C.

4.2.2 Behavioural analysis

The cessation of movement for more than one second, excluding respiratory movement, was used as the threshold for freezing behaviour. Freezing behaviour was sampled every five seconds by a blinded observer. The number of freezing events per session in the chamber was recorded as a percentage of the total time (in

one- or two-minute bins) spent in the chamber for each animal and averaged within each behavioural group.

4.2.3 RNA extraction and cDNA synthesis

Using the micro-tissue punch method described previously (Chapter 2.1.4.2), tissue punches were collected from hippocampal (CA1, CA3 and DG) and PFC (PL and IL) subregions from the 28 brains collected (Figure 2.3). Between two and ten punches were collected per region per animal, with the total weight of punched tissue obtained from a single region being in the approximate range of 2-7 mg. To enable primer validation and efficiency calculations, between 20-30 mg of tissue was also harvested from grossly dissected hippocampi. RNA was extracted and treated to remove genomic DNA contamination using the RNeasy Kit (QIAGEN, Limburg, Netherlands) and TURBO™ DNase (Thermo-Fisher, Massachusetts, USA) respectively. cDNA was synthesised using extracted RNA (10 ng/µl) and cDNA cDNA EcoDry Premix Random Hexamers (Takara Bio Inc., Shiga, Japan) according to manufacturer's protocol. cDNA was diluted 1:15 with nuclease-free water and stored at -80^{o}C until required.

4.2.4 Primer design and validation

As described previously, sequences from genes of interest (*Arc*, *C1qA*, *C3*, *C3aR*, *C4* and *CSMD1*) and housekeeping genes (SDHA and UbC) were obtained from the NCBI database (https://www.ncbi.nlm.nih.gov/gene) and candidate primers identified using the Primer-BLAST webtool (https://www.ncbi.nlm.nih.gov/tools/primer-blast). Specificity of candidate primers was confirmed using the Nucleotide-BLAST webtool (https://www.blast.ncbi.nlm.nih.gov/Blast.cgi). Probes obtained from Sigma-Aldrich

(Dorset, UK) were tested at different concentrations (0.17, 0.33 and 0.42 µM) using cDNA synthesised using mRNA from grossly dissected rat hippocampus. The lowest probe concentration that produced a single peak melt curve, Ct values within an acceptable range (10 to 35) and no signal in negative control wells, had their efficiencies estimated using the calculation presented in Chapter 2. Primer pairs with efficiencies over 90% and under 110% were deemed acceptable for use in further experiments. Table 2.1 contains details of primers optimised and validated for use.

4.2.5 RT-qPCR

96-well plates were loaded with 7.5 µl of SensiFAST® SYBR Hi-ROX master mix (Bioline, London, UK), 1.5 µl of forward and reverse primers diluted to their optimised concentrations (Table 4.1) and 5.0 µl of cDNA. Plates were designed to contain cDNA from the same brain region and a random mix of experimental groups (a minimum of two from each group) run in triplicate for each gene of interest. Each plate was run with probes for two genes of interest and two housekeeping genes. The housekeeping genes selected: polyubiquitin-C (UBC) and succinate dehydrogenase complex flavoprotein subunit A (SDHA), had previously been shown not to alter in expression during both the recall and extinction of fear memories (Scholz *et al.*, 2016). Plates were run on a StepOnePlus system (Thermo-Fisher, Massachusetts, USA) using the standard protocol given in Chapter 2. Briefly, plates underwent 95^{o}C heat activation for 10 minutes, 46 cycles of denaturation (95^{o}C, 15 seconds) and annealing (60^{o}C, 1 minute). Results were analysed using the comparative delta-delta Ct method described previously (Equation 2.3).

4.2.6 Statistics

Percentage freezing from CFC experiments was compared across experimental groups using a multivariate repeated measures general linear model with Mauchly's Test of Sphericity in IBM® SPSS® Statistics (Version 26.0.0.0, IBM, New York, USA). If Mauchly's test was significant then a Greenhouse-Geiser correction was applied.

Gene expression measured for each gene of interest using the comparative delta-delta Ct method using data obtained from RT-qPCR experiments, was analysed using one-way ANOVAs using Prism 8 (GraphPad, California, USA).

4.3 Results

4.3.1 Rats show contextual fear conditioning and extinction of fear memory

Foot shock (US) induced the normal rodent fear response (Figure 4.2). Before the delivery of a US, rats exhibited normal exploratory behaviour and spent the majority of their time moving around the box or grooming. Post-US subjects displayed little to no exploratory behaviour or grooming; instead they displayed classic freezing behaviour (conditioned response, CR) for the majority of the one minute they remained in the box, $F_{(1,23)} = 1310.298$, $p < 0.0001$, repeated-measures ANOVA. Rats reexposed to the context 48 hours later exhibited greater freezing behaviour than they did before receiving the shock, $F_{(1,16)} = 165.293$, $p < 0.0001$, repeated-measures ANOVA. However, freezing behaviour following two minute reexposure was lower than immediately following the shock, $F_{(1,16)} = 9.983$, $p < 0.001$, repeated-measures ANOVA. Freezing was lower following ten minute reexposure to the context compared to the first two minutes of reexposure, $F_{(1,7)} = 99.556$, $p < 0.0001$, repeated-measures ANOVA (Figure 4.2).

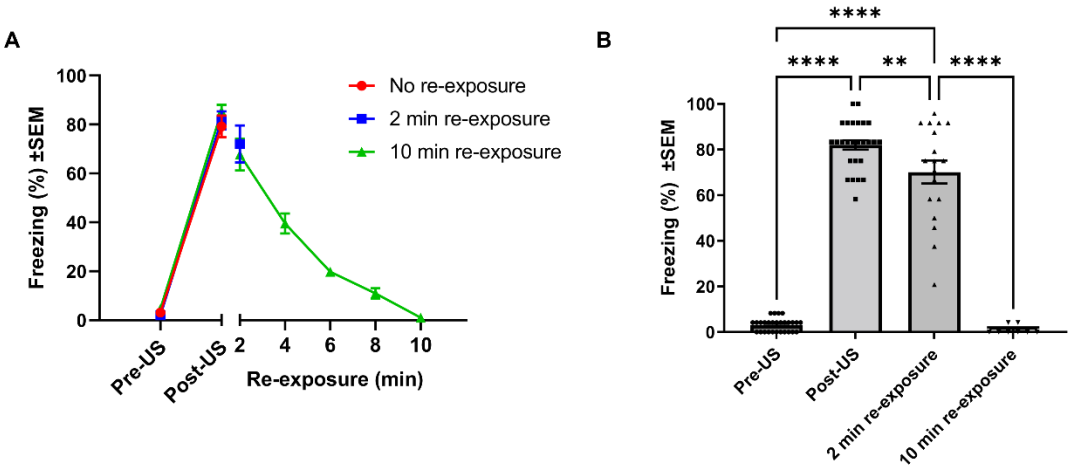

Figure 4.2 – The retrieval and extinction of a contextual fear memories in rat. Subjects froze immediately following a single unconditioned shock in the context. 48 hours post-initial shock rats returned to the context froze initially. Freezing behaviour returned to pre-shock levels after 10 minutes re-exposure to the context. Panel B combines percentage freezing for all three experimental groups, the same changes were observed if each group was analysed separately (Appendix 5). ** denotes 0.001. **** denotes 0.0001.

4.3.2 Micro-tissue punches produce viable RNA for use in RT-qPCR

Micro-tissue punches are not routinely employed in RT-qPCR. Therefore, before experiments progressed, RNA extraction and cDNA synthesis from tissues in the sub-milligram range was optimised and validated. Two RNA extraction kits were compared (both from QIAGEN, Venlo, Netherlands); one designed for a maximum sample size of <30 mg and the other for a sample size of <5 mg. RNA was successfully extracted from CA1 punches by both kits (Figure 4.3). As a comparison, RNA was also extracted from grossly dissected hippocampus using the <30 mg kit. Concentrations of extracted RNA differed between the three different conditions ($F_{(2,230)}$ = 243.3, p <0.0001, ANOVA) (Figure 4.3). Tukey's multiple comparisons revealed no difference in the concentrations obtained from punches using <5mg or <30 mg kits, p = 0.9189. RNA extraction from punches using both kits resulted in lower concentrations than extraction from grossly dissected tissue (<5 mg kit: p <0.0001, <30 mg kit: p <0.0001, Tukey's multiple comparisons). The purity (A260/A280 value) of extracted RNA, whilst differing between the two kits, $F_{(2,131)}$ = 7.562, p = 0.0008, ANOVA (Figure 4.4.), still fell within the acceptable range of 2.0 ± 0.1. The extraction kit designed for <30mg starting tissue was used for all subsequent RNA extractions, due to its lower price and availability from suppliers.

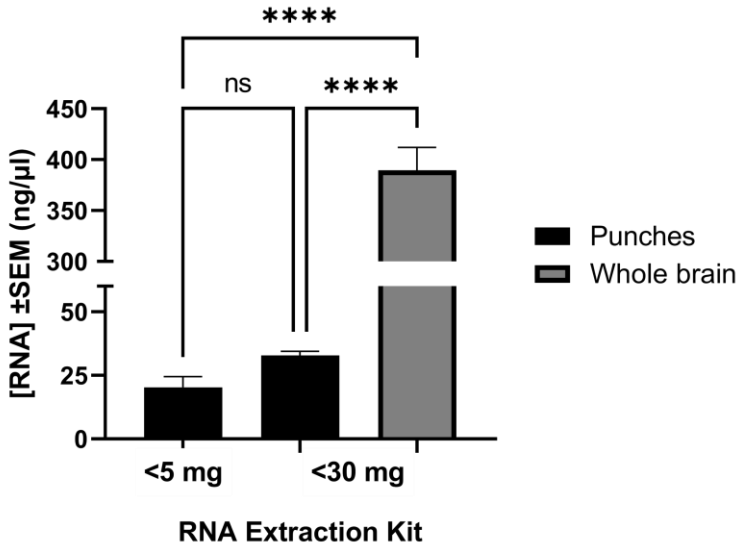

Figure 4.3 – Comparison of RNA extraction kits. RNA extraction from whole brain using the <30 mg kit yielded higher RNA concentrations than from punches. No concentration differences were observed in RNA extracted from punches using the two kits. **** denotes p <0.0001.

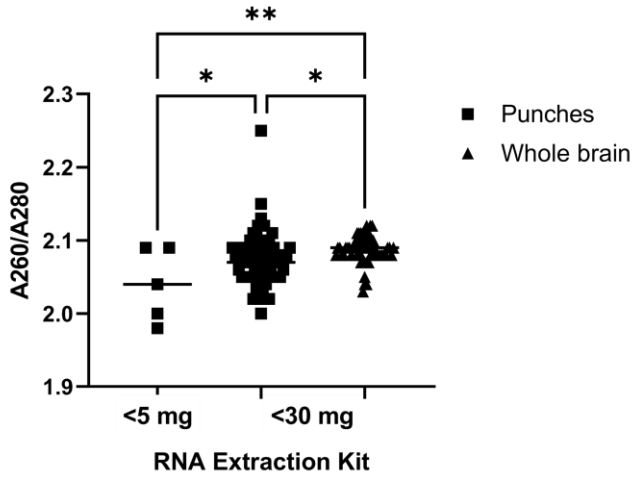

Figure 4.4 – Validation of RNA extraction kits. RNA integrity (A260/A280) was varied based upon RNA extraction kit or source of starting tissue. Despite the variance in RNA integrity the average A260/A280 remained with the acceptable range of 2.0 ± 0.1 across all thee conditions. * denotes p <0.05. ** denotes p <0.01.

The number of punches collected from the hippocampus or the mPFC, within the range that can be obtained from a region of interest in subsequent experiments (2 to 6), does not influence the concentration of extracted RNA, $F_{(3, 84)} = 1.599$, $p = 0.1957$, ANOVA (Figure 4.5). Furthermore, there is no effect of punch location (hippocampus versus mPFC) upon the concentration of RNA extracted from punches $F_{(4, 85)} = 1.603$, $p = 0.1811$, ANOVA (Figure 4.6).

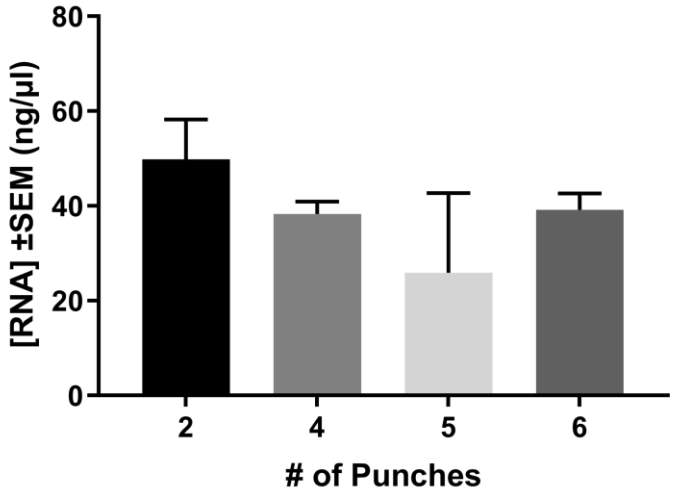

Figure 4.5 – The number of micro-tissue punches; within the range used in subsequent experiments, has no effect upon the RNA concentration obtained during extraction.

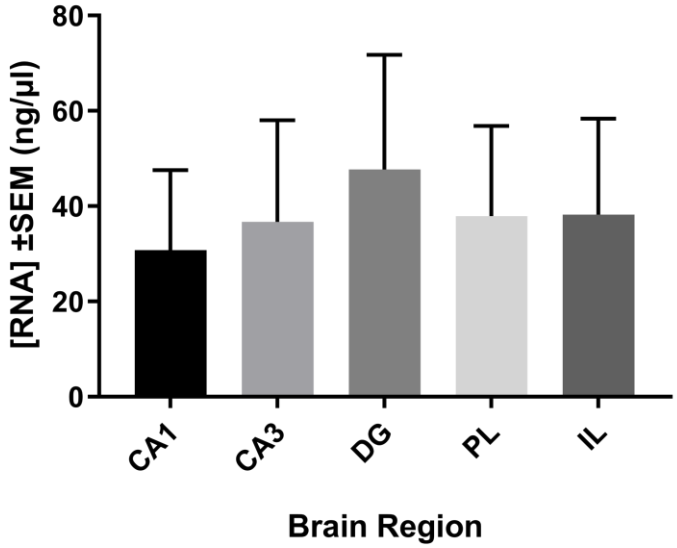

Figure 4.6 – The brain subregion micro-tissue punches are taken from for RNA extraction has no effect upon the RNA concentration obtained.

Due to the relatively low yields of RNA obtained from micro-tissue punches (typically 10-30 ng/µl), a result of the limited the amount of RNA that can be extracted from a small amount of starting tissue, the concentration of RNA used for cDNA synthesis was reduced from the standard 75 ng/µl to 10 ng/µl. A reduction in the amount of RNA used in cDNA synthesis had no effect upon Ct values produced by probes for moderately expressed genes such as *C1q*, compared to cDNA synthesised using 75 ng/µl RNA, $t_{(44)} = 1.801$, p 0.0786, unpaired t-test (Figure 4.7). However, cytokine genes such as *IL1β* and *IL6* were not detectable in cDNA synthesised from 10 ng/µl of RNA, but are detectable in cDNA produced from higher RNA concentrations. Despite this limitation preventing the measurement of cytokine gene expressional changes following the retrieval and/or extinction of a CFM, the ability of tissue punches to provide precise subregional specificity meant it was used for all subsequent RT-qPCR experiments examining changes in the expression of complement system associated genes.

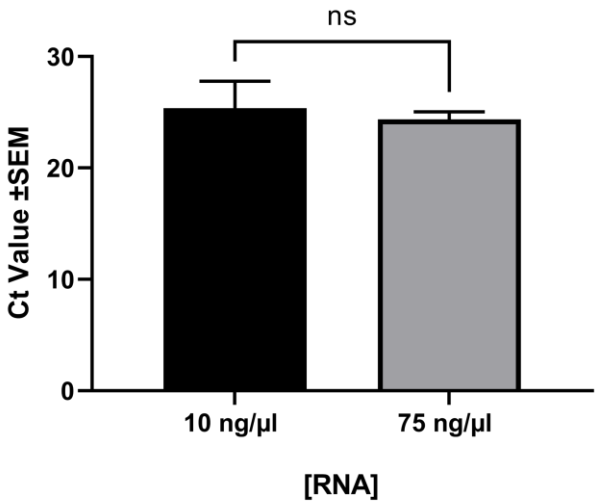

Figure 4.7 – No difference is observable in Ct values obtained from RT-qPCR experiments using probes for C1qA and cDNA synthesised from either 10 ng/µl or 75 ng/µl stock RNA extracted from grossly dissected hippocampus.

4.3.3 RT-qPCR can be used to detect gene expression changes in micro-tissue punches

The expression of the IEG *Arc* has previously been shown to alter following the recall and extinction of CFM in the hippocampus and mPFC (Tayler *et al.*, 2013; Lee *et al.*, 2016; Zhu *et al.*, 2018). The expression of *Arc* was quantified using RT-qPCR in all three experimental groups (no reexposure, two-minute reexposure and ten-minute reexposure) across the five subregions (hippocampus: CA1, CA3 and DG, mPFC: PL and IL) in order to validate that cDNA synthesised from micro-tissue punches can be used to detect changes in the expression of mRNA. The expression of *Arc* mRNA was not altered between experimental groups in the hippocampal subregions CA1 ($F_{(2,18)} = 1.403$, $p = 0.2714$, ANOVA) and CA3 $F_{(2,20)} = 0.3672$, $p = 0.6972$, ANOVA) (Figure 4.8). In the DG there was a group effect, $F_{(2,17)} = 3.725$, $p = 0.0456$, ANOVA, with a trend towards increased expression of *Arc* following 10 min reexposure (no reexposure: $p = 0.0725$, two minute: reexposure $p = 0.0795$). *Arc* mRNA expression increased in the PL and IL sub-regions of the mPFCs of rats (PL: $F_{(2,18)} = 3.592$, $p = 0.0487$, ANOVA IL: PL: $F_{(2,18)} = 9.474$, $p = 0.0015$, ANOVA). This was shown as an increase in the two-minute reexposure compared to no reexposure group.

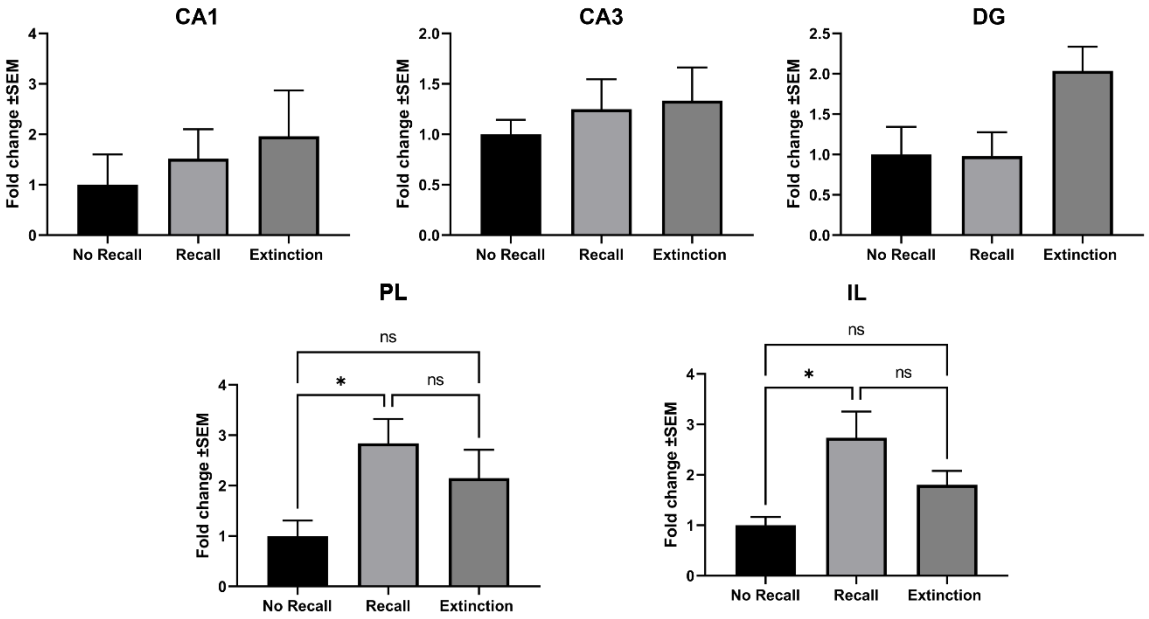

Figure 4.8 – The expression of immediate early gene Arc in hippocampal sub-regions: CA1, CA3 and DG, does not alter following the recall or extinction of contextual fear memory. The recall of contextual fear memory increases expression of Arc in the PL and IL cortices of the mPFC. * denotes $P < 0.05$. No recall and Extinction (n = 8). Recall (n = 10).

4.3.4 The expression of complement-associated genes was regulated in a region-specific manner following reexposure to the conditioned context

4.3.4.1 *C1qA*

The expression of *C1qA* following two-minute, ten-minute or no reexposure to a context associated with foot shock measured using RT-qPCR showed no effect of behavioural group on the levels of *C1qA* mRNA in the CA1 ($F_{(2,19)}$ = 0.004159, p = 0.9959, ANOVA), CA3 ($F_{(2,21)}$ = 0.03196, p = 0.9686, ANOVA), DG ($F_{(2,20)}$ = 0.7003, p = 0.5082), PL ($F_{(2,18)}$ = 2.495, p = 0.1105, ANOVA) and IL ($F_{(2,19)}$ = 0.07983, p = 0.9236, ANOVA) (Figure 4.9).

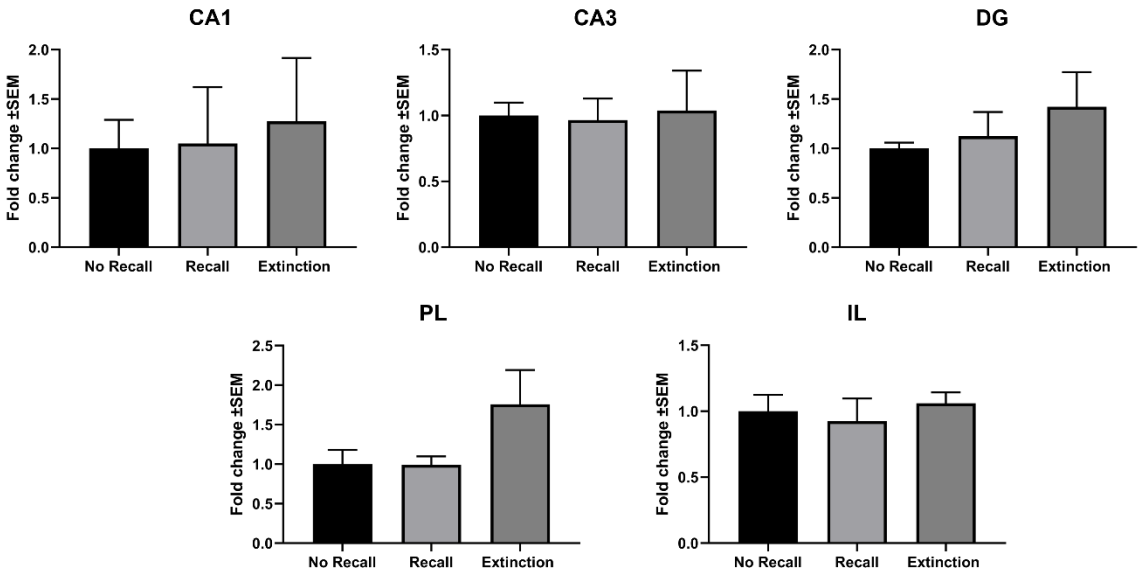

Figure 4.9 – C1qA expression in hippocampal subregions: CA1, CA3 and DC or the mPFC subregions PL and IL, did not alter following the recall or extinction of contextual fear memory. No recall and Extinction (n = 8). Recall (n = 10).

4.3.4.2 *C3*

No difference in the expression of *C3* mRNA was observed across groups in any of the hippocampal (CA1: $F_{(2,21)} = 1.711$, $p = 0.2049$, ANOVA, CA3: $F_{(2,21)} = 1.007$, $p = 0.3839$, ANOVA, DG: $F_{(2,21)} = 0.9210$, $p = 0.4136$, ANOVA) and mPFC (PL: $F_{(2,17)} = 0.5372$, $p = 0.5940$, ANOVA, IL: $F_{(2,20)} = 0.06854$, $p = 0.9340$, ANOVA) subregions (Figure 4.10).

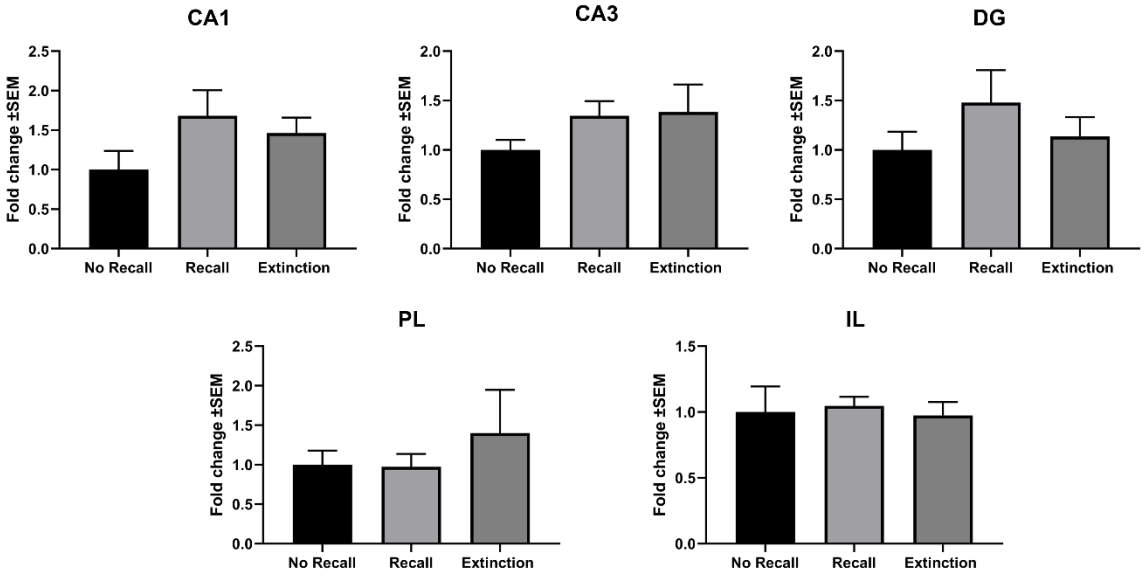

Figure 4.10 – C3 expression in hippocampal subregions: CA1, CA3 and DC or the mPFC subregions PL and IL, did not alter following the recall or extinction of contextual fear memory. No recall and Extinction (n = 8). Recall (n = 10).

4.3.4.3 C3aR

The expression of C3aR differed across groups in the CA1 ($F_{(2,14)}$ = 12.50, p = 0.0008, ANOVA) and multiple comparisons revealed a decrease in expression following two minute reexposure compared to ten minute (p = 0.0182) and no reexposure (p = 0.0006). No difference in expression was observed between ten minute and two-minute reexposure groups (p = 0.0840). No differences in C3aR expression were observed between groups in the CA3 ($F_{(2,16)}$ = 0.6702, p = 0.5254, ANOVA), DG ($F_{(2,15)}$ = 1.444, p = 0.2670, ANOVA), PL ($F_{(2,14)}$ = 0.04539, p = 0.9558, ANOVA) and IL ($F_{(2,18)}$ = 3.257, p = 0.0621, ANOVA) (Figure 4.11).

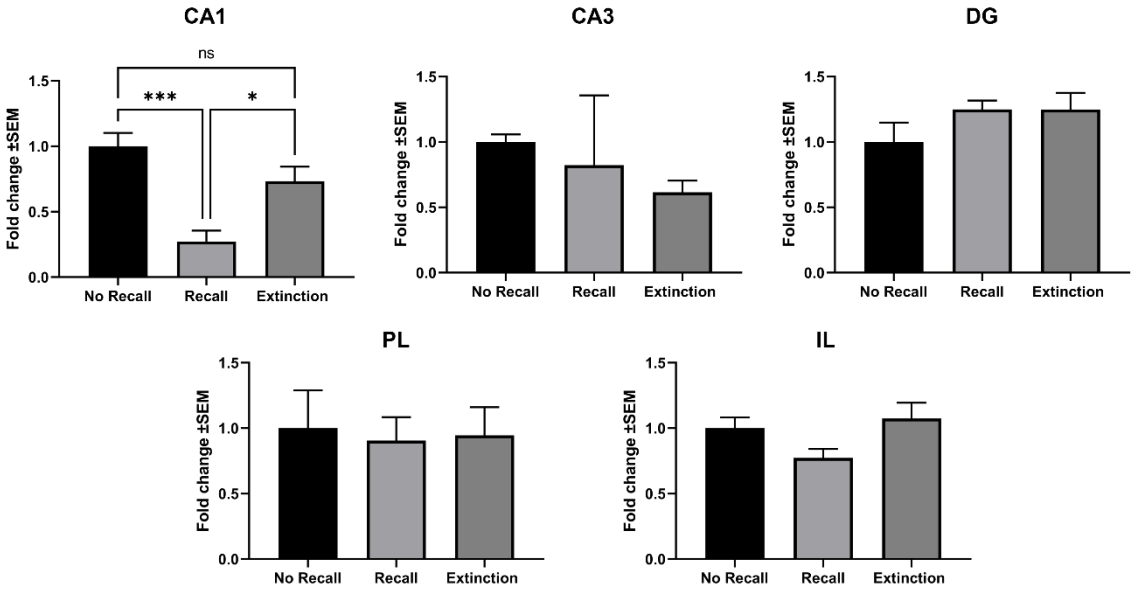

Figure 4.11 – The recall of contextual fear memory was associated with decreased expression of C3aR in the CA1 subregion of the hippocampus. * denotes p < 0.05. *** denotes p < 0.001. No recall and Extinction (n = 8). Recall (n = 10).

4.3.4.4 CSMD1

No differences in the expression of CSMD1 mRNA were observed across groups in any of the hippocampal (CA1: $F_{(2,19)} = 0.3114$, $p = 0.7361$, ANOVA, CA3: $F_{(2,21)} = 0.9139$, $p = 0.4163$, ANOVA, DG: $F_{(2,21)} = 0.2313$, $p = 0.7955$, ANOVA) and mPFC (PL: $F_{(2,15)} = 1.472$, $p = 0.260$, ANOVA, IL: $F_{(2,20)} = 0.3817$, $p = 0.6876$, ANOVA) subregions (Figure 4.12).

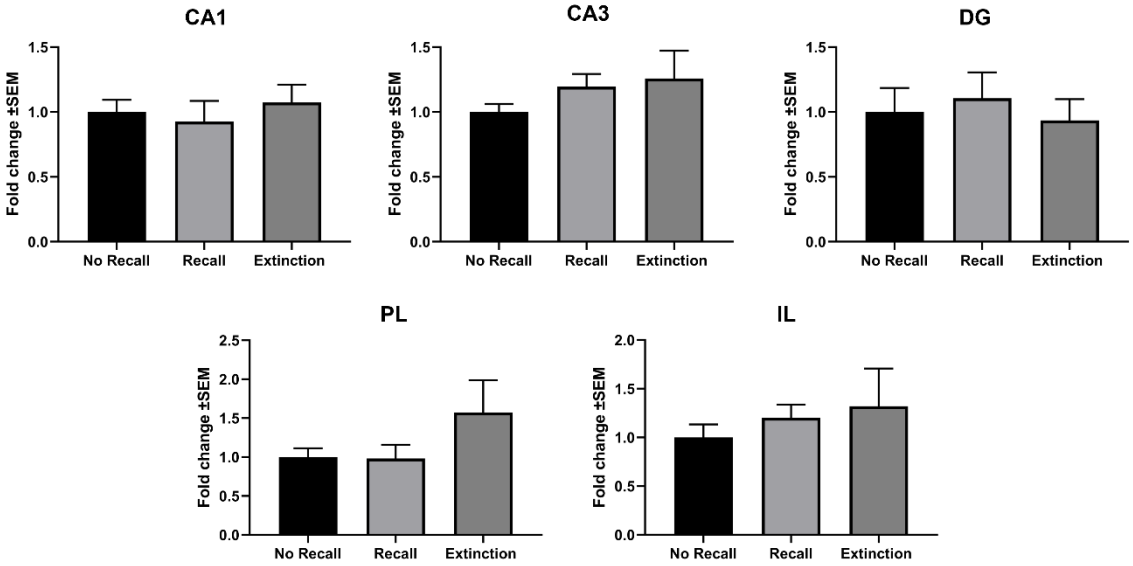

Figure 4.12 – CSMD1 expression in hippocampal subregions: CA1, CA3 and DC or the mPFC subregions PL and IL, did not alter following the recall or extinction of contextual fear memory. No recall and Extinction (n = 8). Recall (n = 10).

4.3.4.5 C4

The expression of C4 was not measured in this experiment as all probes designed using the method described previously produced extremely high Ct values (>40) or no signal at all. In response to these issues, a custom probe was sourced from PrimerDesign (Southampton, UK). However, these primers appear to form primer dimers, as evidenced by the signal in negative control wells (data not shown).

4.4 Discussion

The differential expression of complement associated genes following the recall and/or extinction of CFM was accessed across three hippocampal and two mPFC subregions using RT-qPCR. The ability of the micro-tissue punch technique to achieve subregional specificity and to detect changes in gene expression, was successfully validated using the IEG Arc. Arc expression was observed to increase in the PL and IL cortices of the mPFC following a two-minute reexposure (recall) to the context compared to rats not reexposed to the context. Of the complement associated genes examined, only C3aR showed any change in expression following the recall or extinction of CFM. C3aR expression decreased following a two-minute reexposure to the context (recall) in the CA1 subregion of the hippocampus.

4.4.1 Subjects exhibited the recall and/or extinction of contextual fear memory

Rats displayed robust contextual fear conditioning. Following being exposed to a fearful stimulus (foot shock) in a novel context (conditioning chamber), the rats exhibited fear induced freezing. After being returned to the context, rats recalled the association of the context (conditioned stimulus) with a foot shock (unconditioned stimulus) and froze (conditioned response). However, after prolonged exposure to the conditioned stimulus, the conditioned fear response was attenuated (rats no longer froze in the context). This within session extinction is indexed by the loss of the freezing response to the context represented by the acquisition of a new (extinction) memory: that the context is associated with a fear adverse stimulus i.e., a footshock (Bouton, 2004). This new memory engram for the context out competes the previous one that the box is fearful. However, the former engram is not erased.

Rats who have undergone extinction if returned to the original context and given a subthreshold shock (one that in a naïve rat would not induce freezing), will give salience to fearful association and begin freezing again within the context (Lee, Milton and Everitt, 2006; Deschaux, Motanis, *et al.*, 2011; Deschaux, Spennato, *et al.*, 2011; Williams and Lattal, 2019). In our experiments we do not test whether subjects have a long-term extinction memory, as they were culled shortly after undergoing extinction learning. However previous work using the same extinction paradigm has repeatedly shown the loss of the CR in subsequent reexposures to the context following the acquisition of extinction memory. Therefore, we can conclude that the two-minute reexposure is likely to initiate CFM restabilisation or protein synthesis-dependent mechanisms that prevent extinction (destabilisation), and that a ten-minute reexposure initiated LTP-dependent extinction (Lee, 2009; Trent *et al.*, 2015, 2017).

The CFC paradigm selected for use in these experiments was chosen to match the experimental design of Scholz et al., (2016) as closely as possible, including the time post-reexposure that animals were sacrificed (two hours). Scholz et al., (2016), using a microarray, had previously measured changes in expression of complement associated genes in the CA1 subregion of the hippocampus (Table 4.2). Generating tissue using the same behavioural paradigm as Scholz et al., (2016), we aimed to validate their findings in the CA1 and expand the areas being examined to other hippocampal subregions (CA3 and DG) and mPFC subregions (PL and IL), which, like the CA1, have been shown to play an essential role in the CFM retrieval-initiated processes: re-consolidation and extinction (Maren, Phan and Liberzon, 2013; Giustino and Maren, 2015a; Raber *et al.*, 2019; Kim and Cho, 2020).

4.4.2 Micro-tissue punches can provide subregional specificity in RT-qPCR experiments

Micro-tissue punches gave RT-qPCR experiments subregional specificity that would have been unobtainable using conventional gross dissection methods; particularly for smaller regions such as the CA3 and pre-frontal cortical subregions. Due to the lower amounts of tissue collected using the punching method (~ 2-5 mg) compared to grossly dissected tissue (~ 10-20 mg), RNA extraction yielded lower concentrations of RNA. Subsequent analysis revealed that despite the lower yield, RNA extracted from punches was of comparable quality and purity to RNA extracted from larger sections of the hippocampus. Furthermore, the Ct values obtained using cDNA synthesised using RNA punches and probes for a gene with moderate expression levels, such as C1qA, were equivalent to Ct values produced using cDNA synthesised from grossly dissected hippocampi. This may appear surprising since there is ~90% reduction in the amount of 'starting material' however, the equivalency in average Ct values obtained most likely arises due to biological variability masking the expected 1.5-2 difference expected in Ct values between cDNA obtained from punches versus grossly dissected hippocampi. Genes with lower basal expression, such as the inflammatory cytokines IL1β and IL6, were not detectable in cDNA prepared from tissue punches obtained from healthy adult rats, but were detectable in samples derived from grossly dissected tissue obtained from healthy adult rats, albeit with very high Ct values (>37). The reason for the lack of signal from probes targeting cytokines is not completely clear. It is not purely due to a lack of enough starting material; if punches are pooled to a weight equivalent to grossly dissected tissue, then probes for IL1β and IL6 still produce no meaningful signal. The nature of

punches themselves might play a role in the lack of cytokine signal, due to their small individual size and the protracted process by which punches are obtained and RNA extracted; including several freeze thaw steps during punching and upwards of three hours at room temperature during extraction, is more liable to degradation, thus lowering RNA yields (Copois et al., 2007; Gayral et al., 2011). Future experiments could begin by measuring the RNA integrity number of RNA extracted from tissue punches to assess unambiguously the integrity of RNA obtained, and compared to the integrities of RNA extracted from grossly dissected hippocampi (Schroeder *et al.*, 2006). Following validation of the integrity of RNA extracted from micro-tissue punches, steps could be taken to mitigate any potential degradation by disrupting the punches immediately post-collection instead of freezing them, and performing tissue disruption on a different day. Alternatively, punches could be frozen post-collection but stored in RNA*later* (Thermo Fisher Scientific, Massachusetts, USA) solution to stabilise and protect RNA from degradation.

4.4.3 Arc expression in the mPFC increases following the retrieval of a contextual fear memory

Despite the issues associated with the tissue punch methodology, its unique ability to provide very fine regional specificity to RT-qPCR meant it was used for all experiments in this chapter. However, due to the novelty of using tissue micro-punches to obtain RNA/cDNA for use in RT-qPCR experiments, we sought confirmation that gene expression changes could be measured in RNA extracted from punches. The immediate early gene Arc was selected to confirm the efficacy of RT-qPCR experiments utilising tissue punches, as both the literature and Chapter 3 provide evidence that its expression is altered during CFC and following recall

(particularly in the hippocampus) (Huff *et al.*, 2006; Hudgins and Otto, 2019). Arc expression was found to increase in the pre-frontal cortical subregions PL and IL following the retrieval of a contextual fear memory. No changes were observed following the extinction of a fear memory or in the hippocampus (Figure 4.8). The increases in Arc expression observed here in the mPFC following CFM retrieval contrasts with the changes in Arc protein levels observed in Chapter 3, where increases in Arc were reported in the molecular layer of the DG following the extinction of a CFM. The two experiments examined Arc at different timepoints post-reexposure (RT-qPCR at two hours and IHC at one hour) which could explain the disconnect between the RNA and protein level findings presented here. Additionally, the differences occurred in two different regions of interest; mRNA (mPFC: PL and IL cortices) and protein (hippocampus: CA1 and CA3), which could represent temporal differences in *Arc* expression in the two regions with the mPFC having delayed and/or prolonged increases in *Arc* expression post-retrieval compared to the cornu ammonis subfields of the hippocampus. Previously, evidence has been presented of a similar temporal disconnect in *Arc* expression within the hippocampus with the DG exhibiting sustained expression compared to the CA1 and CA3 (Guzowski *et al.*, 2001; Ramirez-Amaya *et al.*, 2013). These findings warrant further investigation. Using RNA extracted from brains collected one-hour post-reexposure would enable us to match the timepoint used in Chapter 3's IHC experiments. However, in the context of this and subsequent chapters, the *Arc* changes observed in the RT-qPCR experiments stated here are presented primarily to validate the micro-tissue punch methodology, by showing that they cannot only measure changes in *Arc* expression, which we know is activity dependent, but also the expression changes in terms of

time direction and spatial locations as expected (Minatohara, Akiyoshi and Okuno, 2016).

4.4.3 The recall and extinction of fear memory regulates the expression of complement associated genes

Five regions of interest were selected, in which to measure changes in complement system associated genes (*C1qA*, *C3*, *C3aR1* and *CSMD1*), to match in the case of CA1 the experiments of Scholz et al., (2016) and in regions associated with changes post-retrieval or extinction of IEG expression (CA3, DG, PL, and IL) identified in Chapter 3. *C3aR* expression was decreased in the CA1 region of the hippocampus two hours post-retrieval of a CFM (two-minute reexposure), corroborating the findings of Scholz et al., (2016), using microarray analysis. *C3aR* expression was not altered following CFM retrieval in any other regions of interest. Additionally, no changes in *C3aR* expression were observed in subjects assigned to the Extinction group (ten-minute reexposure). No other complement gene included in the RT-qPCR experiments showed any significant alterations in expression in any behavioural group or subregion; which is not consistent with the findings of Scholz et al., (2016), who identified decreased expression of *C1qA* and *C3* following retrieval of a CFM in the CA1. The discordance between our findings and those of Scholz et al., (2016) could reflect a power issue in our experiments, along with the intrinsic limitations of RT-qPCR sensitivity and its ability to detect small changes in expression due to biological variability.

C3aR is expressed by hippocampal neurons, astrocytes, and microglia (Davoust *et al.*, 1999; O'Barr *et al.*, 2001). The role of the immune system in

regulating fear behaviour is not novel. Peripheral administration of immunogens such as LPS or intracerebroventricular treatment with IL1β, at moderate doses, induce the same behavioural phenotype of decreased freezing upon return to the context (Pugh *et al.*, 1998; Pugh, 1999). IL1β along with other cytokines such as IL6 and TNFα, have been shown to attenuate consolidation of fear memories which is thought to be due to their ability to impair hippocampal LTP and the necessity of basal IL1β for plasticity and hippocampal-dependent memory performance (Cunningham *et al.*, 1996; Vereker, O'Donnell and Lynch, 2000a; Yirmiya, 2002; Barrientos *et al.*, 2009a, 2009b; Hao *et al.*, 2014; Yu *et al.*, 2017a; Lyra e Silva *et al.*, 2021). C3aR's ability to regulate the production of cytokines such as IL1β, TNFα, IL6 and prostaglandin E_2 (PGE2) could provide explanations as to why its expression is altered following the retrieval of a fear memory (Coulthard and Woodruff, 2015). Mice genetically lacking *C3aR* display an innate anxiety phenotype and increased production of corticosterone compared to WT mice, when placed on an elevated plus maze (Westacott *et al.*, 2022). The mechanism for why receptor knockout animals display this phenotype is unknown and could be the effect of a developmental defect, but this data gives credence to *C3aR* being associated with behavioural processes.

Both C1q and C3 have previously been implicated in cognitive performance in 'healthy' adult animals, following pathogenic disease and in aged animals (Figueiredo et al., 2019; Perez-Alcazar et al., 2014; Shi et al., 2015; Stephan et al., 2013; Vasek et al., 2016). For example, aged mice lacking *C3* show increased freezing upon return to the context for three-minutes compared to WT mice. However, as with studies involving $C3aR^{-/-}$ mice, the precise role of C3 in cognitive function is muddled as the changes in behaviour could be rooted in developmental

deficits (Shi et al., 2015). Taken together, this body evidence implicates the complement cascade as having a specific role in reversal learning, which, like extinction, is essential for cognitive flexibility. In order to achieve this complement activity could be driving the elimination of glutamatergic synapses in an activity dependent manner during these learning events, processes which have previously been shown to occur during postnatal development in the CNS (Rosa C. Paolicelli *et al.*, 2011a; Schafer *et al.*, 2012; Zhan *et al.*, 2014a). There is also growing evidence that extinction is associated with changes in dendritic spines which, like activity dependent pruning, are processes that the complement system has been shown to facilitate following irradiation and in a mouse model of AD (Lai, Franke and Gan, 2012; Lai, Adler and Gan, 2018; Merlini *et al.*, 2019). Furthermore, complement ability to exert control over learning and memory may not just be limited to synaptic elimination given growing evidence of the neuroimmune system's, and by extension, complement's ability to remodel the ECM and promote AMPA receptor internalisation, which in turn are associated with alterations in synaptic plasticity (Xu *et al.*, 2019; Nguyen *et al.*, 2020b). The hippocampal (CA1) decrease we observed in *C3aR* with two-minute recall may be indicative of a mechanism associated with memory preservation or perhaps retrieval, but not extinction. Potentially, the reduction in *C3aR* expression 'turns down' the constitutive phagocytosis of synapses and thus promote the retention of fear memories. In order to test this hypothesis further, experiments could utilise acute doses of C3aR antagonists (such as SB290157) and/or agonists (such as SQ110–4) administered before conditioned animals are returned to the context (Bellows-Peterson *et al.*, 2012; Lee, Taylor and Woodruff, 2020). These proposed experiments would establish whether the *C3aR*$^{-/-}$

induced fear memory retrieval deficits are developmental in origin, or instead are the result of the C3a/C3aR signalling axis being pivotal in the maintenance of fear memories and, potentially, the inhibition of extinction.

The lack of any changes in any other complement associated genes indicates that the processes facilitating the expression or extinction of a CFM are not dependent upon changes in the expression of complement system components at the two-hour post-reexposure we examined. However, it does not rule out complement's role in the synaptic pruning associated with associative learning (Mendez *et al.*, 2018). The low-grade local activation of the complement system that could underlie this synaptic pruning may not have been detectable with the experimental design used in this chapter. The hallmark of complement activation is the generation of the C3 cleavage products such as iC3b and C3d, which could be examined in regions associated with CFC and may provide an answer to whether complement system is activated during CFM retrieval and/or extinction. Furthermore, we have only a snapshot of expression at two-hours post-reexposure, limited to five regions of interest. Experiments in the future examining complement expression at different time points and in other brain regions associated with CFC expression and extinction; such as the amygdala, could uncover the precise spatiotemporal dynamics of complement's purported role in associative learning. Furthermore, the RT-qPCR experiments we performed are underpowered (G*Power analysis estimates a group size of 22 is required for a small effect size: f = 0.4), so further experiments designed to expand group sizes could uncover further changes in complement expression, particularly in the PL cortex during extension where trends for increases in C1qA, C3 and CSMD1 were observed.

4.4.4 Schizophrenia associated complement gene CSMD1 did not change in expression following the retrieval of contextual fear memory

The experiments in this chapter attempted to establish whether the two-complement system associated genes *C4* and *CSMD1*; that have been implicated in the aetiology of SZ, have differential expression following the retrieval or extinction of a CFM (Ripke, 2011; Sekar *et al.*, 2016). Both genes were not included in the microarray used by Scholz et al., (2016). However, given their association with SZ risk and SZ patients presenting with associative learning deficits, it was deemed prudent to include the two genes in RT-qPCR experiments (Diwadkar, Flaugher, Jones, Zalányi, Ujfalussy, Keshavan and Erdi, 2008; Hall, Romaniuk, Andrew M. McIntosh, *et al.*, 2009).

Several self-designed primers were trialled for C4 which either failed to produce a signal or had signal in the negative control (no cDNA). Following the failure of primers designed in-house, PrimerDesign (Southampton, UK) were tasked with designing and validating a set of probes targeting rat *C4*. Unfortunately, these commercial designed primers produced signals in negative control wells and therefore were not viable for use in further experiments. Despite not being able to measure whether *C4* expression changes during RT-qPCR experiments; based upon the results for *C1qA* and *C3*; genes for two other central complement components, we can make the prediction that ***C4's*** expression does not change during the retrieval or extinction of a CFM. C4 was not identified in Scholz et al., (2016) microarray as having altered expression following either the retrieval or extinction of a CFM, but was a gene of interest to us because of its implication in the etiology of SZ and the overexpression of *C4* in mice promoting anxiety and Y-maze

deficits (Sekar *et al.*, 2016; Yilmaz *et al.*, 2021). There is no biological evidence to explain why one component of the central complement cascade expression would alter without upstream (C1qA) or downstream (C3) components also changing. However, if validated *C4* primers were sourced in the future, further RT-qPCR experiments could be used to confirm this hypothesis.

Primers targeting *CSMD1* were successfully designed and validated. CSMD1 is proposed as a CNS specific complement regulator and a SNP within its gene has been associated with an increased risk for SZ (Ripke, 2011). Additionally, the same *CSMD1* SNP associated with SZ has also been associated with worsened cognitive ability, spatial and visual working memory, and strategy formation (Koiliari *et al.*, 2014). However, mouse models where CSMD1 activity has been disrupted, show limited changes in behaviour (Distler *et al.*, 2012; Steen *et al.*, 2013). In our experiments no differential expression of *CSMD1*; following the retrieval and/or extinction a CFM, was observed in the hippocampus or mPFC. This suggests that CSMD1's purported regulation of classical complement activation is not required in the retrieval of a fear memory or the updating of an existing fear memory (extinction) or at least at the two-hour post-reexposure timepoint used in this investigation (Kraus *et al.*, 2006).

4.5 Conclusions

The data presented in this chapter reveals that out of the five complement associated genes examined, only C3aR was shown be altered in expression in our CFC paradigm. C3aR expression was decreased in the CA1 following the retrieval of a CFM. This data supports previous work that showed the same changes in C3aR

expression in the CA1. This finding opens an avenue for further work to examine the precise role of the receptor in the recall of fear memory and joins a body of work implicating the role of the neuroimmune system in associative learning, the precise mechanisms of which are currently unknown.

Chapter 5: Semi-automated morphological analysis of microglia

5.1 Introduction

Microglia, the adult CNS tissue specific macrophages, have highly dynamic morphologies, which respond to alterations in the brain's immunological environment (Davalos *et al.*, 2005; Nimmerjahn, Kirchhoff and Helmchen, 2005b; Wake, Andrew J. Moorhouse, *et al.*, 2013). In the healthy and uninjured brain, microglia have a small soma, long extended branched processes and are referred to as ramified microglia. Ramified microglia are sometimes termed in the literature as 'non-activated'; however, this is a misnomer. Microglia in the healthy brain are constantly surveying their local environment with their processes, searching for immunological activators such as cellular debris, damage associated molecular patterns (DAMPs), pathogen associated molecular patterns (PAMPs) and pro-inflammatory cytokines, which signal a perturbance to the CNS homeostasis that microglia need to respond to. Microglia also respond to signals not typically considered immunogenic, such as ATP and glutamate (Domercq, Vázquez-Villoldo and Matute, 2013; Miyamoto *et al.*, 2013). Whilst these molecules are released following neuronal injury the ability of microglia to detect them may suggest a mechanism by which they monitor and support neural activity in the healthy adult brain. Historically, activated microglia were classified using the M1 or M2 phenotype. This taxonomy states that macrophages (including microglia) upon activation, initially adopt a M1 phenotype: phagocytic, deleterious and pro-inflammatory and then move along a spectrum to reach a M2 'neuroregenerative' phenotype. However, this taxonomy is flawed and a plethora of evidence has emerged to discredit the M1/M2 taxonomy. Microglial activation is

multidimensional and cannot be defined in such simple terms (Xue *et al.*, 2014). Microglial function post-activation is dynamic, context dependant and modulated by the lingering effects of prior activation (Norden, Muccigrosso and Godbout, 2015; Ransohoff, 2016; Jenna M. Ziebell *et al.*, 2017). A second nomenclature based upon microglial morphology is also prevalent in the literature. Unlike M1/M2 classification, this taxonomy includes ramified microglia and has the capacity for an infinite number of phenotypes to be included. Microglial morphology is an effective proxy for measuring the activation and functionality of microglia as their morphologies shift in a predictable fashion following activation. Upon encountering and recognising a stimulus, microglia undergo a morphological shift retracting their processes, decreasing complexity of processes, and enlarging their somas, adopting an 'activated' morphology (Kloss *et al.*, 2001) (Figure 5.1). During their transition from a ramified to an activated morphology, microglia adopt an intermediary morphology with a 'bushy' appearance, termed hyperramified. Often overlooked, perhaps due to their transitory nature, hyperramified microglia have an intermediary morphology between that of ramified and activated microglia, with multiple spiney processes and enlarged cell bodies. Chronic presence of pro-inflammatory stimuli and neuronal injury pushes microglia further along this path of activation, retracting their process further, becoming spherical and visually indistinguishable from peripheral macrophages (Ayoub and Salm, 2003) (Figure 5.2). Evidence for a new type of microglial activation termed 'dark' microglia has recently emerged; given the moniker 'dark' due to their condensed, electron-dense cytoplasm and nucleoplasm making them appear dark in colour like mitochondria. The current body of work surrounding dark microglia has shown them to be limited in number/non-existent in the healthy

brain and primarily emerge following prolonged neurodegeneration (Bisht *et al.*, 2016). Finally, a rare microglial morphology has been reported sporadically in the uninjured cortex and in greater numbers following a traumatic brain injury, termed rod microglia. These cells have a sausage shaped soma and in the injured brain, extremely polarised processes. Additionally, rod microglia align end to end, forming trains of microglia following neuronal projections and are hypothesised to play a role in the repair and remyelination of neurons post-injury (Taylor *et al.*, 2014).

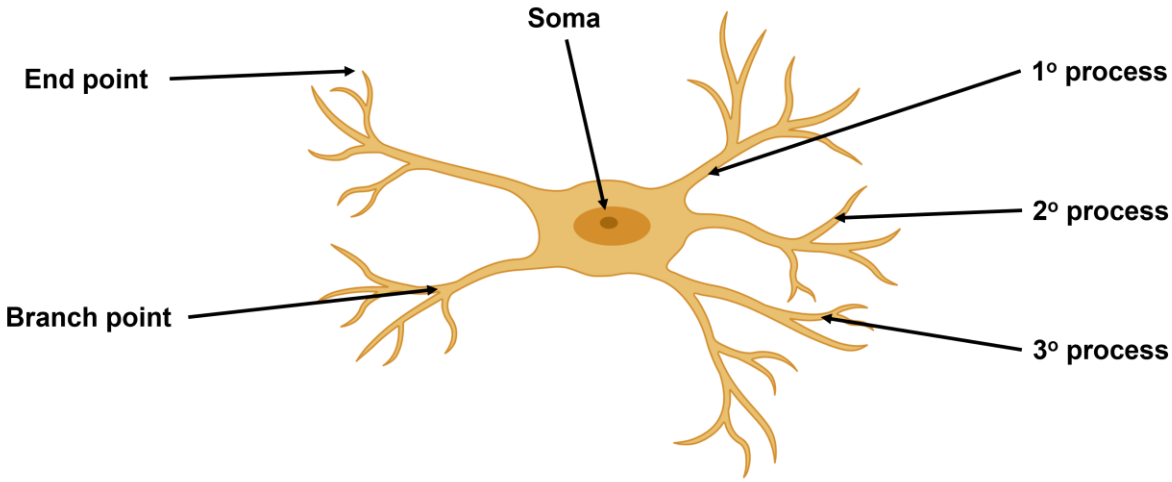

Figure 5.1 – Microglial anatomy. Primary processes emerge directly from the soma (cell body) of the microglia. Secondary processes branch off primary processes at branch points. Branching of secondary processes generates tertiary processes which terminate at end points.

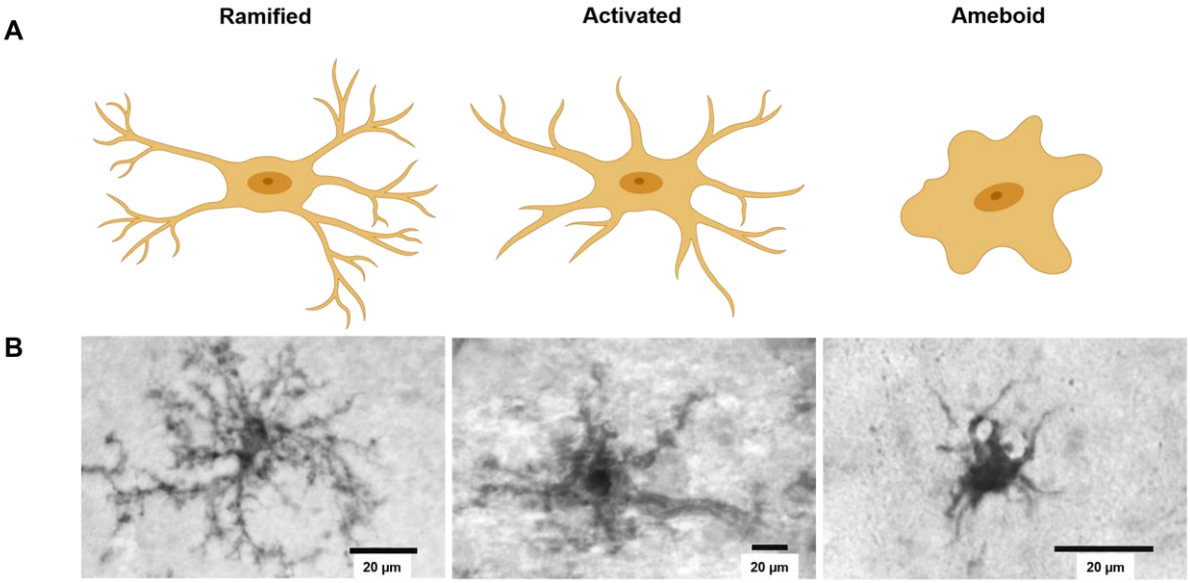

Figure 5.2 – Microglial morphology. **A.** Illustrations of the three most common microglial morphologies. Ramified microglia have long highly complex processes with many secondary and tertiary processes. Activated microglia have thicker, less ramified processes and a larger soma. Ameboid microglia have fully retracted processes with only a large soma remaining. **B.** Photomicrographs of single microglia in each of the three most common morphologies stained using isolectin-B4-HRP. Adapted from Ayoub et. al. (2003).

Experimentally, microglial activation can be achieved in rodents with a physical injury model (fluid percussion or controlled cortical impact) or a peripheral dose of an immunostimulant (LPS or polyinosinic:polycytidylic acid: poly I:C) (Cao *et al.*, 2012; Gibney *et al.*, 2013; Qin *et al.*, 2013). Adult rats receiving a single midline fluid percussion head injury have microglia with shorter processes on average, compared to sham injured rats at 1 day, 7 days and 28 days post-injury at the site of initial shockwave impact and in the S1BF (a region the shockwave travels through), but not in an area remote from the injury site. The decreased average processes length following an experimental TBI reflects microglia de-ramifying and adopting an activated morphology, which appears be retained for at least 28 days post-injury (Morrison *et al.*, 2017b). A single or repeated dosage of the immunostimulant LPS to juvenile or adult mice induces microglial activation throughout the entire brain, with the degree of activation being modulated by the number and strength of dosages and time post-treatment. A single 1.0 mg/kg intraperitoneal dose of LPS to P3 mice increases the number of microglia with an activated morphology, along with increased expression of proinflammatory markers at P6 (Pang *et al.*, 2016). Repeated doses of LPS (four 1.0 mg/kg intraperitoneal doses) in mice induces homogeneous microglial activation throughout the cortical and sub-cortical subregions. 24 hrs following the final LPS injection, microglia have universally adopted an ‘activated’ morphology. No ameboid microglia are present as this LPS treatment regime does not induce the threshold of neuronal injury required for this final stage of microglial activation (Chen *et al.*, 2012). Additionally, at this timepoint following LPS treatment, there is no increase in microglial proliferation; measured by 5-bromo-2’-deoxyuridine (BrdU) immunopositivity, compared to mice treated with

PBS. Physical injury models do not produce global activation; instead activated microglia are concentrated around the injury site and the resulting dying neurons. The morphological make up of microglia following an experimental traumatic brain injury is very heterogenous, with a mixture of ramified, activated, rod and amoeboid morphologies being present post-injury (Cao *et al.*, 2012).

Several methods have arisen to assess the morphology of microglia. *In vivo* live imaging using two-photon microscopy can be used to monitor dynamic changes in microglial morphology in real-time. (Nimmerjahn, Kirchhoff and Helmchen, 2005b) used a GFP-tagged microglia mouse line ($CX_3CR1^{GFP/+}$) and two-photon microscopy to show how ramified microglia in adult mouse neocortex are highly dynamic, continually surveying their microenvironment through the retraction and extension of their processes. Upon experimental BBB disruption with localised laser lesions, microglia in were shown to rapidly shift to an activated morphology and processes moving to engage with the damaged blood vessel. Whilst two-photon microscopy is very effective for monitoring even minuscule movements of microglial processes, morphological data is only gathered for a very small population of cells and the technique requires complex surgical procedures and specialised imaging hardware (Marker *et al.*, 2010; Nimmerjahn, 2012). Sampling microglial morphology across a larger number of cells than two-photon imaging requires the sectioning of GFP-tagged microglia brains or IHC staining of brain sections using a pan-microglial marker such as IBA1, which are then imaged using a confocal microscopy to capture 3D dimensional images containing hundreds of microglia from regions of interest. Manual classification of microglia in these images by an independent observer of microglia into morphological groups allows for hundreds of microglia to be sampled

per animal. This method is both time consuming and requires verification by at least one independent observer to avoid bias and reduce observer variability. Based upon our prior experience with manual classification, no matter how well written criteria and applied the classifications are, there will always be an element of subjectivity and the potential for variability in data produced by this method of morphological analysis. To overcome some of these issues, manual and semi-automated tracing of microglia with subsequent automated measurement of morphological parameters, using software packages such as IMARIS (Oxford Instruments, Oxfordshire, UK) and Neurolucida® 360 (MBF Bioscience, Vermont, USA), are currently being used and are considered the gold standard for assessing microglial morphology *in vivo* (Kongsui *et al.*, 2014; García-Magro *et al.*, 2020). Methods employing tracing entail less subjectivity than manual classification but have caveats. These methods require the manual selection of microglia to be traced, which may introduce bias into analyses, particularly as the user often favours isolated and less complex cells that are easier for the software to trace. Additionally, the software packages required for tracing are extremely costly (~ £10,000, circa 2021) and require dedicated high-end computer hardware.

In response to cost, time, and bias issues with the existing methods of morphological analysis, York et al., (2018) have developed 3DMorph - a free and open-source MATLAB (MathWorks, Massachusetts, USA) based script which analyses morphology from 3D images of microglia. 3DMorph allows for rapid analysis of microglia morphology and is infinitely scalable. The software requires the user to set signal thresholds, minimum and maximum cell sizes for one image. The same parameters can then be used to facilitate completely automated and unbiased

gathering of cells' morphological parameters from additional images. Output data from 3DMorph includes cell volume, cell territory volume, ramification index, branch lengths, number of endpoints, and number of branch points (Figure 5.2). Several research groups have successfully used 3DMorph to quantify microglial morphological changes in their experimental paradigms. Fernández-Arjona, et. al. (2019) employed 3DMorph to show that morphological parameters correlate with expression level of lL1β (Fernández-Arjona *et al.*, 2019). (Bernier, Bohlen, York, Choi, Kamyabi, Dissing-Olesen, Hefendehl, Collins, Stevens and Barres, 2019), using 3DMorph, showed that manipulation of cAMP in microglia can alter their morphological parameters. Both these studies used the 'off the shelf' version of 3DMorph and measured between 10 and 20 microglia per animal to produce the findings they report.

The experiments in this chapter attempted to implement 3DMorph's semi-automated collection of microglial morphological data and to scale up the amount of microglia sampled by 3DMorph compared to previous studies using the software. Developing 3DMorph into a high throughput quantitative analysis tool required the optimisation of semi-automated confocal image acquisition and the modification of 3DMorph to remove graphical user interfaces enabling it to be run on Cardiff University's Hawk high-performance computing cluster. Additionally, the experiments in the chapter also attempted to develop a fully automated unbiased method of analysing morphological data generated by 3DMorph using machine learning. The goal of this analysis at this early stage was to binarily classify microglial based upon morphological parameters as either ramified or activated. Machine learning has previously been successfully employed for similar morphological classification

biological problems. Li et al., (2018) used deep convolutional neural networks to classify lymphocytes based upon their morphology from mice post-skin graft and produced a model that outperformed existing lymphocyte classification methods. Machine learning has also been successful in the detection of metastatic tumour cells which have a distinctive morhphogy compared to their healthy counterparts. Hasan et al., (2018) used time lapse images of human glioblastoma cells and healthy astrocytes obtained from patients to train three different models: support vector machine, random forest tree and naïve Bayes classifier, to detect cancer cells with an average accuracy of 82%. To develop a predictive model for classifying microglia as ramified or activated, a training dataset is required to 'teach' the algorithm the parameters that differentiate ramified microglia from activated ones. Rats were treated with or without 0.1 mg/kg intraperitoneal LPS, culled at 24 hrs post-injection and brains stained for IBA1 using IHC. Thousands of microglia confocal images were collected from the sensory barrel fields and motor cortices of stained sections using an automated slide scanner. Microglia contained within images gathered were processed and had their morphological parameters measured using 3DMorph running on Hawk supercomputing cluster. The two groups contained in this dataset: no LPS (no microglial activation) and LPS treated (microglial activation), were used to train four different machine learning models capable of classifying microglia as being activated or non-activated based upon morphological parameters alone.

5.2 Materials and methods

5.2.1 Animals

Seven Lister Hooded rats were housed in pairs or trios with ad libitum access to food and water as previously described, on a reverse light cycle. At five months old four male rats received intraperitoneal injections of LPS (0.1 mg/kg, in 0.1 M PBS, E. col 0111:B4, InvivoGen, California, USA) between 09:00 and 11:00 before being returned to home cages. The remaining three rats, at the same timepoint as the LPS injections, received control intraperitoneal injections of PBS. Following LPS or PBS treatment, rats were kept under close observation for 30 minutes. No formal scale was used, or measurement of sickness behaviour taken however, all rats receiving LPS displayed classical sickness behaviour: lethargy, reduced locomotion, and decreased socialisation. Rats given no LPS displayed no sickness behaviour. 24 hours post-LPS injection, subjects were sacrificed using an overdose of pentobarbital (200 mg/ml Euthatal, Boehringer Ingelheim Animal Health, Surrey, UK) administered via intraperitoneal injection. Rats that received no injection of LPS were culled alongside other animals, using the same method.

5.2.2 Perfusion

Immediately following sacrifice, rats were transcardially perfused with 0.1 M PBS followed by ice cold 4% PFA (flowrate: 20 ml/min) until the liver cleared and fixation tremors had ceased (approximately 15-20 min, 300-400 ml 4% PFA per animal). Subjects were then decapitated, brains removed and submerged in 4% PFA for 24 hrs at 4^{o}C. Post-fixation brains were washed with 0.1 M PBS and transferred to 30% sucrose in 0.1 M PBS for cryoprotection. Post-cryoprotection brains were

embedded in OCT compound (Scigen, California, USA), frozen on dry ice and stored at -80^{o}C until required.

5.2.3 Tissue preparation

Brains imbedded in OCT compound were sliced into 40 µm thick coronal sections. Slices were collected from the appearance of the dorsal hippocampus (Bregma -2.28 mm, Paxinos and Watson Rat Brain Atlas) until its ventralisation (Bregma -4.44 mm). A 1/12 series of sections were stored at 4^{o}C in 12-well plates containing 0.1 M PBS until required.

5.2.4 Immunohistochemical staining

Sections were blocked with NDS 1/10 NDS and 1% v/v Triton X-100 before being incubated with anti-IBA1 primary antibodies (1/1000, Fujifilm Wako Chemicals, North Rhine-Westphalia, Germany) overnight at 4^{o}C. Following a two-hour incubation with secondary antibodies (1/1000, Alexa Fluor 488 polyclonal antibody, A-11094, Thermo-Fisher, Massachusetts, USA) and a ten minute wash with PBS containing DAPI (0.1 ng/ml, 62248, Thermo-Fisher, Massachusetts, USA), sections were mounted on to glass slides and cover slipped using MOWIOL® 4-88 (Merck & Co., New Jersey, USA).

5.2.5 Sampling and image acquisition

Z-stack images (1 µm increments) at 20x magnification of the somatosensory and motor cortices (representative image provided in Figure 5.3) were collected from stained sections covering Bregmas -2.28 mm to -4.44 mm (Paxinos and Watson Rat Brain Atlas) using a Zeiss Axio Scan.Z1 (Carl Zeiss AG, Baden-Württemberg, Germany). Two ROIs were collected per section (bilaterally) with an average of ten

images being collected per animal. Preview images (brightfield: BF, 10x magnification) of sections were used within ZEN 3.2 Blue Edition (Carl Zeiss AG, Baden-Württemberg, Germany) to designate ROIs for automated image collection.

Following acquisition, images were converted into single channel BigTIFFs using ZEN 3.2 Blue Edition. Using the Fiji distribution of ImageJ (version 1.53c, NIH, Maryland, USA), running the Bio-Formats Plugin (The Open Microscopy Environment, Dundee, UK), images were converted to 8-bit, digitally divided into 500 x 500 px squares and saved as induvial TIFFs.

5.2.6 Semi-automated morphological analysis in 3D-Morph

3DMorph was obtained from GitHub (https://github.com/ElisaYork/3DMorph) and run in MATLAB R2019b. To optimise automated processing, a cropped image file was selected at random and loaded into 3D-Morph. A maximum intensity Z-projection was generated for the image loaded into 3DMorph. This projection examines each pixel in the image and creates a 2D image where each pixel is sourced from the pixel within the Z-stack with the highest intensity. The maximum intensity projection allows the user to see all microglia within the image without having to scroll along the Z-axis and is used as a reference image when setting the threshold and noise filters in 3DMorph. Filters were adjusted in 3DMorph until the software identified the number of microglia present in the original image. The resulting preview image was used to identify the largest single cell; any larger ‘cells’ underwent deconvolution in 3DMorph. Any signal that was not a complete cell was removed from analysis. Any cells touching the image border were also removed. The image was subsequently processed by 3D-Morph to trace the cell bodies, processes, and branches of all remaining microglia. Resultant microglial trace images and

morphological parameters were validated through visual comparison to the maximum intensity projection. If discrepancies between traces and the original image occurred, the image was run through ‘interactive mode’, again adjusting the threshold and noise filters, until traces produced an accurate reflection of the microglia in the image.

For final validation, the parameters file containing the threshold, noise filter and size cut-offs, generated by ‘interactive mode’ 3D-Morph was run in ‘automatic mode’ on a single image file from each animal. Traces from these images were visually inspected against the original image to confirm that the parameters selected generated an accurate facsimile of stained microglia in the original unprocessed image.

Following validation of the parameters selected, all images were run through a customised version of the 3D-Morph (described in Chapter 2) script using MATLAB R2019b Cardiff University’s high-performance computing cluster Hawk. The custom script output each individual trace and compiled all morphological data (cell volume, cell territory, number of end points, average branch length, maximum branch length and minimum branch length) into a single CSV file.

5.2.7 Morphological classification using machine learning

RStudio (v1.4.1103, RStudio, Massachusetts, USA) using several addon packages: dplyr (v1.0.3, Hadley Wickham, Texas, USA), tidyr (v1.1.2, Hadley Wickham, Texas, USA), reshape2 (v1.4.4, Hadley Wickham, Texas, USA), caret (v6.0-86, Max Kuhn, Connecticut, USA), mlr3 (v0.9.0, Michel Lang, Dortmund, Germany), pROC (v1.17.0.1, Xavier Robin, Basel, Switzerland), DMwR (v0.4.1, Luis

Torgo, Porto, Portugal), ggplot2 (v3.3.3, Hadley Wickham, Texas, USA), magrittr (v2.0.1, Stefan Milton Bache, Victoria Australia), GGally (v2.1.0, Barret Schloerke, Virginia, USA), car (v3.0-10, John Fox, Ontario, Canada) and Hmisc (v4.4-2, Frank Harrell, Tennessee, USA), was used for all machine learning.

5.2.7.1 Pre-processing of output data from 3D-Morph

LPS and PBS datasets were loaded into RStudio and microglia with one or more parameters with a value of zero were eliminated. Zero values were only found in parameters relating to process number and length. The lack of biological evidence to support the presence of processless microglia in our dataset having no processes (which a zero value in process number reflects) and ability to unduly weight predictive models warranted their removal from the dataset (Chen *et al.*, 2012). To identify whether the appearance of zeroes in the two datasets was random, the number of cells with a zero parameter as a percentage of total cells traced was compared between the PBS and LPS groups. Data underwent centring and scaling to normalise the dataset and change the values of parameters to common scale. A pairwise correlation of all parameters was calculated and a measure of multicollinearity, a VIF was calculated for each parameter to identify correlated parameters. If no correlation was observed, a VIF of one is returned. A VIF between 5 and 10 indicates a high correlation that could induce variance into estimated regression coefficients used in a regression model. VIF over 10 guarantees that regression coefficients will be poorly estimated (Craney and Surles, 2002). Principal component analysis was performed to estimate the number of components (e.g cell volume, number of endpoints) to fully describe the dataset.

5.2.7.2 Modelling the data with machine learning

Data was partitioned using a reproducible random seed (107) into test (25%) and training (75%) datasets. To account for variation in the number of cells between the LPS and PBS groups, sample re-weighting was performed to impose a penalty upon the most common class (LPS), ensuring that an imbalance between groups does not bias the model's development. Using 10-fold cross validation, candidate models were evaluated using the testing dataset. Models trialled were: GLM, GBM, SVM using RBF kernel and random forest, all well-established models for in use in binary classification problems. Resampling using 10-fold cross-validation was used to evaluate the machine learning models. The AUC generated by cross-validation was used as the metric to evaluate models. The model with the highest AUC was calibrated using Platt scaling and selected to be used in all future analysis. Details of the final model are provided in Appendix 3.

5.2.8 Statistics

GraphPad Prism 8 was used for all statistical analysis of morphological parameters generated by 3DMorph. Where appropriate, a t-test was used for all statistical tests with an alpha level of 0.05. RStudio was used for all machine learning steps including pre-processing.

5.3 Results

5.3.1 3D-Morph detected microglial morphological changes 24 hours post-LPS treatment

Over 22,000 microglia of three PBS and four LPS (0.1 mg/kg) treated rats were successfully traced using 3D-Morph. For each trace eight morphological parameters were measured: cell territory volume, cell volume, ramification index, number of endpoints, number of branchpoints, average branch length, maximum branch length and minimum branch length. Several differences in microglial morphology were observed between PBS and LPS treated animals. Cell territory ($t(21791) = 14.23$, $p < 0.0001$) and cell volume ($t(21791) = 17.08$, $p < 0.0001$) decreased in LPS treated animals compared to PBS. Decreases in the number of endpoints and branch points were also observed following LPS treatment, $t(21791) = 2.655$, $p = 0.0079$, $t(21791) = 5.338$, $p < 0.0001$, respectively. Ramification index increased in LPS treated animals, $t(21791) = 2.048$, $p = 0.0406$. Both average and maximum branch length increased in LPS treated animals, $t(21791) = 6.755$, $p < 0.0001$, $t(21791) = 7.063$, $p < 0.0001$, respectively (Figure 5.3). No difference in minimum branch length was observed between groups. A representative image of IBA1 immunohistochemical staining is provided in Figure 5.4 and results are summarised in Table 5.1.

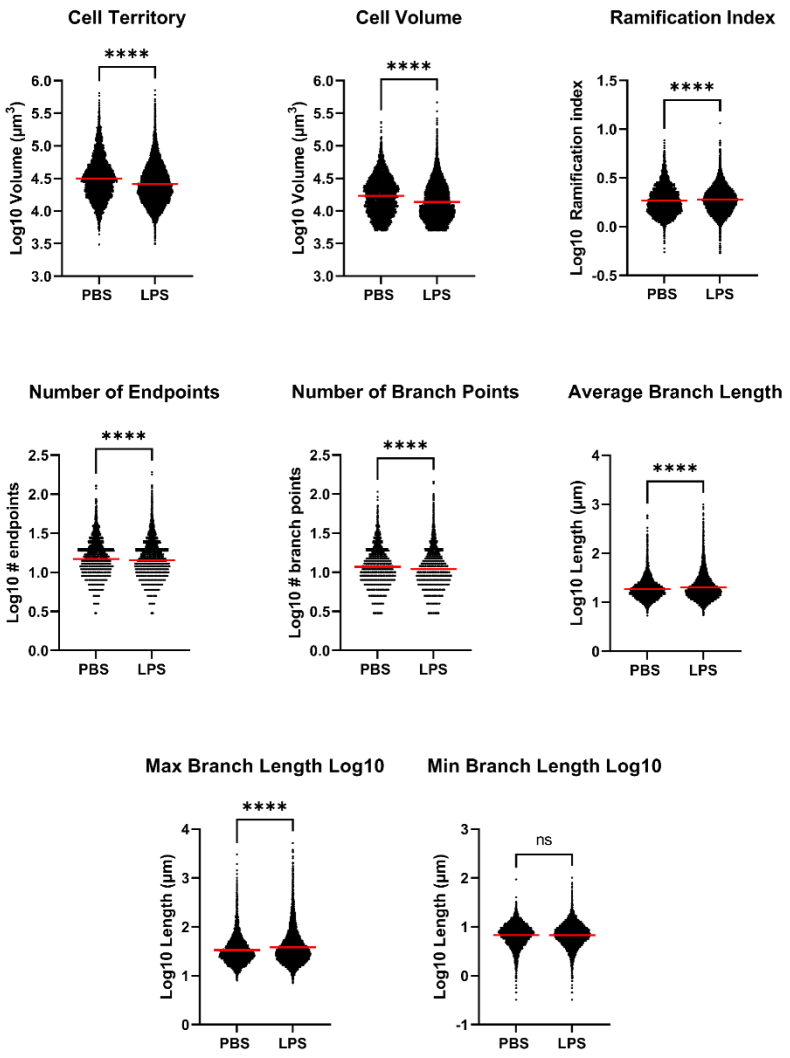

Figure 5.3 – Changes in microglial morphological parameters following LPS treatment. LPS treatment induced a decrease in cell territory, cell volume, number of endpoints and number of branch points. Treatment with LPS increased ramification index, average and maximum branch length. No change in the minimum branch length was observed between treatment groups. Summary of results can be found in Table 5.1.

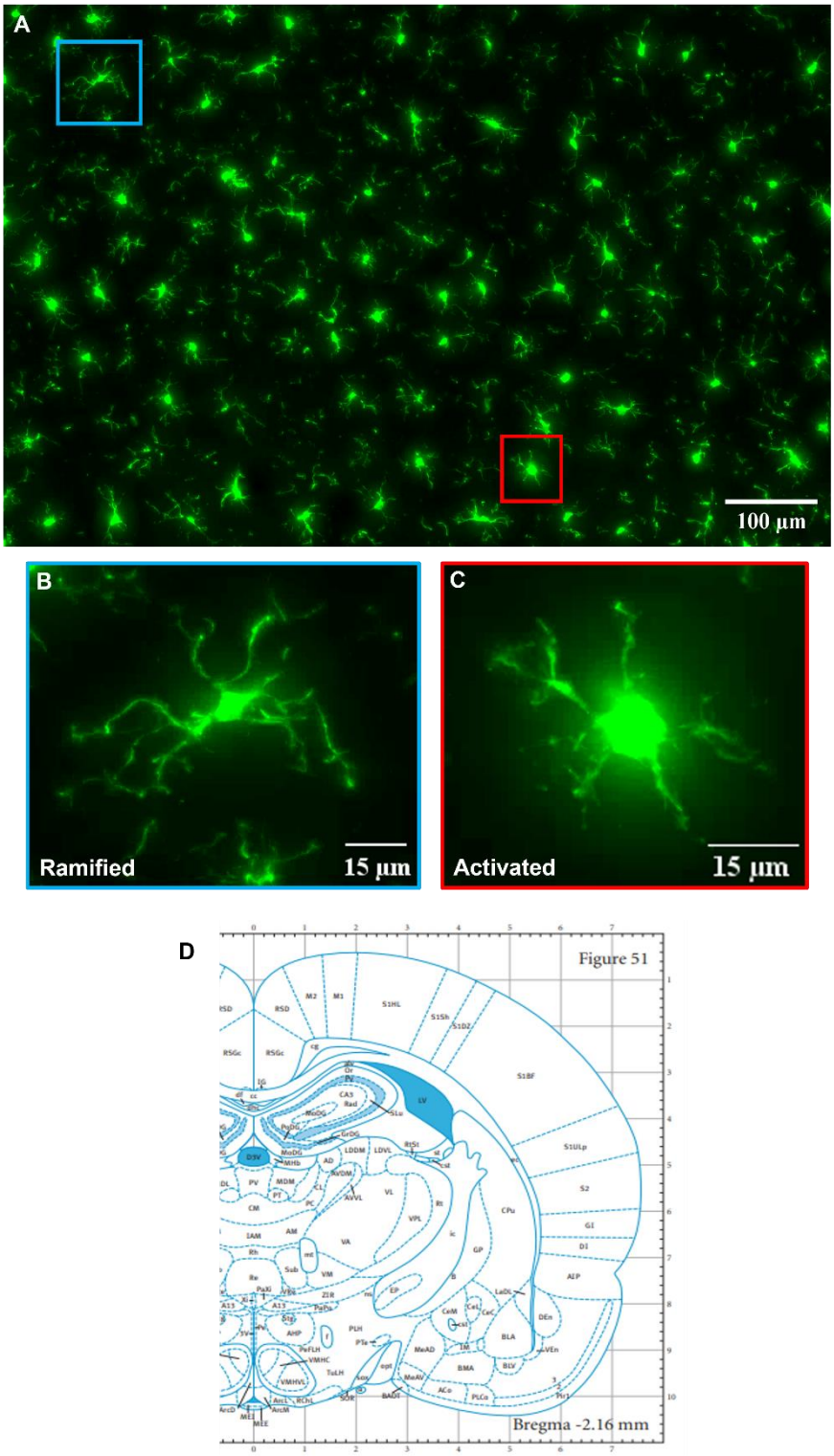

Figure 5.4 – Z-stack images gathered from the somatosensory and motor cortices of LPS and PBS treated rats stained with IBA1. **A.** Representative maximum intensity projection image of IBA1 staining within the somatosensory barrel cortex at ~ Bregma 2.16 mm, 20X magnification and 1 µm Z-axis increments (40 µm thick sections). Representative images of IBA1 negative controls are provided in Appendix 9. **B.** Representative image of a cortical microglia with a ramified morphology. **C.** Representative image of a cortical microglia with an activated morphology. **D.** Location of the ROI used during the acquisition of microglial images from LPS and PBS treated animals. Adapted from Paxinos and Watson Rat Brain Atlas.

Parameter	Change (LPS vs PBS)	DF	T value	P value
Cell territory	↓	21791	14.23	< 0.0001
Cell volume	↓	21791	17.08	< 0.0001
Ramification index	↑	21791	2.048	0.0406
Number of end points	↓	21791	2.655	0.0079
Number of branch points	↓	21791	5.338	< 0.0001
Average branch length	↑	21791	6.755	< 0.0001
Maximum branch length	↑	21791	7.063	< 0.0001
Minimum branch length	No difference	21791	0.040	0.9679

Table 5.1 – Tabular summary of changes observed in microglial morphological parameters between animals treated with PBS or LPS.

5.3.2 Development of a predictive model of microglial activation status

5.3.2.1 Pre-processing revealed collinearity in morphological parameters

The morphological data of 21983 microglia from mice treated with PBS (5314 cells) or LPS (16669 cells) was imported in RStudio. 195 cells with zero values for one or more parameter (zeros) were removed from the dataset. To confirm that the incidence of zeros was not affected by treatment, cells treated with LPS were assigned the identifier “1” and PBS treated cells were assigned the identifier “2". The mean of these identifiers across this dataset was compared before and after the removal of cells with zero values. Before removal, the mean was 1.23 and post-removal 1.24. As the mean varied by less than 1% (0.8%), it indicates that the incidence of cells with one or more zero parameters was not influenced by LPS treatment and was random. Examining the distribution of each parameter revealed that they were all highly skewed (Figure 5.5A, Table 5.2). Log transformation, Yeo-Johnson transformation or centring and scaling of data reduced the skewness of distributions (Figures 5.5C and D). Ramification index and minimum branch length had long tails on their distribution plots. Forty-eight extreme values for the ramification index and 244 for minimum branch length formed the tails of distribution plots; as these extremes represent a very small proportion of the dataset at large (0.2% and 1.1% respectively) and were biologically feasible, they were retained (Ziebell, Adelson and Lifshitz, 2015). Centred and scaled data was randomly split into two datasets: training (75%, 16342 cells) and testing (25%, 5446 cells).

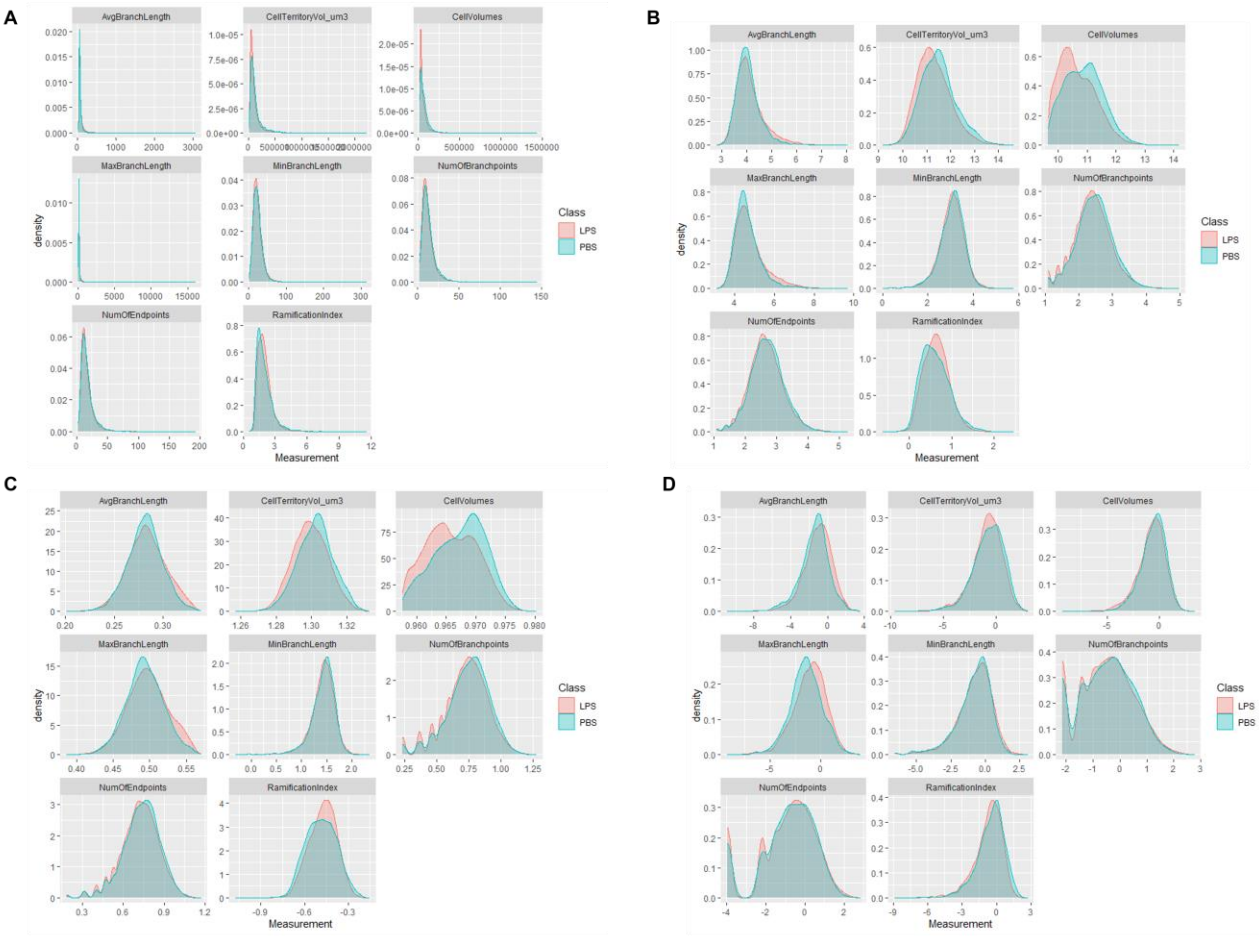

Figure 5.5 – Distributions of microglial parameters. **A.** Distributions of raw data without transformation. **B.** Distributions following logarithmic transformation. **C.** Distributions following Yeo-Johnson transformation. **D.** Distributions following centring and scaling.

Parameter	Skewness		Skewness (post-log_{10} transform)	
	PBS	***LPS***	***PBS***	***LPS***
Cell territory	4.167	4.880	0.4577	0.516
Cell volume	3.047	5.766	0.2847	0.6605
Ramification index	1.870	1.599	0.5826	0.2854
Number of end points	2.510	3.265	0.1046	0.2550
Number of branch points	2.406	3.117	-0.0025	0.1018
Average branch length	12.49	10.15	1.506	1.347
Maximum branch length	16.90	14.83	1.510	1.291
Minimum branch length	2.910	3.388	-0.847	-0.588

Table 5.2 – Tabular summary of in microglial morphological parameters obtained from animals treated with PBS or LPS.

Multicollinearity analysis on transformed data revealed a very high correlation amongst all parameters, with VIFs for cell territory, cell volume, number of endpoints and number of branch points all being over 10 average and max branch length greater than 5. Only minimum branch length and ramification index had VIFs less than 5. VIFs are presented in Table 5.3. Pairwise correlation revealed strong correlation between multiple features of the dataset. The strongest correlation (denoted by a Pearson correlation coefficient close to one) was observed between maximum branch length and average branch length (ρ = 0.93), closely followed by cell territory volume and cell volume (ρ =0.91). A correlation matrix in Figure 5.6 provides a complete summary of all Pearson correlation coefficient calculated for the dataset. Principal component analysis was used to explore the multidimensionality of the dataset. The plot of cumulative variance produced during principal component analysis shows that the variance in the dataset can be summarised in six dimensions, indicating that parameters are highly correlated.

Parameter	VIF Factor
Cell territory	13.92
Cell volume	11.70
Ramification index	2.17
Number of end points	18.52
Number of branch points	16.76
Average branch length	9.31
Maximum branch length	8.18
Minimum branch length	1.36

Table 5.3 – Tabular summary of VIFs calculated for each morphological parameter used within the classification model.

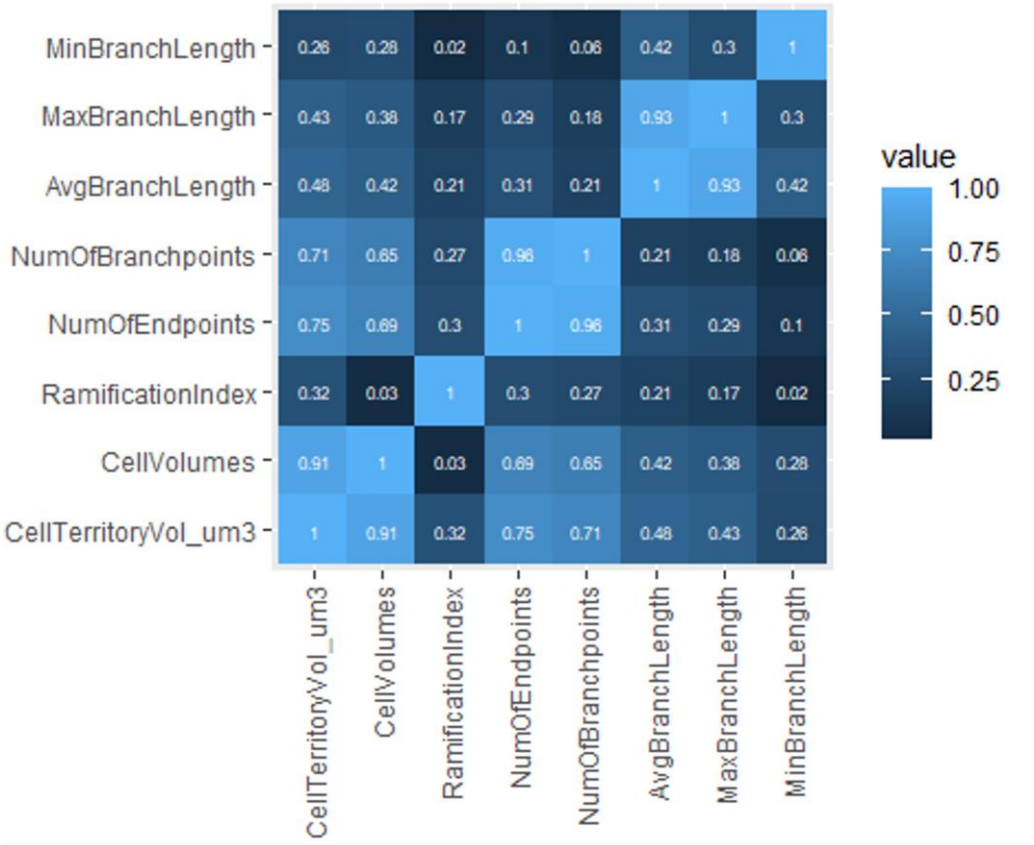

Figure 5.6 – Pairwise correlation matrix of microglial morphological parameters from the PBS/LPS dataset.

5.3.2.2 Model selection

Four different statistical models: GLM, GBM, SVM using a RBF kernel trick and RF (detailed in Chapter 2), were trained using two versions of the LPS and PBS treated microglia dataset: one Yeo-Johnson transformed and the other centred and scaled. Each model and version of the dataset combination was run with and without weighting of data, to examine whether the disparity between the number of microglia from LPS and PBS treated animals (16669 and 5314 cells respectively) should be accounted for. Following training, models were tested using a similarly transformed test dataset using 10-fold cross-validation. Models were ranked based upon one metric; AUC, with an AUC of at least ~0.7 being considered good for this biological scenario.

The method of transformation had no effect upon the estimated AUC (Table 5.4). Centring and scaling was selected as the optimum method for normalising datasets going forward as it drastically reduces the processing power required to run the model. Weighting the dataset had no effect on estimated AUCs in all models besides GLM, where weighting decreased the AUC by 0.008 (Table 5.4). As weighting had no effect upon the quality; measured by AUC, of the trained models, the model selected for use in further analyses was trained using a non-weighted dataset.

All four models performed close to 0.7, however, only one exceeded the target AUC of 0.7 (Table 5.3). The SVM model performed the worst with an estimated AUC of 0.656, followed by GLM and GBM with AUCs of 0.678 and 0.700, respectively. RF was the best performing model with an AUC of 0.707. The RF model was selected for calibration and further development.

Platt scaling was employed to calibrate the RF model trained with the PBS/LPS dataset. This allowed the model to optimise the classification threshold between the two groups and maximise the model's specificity and sensitivity. Following Platt scaling, the RF model had a sensitivity of 72.98% and a specificity of 69.76%.

Model	AUC
GLM non-weighted	0.678
GLM weighted	0.670
GBM non-weighted	0.700
GBM weighted	0.699
SVM non-weighted	0.656
SVM weighted	0.656
Random forest non-weighted	0.707
Random forest weighted	0.707

Table 5.4 – Tabular summary of AUCs, sensitivities and specificities obtained from the four different machine learning models trialled.

5.4 Discussion

The experiments in this chapter effectively implemented 3D-Morph to collect morphological data from confocal photomicrographs of microglia immunohistochemically stained with IBA1. This gathering of morphological data was successfully scaled up using a modified version of 3D-Morph running without a graphical user interface on Cardiff University's Hawk supercomputing cluster, enabling thousands of microglia to be analysed in a matter of hours. Using this high throughput methodology, the morphological parameters of over 21,000 microglia from rats treated with LPS or PBS were gathered. Comparison of morphometrics between the two treatment groups revealed morphological differences in microglia. The dataset of morphological parameters from LPS and PBS treated animals was used to develop a binary classification machine learning model, which can be used to predict activation status of microglia from morphological parameters alone in future experiments.

5.4.1 Optimising image processing and semi-automated morphological analysis

3D-Morph can analyse smaller single images (15,000 px, 20x magnification); like those in previous studies, without any post-imaging processing steps, however, the size of image file generated by semi-automated slider scanner imaging cannot be processed and exceed the maximum file size (4 GB) of the TIFF file type that the 3D-Morph requires. To circumvent the limitations of the software and TIFF file format, the images acquired via the Zeiss Axio Scan were divided into uniform squares well under the 4 GB limit using a custom ImageJ macro.

Dividing large photomicrographs captured of ROIs into smaller images provided additional benefits. During the analysis of morphology, 3D-Morph attempts to deconvolute inaccurate traces when containing multiple overlapping microglia. This deconvolution step is usually successful, however, in a small number of cases it fails and a large multi-cell bodied microglia remains. By using smaller images (500x500 px) these multi-cell microglia are not traced, as due to their size at least one part of the 'cell mass' will contact the image border and were automatically eliminated and not traced. If larger images were used these erroneous 'cell masses' would be traced and therefore require extensive quality control in post-data acquisition.

5.4.2 LPS treatment induced microglial activation

Previous studies have shown that rats treated with LPS with a single 0.1 mg/kg dose, as used in the experiments within this chapter, induce morphological changes in microglia within the CNS (Abd-El-Basset and Fedoroff, 1995; Hines *et al.*, 2013; Obuchowicz *et al.*, 2014). Morphological assessment of microglia in rats that had received 0.1 mg/kg LPS treatment in this study revealed concordant changes in measured morphological parameters. The decreases in cell territory, cell volume, number of endpoints and number of branch points are consistent with the classical description of activated microglia. Reduced volume and territory reflects the retraction of processes observed post-microglial activation, as they switch from surveying their local environment to mounting an inflammatory response to a pathogen, cell debris, apoptosis, or cell death. Likewise, the decreased number of endpoints and branch points show microglia post-LPS treatment are becoming less complex, processes are beginning to retract, and distal ramified processes are lost.

The increases in average and maximum branch lengths observed appear to contradict the argument that post-LPS microglia have adopted activated morphologies with shorter and less ramified processes. However, by understanding how 3D-Morph measures and defines processes, these changes in branch length can be interpreted correctly. Unlike software packages such as IMARIS and Neurolucida, 3D-Morph does not distinguish between primary, secondary, or tertiary processes. When determining branch length, 3D-Morph measures a process until reaching a branch point then stops measuring and starts new measurements for the two processes emerging from the branch point. This method of measuring processes means that as ramification and the number of branch points decrease, branch lengths increase as there are fewer interruptions stopping process length measurements (Figure 5.7).

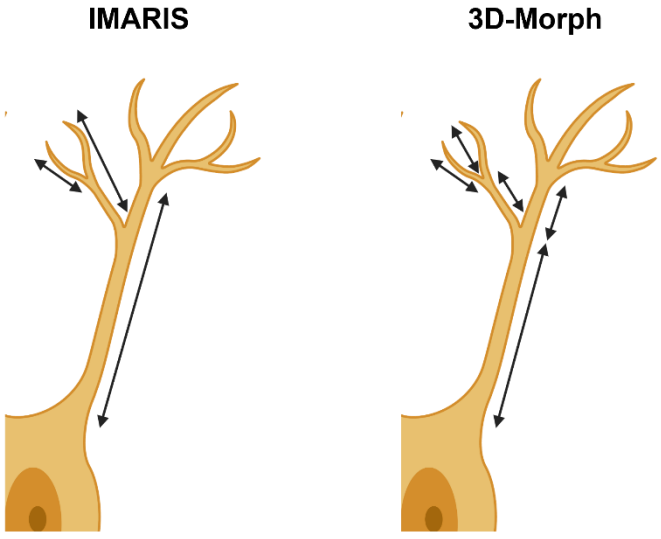

Figure 5.7 – Representation of how IMARIS and 3D-Morph measure process length. IMARIS differentiates between primary, secondary and tertiary processes so continues measuring a process following its branching. 3D-Morph stops measuring a process at a branch point and starts new measurements for the processes emerging from the fork.

5.4.3 Morphological data from LPS and PBS treated animals provided a training dataset for a predictive model of microglial activation status

Microglial morphological datasets from PBS and LPS treated rats were generated with the intention of using them to develop a predictive model of microglial activation for future experimental use. 75% of the dataset was used to train four different classification models, which were evaluated based upon their respective AUCs using the remaining 25% of the dataset. The AUC was used as the metric to compare the four models; the one with an AUC closest to one being selected for use in further analysis. The RF model produced the highest AUC (0.707), a sensitivity (true positive rate) of 72.98% and a specificity (true negative rate) of 69.76%. The model developed is a binary classifier, however, the classification of microglia as being either PBS or LPS treated is pseudo binary. Microglia in the healthy brain and post-immunogenic stimulus are on average morphologically distinct (Figure 5.4). However, within each group an individual microglia's morphology falls along a spectrum. The morphological spectrums of the two treatment groups overlap, meaning model training becomes more complex and inevitably leads to increased rates of false positives and false negatives. Other binary classification models used in biological scenarios, such as those used in cancer diagnosis, have their thresholds set to maximise sensitivity (true positive rate) because specificity (true negative rate) is not of huge concern. In cancer diagnosis, the purpose of a predictive model is to identify potential cases and therefore it is imperative that 'positive' cases (i.e. those with cancer) are not lost as false negatives. By moving the threshold to prevent false negatives, the true negative rate (specificity) decreases however, this is not of huge of concern in cancer diagnosis as these 'healthy'

individuals identified will be eliminated during in person consultations and subsequent diagnostic tests (blood biomarkers and computerised tomography scans) (Kourou *et al.*, 2015). However, there is a trade-off between sensitivity and specificity; by increasing one, the other will naturally decrease. The model we are developing here does not have to be perfect for every 'positive' case; in fact we actually just as interested in the 'negatives' as we are the 'positive' cases, so the threshold in our model was set to equally favour sensitivity and specificity. Unlike cancer diagnostics, our model is not trying to be perfect in every prediction; instead the experimental questions it is trying to solve are related to global shifts in activation status.

The 0.707 AUC value achieved by our RF model met the criteria set out in the aims of this chapter (being over 0.7) and is in keeping with the AUC's generated by models tackling similar biological problems. SVM, artificial neural network (ANN) and self-supervised learning (SSL) based models developed (Park *et al.*, 2013) to predict cancer survivability had AUCs ranging between 0.7 and 0.8. Additionally, the sensitivity (72.98%) and specificity (69.76%) of the RF model we developed for microglial analysis are comparable those achieved by (Park *et al.*, 2013) ANN model (73% and 58% respectively).

The model rests upon two key assumptions: that all microglia from the cortex of LPS treated animals are activated and likewise all microglia from PBS treated ones are non-activated, and that the morphological shift of microglia observed in these experiments is not unique to LPS treatment, instead being the widely reported activated morphology seen following any immunogenic stimuli e.g., TBI, ischemia and stress. In considering the first assumption, whilst LPS will not achieve 100%

microglial activation, the scale of the training dataset and future datasets on which predictions were made, should minimise the impact of this false assumption and predicted global shifts in microglial morphology were indeed observed. To verify that we do have virtually complete microglial activation in our dataset, a small subset (~250) of microglial from both treatment groups needs to be manually classified as activated or not activated. This would provide a reliable measure of the error we are incorporating into our model by default through our assumption that all microglia are active post-LPS and all are inactive if treated with PBS. The second assumption we used in generating our model was that it would generalise microglial activation by other immunogenic agents, rather than specifically LPS-induced activation was grounded in there being no evidence of stimuli-specific microglial morphologies. Activated microglia from a rat treated with LPS are morphologically indistinguishable from activated microglia from a rat post-mFPI. To confirm we have produced a model that can identify non-LPS induced activation, a microglial morphology dataset produced by 3D-Morph from brain injured, ischaemic or poly I:C treated rats with an appropriate control should be generated. If our model is valid, it will correctly identify increases the proportion of microglia active following injury or treatment compared to control.

5.5 Conclusion

The experiments in this chapter successfully scaled up the existing 3D-Morph platform developed by York et al., (2018) to gather morphological data from thousands of microglia using Cardiff University's supercomputing cluster Hawk. Secondly, experiments contained within this chapter demonstrated that 3D-Morph

running at scale was able to detect the changes in microglial morphology previously reported following LPS treatment in rats. The large dataset generated from microglial treated with LPS or PBS was used to successfully develop and train a binary classification model, which was able to rapidly distinguish, with an acceptable degree of accuracy, activated from non-activated microglia in an automated and non-biased manner.

Chapter 6: Microglial activation and CFC

6.1 Introduction

Microglia comprise approximately 10% of cells in the CNS and function as its tissue specific macrophages. Microglia are essential for the normal development of the brain, and loss or perturbance of microglia during the developmental window has transient effects upon neural anatomy and synaptic connectivity. During post-natal development of the thalamus, hippocampus, olfactory bulb and cerebellum, microglia adopt activated morphologies, and their processes preferentially engage with mature (mushroom shaped) dendritic spines (Perry, Hume and Gordon, 1985; Dalmau *et al.*, 1998; Fiske and Brunjes, 2000; Tremblay, Lowery and Majewska, 2010a; Reshef *et al.*, 2017). Mice lacking the microglia-specific receptor CX3CR1 exhibit reduced numbers of microglia in the hippocampus during the post-natal period. This reduction in microglial density is coupled with immature synaptic function and connectivity, compared to WT mice, reflected in higher miniature synaptic activity amplitudes and frequency, along with a reduced frequency of spontaneous excitatory postsynaptic currents recorded from CA1 pyramidal neurons. Additionally, CX3CR1 knockout mice also exhibit decreased sensitivity to the pro-convulsant drug pentylene tetrazole, which is indicative of immature circuit development at the whole animal level (Rosa C. Paolicelli *et al.*, 2011b). The effects of microglial depletion or inhibition during the post-natal developmental window in the example given above and others, including the work of Schafer et al., (2012) who examined microglial mediated pruning of RGC's supernumerary synapses, have all been transient, with the effects not being present in adulthood, suggesting that there is compensatory mechanism

which is engaged if microglial pruning fails or is inhibited. Pruning by astrocytes and neuron-driven synapse degeneration have both been proposed as alternative mechanisms by which supernumerary synapses are eliminated during development (Nikolaev *et al.*, 2009; Chung *et al.*, 2013, 2016). Whilst post-natal synaptic pruning does eventually occur in a non-microglial mediated manner; albeit with a delay, their loss during development does have persistent effects upon behaviour. Nelson & Lenz, (2017) depleted microglia in male and female Sprague Dawley rats using bilateral intracerebroventricular injections of liposomal clodronate on post-natal days one and four. Upon reaching adulthood, rats, who had their microglia depleted, displayed impaired social play, lower anxiety, and increased locomotor behaviour.

In addition to their developmental role, microglia also play an essential role in the ongoing synaptic structural and functional process in the healthy adult brain. In mouse hippocampal slices, microglial activation (via LPS administration) induced increases in the frequency of spontaneous activity from AMPAergic synapses (Tremblay *et al.*, 2011). Whilst this example of microglia control of short-term neuronal activity in the adult brain is from ex-vivo brains being treated with an exogenous immunogen, it represents a mechanism by which neuronal activity can be acutely modulated by microglia. Beyond acute modulation of hippocampal circuitry, microglia also participate in long term experience-dependent remodelling and elimination of synapses in the adult visual and auditory cortices. Using two-photon imaging, microglial were shown in the adult visual cortex to interact in a random fashion with dendritic spines, which in turn transiently swelled in a similar fashion to synaptically active spines. Spines contacted by microglia were nearly

three and a half times more likely to disappear two days following their initial observation (Tremblay et al., 2010).

In a chronic mild stress rat model of major depressive disorder, the CNS adopts a neuroinflammatory state, indicated by increases in the expression of microglial markers: translocator protein (TSPO), IBA1 and cluster of differentiation 11b (CD11b) and inflammatory cytokines: IL1β (pro), IL4 (anti), IL6 (pro), IL10 (anti) and IL18 (pro). If microglial activation is inhibited via chronic minocycline administration (50 mg/kg, intraperitoneal), the increases in cytokines and microglial activity markers post-stress are ameliorated. Additionally, stressed rats treated with minocycline no longer display depressive-like behaviour. Together, these results indicate that microglial activation plays a pivotal role in the expression of depressive behaviours (Y.-L. Wang *et al.*, 2018). These findings support the established theories surrounding sickness behaviour, which states that acute infection and tissue damage in mammals induces malaise, hyperalgesia, hypersomnia, pyrexia, listlessness and decreased sociability. These behaviours are routed deep in evolutionary history, the idea being that if an individual is sick then it is advantageous to the group/pack if they isolate themselves and reduce the risk of disease transmission (Maes *et al.*, 2012; Shakhar and Shakhar, 2015). As with the stress induced depression model discussed previously, sickness behaviour is thought be mediated by increases in the expression of pro-inflammatory cytokines: IL1, TNFα and IL6 (Maier *et al.*, 1993; Qin *et al.*, 2007; Burton, Sparkman and Johnson, 2011). Collectively, these findings highlight microglia's ability to modulate behaviour through immune signalling pathways.

There is growing evidence that microglia are regulators of memory formation, for instance the microglial chemokine receptor CX3CR1 appears to play an integral role in cued fear conditioning, novel object recognition, social behaviour, and spatial learning (Rogers *et al.*, 2011b; Parkhurst *et al.*, 2013; Zhan *et al.*, 2014b). Furthermore, depletion of hippocampal microglia via administration of clodronate impairs spatial learning (Parkhurst *et al.*, 2013). A more limited body of evidence also suggest that via similar mechanism, microglia can influence the acquisition, recall and extinction of CFM. Following a social isolation behavioural paradigm, Sprague-Dawley rats show impaired acquisition of CFM. Pugh, (1999) found that these deficits were paired with an increased expression of IL-1 protein in the hippocampus and cerebral cortex following social isolation. The administration of an intracerebroventricular IL1 receptor antagonist post-conditioning prevented the CFM acquisition impairments following social isolation. Additionally, intracerebroventricular administration of IL1β replicates the same retrieval deficits seen post-social isolation. Together, these results show that the pro-inflammatory cytokine IL1, likely produced solely or in part by microglia, can modulate the neural processes contributing to CFC (Ferrari *et al.*, 1997; Grahames *et al.*, 1999). Further support for IL1's role in retrieval-associated processes has been provided by gene arrays looking at changes in mRNA expression following the reactivation of a CFM. Said arrays identified an increase in IL1 expression post-retrieval, along with a similar increase in expression of another pro-inflammatory cytokine IL6 which, like IL1, is expressed by microglia (Bobbo *et al.*, 2019). Further evidence of IL6's ability to modulate fear conditioning is presented by Burton & Johnson, (2012). LPS induced deficits in contextual fear conditioning (impaired recall) were rescued with an intracerebroventricular injection

of sgp130; a partial agonist or decoy receptor for IL6 such as soluble IL-6 receptor (sIL6R). Scholz et al., (2016) also found that several other cytokines produced by microglia exhibited increases in expression post-CFM extinction, including members of the TGFβ and TNF families. Additionally, following recall (associated with memory restabilisation), increases in pro-inflammatory cytokine IL1 have also been reported and administration of pro-inflammatory cytokine receptor antagonists can block CFM retrieval or extinction (Barnes, Kirtley and Thomas, 2012). CX_3CR1, a chemokine receptor expressed by microglia, has also been implicated in facilitating the consolidation of CFMs. Mice lacking CX_3CR1 successfully enhances CFM acquisition during training however, upon return to the context 24 hours later, show reduced freezing compared to WT (Rogers et al., 2011). Taken together, this body of evidence suggests that pro-inflammatory cytokines, either released and/or recognised by microglia, modulate the molecular mechanisms underlying contextual fear conditioning.

The mechanism by which cytokines exert their effects upon associative learning has not been fully elucidated however, their ability to modulate synaptic plasticity has been put forward as a likely candidate (Rizzo *et al.*, 2018). CFMs are stored in engrams through functional and structural changes in synaptic efficiency (Lynch, 2004; Malenka & Nicoll, 1999). Strengthening of synapses through LTP is thought to facilitate associative learning and is mediated by the activation of NMDA receptors (Bliss and Gardner-Medwin, 1973; Bliss and Collingridge, 1993; Malenka and Nicoll, 1999; Cooke and Bear, 2012). Any interaction of cytokine signalling cascades with the mechanisms of LTP could explain pro-inflammatory cytokines' ability to alter associative learning (Gruart *et al.*, 2015; Levin and Godukhin, 2017).

Several studies have provided support for this hypothesis. TNF signalling via tumour necrosis factor receptor 1 (TNFR1) and TNFR2 is required for the maintenance of LTP, and microglial derived TNF improves LTP in C-giber synapses following spinal injury (Hanisch and Kettenmann, 2007; Becker, Deller and Vlachos, 2015). Conversely, in a different study, TNF originating from the CA1 was shown to impair hippocampal LTP in the CA1; additionally an ICV injection of TNF impairs LTP at CA3-CA1 synapses (Ren *et al.*, 2011). Unlike TNF's regulation of synaptic plasticity, IL1β's role appears to be unidirectional. ICV administration of IL-1β inhibits LTP across the hippocampus (CA1, CA3 and DG) through the modulation of NMDARs' Ca^{2+} conductance and disruption of BDNF signalling cascades (Vezzani *et al.*, 1999; Vereker, O'Donnell and Lynch, 2000b; Tong *et al.*, 2012). The chemokine CX_3CL1 expressed in the hippocampus, especially during neurogenesis, inhibits LTP when the CX_3CR1 signalling axis knocked out LTP induced through weak stimulation in hippocampal slices is either completely absent or more sustained than LTP in WT littermates (Maggi, 2011; Paolicelli et al., 2014; Rogers et al., 2011).

Outside of Scholz et al., (2016) there is limited evidence of cytokine signalling and by association microglia, having a role in extinction. IFNα infusion into the amygdala of rats impairs fear extinction; an effect that is attenuated following minocycline induced microglial depletion (Bi *et al.*, 2016). Furthermore, increased microglial production of TNFα is associated with the retention of fear memories, whereas decreased TNFα appears to facilitate their extinction (Yu *et al.*, 2017b). The experiments presented in this chapter were intended to expand the body of evidence on the role of microglia in the retrieval and extinction of associative memories. Morphometric analysis of microglia in the hippocampus and mPFC; brain regions

identified in Chapter 3 as being engaged during associative learning processes, was performed using a version of 3D-Morph customised for high throughput large scale analysis, the development of which is presented in Chapter 5. Microglial morphometrics and a prediction engine trained in Chapter 5 were used to quantify changes in the microglial activation status following the retrieval and/or extinction of a CFM. Unlike Burton & Johnson, (2012) and Pugh, (1999), all experiments were conducted in healthy uninjured and non-stressed rats. The aim was to assess whether microglia are activated and potentially play a faciliatory role in associative learning processes, rather than whether post-injury large-scale microglial activity negatively impacts learning and memory. If microglia are indeed activated as the influence of cytokines on associative learning suggests, then during either the retrieval or extinction microglia in brain regions engaged in these learning processes should shift towards an activated morphology. Such shifts may be subtle and may only occur in a small sub-population of microglia, potentially those directly associated with neurons encoding engrams relating to the associative memory (Tonegawa, Morrissey and Kitamura, 2018; Josselyn and Tonegawa, 2020). The high throughput analysis employed in this chapter has been designed to enable subtle changes to be identified if present, by sampling the morphology of hundreds of microglia per region/per animal; we aimed to capture both small- and large-scale microglial changes following the retrieval and extinction of CFM.

6.2 Materials and methods

Animals used in this chapter are the same as those used in Chapter 3; please refer to Chapter 3.2.1 for greater detail of animals, behavioural procedures, and tissue preparation.

6.2.1 Animals

17 adult male Lister Hooded rats underwent the husbandry practices and CFC paradigm described in detail previously in Chapter 3.2.1. Briefly, on day one of the experiment, subjects were exposed to a novel context and allowed to explore and familiarise themselves with it for two minutes after which they received a single scrambled, 2 s, 0.5 mA foot shock, before being returned to their home cages. 48 hours later, 12 rats were reexposed to the context for either two minutes (six rats) or ten minutes (six rats) to facilitate the retrieval and extinction of the CFM respectively. One-hour post-reexposure, subjects were sacrificed with an intraperitoneal injection of pentobarbital (200 mg/ml Euthanal, Boehringer Ingelheim Animal Health, Surrey UK). The five rats not reexposed to the context were sacrificed alongside those that underwent reexposure.

6.2.2 Perfusion

Following sacrifice, rats underwent the perfusion and brain collection methods described in Chapter 3.2.2. Rats were transcardially perfused with 0.1 M PBS followed by 4% PFA in 0.1 M PBS until the liver cleared and fixation tremors ceased. Brains were removed and stored for 24 hours in 4% PFA at 4°C, before being transferred to 30% sucrose (in 0.1 M PBS) for three days and embedded in OCT compound (Scigen, California, USA) and stored at -80°C.

6.2.3 Sectioning

Sectioning of OCT imbedded brains is covered in Chapter 3.2.3. In short, 40 µm coronal sections were collected from Bregma +5.16 mm to Bregma +2.52 mm (covering the mPFC, Paxinos and Watson Rat Brain Atlas), Bregma -1.44 mm to Bregma -4.36 mm (covering the hippocampus). Sections from the two series were stored at 4°C in 12-well plates containing 0.1 M PBS.

6.2.4 Staining

A set of 12 sections from each series collected were stained from each rat for IBA1. Sections were blocked with 1/10 NDS and 1% v/v Triton X-100 (0.1 M PBS diluent) for two hours at room temperature with agitation. Incubation with an anti-IBA1 primary antibody (1/1000, Fujifilm Wako Chemicals, North Rhine-Westphalia, Germany) followed. Sections were incubated with the primary antibody with agitation overnight at 4°C. The next day, sections were washed with 0.1 M PBS and incubated for two hours at room temperature with anti-rabbit secondary antibodies (Alexa Fluor 488, 1/1000, A-11094, Thermo-Fisher, Massachusetts, USA). Following a ten a minute wash with PBS containing DAPI (0.1 ng/ml, 62248, Thermo-Fisher, Massachusetts, USA), sections were mounted onto glass slides and cover slipped with MOWIOL® 4-88 (Merck & Co., New Jersey, USA).

6.2.5 Image acquisition

Z-stack images (1 µm increments) at 20x magnification, encompassing the entirety of each section stained for IBA1 (representative image shown in Figure 6.1), were taken using a Zeiss Axio Scan Z.1 (Carl Zeiss AG, Baden-Württemberg, Germany) running Zen Blue Edition (v3.2 Carl Zeiss AG, Baden-Württemberg, Germany). Post-acquisition, images were converted into single channel (488)

BigTIFFs using Zen Blue Edition (v3.2). Using the Fiji distribution of ImageJ (v1.53c), with the Bio-Formats plugin installed and custom macro (Appendix 1), images were digitally divided into 500 x 500 px squares and converted to the TIFF image format.

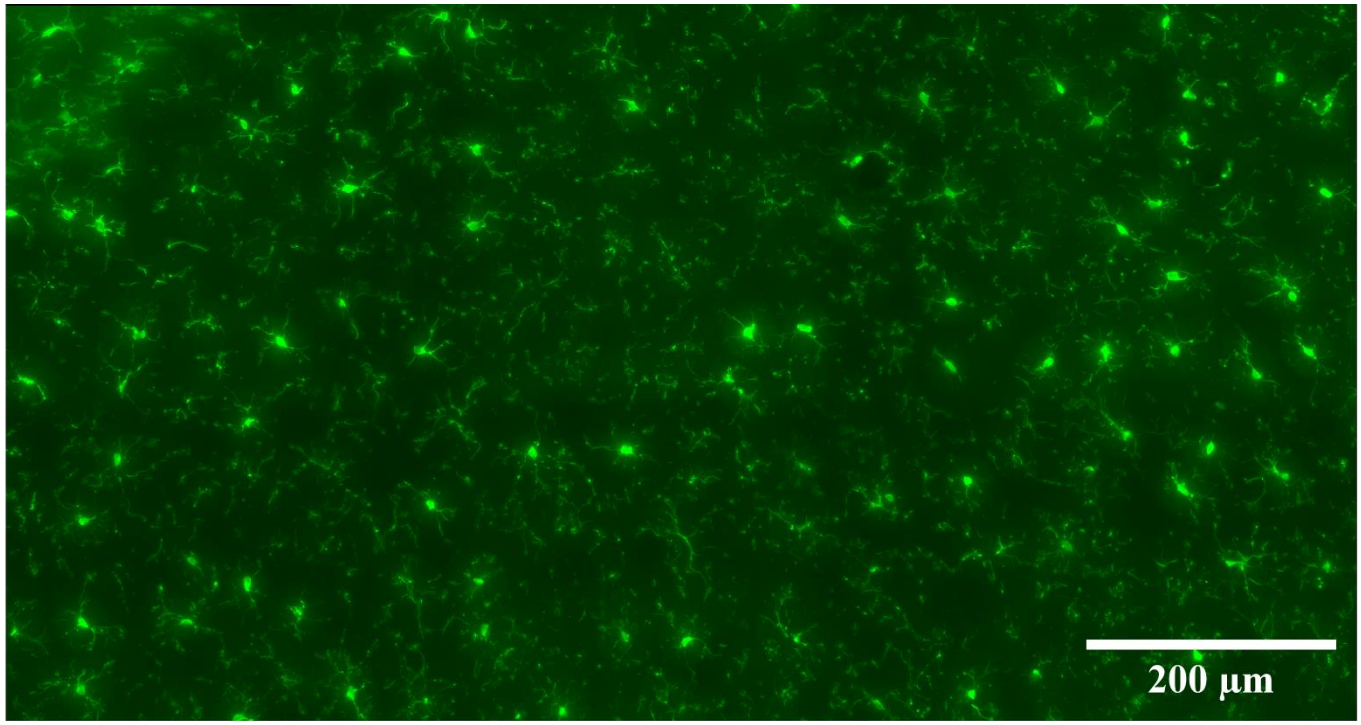

Figure 6.1 – Representative image of IBA1 staining from the PL cortex of the mPFC, used for microglial morphometric analysis with a version of 3DMorph modified for high throughput analysis.

6.2.6 Semi-automated morphological analysis in 3D-Morph

Morphological analysis of microglia from 500 x 500 px images obtained from the hippocampus and mPFC was carried out following the same protocol described in Chapter 5.2.6. Briefly, using the stock 3D-Morph script obtained from GitHub (https://github.com/ElisaYork/3DMorph) running in MATLAB R2019b (MathWorks, California, USA) a parameters file was generated manually (using 'interactive mode') from a randomly selected representative image and using its maximum intensity Z-projection image for reference. The parameters file was then validated against one image from each animal in 'automatic mode'. Traces produced from these validatory images were visually inspected against their maximum intensity Z-projections to confirm the parameters file generated an accurate facsimile of microglial morphology. Following validation of the parameters file, all images were run though a customised version of 3D-Morph (described in Chapter 2.3.2.4.3) using Cardiff University's high-performance computing cluster Hawk. The custom script output each individual trace and compiled all morphological data (cell volume, cell territory, ramification index, number of end points, average branch length, maximum branch length and minimum branch length) into a single CSV file for each region of interest.

6.2.7 Morphological classification using machine learning

RStudio (v1.4.1103, RStudio, Massachusetts, USA) using several addon packages: dplyr (v1.0.3, Hadley Wickham, Texas, USA), tidyr (v1.1.2, Hadley Wickham, Texas, USA), reshape2 (v1.4.4, Hadley Wickham, Texas, USA), caret (v6.0-86, Max Kuhn, Connecticut, USA), mlr3 (v0.9.0, Michel Lang, Dortmund, Germany), pROC (v1.17.0.1, Xavier Robin, Basel, Switzerland), DMwR (v0.4.1, Luis

Torgo, Porto, Portugal), ggplot2 (v3.3.3, Hadley Wickham, Texas, USA), magrittr (v2.0.1, Stefan Milton Bache, Victoria Australia), GGally (v2.1.0, Barret Schloerke, Virginia, USA), car (v3.0-10, John Fox, Ontario, Canada) and Hmisc (v4.4-2, Frank Harrell, Tennessee, USA), was used for all machine learning. Morphometric parameters generated by 3D-Moph were used to classify microglia as either activated or non-activated using the random forest binary classification model developed in Chapter 5.

6.2.8 Statistics

GraphPad Prism 8 was used for all statistical analysis of morphological parameters generated by 3DMorph. Where appropriate, a nested one-way ANOVA followed by multiple comparisons with an alpha level of 0.05 was used to compare morphological parameters between each behavioural group.

Following a prediction of the activation status from microglial morphological data generated by the trained machine learning algorithm (Chapter 5), the proportion of total microglia activated was calculated using Equation 6.1 and reported as percentage activation. GraphPad Prism 8 was used for all statistical comparisons of percentage activations. Where appropriate, an ordinary one-way ANOVA with multiple comparisons was used for all statistical tests with an alpha level of 0.05.

$$\%\ \boldsymbol{activation} = \frac{\boldsymbol{number\ of\ activated\ microglia}}{\boldsymbol{total\ number\ of\ microglia}} \times \mathbf{100}$$

Equation 6.1 – Equation used to calculate percentage activation of microglia using predictions made by a machine learning algorithm.

6.3 Results

6.3.1 Rats show contextual fear conditioning and extinction of fear memory

Behavioural data from rats used in this chapter's experiments are presented in Chapter 3.3.1. In short, rats displayed fear induced freezing post-shock in a novel context. Subjects, upon return to the context 48 hours post-conditioning for two-minutes showed conditioned freezing response. However, those reexposed for an extended period (ten-minutes) returned to pre-shock levels of freezing behaviour, indicating within session extinction (Figure 4.2).

6.3.2 Comparison of microglial morphometrics revealed limited differences between experimental groups

6.3.2.1 mPFC

Comparison of microglial morphology from the PL and IL cortices of the mPFC using a version of 3DMorph modified for high throughput analysis, revealed no differences between the three behavioural groups (no reexposure, two-minute reexposure and ten-minute reexposure) in any of the eight morphometrics obtained from the microglia (Tables 6.1 and 6.2, Figures 6.2 and 6.3).

	DF	F value	P value	NR vs 2 min	NR vs 10 min	2 min vs 10 min
Cell Territory	2,14	0.3479	0.7121	0.9915	0.7323	0.7860
Cell Volume	2,14	0.8619	0.4436	0.8937	0.7145	0.4183
Ramification Index	2,14	1.794	0.2025	0.2025	0.8675	0.3905
Number of Endpoints	2,14	0.4333	0.6568	0.9876	0.6768	0.7460
Number of Branches	2,14	0.7982	0.4696	0.9354	0.6894	0.4533
Average Branch Length	2,14	1.148	0.3454	0.3291	0.8549	0.5981
Maximum Branch Length	2,14	1.460	0.2656	0.2529	0.8340	0.5116
Minimum Branch Length	2,14	1.628	0.2313	0.2189	0.8172	0.4803

Table 6.1 – Tabular summary of changes observed in microglial morphometric parameters following CFM recall and extinction in the PL cortex of the mPFC.

	DF	F value	P value	NR vs 2 min	NR vs 10 min	2 min vs 10 min
Cell Territory	2,13	0.6743	0.5265	0.6742	0.5222	0.9508
Cell Volume	2,13	0.04632	0.9549	0.9506	0.9834	0.9917
Ramification Index	2,13	0.7517	0.4910	0.8261	0.4601	0.7759
Number of Endpoints	2,13	1.031	0.3842	0.4559	0.4350	0.9950
Number of Branches	2,13	1.143	0.3490	0.3995	0.4213	0.9999
Average Branch Length	2,13	1.602	0.2387	0.4743	0.8689	0.2309
Maximum Branch Length	2,13	1.936	0.1837	0.3536	0.9153	0.1905
Minimum Branch Length	2,13	1.546	0.2498	0.2217	0.6297	0.7136

Table 6.2 – Tabular summary of changes observed in microglial morphometric parameters following CFM recall and extinction in the IL cortex of the mPFC.

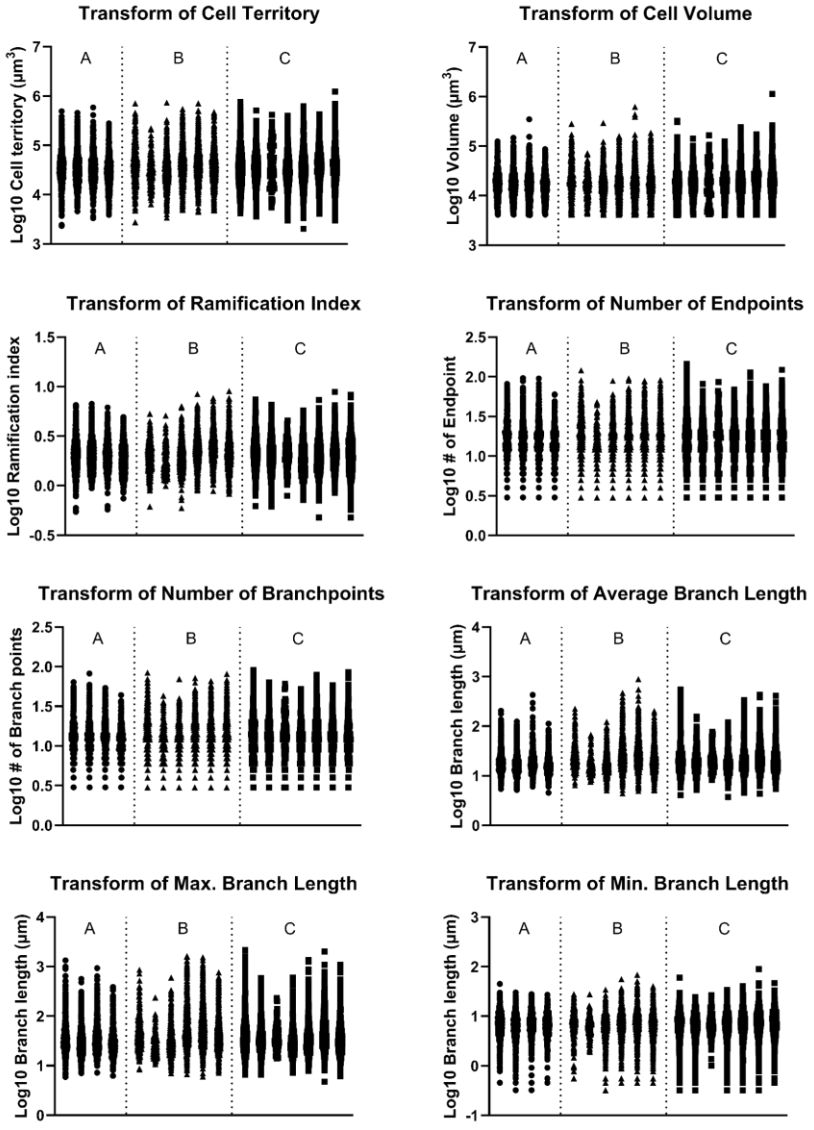

Figure 6.2 – Morphometric parameters taken from microglia contained within the PL cortex of the mPFC. A, B and C denote animals reexposed to the context for zero, two and ten minutes respectively.

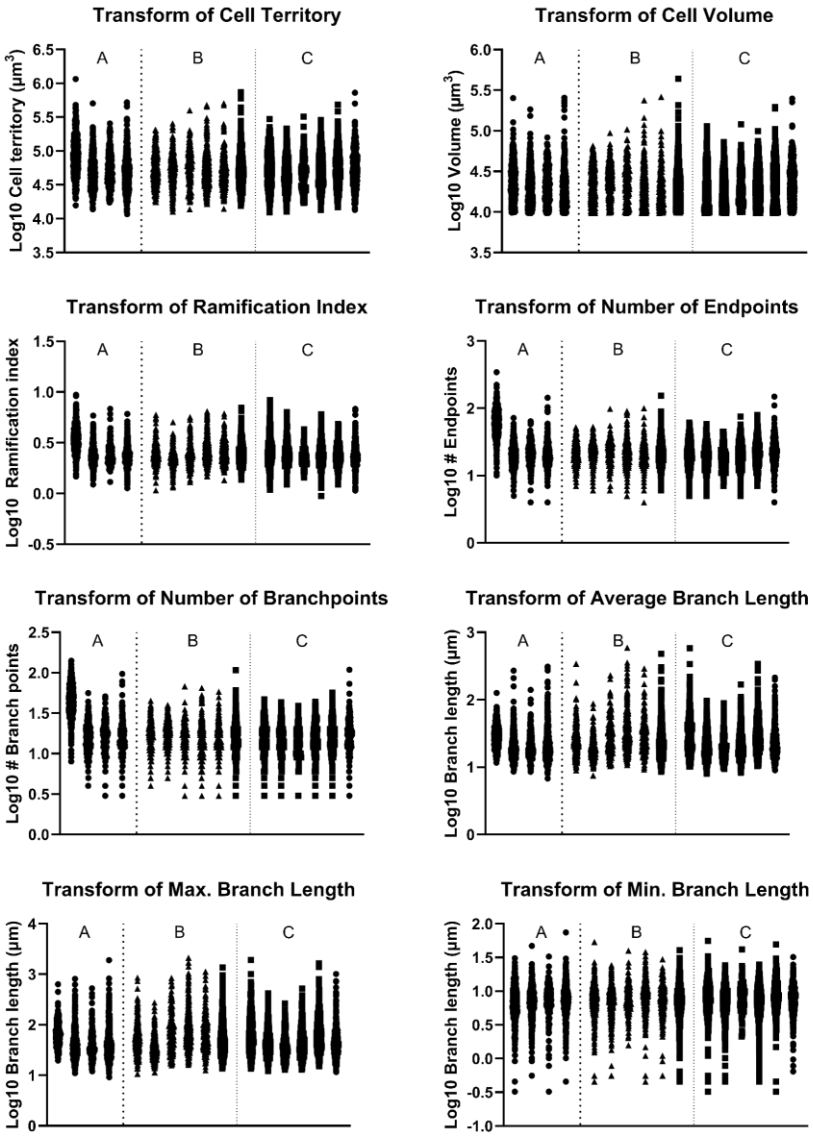

Figure 6.3 – Morphometric parameters taken from microglia contained within the IL cortex of the mPFC. A, B and C denote animals reexposed to the context for zero, two and ten minutes respectively.

6.3.2.2 Hippocampus

Comparison of microglial morphology using a version of 3DMorph modified for high throughput analysis, revealed changes in the ramification index of microglia in the DG ($F_{(2, 12)} = 6.814$, $p = 0.0011$, ANOVA, Figure 6.6). Subsequent multiple comparisons revealed that this change was an increase in ramification index in rats reexposed to the context for two-minutes, compared those reexposed for ten-minutes ($p = 0.0007$), but not compared to those not reexposed to the context. No further differences in microglial morphometrics across the DG or other hippocampal subregions (CA1 and CA3) were observed between behavioural groups (Tables 6.3, 6.4 and 6.5 and Figures 6.4, 6.5 and 6.6).

	DF	F value	P value	NR vs 2 min	NR vs 10 min	2 min vs 10 min
Cell Territory	2,12	2.154	0.1588	0.1778	0.9295	0.2391
Cell Volume	2,12	2.399	0.1329	0.2470	0.9696	0.1356
Ramification Index	2,12	0.09219	0.9126	0.9413	0.9990	0.9143
Number of Endpoints	2,12	0.7819	0.4795	0.4670	0.9084	0.6625
Number of Branches	2,12	0.003365	0.9966	0.9980	>0.9999	0.9966
Average Branch Length	2,12	1.588	0.2444	0.5361	0.8537	0.2225
Maximum Branch Length	2,12	1.780	0.2104	0.5362	0.7974	0.1873
Minimum Branch Length	2,12	1.232	0.3262	0.3716	0.9803	0.4098

Table 6.3 – Tabular summary of changes observed in microglial morphometric parameters following CFM recall and extinction in the CA1.

	DF	F value	P value	NR vs 2 min	NR vs 10 min	2 min vs 10 min
Cell Territory	2,12	0.1197	0.8872	0.8944	0.9987	0.9133
Cell Volume	2,12	0.3696	0.6986	0.70503	0.7903	0.9822
Ramification Index	2,12	0.1013	0.9044	0.8990	0.9464	0.9881
Number of Endpoints	2,12	0.8863	0.4375	0.5870	0.4337	0.9704
Number of Branches	2,12	1.259	0.3190	0.4282	0.3336	0.9886
Average Branch Length	2,12	0.3325	0.7236	0.9090	0.9434	0.7011
Maximum Branch Length	2,12	0.2408	0.7897	0.9390	0.9527	0.7714
Minimum Branch Length	2,12	0.09220	0.9126	>0.9999	0.9315	0.9289

Table 6.4 – Tabular summary of changes observed in microglial morphometric parameters following CFM recall and extinction in the CA3.

	DF	F value	P value	NR vs 2 min	NR vs 10 min	2 min vs 10 min
Cell Territory	2,12	0.3031	0.7440	0.9498	0.7279	0.9165
Cell Volume	2,12	0.08760	0.9167	0.9148	0.9496	0.9878
Ramification Index	2,12	6.814	0.0011	0.1269	0.2266	0.0007
Number of Endpoints	2,12	1.604	0.2413	0.2324	0.4112	0.8346
Number of Branches	2,12	2.853	0.0969	0.0820	0.3408	0.5166
Average Branch Length	2,12	2.963	0.0900	0.2084	0.9415	0.0892
Maximum Branch Length	2,12	3.734	0.0548	0.1315	0.9604	0.0574
Minimum Branch Length	2,12	1.496	0.2629	0.4210	0.9734	0.2613

Table 6.5 – Tabular summary of changes observed in microglial morphometric parameters following CFM recall and extinction in the DG.

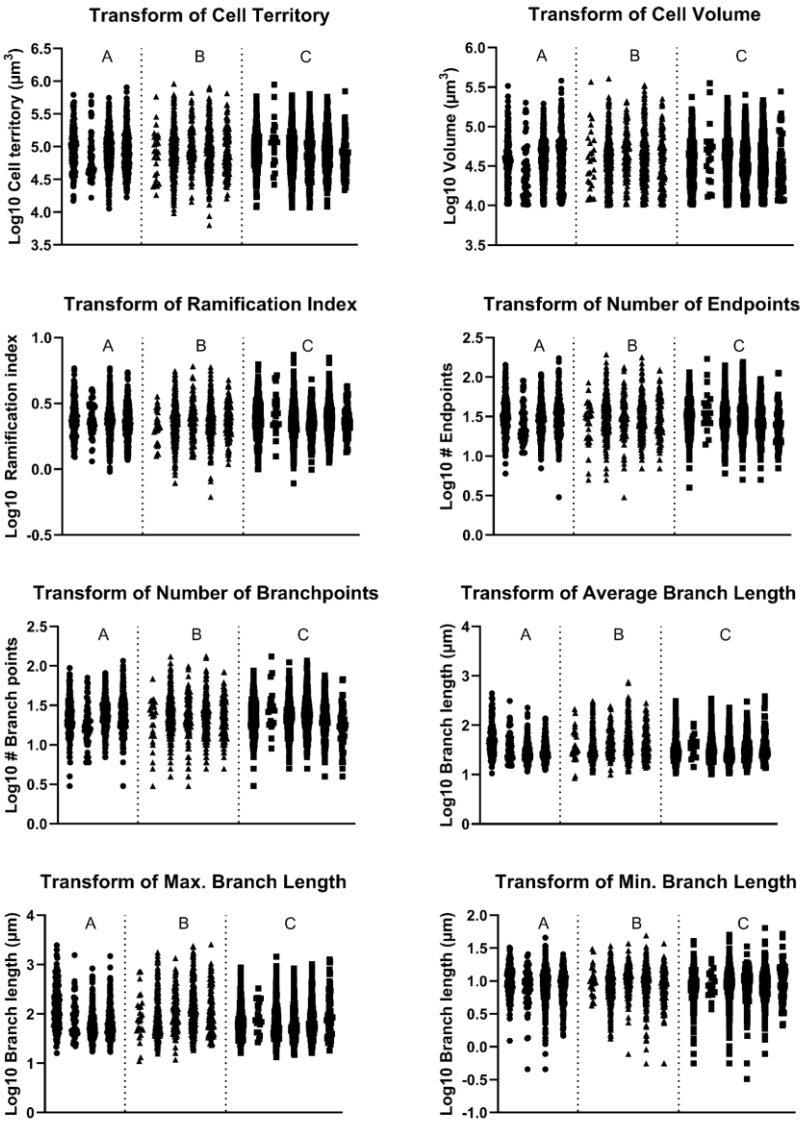

Figure 6.4 – Morphometric parameters taken from microglia contained within the CA1 hippocampal sub-region. A, B and C denote animals reexposed to the context for zero, two and ten minutes respectively.

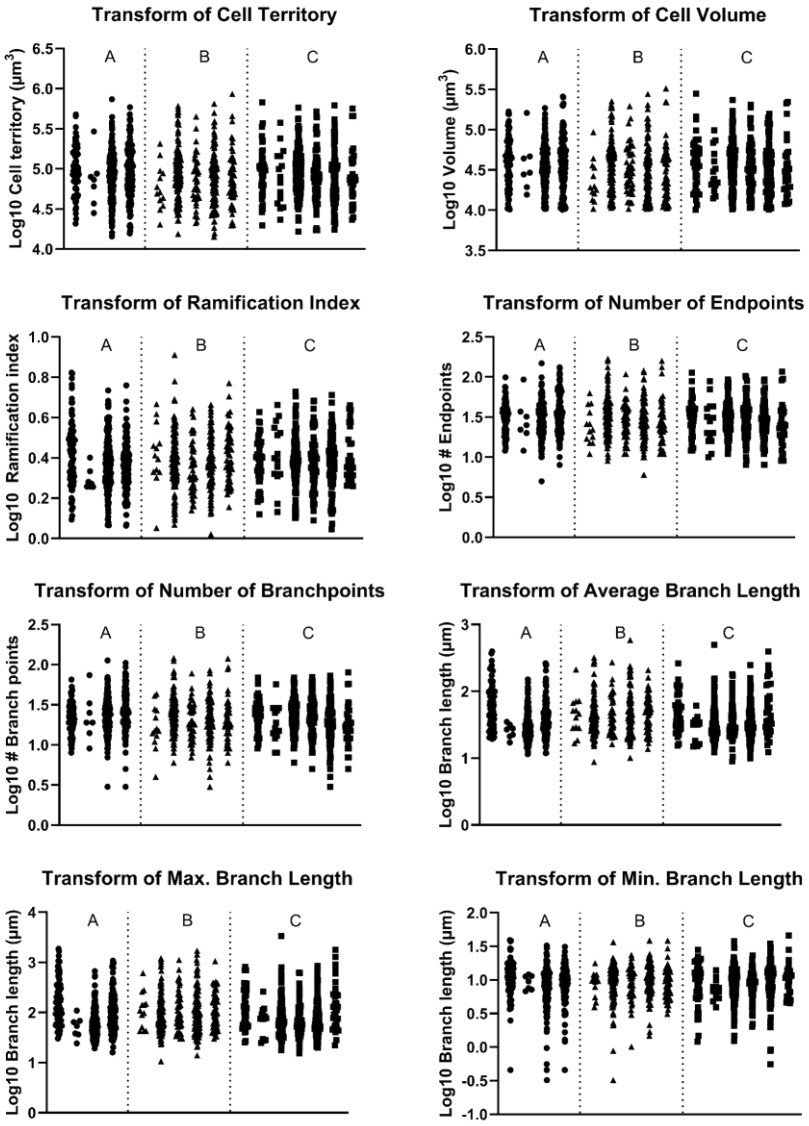

Figure 6.5 – Morphometric parameters taken from microglia contained within the CA3 hippocampal sub-region. A, B and C denote animals reexposed to the context for zero, two and ten minutes respectively.

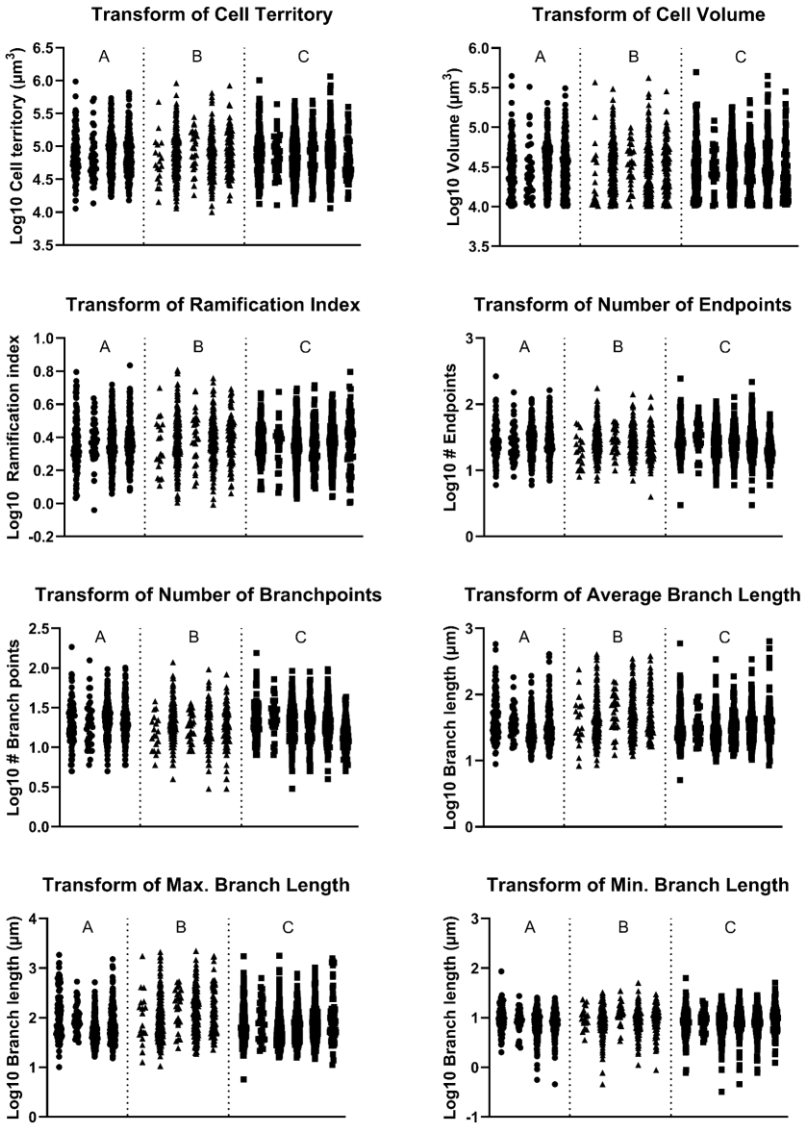

Figure 6.6 – Morphometric parameters taken from microglia contained within the DG hippocampal sub-region. A, B and C denote animals reexposed to the context for zero, two and ten minutes respectively. *** denotes $p < 0.001$

6.3.3 Microglia activation post-CFM retrieval and extinction

6.3.3.1 mPFC

Using the raw morphometric data generated by 3DMorph from microglia in the PL and IL cortices, the machine learning algorithm developed in Chapter 5 made predictions of each cell's activation status (activated or non-activated). After microglia had been assigned activation status predictions, they were used to calculate a percentage activation value from each animal (i.e. the proportion of active microglia present in the total population). Comparing percentage activation of microglia in the PL and IL cortices of the mPFC revealed no differences in the levels of microglial activation between behavioural groups (no reexposure, two minutes reexposure and ten minutes reexposure) (Table 6.6 and Figure 6.6). The number of microglia obtained from each animal are detailed in Table 6.7.

	DF	F value	P value	NR vs 2 min	NR vs 10 min	2 min vs 10 min
CA1	2,12	3.067	0.0840	0.2002	0.5739	0.6288
CA3	2,11	0.7131	0.5115	0.4828	0.8333	0.7978
DG	2,12	3.132	0.0805	0.3525	0.1665	0.8788
IL	2,13	0.8125	0.4651	0.5383	>0.9999	0.5383
PL	2,14	0.8523	0.4474	0.9986	0.5499	0.4886

Table 6.6 – Tabular summary of changes observed in microglial activation status in different brain regions following CFM recall and extinction.

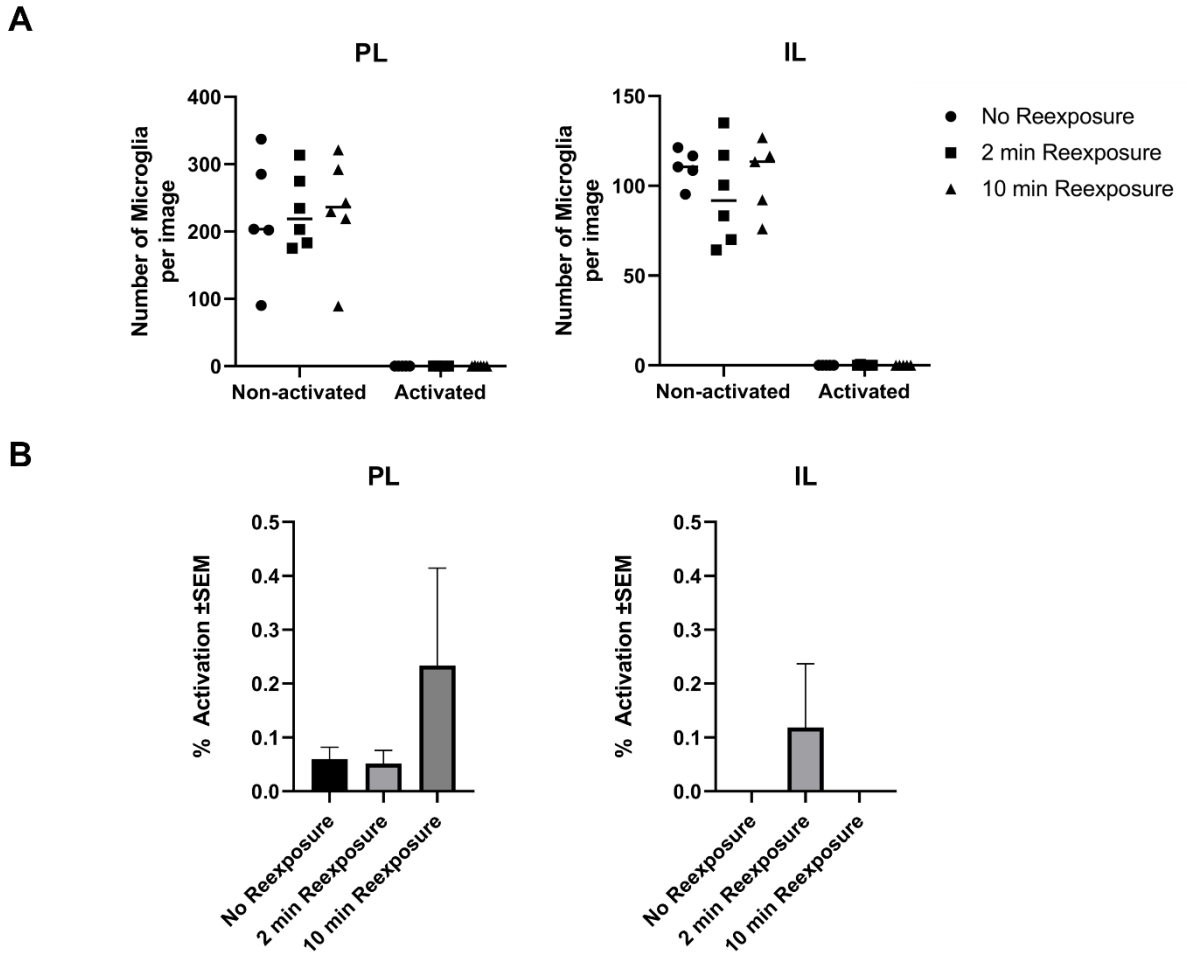

Figure 6.7 – mPFC microglial activation status predictions obtained from morphometric parameters and machine learning. **A.** Raw counts of activated and non-activated microglia obtained from the PL and IL cortices of the mPFC. **B.** Proportions of microglial activation calculated from raw counts of non-activated and activated microglia.

6.3.3.2 Hippocampus

Microglial morphometrics from the hippocampus were used to obtain predictions of microglial activation status and calculate percentage activation in the hippocampal subregions: CA1, CA3 and DG. Comparison of percentage activations between behavioural groups revealed no differences in the levels of microglial activation across the three hippocampal subregions (Table 6.6 and Figure 6.8). The number of microglia obtained from each animal are detailed in Table 6.7.

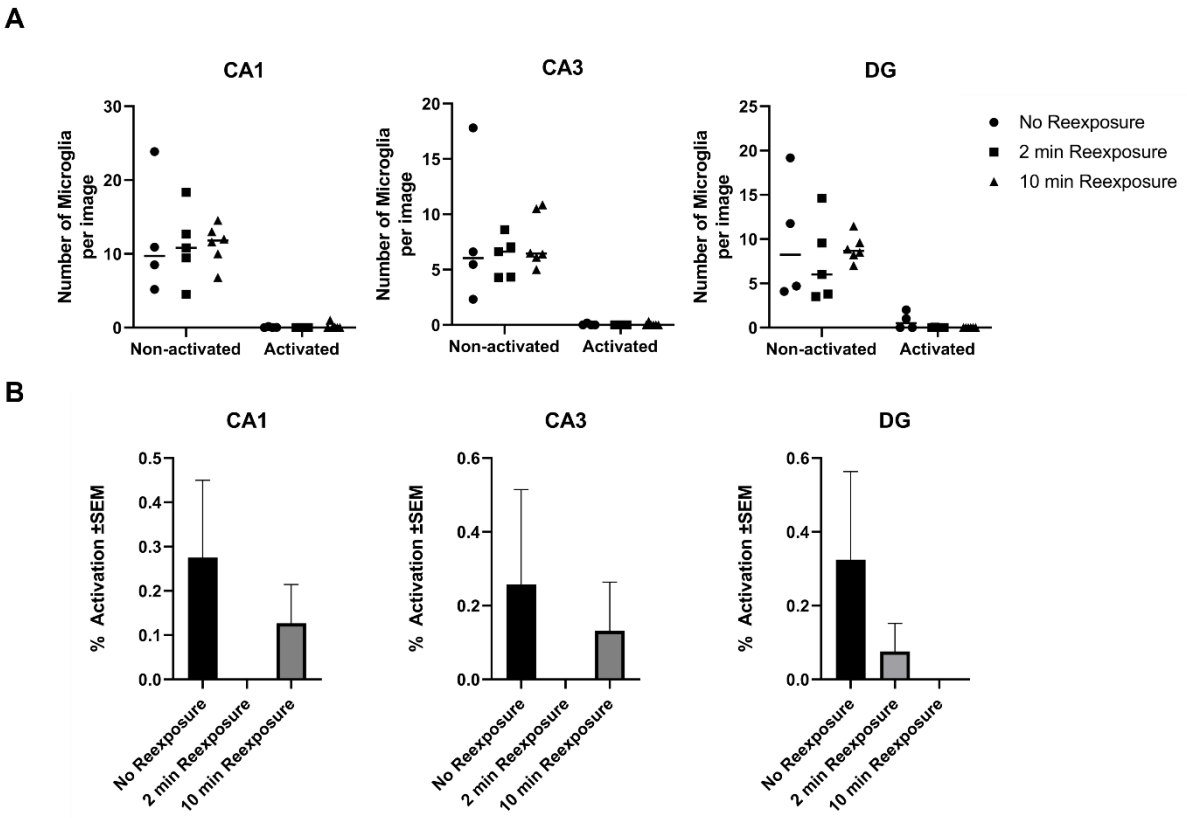

Figure 6.8 – Hippocampus microglial activation status predictions obtained from morphometric parameters and machine learning. **A.** Raw counts of activated and non-activated microglia obtained from the CA1, CA3 and DG hippocampal subregions cortices of the mPFC. **B.** Proportions of microglial activation calculated from raw counts of non-activated and activated microglia.

Behavioural group	Animal Number	Number of Microglia	Total
No reexposure	1	2566	7438
	2	2697	
	3	813	
	4	1001	
	5	361	
2 minute reexposure	6	183	9667
	7	1373	
	8	1876	
	9	2103	
	10	2506	
	11	1626	
10 minute reexposure	12	1754	7686
	13	89	
	14	1148	
	15	1928	
	16	1456	
	17	1311	

Table 6.7a Details of the number of PL microglia obtained from each animal from which morphometrics were generated using 3DMorph software.

Behavioural group	Animal Number	Number of Microglia	Total
No reexposure	1	434	1491
	2	485	
	3	221	
	4	350	
2 minute reexposure	6	468	2826
	7	140	
	8	502	
	9	250	
	10	1080	
	11	386	
10 minute reexposure	12	761	2757
	14	152	
	15	816	
	16	461	
	17	567	

Table 6.7b Details of the number of IL microglia obtained from each animal from which morphometrics were generated using 3DMorph software.

Behavioural group	Animal Number	Number of Microglia	Total
No reexposure	1	170	1044
	2	57	
	3	545	
	4	272	
2 minute reexposure	6	27	1011
	7	406	
	9	110	
	10	335	
	11	123	
10 minute reexposure	12	247	1541
	13	20	
	14	598	
	15	191	
	16	417	
	17	68	

Table 6.7c Details of the number of CA1 microglia obtained from each animal from which morphometrics were generated using 3DMorph software.

Behavioural group	Animal Number	Number of Microglia	Total
No reexposure	1	82	415
	2	7	
	3	194	
	4	132	
2 minute reexposure	6	13	353
	7	141	
	9	43	
	10	103	
	11	53	
10 minute reexposure	12	15	380
	13	152	
	14	76	
	15	105	
	17	32	

Table 6.7d Details of the number of CA3 microglia obtained from each animal from which morphometrics were generated using 3DMorph software.

Behavioural group	Animal Number	Number of Microglia	Total
No reexposure	1	108	691
	2	41	
	3	344	
	4	198	
2 minute reexposure	6	19	581
	7	262	
	9	28	
	10	182	
	11	90	
10 minute reexposure	12	133	1073
	13	34	
	14	447	
	15	115	
	16	260	
	17	84	

Table 6.7e Details of the number of DG microglia obtained from each animal from which morphometrics were generated using 3DMorph software.

6.4 Discussion

6.4.1 Comparison of gross microglial morphometrics proved unsuitable for analysing microglial activation status post-CFM retrieval and extinction

Individual measures of microglial morphology are unlikely to identify shifts in microglial morphology under physiological conditions, such as following retrieval of a CFM or acquisition of an extinction memory. This was the case for all the morphological parameters obtained from microglia during the experiments presented in this chapter. Only one difference in morphological parameters was observed between behavioural groups (no reexposure, two-minute and ten-minute reexposure); an increase in ramification index of microglia following a retrieval of a CFM.

In total, across all regions of interest, we assessed the morphology of over 40,000 microglia, which is a major improvement on the numbers used for similar analyses in the literature (Ziebell, Ray-Jones and Lifshitz, 2017; Bernier, Bohlen, York, Choi, Kamyabi, Dissing-Olesen, Hefendehl, Collins, Stevens, Barres, *et al.*, 2019; Fernández-Arjona *et al.*, 2019; Franco-Bocanegra *et al.*, 2021). The effectiveness of our semi-automated pipeline to detect morphological changes following microglial activation was confirmed with the LPS/PBS experiments presented in Chapter 5. We can therefore conclude that the lack of changes observed in the experiments presented in this chapter are an accurate representation of the global microglial population in regions of interest following CFM retrieval and extinction. This finding fits with our original hypothesis, that changes in microglial activation during CFC is limited in number and limited to sparsely

distributed reactivated engrams in the regions of interest (Josselyn and Tonegawa, 2020). We therefore did not expect to see gross changes in raw microglial morphometrics seen following CFM retrieval in intense CFC paradigms where repeated and high amplitude shocks induce hyper-ramification of microglia in the hippocampus and mPFC in a mouse model of PTSD (Sun *et al.*, 2016; W. Wang *et al.*, 2018; Smith *et al.*, 2019).

A single increase in morphometric parameter was observed in the DG where ramification index increased in rats reexposed to the context for ten minutes, compared to those reexposed for only two minutes, but not compared to rats that were not returned to the context. The increase in ramification index suggests that microglia in the DGs of rats that underwent the CFM extinction inducing paradigm, become more ramified indicating that they are less active compared to those from mice who only experience CFM retrieval (Donat *et al.*, 2017; Savage, Carrier and Tremblay, 2019b). It is particularly interesting that the sole difference was seen in ramification index, a metric calculated using two other morphometrics (the ratio between cell volume and cell territory). This result potentially shows the power of ramification index and why its inclusion is warranted in subsequent morphology analyses. Taken as a whole, the analysis of microglial morphology using single morphometric parameters cannot be used to make any meaningful conclusions about the extent of/changes in microglia activation during the retrieval and/or extinction of a CFM. However, the increase in ramification index in the DG was encouraging and gave us confidence that further analysis of microglial morphometrics in combination with each other, rather than singularly, could uncover whether there are microglial morphological changes following our CFC paradigm.

6.4.2 A novel machine learning analysis tool was successfully implemented for the analysis of microglial activation following CFM retrieval and extinction

The raw morphometric data generated by 3DMorph's analysis of microglial morphology would be more than capable of identifying the activation of microglia that accompanies events such as TBI or ischemia and neurodegenerative diseases including AD and multiple sclerosis (MS) (Schilling *et al.*, 2003; Cao *et al.*, 2012; Donat *et al.*, 2017; Luo *et al.*, 2017; Hansen, Hanson and Sheng, 2018; O'Loughlin *et al.*, 2018; Zhang, 2019; Guerrero and Sicotte, 2020; Leng and Edison, 2021; Park *et al.*, 2021). This is because the microglial activation observed in these conditions is widespread, sustained and affects the majority of the global microglial population (MS) or microglia around an injury site (TBI and ischemia) or plaques (AD). Events associated with low-grade and highly localised neuroimmune activation, such as learning and memory tasks (e.g., CFC) and mild stress inducing paradigms (e.g., restraint stress and social defeat), require a method to pull out small numbers of activated microglia out of a 'sea' of non-activated microglia (Calcia *et al.*, 2016; Scholz *et al.*, 2016; Chaaya *et al.*, 2019). The machine learning algorithm developed in Chapter 5 was designed to meet this problem, by designating each microglia as either activated or non-activated using a range of morphometrics and subsequent calculation of percentage microglial activation. This approach better ensures subtle changes in the microglial population are not 'hidden' by large numbers of unchanging non-activated microglia.

However, no differences in percentage activation were observed between experimental groups using ML, indicating that microglia are not differentially activated following CFM retrieval or extinction compared to rats not reexposed to the

context. Given that, we sampled thousands of microglia and used a novel machine learning algorithm to tease out even the most subtle changes in microglial activation. The conclusion could be reached that morphological changes are not a viable method to assess the role of microglia during CFC and alternative methods are needed to uncover the purported role of microglia in facilitating CFM retrieval and/or extinction. When taking into consideration the finding that the expression of C3aR decreased in the CA1 following the retrieval of a CFM, along with data from the wider literature that the brain's immune system is engaged during CFM retrieval and extinction, the null results from this chapter's experiments somewhat muddy the waters (Scholz *et al.*, 2016). However, we did observe some biological plausible trends in the microglial activation, such as decreased activity following CFM retrieval in the hippocampus and increased activity in the PL following extinction. Future experiments, which increase the number of animals in each behavioural group, could be employed to expand upon the data from these pilot experiments.

The immune stimulus and thus microglial activation that accompanies these behavioural events, could be so low-grade that, whilst expression of cytokines (e.g. IL1β and TNFα), drivers of synaptic pruning (e.g. C1q and C3) and regulatory components of the innate immune system (e.g. C3aR and Serping1) (Table 4.2) may change, but not the overall morphology (Gorelik *et al.*, 2017; Presumey, Bialas and Carroll, 2017; Györffy *et al.*, 2018; Young, Yan and Picketts, 2019). Several alternative and/or complimentary approaches could have been used instead/alongside our assessment of microglial morphology. Dual labelling of microglia (via IHC) with IBA1, along with a marker of activation (e.g. CD16, CD32 and CD86), could be employed to assess whether the number of active microglia is

altered during CFC associated processes (Györffy *et al.*, 2018). However, this method has its limitations; microglia are not homogenous in their expression profiles post-activation, so selecting the right marker would be key if microglial activation is to be assessed using this approach (Zhang, Lam and Tso, 2005; Xu *et al.*, 2017; Lee *et al.*, 2019). Another method regularly employed to assess microglial activation is measuring the intensity of IBA1 staining, as microglial activation results in increased expression of IBA1. This is because IBA1 is required for actin-crosslinking driven membrane ruffling, which facilitates gross morphological changes (Sasaki *et al.*, 2001). Whilst the images produced by the experiments contained within this chapter could have been used to measure any potential changes in the levels of IBA1 between behavioural groups, reports suggest this approach struggles to measure low grade non-global microglial activation, making it ill-suited for our experimental questions (Hovens, Nyakas and Schoemaker, 2014).

Putting aside the lack of changes observed in the microglia activation status between behavioural groups, we can consider the implementation of our novel semi-automated machine learning driven tool for assessing microglial activation. We successfully gathered morphological data from over 40,000 cells, from which predictions were made of their activation status using an algorithm trained with microglia treated with either PBS or LPS. The predictions made by our algorithm for the dataset generated in this chapter are biologically feasible; the majority of microglia assessed were assigned a non-activated status opposed to activated. This distribution of activation statuses was to be expected, as the rats did not experience global immune activation as they were healthy adults. This is encouraging that the algorithm is working as intended and gives confidence to conclusions made based

on the algorithm's predictions. During the model's design and validation, its sensitivity and specificity set so they both maximised (rather than favouring one over the other) if there was a problem with predictive ability of the model, then we would expect incorrect predictions in both directions i.e., activated cells would be classed as non-activated and vice versa. The experiments in this chapter therefore stand as a proof of concept for our microglial analysis pipeline and is in a form which can be shared with other researchers for their investigations. The platform we have developed is a rapid (analysis of ~40,000 cells can be completed in under a week), semi-automated platform for researchers to assess the state of microglia in the CNS in their experimental models, post-drug administration or following a behaviour paradigm in a rapid reproducible manner. Additionally, preliminary experiments have showed that our pipeline is effective at gathering morphometrics primary microglia in culture, paraffin imbedded sections of human brain and sectioned stained using 3, 3'-diaminobenzidine (DAB). Exploratory experiments have shown that 3DMorph struggles with microglia from embryonic brains.

6.5 Conclusions

The data presented in this chapter revealed that following the retrieval and/or extinction of a CFM, the morphology of microglia; a proxy measurement of microglial activation status, in five ROIs (CA1, CA3, DG, PL, and IL) was not altered however, this may have been due to the experiment being under powered (G*Power analysis estimates a group size of 22 is required for a small effect size: f = 0.4) or the wrong immune points post-reexposure being selected. However, the experiments in this chapter do represent a successful 'real-world' implementation of a novel algorithm

which makes machine learning driven predictions of microglia's activation status and therefore serve as an example of how this approach can be incorporated into future investigations in the field of neuroimmunology.

Chapter 7: General Discussion

7.1 Introduction

A wide body of evidence has shown that microglia, the CNS' tissue specific macrophages, have been co-opted for synaptic pruning and refinement of neural networks due to their ability to recognise and engulf cellular material and/or whole cells. Based upon these observations, microglia have been proposed as the facilitators of the changes in neuronal circuitry and plasticity required for the acquisition and expression of fear and extinction memories (Chapters 1.2.2 and 6.1.1). Establishing the precise neuroimmune mechanisms behind associative fear learning will allow us to understand how deviances in mechanisms, due to the impact of both genetic variations in immune system components and environmental stressors, are implicated in the etiology of associative learning deficits seen in psychiatric disorders such as SZ and PTSD (Chapters 1.1 and 4.1). If both genetic and environmental factors converge on the same neuroimmune pathways, it could inform upon prospective novel targets for drug intervention and treatments for individuals with SZ and PTSD.

This chapter summarises the main conclusions from each chapter's results contained within this thesis and consider their place in the context of the wider literature on their respective fields. This chapter also discusses the limitations of the experiments in this thesis and proposes further experiments that could be performed to expand upon our findings.

7.2 Summary of findings

Chapter 3: Immediate early gene expression is altered in a region-specific manner following CFM extinction

- Measuring freezing behaviour by sampling every five seconds shown to be no different from measuring the actual time spent frozen, in terms of overall trends observed.
- Rats exposed to the CFC paradigm used throughout this thesis displayed the acquisition, expression, and extinction of contextual fear memories.
- Using IHC, several changes in IEG protein levels (Arc, cFOS and zif268) were observed in the mPFC, hippocampus and RE following CFM expression and extinction, reflecting differential engagement of these regions and roles of IEGs in fear memory associated processes.
    - ❖ Arc expression decreased in the ML of the hippocampus' DG following CFM extinction.
    - ❖ No changes in Arc expression were observed following CFM retrieval.
    - ❖ cFOS expression increased in the hippocampal subregions: CA1, CA3 GL, hilus and ML, mPFC subregions PL and IL, and in the RE following CFM extinction.
    - ❖ cFOS expression increased in the ML of the hippocampus' DG following CFM retrieval.
    - ❖ zif268 expression increased in the GL of the DG and the mPFC subregions PL and IL following CFM extinction.

- ❖ No changes in zif268 expression were observed following CFM retrieval.

- Changes in IEG expression were used to identify regions of interest in which microglial and complement system activity were to be assessed in subsequent Chapters' experiments.

Chapter 4: Expression of complement associated genes following the retrieval and extinction of a contextual fear memory

- The CFC paradigm established in Chapter 3 was performed on male rats producing groups of animals that were not reexposed to the context, reexposed to the context and underwent fear memory extinction learning.
- RNA was isolated from hippocampal and mPFC subregions using novel microtissue punch methodology that was shown to be viable for use in RT-qPCR experiments.
- RT-qPCR experiments using cDNA synthesised from RNA obtained from microtissue punches were validated with experiments measuring Arc mRNA levels following CFM retrieval and extinction.
- RT-qPCR experiments measuring complement system component expression in the hippocampal and mPFC subregions, found a decrease in the expression of C3aR in the CA1 accompanying reexposure to the context at a level not sufficient to induce CFM extinction.
- This observation suggests that the C3a/C3aR signalling axis may play a role in the processes underlying the expression of previously acquired CFMs and

paves the way for future experiments which aim to investigate the effects of complement system modulating drugs upon CFM retrieval.

Chapter 5: Semi-automated morphological analysis of microglia

- In order to detect subtle subregion specific changes in microglial activation that might be indicative of their role in the reshaping/strengthening of neural circuits during fear learning, we identified a need for a method to assess microglial activation that sampled from a larger population of cells than is normally seen in the wider literature.
- Microglial morphology was selected as the best proxy measure of microglial activation given the comprehensive literature surrounding the topic; showing that activated microglia have reduced process branching, shorter processes, fewer processes and enlarged somas compared to ramified ‘resting’ microglia.
- 3DMorph, a piece of morphological analysis software developed by York et. al., (2018) was identified and modified to run on a supercomputing cluster allowing for morphometrics to be gathered from thousands of images of microglia obtained using an automated slide scanner.
- A model dataset of activated and non-activated microglia was generated using PBS and LPS treated rats. Morphometrics obtained using 3DMorph from these PBS and LPS treated microglia followed the trends expected, based upon evidence presented in the literature. Microglia from LPS treated rats had reduced process branching, shorter processes and fewer processes compared to microglia obtained from rats that received IP injections of PBS.

- Using the model PBS/LPS dataset, a machine learning algorithm was successfully trained and validated that can predict microglia activation status from morphometric parameters.
- The model developed has wide ranging applications for measuring microglial activation in a variety of disease models and developmental stages in a rapid, reproducible, and non-biased manner.
- The ability of the model to sample an extremely large population of microglia makes it well suited to detect the hypothesised low-grade microglial activation that accompanies the expression and extinction of CFMs.

Chapter 6: Microglial activation and CFC

- The coronal brain sections from the same animals used in Chapter 3's experiments that had undergone our CFC paradigm were stained for the pan-microglial marker IBA1.
- Microglia from these sections were imaged using an automated slider scanner and underwent morphological assessment with a modified version of 3DMorph software, followed by activation status classification using the novel machine learning algorithm developed and validated in Chapter 5.
- No changes in the raw morphometric parameters obtained from microglia from conditioned animals were observed between the three behavioural groups.
- No changes in microglial activation status predicted by our machine learning algorithm were observed between the three behavioural groups.

- Despite no changes being observed, these experiments provided a ‘test-bed’ for a novel machine learning driven pipeline for microglial morphological classification, whilst also signposting the refinements and improvements that could be made to this analytical tool in the future.

This thesis contributed to the wider literature surrounding the expression of IEG in processes associated with CFC, whilst also developing the limited body of work that surrounds the role of the innate immune system, particularly the part the complement system plays in the presentation of contextual fear memories and extinction memories. Furthermore, in the course of this thesis, a novel method for analysing microglial morphology and activation was presented for the first time, which has broad potential applications outside the context of this thesis.

7.3 To what extent is the innate immune system engaged during the expression and extinction of CFMs?

The ability of the brain’s innate immune system to strengthen and shape synaptic circuitry has been well established during development and tissue repair post-injury (Ziebell and Morganti-Kossmann, 2010; Hovens, Nyakas and Schoemaker, 2014; Simon *et al.*, 2017; VanRyzin, 2021). Preliminary evidence has implicated the innate immune system in the expression of CFMs and the acquisition of fear extinction memories (Scholz *et al.*, 2016; Chaaya *et al.*, 2019). The precise mechanisms of how the neuroimmune pathways control these processes are yet to be fully elucidated however, it has been proposed that the same mechanisms that underly developmental and disease associated neural circuit remodelling, also drive the changes required during CFC associated processes. The findings of Barnes et

al., (2012) and Scholz et al., (2016) showed that the expression of genes associated with the neuroimmune system, particularly those associated with the complement system (Table 4.2), altered their expression following the retrieval and extinction of a CFM. We expanded these experiments to regions outside the CA1 which had been identified in Chapter 3 as being engaged during fear learning. Using RT-qPCR experiments targeting the components of the complement system, we found limited changes in expression apart from a decrease in C3aR expression in the CA1 (also seen in Scholz et. al., 2016's microarrays). Although only one change was observed at the time point we studied, it does highlight that the C3a/C3aR signalling axis is potentially required for the expression of fear memories which would require the involvement of all complement system components upstream of C3a (Figure 1.7), despite their expression levels not changing. To further investigate the contribution of the complement system to the plastic and structural changes required during CFC, experiments are required to investigate the effect of complement modulation upon the expression and extinction of CFMs. This could be achieved by combining stereotaxicadministration into the hippocampus and mPFC of drugs targeting the complement system with different time points i.e., post-acquisition or pre-reexposure. Compounds that could be used include C1q inhibitors such as the nanobody C1qNb75 or drugs targeting C3aR such as the antagonist SB290157 and agonist SB290157 (Mathieu *et al.*, 2005; Therien, 2005; Morgan and Harris, 2015; Laursen *et al.*, 2020; Lee, Taylor and Woodruff, 2020). Administration into the CA1 of a C3aR receptor antagonist before reexposure to the context could be used to investigate the hypothesis that a C3a/C3aR signalling axis plays a role in supressing CFM extinction or promoting its restabilisation, as our RT-qPCR experiments in Chapter 4 have

suggested. Several mouse models exist lacking components of the complement system including C1q, C3 and C3aR. Whilst these models may appear as suitable for testing our hypothesis of complement's role in CFC, they would not be able to differentiate between the developmental effects of complement system deficits and the acute effects of disrupted complement pathways upon fear and extinction memories (Holers, 2000). However, recently an inducible C3 conditional knockout mouse model has been developed, which could be used in experiments to measure the effect of a lack of complement activity upon the expression and extinction of CFMs (Batista *et al.*, 2020).

In response to other investigators' and our findings that implicated the complement system in CFM extinction and recall, we wanted to investigate whether the cells producing many of the brains' complement proteins and mediators of synaptic pruning; microglia, had altered activities between our behavioural groups, in brain regions associated with CFC (R Veerhuis *et al.*, 1999; M Sta *et al.*, 2011; Shi *et al.*, 2015a; Scholz *et al.*, 2016) (Table 1.2). We used microglial morphometrics as a proxy for their activation status to investigate this hypothesis. We identified changes in microglial morphology indicative of microglial activation following LPS treatment in rats however, when considering microglia activation following CFM retrieval or extinction, no changes in microglial activation were observed. This is intriguing given the findings reported by researchers - that acquisition of a CFM is accompanied by increased numbers of microglia in the DG and adoption of what the authors describe as an 'amoeboid' morphology (Chaaya *et al.*, 2019). The authors used manual tracing within Neurolucida 360 (MBF Bioscience, Vermont, USA) to analyse microglial morphology and appear to use the term 'amoeboid' very loosely, as from

the representative images and data provided the cells they term ‘amoeboid’ clearly have complex processes and multiple endpoints. Using the schema of microglial morphologies used throughout the rest of thesis, we would define these cells has having an activated morphology (Figure 1.6). These experiments, whilst not identical to the ones presented in this thesis, as they looked at CFM acquisition rather CFM expression and extinction, suggest that the behavioural processes can induce detectable microglial activation in the ‘healthy’ adult rat brain. The authors in this paper were able to detect their morphological changes in a relatively small population of microglia samples per group (25-30 equal to 4-5 per animal) and propose that this reflects the involvement of these microglia in the plasticity required for CFM acquisition (Chaaya *et al.*, 2019). Given the changes are observed across the entire microglial population of the DG and are so robust that they are detectable in a very small sample size, we propose they may be the result of the well documented impact of psychological stressors upon the microglial population in the hippocampus, rather than CFC associated synaptic plasticity (Rohan Walker, Nilsson and Jones, 2013; Sugama *et al.*, 2019; Sugama and Kakinuma, 2020). Further experiments could establish whether this is the case by examining microglial morphological shifts in other hippocampal subregions, such as the CA1 and CA3 following CFM acquisition. If the same morphological changes were observed across the hippocampus, stress will emerge as the most likely candidate for microglial activation however, if they are specific to the DG then the case for CFM acquisition’s association with microglial activity is given credence. The corollary to this would be to investigate microglial changes in a learning/memory task that is not dependent upon stress, such as a reward based associative learning (Tronel and Sara, 2002).

Confirmation of Chaaya et. al.'s (2019) conclusions could represent a new avenue of research into the potential neuroimmune mechanism underpinning fear memory acquisition. A similar methodology to that applied in Chapter 4's RT-qPCR experiments could be used to measure changes in the expression of pro-inflammatory cytokines and complement system associated genes in hippocampal subregions following CFM acquisition. Such experiments could be vital to develop our understanding of how known risk variants in genes, such as C4A/B, are associated with an increased risk of developing SZ and specifically how they are implicated in the etiology of associative memory acquisition deficits seen in said patients (Hall, Romaniuk, Andrew M. McIntosh, *et al.*, 2009; Sekar *et al.*, 2016; Clifton *et al.*, 2017).

Regarding the findings presented in this thesis, several approaches could be taken to confirm whether our observations are accurate; that microglial activity is not altered following the expression of a fear memory or the acquisition of an extinction memory. The images we acquired for our morphological analyses could also be used to measure IBA1 staining intensity. IBA1 is an actin associated calcium binding protein involved in the folding and ruffling of microglial membrane. Therefore, during microglial activation, when there are changes in microglial morphology, its expression increases accordingly (Ohsawa *et al.*, 2004b). Any changes in IBA1 staining intensity within our regions of interest between our behavioural groups could indicate differential microglial activation during expression and extinction of CFMs. Furthermore, a second primary antibody could also be run alongside anti-IBA1 antibodies which targets other microglial markers associated with increases in their activity such as CD45 (transmembrane regulator of antigen receptor signalling),

CD68 (transmembrane involved in the promotion of phagocytosis and macrophage recruitment) or even neuronal markers such as PSD95 or synaptophysin that would be indicative of synaptic pruning by microglia during CFC (Appel *et al.*, 2018; Brioschi *et al.*, 2020; Comer *et al.*, 2020; Jurga, Paleczna and Kuter, 2020b).

However, with all these proposed experiments the issue remains that the activation and engagement of microglia during CFC is too low-grade, and we are looking for a 'needle in a haystack'. The discrete and localised changes in very small populations associated with engram 'hotspots' are too small to be readily detectable by methods that are commonly used in models of development and disease. To combat this an alternative could be used to ask what happens to CFM expression and extinction if there is no microglial activation in the brain? Minocycline hydrochloride, a tetracycline a broad-spectrum antibiotic administered intraperitoneally 20-50 mg/kg/day for two weeks, is sufficient to attenuate microglial activation (Yrjanheikki *et al.*, 1998; W. Wang *et al.*, 2018). Minocycline treated rats could be used to study whether microglia are essential for the expression and extinction of CFMs, however the same behavioural paradigm used in this thesis would not be suitable as the gap between CFM acquisition and reexposure to the context (two days) is not long enough for microglial activation to be attenuated with minocycline. However, with an adapted behavioural paradigm incorporating a two-week period post-CFM acquisition for minocycline treatment, the necessity of microglial activity for the expression and extinction of fear memories can be determined conclusively.

7.4 Potential applications and improvements for a novel pipeline of microglial morphological assessment

Microglial morphology has long been used as proxy measurement of microglial activation in the CNS following a wide range of stimuli including drugs, injury, and disease. However, traditional methods of assessing morphological changes, whilst not requiring expensive RNA sequencing or precise marker selected coupled with IHC dual labelling as other methods of measuring microglial activation used, does involving time consuming manual classification or manual cell tracing. Both morphological assessment methods result in a low percentage of the total microglial population being assessed and an operator driven selection of cells introduces bias into any analyses performed. The experiments presented in Chapters 5 and 6 developed an innovative approach to assess microglial morphometrics from tens of thousands of microglial in a non-biased and high-throughput manner, with the vision being that the pipeline could be used to assess changes in microglial activation, not just post-injury or during disease progression, but also in scenarios where subtle low-grade microglial activation is believed to occur such as during learning/memory associated plasticity and developmental circuit refinement. We succeeded in developing a pipeline for morphological assessment starting with automated image acquisition using a slider scanner, followed using a modified version of 3DMoprh software and culminating with binary classification of activation status using a random forest-based machine learning model trained with a LPS/PBS dataset. Going forward, this model could be useful for investigating microglial activation in other scenarios, enabling rapid assessment of changes in the neuroimmune environment, using pre-existing tissue and a robust easily obtainable

antibody (anti-IBA1, 019-19741, Fujifilm, Tokyo, Japan). Whilst these assessments would not provide conclusive proof of changes or deficits in the neuroimmune system, they could signpost a new avenue for research. The platform could also be used to monitor, in a rapid and reproducible manner, microglial response to different concentration/dosage regimens of drugs or severities of aversive stimuli. Furthermore, following validation that the platform can detect and classify human microglia, it could be used to study microglial activation post-mortem brain sections (exploratory experiments with brains from MS patients have been encouraging regarding this). Further exploratory experiments using primary cultures of microglia have shown the pipeline is able to trace and classify microglia in culture. In fact, tracing cultured microglia has a lower failure rate, most likely because cells are in a monolayer rather than 3D-dimensional space as is the case with brain sections.

The binary classifier we developed was internally validated using the testing LPS/PBS dataset however, validation with new dataset from a model system that is known to contain both active and ramified microglia is needed. Potential microglial datasets that could be used to further validate the classifier include animals treated with poly I:C, a mouse model of AD such as APP or animals that have undergone an experimental model of TBI such as midline fluid-percussion injury (Patro *et al.*, 2010; Cao *et al.*, 2012; Loane and Kumar, 2016; Manocha *et al.*, 2016; Datta, 2017; Donat *et al.*, 2017; Wegrzyn *et al.*, 2021). Validation of our model's ability to detect small changes in microglial activation could be achieved by treating rats/mice with a series of different LPS concentrations. Each stepwise decrease in LPS concentration should be accompanied by a complimentary slight decrease in microglial activation detected by our pipeline. A final potential validation for our random forest model is to

determine its ‘true’ accuracy. The model rests upon the assumption that all microglia from LPS treated rats are activated and all microglia from PBS treated rats are not activated. However, the population of microglia from each treatment group is not entirely homogenous, therefore the model has been trained with a certain degree of inaccuracy in its training dataset. In order to calculate how the potential inaccuracy this assumption incorporates into the model, we propose that a small subset of microglia from which we have obtained predictions of their activation status are manually classified by independent observers and then the percentage of classifications that our model got ‘correct’ is calculated. As it stands, the model performs the function of classifying microglial activation status with an acceptable accuracy of nearly 70%. However, the model could be improved by increasing the number of morphological parameters generated by 3DMorph, which would give a future machine learning algorithm more components to use during its training. Potential new parameters could be the number of process intersections with Sholl radii, branching angle and process endpoint distance from origin. Integration of these parameters into 3Dmorph would be relatively simple and require little modification to the existing script. Other improvements requiring more extensive alterations to 3DMorph would be to stitch back together (using their coordinates) the large images generated by the slide scanner after their microglia have been traced, enabling measurements of microglial density and nearest neighbour to be obtained. This improvement to the software could aid in the identification of the small, localised changes expected in microglial activation around fear memory engrams during associative memory retrieval and/or activation.

Astrocytic morphology also reflects their function/activation status (Zhou, Zuo and Jiang, 2019; Sofroniew, 2020). Astrocytes responding to CNS disease injury and infection are termed reactive astrocytes. Reactive astrocytes are distinguished from non-reactive ones primarily by their increased expression of glial fibrillary protein (GFAP) but also hypertrophy, process extension and elongation (Escartin *et al.*, 2021). The pipeline we have presented in this thesis for morphological analysis can also be used to assess astrocyte morphology simply by altering the parameters file used in 3DMorph via manual calibration with a subset of astrocyte images. Furthermore, astrocytes could be another target for investigating the neuroimmune system's role in the recall and extinction of CFMs given their well-documented role in synaptic plasticity and association with psychiatric disease (de Pittà, Brunel and Volterra, 2016; Notter, 2021).

Whilst preparing this thesis, a methods paper from Leyh et al., (2021) was published, in which they described their development of a pipeline involving machine learning designed for classification of microglial morphological phenotypes on a large scale (thousands of cells at a time). Although the concept and end goal were similar to ours, the authors' approach was markedly different. Leyh et al., (2021), trained their model using a dataset from a mouse model of diabetes (db/db and db/+) which contains, like our PBS/LPS treated dataset, ramified and activated morphological, but also rod and amoeboid shaped microglia. Therefore, their model is more comprehensive in the microglial phenotypes of microglia it covers than the one presented in this thesis, as our model of LPS induced microglial activation does not induce the neuronal damage that is required for the adoption of rod and amoeboid morphologies. These additional morphologies could be incorporated into our model

by acquiring datasets containing only rod or amoeboid microglia and using these to train our model from a binary to a quaternary classifier.

Exploratory experiments we performed attempted to generate a purely amoeboid dataset using images of microglia obtained from pre-natal mouse brains which contain immature microglia with an amoeboid morphology. However, several issues arose with this approach. Firstly, there was concern over whether developmental microglia, despite having the same overall shape as mature amoeboid microglia, may not have the same morphometrics dimensions, which would lead to the development of a model that might not correctly identify round processless cells in the adult brain as ‘amoeboid’, only those in the immature brain. Secondly, following the attempts to pass images of immature ‘amoeboid’ microglia through 3DMorph software, it struggled to separate apart individual cells due to their tendency to cluster together in three-dimensional space. Alternatively, peripheral macrophages which have an amoeboid morphology could be used to produce an amoeboid training dataset. Peripheral macrophages upon infiltration into the CNS are morphologically indistinguishable from amoeboid microglia which makes them perfect for generating a purely amoeboid dataset (Koeniger and Kuerten, 2017; Sevenich, 2018). Leyh et al., (2021) circumvented the need for a pure population of one microglial phenotype by not training their model with morphometric parameters. Instead, they generated ‘masks’ of their imaged microglia which were then run through a VGG16 neural network (a machine learning algorithm) developed by (Simonyan and Zisserman, 2014) that is capable of classifying cells based on their architecture into the four separate phenotypes. Leyh et al., (2021) model proved to be highly accurate (>95%) which was a great improvement on our random forest-

based model (~70%). This suggests that going forward, we should try use neural networking to develop our classification algorithm. The neural network model could still use the morphometric parameters generated by the base 3DMorph, or a modified version of 3DMorph, which gathers additional morphometrics from microglia and would still have the advantage of being less biased, quicker, and more high throughput than the pipeline developed by Leyh et. al. (2015). Bias is introduced to the approach taken by Leyh et. al. (2015) as it requires manual selection of cells to be tested and non-automated generation of cell masks, whereas our approach from imaging to output of morphometrics from 3DMorph requires no user input and can be completed in a day. A future microglial activation classifier could incorporate the best features of Leyh et. al.'s classifier (high accuracy achieved with a neural network and quaternary classification), with the faster and non-biased acquisition of morphometrics that we incorporated into the classification pipeline presented in this thesis. Another approach, using clustering analysis for automated analysis of microglial morphology, was developed by Salamanca et. al. (2019) named MIC-MAC. MIC-MAC generates two masks per cell, one of which focusses on extracting the fine detail of microglial arborisation, and the other captures its overall composition. The two masks are combined within MATLAB and segmented to disassociate individual cell structure to produce 3D microglial *in-silico* reconstructions. Using feature extraction in MATLAB, morphological characteristics are extricated from said reconstructions and undergo feature reduction using PCA. Remaining morphological parameters (features) underwent k-means clustering analysis and microglia were assigned to one of ten different clusters. A similar clustering-based approach was considered for use for the

experiments presented in Chapters 5 and 6, however it was not selected due to several concerns. Firstly, clustering analysis is specific to one dataset, meaning it cannot be used as a universal classifier, like the machine learning approach we selected. Secondly, the interpretation of clustering analysis' results is difficult as the clusters generated do not necessarily fall into the classical microglial morphophenotypes (ramified, hyper-ramified, activated, rod and ameboid) due to the unsupervised nature of k-means clustering. Finally, the ability of clustering analysis to detect subtle changes in microglial morphology (activation) is debateable, so is not suitable for the biological questions regarding microglial activation following CFM retrieval and extinction addressed in Chapter 5. Whilst the cluster analysis of microglial morphometrics employed by Salamanca et. al. (2019) in their MIC-MAC pipeline has its issues, the cluster distribution tool included in the software package is something that in the future should be incorporated into out machine learning driven pipeline. The cluster distribution tool maps microglial traces and their corresponding classifications onto the original tile scanned image of the brain. The inclusion of this feature would allow for spatial mapping of where activated microglia are localised in the brain following a behavioural manipulation i.e., are they located in discrete clusters or are they uniformly distributed across a specific subregion.

7.5 Concluding remarks

The brain's neuroimmune system may indeed play a role in facilitating the synaptic plasticity and strengthening required for the expression and extinction of contextual fear memories. The experiments presented in this thesis have confirmed some of the findings of Scholz et. al. (2016); that the complement system appears to

play a role in hippocampal mediated expression of fear memories. Whilst a change in expression was only observed in C3aR, its ligand C3a is generated only by the complement cleavage cascade, therefore we can hypothesise that the complement system at large is implicated in CFC-associated process. However, further experiments are required to establish what precisely this complement system associated signalling cascade is doing in the CA1 during fear learning/memory (retrieval-associated mnemonic processing) and to elucidate the mechanisms and ligands driving its activation. Establishing the role the complement system potentially plays in facilitating associative learning and its extinction, may highlight potential therapeutic targets for the treatment of psychiatric disorders where deficits in associative learning are seen, such as schizophrenia and PTSD.

Microglia are highly dynamic cells essential for the normal development and homeostasis of the CNS. Understanding which biological processes microglia are actively participating in is essential to develop our comprehension of a wide range of diseases and disorders of the brain. During this thesis, we presented a novel pipeline for assessing microglial activation via their morphometrics. The applications of this pipeline are not limited to the proof-of-concept experiments presented in this thesis, but with some further validations and refinement could represent a new tool for studying both animal models of CNS disease and post-mortem human brain sections.

Bibliography

Abd-El-Basset, E. and Fedoroff, S. (1995) “Effect of bacterial wall lipopolysaccharide (LPS) on morphology, motility, and cytoskeletal organization of microglia in cultures,” *Journal of neuroscience research*, 41(2), pp. 222–237.

Aggleton, J. (2000) “The Amygdala: A Functional Analysis.”

Ahmed, Z. *et al.* (2007) “Actin-binding Proteins Coronin-1a and IBA-1 are Effective Microglial Markers for Immunohistochemistry,” *Journal of Histochemistry & Cytochemistry*, 55(7), pp. 687–700. doi:10.1369/jhc.6A7156.2007.

Akdis, M. *et al.* (2011) “Interleukins, from 1 to 37, and interferon-γ: Receptors, functions, and roles in diseases,” *Journal of Allergy and Clinical Immunology*, 127(3), pp. 701-721.e70. doi:10.1016/j.jaci.2010.11.050.

Alhadidi, Q. and Shah, Z.A. (2018) “Cofilin Mediates LPS-Induced Microglial Cell Activation and Associated Neurotoxicity Through Activation of NF-κB and JAK–STAT Pathway,” *Molecular Neurobiology*, 55(2), pp. 1676–1691. doi:10.1007/s12035-017-0432-7.

Alluri, H. *et al.* (2015) “Blood–brain barrier dysfunction following traumatic brain injury,” *Metabolic Brain Disease*, 30(5), pp. 1093–1104. doi:10.1007/s11011-015-9651-7.

Almitairi, J.O.M. *et al.* (2018) “Structure of the C1r–C1s interaction of the C1 complex of complement activation,” *Proceedings of the National Academy of Sciences*, 115(4), pp. 768–773. doi:10.1073/pnas.1718709115.

American Psychiatric Association (2013) *Diagnostic and Statistical Manual of Mental Disorders*. American Psychiatric Association. doi:10.1176/appi.books.9780890425596.

Ames, J.B. and Lim, S. (2012) “Molecular structure and target recognition of neuronal calcium sensor proteins,” *Biochimica et Biophysica Acta (BBA) - General Subjects*, 1820(8), pp. 1205–1213. doi:10.1016/j.bbagen.2011.10.003.

Anagnostaras, S.G. (2010) “Automated assessment of Pavlovian conditioned freezing and shock reactivity in mice using the VideoFreeze system,” *Frontiers in Behavioral Neuroscience*, 4. doi:10.3389/fnbeh.2010.00158.

Anagnostaras, S.G., Maren, S. and Fanselow, M.S. (1999) “Temporally graded retrograde amnesia of contextual fear after hippocampal damage in rats: within-subjects examination.,” *The Journal of neuroscience : the official journal of the Society for Neuroscience*, 19(3), pp. 1106–14.

Anderson, M.L. *et al.* (2011) “Associative learning increases adult neurogenesis during a critical period,” *European Journal of Neuroscience*, 33(1), pp. 175–181.

Andreasen, N.C. *et al.* (2011) “Progressive Brain Change in Schizophrenia: A Prospective Longitudinal Study of First-Episode Schizophrenia,” *Biological Psychiatry*, 70(7), pp. 672–679. doi:10.1016/j.biopsych.2011.05.017.

Aoki, T. and Narumiya, S. (2012) “Prostaglandins and chronic inflammation.,” *Trends in pharmacological sciences*, 33(6), pp. 304–11. doi:10.1016/j.tips.2012.02.004.

Appel, J.R. *et al.* (2018) “Increased microglial activity, impaired adult hippocampal neurogenesis, and depressive-like behavior in microglial VPS35-depleted mice,” *Journal of Neuroscience*, 38(26), pp. 5949–5968.

Auchter, A. *et al.* (2017) “Reconsolidation-Extinction Interactions in Fear Memory Attenuation: The Role of Inter-Trial Interval Variability,” *Frontiers in Behavioral Neuroscience*, 11. doi:10.3389/fnbeh.2017.00002.

Ayoub, A.E. and Salm, A.K. (2003) “Increased Morphological Diversity of Microglia in the Activated Hypothalamic Supraoptic Nucleus,” *The Journal of Neuroscience*, 23(21), pp. 7759–7766. doi:10.1523/JNEUROSCI.23-21-07759.2003.

Bachiller, S. *et al.* (2018) “Microglia in Neurological Diseases: A Road Map to Brain-Disease Dependent-Inflammatory Response,” *Frontiers in Cellular Neuroscience*, 12. doi:10.3389/fncel.2018.00488.

Baldi, E. (2004) “Footshock intensity and generalization in contextual and auditory-cued fear conditioning in the rat,” *Neurobiology of Learning and Memory*, 81(3), pp. 162–166. doi:10.1016/j.nlm.2004.02.004.

Baranes, D. *et al.* (1998) “Tissue Plasminogen Activator Contributes to the Late Phase of LTP and to Synaptic Growth in the Hippocampal Mossy Fiber Pathway,” *Neuron*, 21(4), pp. 813–825. doi:10.1016/S0896-6273(00)80597-8.

Barnes, P., Kirtley, A. and Thomas, K.L. (2012) “Quantitatively and qualitatively different cellular processes are engaged in CA1 during the consolidation and reconsolidation of contextual fear memory,” *Hippocampus*, 22(2), pp. 149–171. doi:10.1002/hipo.20879.

Barnes, P. and Thomas, K.L. (2008) “Proteolysis of proBDNF Is a Key Regulator in the Formation of Memory,” *PLoS ONE*, 3(9), p. e3248. doi:10.1371/journal.pone.0003248.

Barrientos, R.M. *et al.* (2009) “Time course of hippocampal IL-1 β and memory consolidation impairments in aging rats following peripheral infection,” *Brain, Behavior, and Immunity*, 23(1), pp. 46–54. doi:10.1016/j.bbi.2008.07.002.

Bartles, J.R. (2000) “Parallel actin bundles and their multiple actin-bundling proteins.,” *Current opinion in cell biology*, 12(1), pp. 72–8. doi:10.1016/s0955-0674(99)00059-9.

Basu, J. and Siegelbaum, S.A. (2015) “The Corticohippocampal Circuit, Synaptic Plasticity, and Memory.,” *Cold Spring Harbor perspectives in biology*, 7(11). doi:10.1101/cshperspect.a021733.

Batista, A.F. *et al.* (2020) “A novel inducible complement C3 conditional knockout mouse model: Generation and characterization,” *Alzheimer’s & Dementia*, 16(S3). doi:10.1002/alz.047192.

Baud, V. and Karin, M. (2001) “Signal transduction by tumor necrosis factor and its relatives,” *Trends in Cell Biology*, 11(9), pp. 372–377. doi:10.1016/S0962-8924(01)02064-5.

Becker, D., Deller, T. and Vlachos, A. (2015) “Tumor necrosis factor (TNF)-receptor 1 and 2 mediate homeostatic synaptic plasticity of denervated mouse dentate granule cells,” *Scientific Reports*, 5(1), p. 12726. doi:10.1038/srep12726.

Beckmann, A.M. and Wilce, P.A. (1997) “Egr transcription factors in the nervous system,” *Neurochemistry International*, 31(4), pp. 477–510. doi:10.1016/S0197-0186(96)00136-2.

Bellows-Peterson, M.L. *et al.* (2012) “De Novo Peptide Design with C3a Receptor Agonist and Antagonist Activities: Theoretical Predictions and Experimental Validation,” *Journal of Medicinal Chemistry*, 55(9), pp. 4159–4168. doi:10.1021/jm201609k.

Bender, C.L. *et al.* (2018) “Stress influences the dynamics of hippocampal structural remodeling associated with fear memory extinction,” *Neurobiology of Learning and Memory*, 155, pp. 412–421. doi:https://doi.org/10.1016/j.nlm.2018.09.002.

Berardi, N., Pizzorusso, T. and Maffei, L. (2004) “Extracellular Matrix and Visual Cortical Plasticity,” *Neuron*, 44(6), pp. 905–908. doi:10.1016/j.neuron.2004.12.008.

van den Berg, R.A. *et al.* (2006) “Centering, scaling, and transformations: improving the biological information content of metabolomics data,” *BMC Genomics*, 7(1), p. 142. doi:10.1186/1471-2164-7-142.

Bernier, L.-P., Bohlen, C.J., York, E.M., Choi, H.B., Kamyabi, A., Dissing-Olesen, L., Hefendehl, J.K., Collins, H.Y., Stevens, B. and Barres, B.A. (2019) “Nanoscale surveillance of the brain by microglia via cAMP-regulated filopodia,” *Cell reports*, 27(10), pp. 2895–2908.

Berretta, S., Robertson, H.A. and Graybiel, A.M. (1992) “Dopamine and glutamate agonists stimulate neuron-specific expression of Fos-like protein in the striatum,” *Journal of Neurophysiology*, 68(3), pp. 767–777. doi:10.1152/jn.1992.68.3.767.

Besnard, A., Laroche, S. and Caboche, J. (2014) “Comparative dynamics of MAPK/ERK signalling components and immediate early genes in the hippocampus and amygdala following contextual fear conditioning and retrieval,” *Brain Structure and Function*, 219, pp. 415-430.

Bi, Q. *et al.* (2016) “Minocycline attenuates interferon-α-induced impairments in rat fear extinction,” *Journal of Neuroinflammation*, 13(1), p. 172. doi:10.1186/s12974-016-0638-z.

Bialas, A.R. and Stevens, B. (2013) “TGF-β signaling regulates neuronal C1q expression and developmental synaptic refinement,” *Nature Neuroscience*, 16(12), pp. 1773–1782. doi:10.1038/nn.3560.

Bisht, K. *et al.* (2016) “Dark microglia: A new phenotype predominantly associated with pathological states,” *Glia*, 64(5), pp. 826–839. doi:10.1002/glia.22966.

Blanchoin, L. *et al.* (2014) “Actin Dynamics, Architecture, and Mechanics in Cell Motility,” *Physiological Reviews*, 94(1), pp. 235–263. doi:10.1152/physrev.00018.2013.

Bliss, T.V.P. and Collingridge, G.L. (1993) “A synaptic model of memory: long-term potentiation in the hippocampus,” *Nature*, 361(6407), pp. 31–39. doi:10.1038/361031a0.

Bliss, T.V.P. and Gardner-Medwin, A.R. (1973) “Long-lasting potentiation of synaptic transmission in the dentate area of the unanaesthetized rabbit following stimulation of the perforant path,” *The Journal of Physiology*, 232(2), pp. 357–374. doi:10.1113/jphysiol.1973.sp010274.

Bloomer, W.A.C., VanDongen, H.M.A. and VanDongen, A.M.J. (2007) “Activity-regulated cytoskeleton-associated protein Arc/Arg3.1 binds to spectrin and associates with nuclear promyelocytic leukemia (PML) bodies.,” *Brain research*, 1153, pp. 20–33. doi:10.1016/j.brainres.2007.03.079.

Bloomer, W.A.C., VanDongen, H.M.A. and VanDongen, A.M.J. (2008) “Arc/Arg3.1 translation is controlled by convergent N-methyl-D-aspartate and Gs-coupled receptor signaling pathways.,” *The Journal of biological chemistry*, 283(1), pp. 582–592. doi:10.1074/jbc.M702451200.

Bobbo, V.C.D. *et al.* (2019) “Interleukin-6 Expression by Hypothalamic Microglia in Multiple Inflammatory Contexts: A Systematic Review,” *BioMed Research International*, 2019, pp. 1–11. doi:10.1155/2019/1365210.

Bolmont, T. *et al.* (2008) “Dynamics of the Microglial/Amyloid Interaction Indicate a Role in Plaque Maintenance,” *Journal of Neuroscience*, 28(16), pp. 4283–4292. doi:10.1523/JNEUROSCI.4814-07.2008.

Bono, R., Alarcón, R. and Blanca, M.J. (2021) “Report Quality of Generalized Linear Mixed Models in Psychology: A Systematic Review,” *Frontiers in Psychology*, 12. doi:10.3389/fpsyg.2021.666182.

Booth, C. (1986) “The limulus amoebocyte lysate (LAL) assay--a replacement for the rabbit pyrogen test.,” *Developments in biological standardization*, 64, pp. 271–5.

Botterill, J.J. *et al.* (2021) “Bidirectional Regulation of Cognitive and Anxiety-like Behaviors by Dentate Gyrus Mossy Cells in Male and Female Mice,” *The Journal of Neuroscience*, 41(11), pp. 2475–2495. doi:10.1523/JNEUROSCI.1724-20.2021.

Bourgognon, J.-M. and Cavanagh, J. (2020) “The role of cytokines in modulating learning and memory and brain plasticity,” *Brain and Neuroscience Advances*, 4, p. 239821282097980. doi:10.1177/2398212820979802.

Bourtchuladze, R. *et al.* (1994) “Deficient long-term memory in mice with a targeted mutation of the cAMP-responsive element-binding protein,” *Cell*, 79(1), pp. 59–68. doi:https://doi.org/10.1016/0092-8674(94)90400-6.

Bouton, M.E. (2004) “Context and behavioral processes in extinction,” *Learning & memory*, 11(5), pp. 485–494.

Bowie, C.R. and Harvey, P.D. (2006) “Cognitive deficits and functional outcome in schizophrenia,” *Neuropsychiatric Disease and Treatment*, 2(4), pp. 531–536. doi:10.2147/nedt.2006.2.4.531.

Branco, A.C.C.C. *et al.* (2018) “Role of Histamine in Modulating the Immune Response and Inflammation,” *Mediators of Inflammation*, 2018, pp. 1–10. doi:10.1155/2018/9524075.

Brinley-Reed, M., Mascagni, F. and McDonald, A.J. (1995) “Synaptology of prefrontal cortical projections to the basolateral amygdala: an electron microscopic study in the rat.,” *Neuroscience letters*, 202(1–2), pp. 45–8. doi:10.1016/0304-3940(95)12212-5.

Brioschi, S. *et al.* (2020) “Detection of synaptic proteins in microglia by flow cytometry,” *Frontiers in molecular neuroscience*, 13, p. 149.

Brucato, F.H. and Benjamin, D.E. (2020) “Synaptic pruning in Alzheimer’s disease: role of the complement system,” *Global journal of medical research*, 20(6).

Bryant, R.A. (2019) “Post-traumatic stress disorder: a state-of-the-art review of evidence and challenges.,” *World psychiatry : official journal of the World Psychiatric Association (WPA)*, 18(3), pp. 259–269. doi:10.1002/wps.20656.

Burgos-Robles, A. *et al.* (2007) “Consolidation of fear extinction requires NMDA receptor-dependent bursting in the ventromedial prefrontal cortex.,” *Neuron*, 53(6), pp. 871–80. doi:10.1016/j.neuron.2007.02.021.

Burton, M.D. and Johnson, R.W. (2012a) “Interleukin-6 trans-signaling in the senescent mouse brain is involved in infection-related deficits in contextual fear conditioning,” *Brain, Behavior, and Immunity*, 26(5), pp. 732–738. doi:https://doi.org/10.1016/j.bbi.2011.10.008.

Burton, M.D., Sparkman, N.L. and Johnson, R.W. (2011) “Inhibition of interleukin-6 trans-signaling in the brain facilitates recovery from lipopolysaccharide-induced sickness behavior,” *Journal of Neuroinflammation*, 8(1), p. 54. doi:10.1186/1742-2094-8-54.

Calcia, M.A. *et al.* (2016) “Stress and neuroinflammation: a systematic review of the effects of stress on microglia and the implications for mental illness,” *Psychopharmacology*, 233(9), pp. 1637–1650.

Cao, T. *et al.* (2012) “Morphological and genetic activation of microglia after diffuse traumatic brain injury in the rat,” *Neuroscience*, 225, pp. 65–75. doi:https://doi.org/10.1016/j.neuroscience.2012.08.058.

Carmichael, R.E. and Henley, J.M. (2018) “Transcriptional and post-translational regulation of Arc in synaptic plasticity,” *Seminars in Cell & Developmental Biology*, 77, pp. 3–9. doi:10.1016/j.semcdb.2017.09.007.

Caspi, A. (2003) “Cognitive performance in schizophrenia patients assessed before and following the first psychotic episode,” *Schizophrenia Research*, 65(2–3), pp. 87–94. doi:10.1016/S0920-9964(03)00056-2.

Cassini, L.F. *et al.* (2017) “On the transition from reconsolidation to extinction of contextual fear memories,” *Learning & Memory*, 24(9), pp. 392–399. doi:10.1101/lm.045724.117.

Cengiz, P. *et al.* (2019) “Developmental differences in microglia morphology and gene expression during normal brain development and in response to hypoxia-ischemia.,” *Neurochemistry international*, 127, pp. 137–147. doi:10.1016/j.neuint.2018.12.016.

Chaaya, N. *et al.* (2019) “Contextual Fear Conditioning Alter Microglia Number and Morphology in the Rat Dorsal Hippocampus,” *Frontiers in Cellular Neuroscience*, 13. doi:10.3389/fncel.2019.00214.

Chakraborty, T. *et al.* (2016) “Variants of contextual fear conditioning induce differential patterns of Egr-1 activity within the young adult prefrontal cortex,” *Behavioural Brain Research*, 302, pp. 122–130. doi:10.1016/j.bbr.2016.01.018.

Chang, C. and Maren, S. (2010) “Strain difference in the effect of infralimbic cortex lesions on fear extinction in rats.,” *Behavioral Neuroscience*, 124(3), pp. 391–397. doi:10.1037/a0019479.

Chater, T.E. and Goda, Y. (2021) “My Neighbour Hetero—deconstructing the mechanisms underlying heterosynaptic plasticity,” *Current Opinion in Neurobiology*, 67, pp. 106–114. doi:https://doi.org/10.1016/j.conb.2020.10.007.

Chaudhuri, A. *et al.* (2000) “Molecular maps of neural activity and quiescence.,” *Acta neurobiologiae experimentalis*, 60(3), pp. 403–10.

Chen, Z. *et al.* (2012) “Lipopolysaccharide-induced microglial activation and neuroprotection against experimental brain injury is independent of hematogenous TLR4,” *Journal of Neuroscience*, 32(34), pp. 11706–11715.

Cheval, H. *et al.* (2012) “Distinctive features of Egr transcription factor regulation and DNA binding activity in CA1 of the hippocampus in synaptic plasticity and consolidation and reconsolidation of fear memory,” *Hippocampus*, 22(3), pp. 631–642. doi:10.1002/hipo.20926.

Chistiakova, M. *et al.* (2015) “Homeostatic role of heterosynaptic plasticity: models and experiments,” *Frontiers in Computational Neuroscience*, 9. doi:10.3389/fncom.2015.00089.

Chiu, R. *et al.* (1988) “The c-fos protein interacts with c-JunAP-1 to stimulate transcription of AP-1 responsive genes,” *Cell*, 54(4), pp. 541–552. doi:https://doi.org/10.1016/0092-8674(88)90076-1.

Choi, D.C. *et al.* (2007) “Bed nucleus of the stria terminalis subregions differentially regulate hypothalamic-pituitary-adrenal axis activity: implications for the integration of limbic inputs.,” *The Journal of neuroscience : the official journal of the Society for Neuroscience*, 27(8), pp. 2025–34. doi:10.1523/JNEUROSCI.4301-06.2007.

Chowdhury, S. *et al.* (2006) “Arc/Arg3.1 Interacts with the Endocytic Machinery to Regulate AMPA Receptor Trafficking,” *Neuron*, 52(3), pp. 445–459. doi:10.1016/j.neuron.2006.08.033.

Chung, L. (2015) “A Brief Introduction to the Transduction of Neural Activity into Fos Signal,” *Development & Reproduction*, 19(2), pp. 61–67. doi:10.12717/DR.2015.19.2.061.

Chung, W.-S. *et al.* (2013) “Astrocytes mediate synapse elimination through MEGF10 and MERTK pathways,” *Nature*, 504(7480), pp. 394–400. doi:10.1038/nature12776.

Chung, W.-S. *et al.* (2016) “Novel allele-dependent role for APOE in controlling the rate of synapse pruning by astrocytes,” *Proceedings of the National Academy of Sciences*, 113(36), pp. 10186–10191. doi:10.1073/pnas.1609896113.

Ciocchi, S. *et al.* (2010) “Encoding of conditioned fear in central amygdala inhibitory circuits.,” *Nature*, 468(7321), pp. 277–82. doi:10.1038/nature09559.

Clifton, N.E. *et al.* (2017) “Schizophrenia copy number variants and associative learning,” *Molecular Psychiatry*, 22(2), pp. 178–182. doi:10.1038/mp.2016.227.

Clifton, N.E., Thomas, K.L. and Hall, J. (2018) “The effect of ketamine on the consolidation and extinction of contextual fear memory,” *Journal of Psychopharmacology*, 32(2), pp. 156–162. doi:10.1177/0269881117748903.

Cogswell, P.C., Mayo, M.W. and Baldwin, A.S. (1997) “Involvement of Egr-1/RelA Synergy in Distinguishing T Cell Activation from Tumor Necrosis Factor-α–induced

NF-κB1 Transcription," *Journal of Experimental Medicine*, 185(3), pp. 491–498. doi:10.1084/jem.185.3.491.

Comer, A.L. *et al.* (2020) "Increased expression of schizophrenia-associated gene C4 leads to hypoconnectivity of prefrontal cortex and reduced social interaction," *PLOS Biology*, 18(1), p. e3000604. doi:10.1371/journal.pbio.3000604.

Cooke, S.F. and Bear, M.F. (2012) "Stimulus-Selective Response Plasticity in the Visual Cortex: An Assay for the Assessment of Pathophysiology and Treatment of Cognitive Impairment Associated with Psychiatric Disorders," *Biological Psychiatry*, 71(6), pp. 487–495. doi:https://doi.org/10.1016/j.biopsych.2011.09.006.

Cooper, J.F., Hochstein, H.D. and Seligmann, E.B. (1972) "The Limulus test for endotoxin (Pyrogen) in radiopharmaceuticals and biologicals.," *Bulletin of the Parenteral Drug Association*, 26(4), pp. 153–62.

Copois, V. *et al.* (2007) "Impact of RNA degradation on gene expression profiles: Assessment of different methods to reliably determine RNA quality," *Journal of Biotechnology*, 127(4), pp. 549–559. doi:https://doi.org/10.1016/j.jbiotec.2006.07.032.

Corcoran, K.A. and Quirk, G.J. (2007) "Activity in Prelimbic Cortex Is Necessary for the Expression of Learned, But Not Innate, Fears," *Journal of Neuroscience*, 27(4), pp. 840–844. doi:10.1523/JNEUROSCI.5327-06.2007.

Correll, C.U. and Schooler, N.R. (2020) "Negative Symptoms in Schizophrenia: A Review and Clinical Guide for Recognition, Assessment, and Treatment.,"

Neuropsychiatric disease and treatment, 16, pp. 519–534. doi:10.2147/NDT.S225643.

Coulthard, L.G. *et al.* (2018) “Complement C3a receptor modulates embryonic neural progenitor cell proliferation and cognitive performance,” *Molecular Immunology*, 101, pp. 176–181. doi:https://doi.org/10.1016/j.molimm.2018.06.271.

Coulthard, L.G. and Woodruff, T.M. (2015) “Is the Complement Activation Product C3a a Proinflammatory Molecule? Re-evaluating the Evidence and the Myth,” *The Journal of Immunology*, 194(8), pp. 3542–3548. doi:10.4049/jimmunol.1403068.

Craney, T.A. and Surles, J.G. (2002) “Model-dependent variance inflation factor cutoff values,” *Quality Engineering*, 14(3), pp. 391–403.

Crehan, H., Hardy, J. and Pocock, J. (2012) “Microglia, Alzheimer’s Disease, and Complement,” *International Journal of Alzheimer’s Disease*, 2012, pp. 1–10. doi:10.1155/2012/983640.

Crider, A. *et al.* (2018) “Complement component 3a receptor deficiency attenuates chronic stress-induced monocyte infiltration and depressive-like behavior.,” *Brain, behavior, and immunity*, 70, pp. 246–256. doi:10.1016/j.bbi.2018.03.004.

Cudrici, C. *et al.* (2008) “Complement C5 regulates the expression of insulin-like growth factor binding proteins in chronic experimental allergic encephalomyelitis,” *Journal of Neuroimmunology*, 203(1), pp. 94–103. doi:10.1016/j.jneuroim.2008.06.040.

Cuneo, A.A. and Autieri, M. v (2009) “Expression and function of anti-inflammatory interleukins: the other side of the vascular response to injury.,” *Current vascular pharmacology*, 7(3), pp. 267–76. doi:10.2174/157016109788340721.

Cunha (2010) “A simple role for BDNF in learning and memory?,” *Frontiers in Molecular Neuroscience* [Preprint]. doi:10.3389/neuro.02.001.2010.

Cunningham, A.J. *et al.* (1996) “Interleukin-1β (IL-1β) and tumour necrosis factor (TNF) inhibit long-term potentiation in the rat dentate gyrus in vitro,” *Neuroscience Letters*, 203(1), pp. 17–20. doi:10.1016/0304-3940(95)12252-4.

Curzon, P., Rustay, N. and Browman, K. (2009) “Chapter 2 Cued and Contextual Fear Conditioning for Rodents,” in *Methods of Behavior Analysis in Neuroscience*. 2nd edn.

Dalmau, I. *et al.* (1998) “Development of microglia in the postnatal rat hippocampus,” *Hippocampus*, 8(5), pp. 458–474. doi:10.1002/(SICI)1098-1063(1998)8:5<458::AID-HIPO6>3.0.CO;2-N.

van Dam, H. and Castellazzi, M. (2001) “Distinct roles of Jun : Fos and Jun : ATF dimers in oncogenesis,” *Oncogene*, 20(19), pp. 2453–2464. doi:10.1038/sj.onc.1204239.

Daneman, R. and Prat, A. (2015) “The Blood–Brain Barrier,” *Cold Spring Harbor Perspectives in Biology*, 7(1), p. a020412. doi:10.1101/cshperspect.a020412.

Dashiell, S.M., Rus, H. and Koski, C.L. (2000) “Terminal complement complexes concomitantly stimulate proliferation and rescue of Schwann cells from apoptosis,”

Glia, 30(2), pp. 187–198. doi:10.1002/(SICI)1098-1136(200004)30:2<187::AID-GLIA8>3.0.CO;2-7.

Datta, D. (2017) “APP Modulates Aβ-Induced Activation of Microglia in Mouse Model of Alzheimer’s Disease,” *The Journal of Neuroscience*, 37(2), pp. 238–240. doi:10.1523/JNEUROSCI.3122-16.2017.

Davalos, D. *et al.* (2005) “ATP mediates rapid microglial response to local brain injury in vivo,” *Nature Neuroscience*, 8(6), pp. 752–758. doi:10.1038/nn1472.

Davis, M. (1997) “Neurobiology of fear responses: the role of the amygdala.,” *The Journal of neuropsychiatry and clinical neurosciences*, 9(3), pp. 382–402. doi:10.1176/jnp.9.3.382.

Davoust, N. *et al.* (1999) “Receptor for the C3a anaphylatoxin is expressed by neurons and glial cells,” *Glia*, 26(3), pp. 201–211.

Decker, E.L. (2003) “Early growth response proteins (EGR) and nuclear factors of activated T cells (NFAT) form heterodimers and regulate proinflammatory cytokine gene expression,” *Nucleic Acids Research*, 31(3), pp. 911–921. doi:10.1093/nar/gkg186.

Degn, S.E. *et al.* (2012) “Mannan-Binding Lectin-Associated Serine Protease (MASP)-1 Is Crucial for Lectin Pathway Activation in Human Serum, whereas neither MASP-1 nor MASP-3 Is Required for Alternative Pathway Function,” *The Journal of Immunology*, 189(8), pp. 3957–3969. doi:10.4049/jimmunol.1201736.

Deisseroth, K. *et al.* (2003) “Signaling from synapse to nucleus: the logic behind the mechanisms,” *Current Opinion in Neurobiology*, 13(3), pp. 354–365. doi:10.1016/S0959-4388(03)00076-X.

Deschaux, O., Spennato, G., *et al.* (2011) “Chronic treatment with fluoxetine prevents the return of extinguished auditory-cued conditioned fear,” *Psychopharmacology*, 215(2), pp. 231–237. doi:10.1007/s00213-010-2134-y.

Deschaux, O., Motanis, H., *et al.* (2011) “Re-emergence of extinguished auditory-cued conditioned fear following a sub-conditioning procedure: Effects of hippocampal and prefrontal tetanic stimulations,” *Neurobiology of Learning and Memory*, 95(4), pp. 510–518. doi:https://doi.org/10.1016/j.nlm.2011.03.002.

Diaz-Aparicio, I. *et al.* (2020) “Microglia Actively Remodel Adult Hippocampal Neurogenesis through the Phagocytosis Secretome,” *The Journal of Neuroscience*, 40(7), pp. 1453–1482. doi:10.1523/JNEUROSCI.0993-19.2019.

Dickinson, A. (2012) “Associative learning and animal cognition.,” *Philosophical transactions of the Royal Society of London. Series B, Biological sciences*, 367(1603), pp. 2733–42. doi:10.1098/rstb.2012.0220.

Difede, J. *et al.* (2014) “D-cycloserine augmentation of exposure therapy for post-traumatic stress disorder: a pilot randomized clinical trial.,” *Neuropsychopharmacology : official publication of the American College of Neuropsychopharmacology*, 39(5), pp. 1052–8. doi:10.1038/npp.2013.317.

Distler, M.G. *et al.* (2012) “Assessment of Behaviors Modeling Aspects of Schizophrenia in Csmd1 Mutant Mice,” *PLoS ONE*, 7(12), p. e51235. doi:10.1371/journal.pone.0051235.

Dityatev, A. and Fellin, T. (2008) “Extracellular matrix in plasticity and epileptogenesis,” *Neuron Glia Biology*, 4(3), pp. 235–247. doi:10.1017/S1740925X09000118.

Diwadkar, V.A., Flaugher, B., Jones, T., Zalányi, L., Ujfalussy, B., Keshavan, M.S. and Érdi, P. (2008) “Impaired associative learning in schizophrenia: behavioral and computational studies,” *Cognitive Neurodynamics*, 2(3), p. 207. doi:10.1007/s11571-008-9054-0.

Dolleman-van der Weel, M.J. *et al.* (2019) “The nucleus reuniens of the thalamus sits at the nexus of a hippocampus and medial prefrontal cortex circuit enabling memory and behavior,” *Learning & Memory*, 26(7), pp. 191–205. doi:10.1101/lm.048389.118.

Domercq, M., Vázquez-Villoldo, N. and Matute, C. (2013) “Neurotransmitter signaling in the pathophysiology of microglia,” *Frontiers in Cellular Neuroscience*, 7. doi:10.3389/fncel.2013.00049.

Do-Monte, F.H. *et al.* (2015) “Revisiting the Role of Infralimbic Cortex in Fear Extinction with Optogenetics,” *Journal of Neuroscience*, 35(8), pp. 3607–3615. doi:10.1523/JNEUROSCI.3137-14.2015.

Donat, C.K. *et al.* (2017) “Microglial Activation in Traumatic Brain Injury,” *Frontiers in Aging Neuroscience*, 9. doi:10.3389/fnagi.2017.00208.

Druart, M. and le Magueresse, C. (2019) “Emerging Roles of Complement in Psychiatric Disorders,” *Frontiers in Psychiatry*, 10. doi:10.3389/fpsyt.2019.00573.

Duclot, F. and Kabbaj, M. (2017) “The Role of Early Growth Response 1 (EGR1) in Brain Plasticity and Neuropsychiatric Disorders,” *Frontiers in Behavioral Neuroscience*, 11. doi:10.3389/fnbeh.2017.00035.

Ducruet, A.F. *et al.* (2012) “Complement Inhibition Promotes Endogenous Neurogenesis and Sustained Anti-Inflammatory Neuroprotection following Reperfused Stroke,” *PLoS ONE*, 7(6), p. e38664. doi:10.1371/journal.pone.0038664.

Dunkelberger, J.R. and Song, W.-C. (2010) “Complement and its role in innate and adaptive immune responses,” *Cell Research*, 20(1), pp. 34–50. doi:10.1038/cr.2009.139.

Escartin, C. *et al.* (2021) “Reactive astrocyte nomenclature, definitions, and future directions,” *Nature Neuroscience*, 24(3), pp. 312–325. doi:10.1038/s41593-020-00783-4.

Escudero-Esparza, A. *et al.* (2013) “The novel complement inhibitor human CUB and Sushi multiple domains 1 (CSMD1) protein promotes factor I-mediated degradation of C4b and C3b and inhibits the membrane attack complex assembly,” *The FASEB Journal*, 27(12), pp. 5083–5093. doi:10.1096/fj.13-230706.

Etienne-Manneville, S. (2004) “Actin and Microtubules in Cell Motility: Which One is in Control?,” *Traffic*, 5(7), pp. 470–477. doi:10.1111/j.1600-0854.2004.00196.x.

Eugen-Olsen, J. *et al.* (1997) “Serotonin Modulates Immune Function in T Cells from HIV-Seropositive Subjects,” *Clinical Immunology and Immunopathology*, 84(2), pp. 115–121. doi:10.1006/clin.1997.4384.

Eyo, U.B. *et al.* (2014) “Neuronal Hyperactivity Recruits Microglial Processes via Neuronal NMDA Receptors and Microglial P2Y12 Receptors after Status Epilepticus,” *Journal of Neuroscience*, 34(32), pp. 10528–10540. doi:10.1523/JNEUROSCI.0416-14.2014.

Falls, W.A., Miserendino, M.J. and Davis, M. (1992) “Extinction of fear-potentiated startle: blockade by infusion of an NMDA antagonist into the amygdala.,” *The Journal of neuroscience : the official journal of the Society for Neuroscience*, 12(3), pp. 854–63.

Fernández-Arjona, M. del M. *et al.* (2017) “Microglia Morphological Categorization in a Rat Model of Neuroinflammation by Hierarchical Cluster and Principal Components Analysis,” *Frontiers in Cellular Neuroscience*, 11. doi:10.3389/fncel.2017.00235.

Fernández-Arjona, M. del M. *et al.* (2019) “Microglial Morphometric Parameters Correlate With the Expression Level of IL-1β, and Allow Identifying Different Activated Morphotypes,” *Frontiers in Cellular Neuroscience*, 13. doi:10.3389/fncel.2019.00472.

Ferrari, D. *et al.* (1997) “Purinergic Modulation of Interleukin-1β Release from Microglial Cells Stimulated with Bacterial Endotoxin,” *Journal of Experimental Medicine*, 185(3), pp. 579–582. doi:10.1084/jem.185.3.579.

Figueiredo, C.P. *et al.* (2019) “Zika virus replicates in adult human brain tissue and impairs synapses and memory in mice,” *Nature Communications*, 10(1), p. 3890. doi:10.1038/s41467-019-11866-7.

Filipkowski, R.K., Knapska, E. and Kaczmarek, L. (2006) “c-Fos and Zif268 in Learning and Memory—Studies on Expression and Function,” in *Immediate Early Genes in Sensory Processing, Cognitive Performance and Neurological Disorders*. Springer US, pp. 137–158. doi:10.1007/978-0-387-33604-6_8.

Fiske, B.K. and Brunjes, P.C. (2000) “Microglial activation in the developing rat olfactory bulb,” *Neuroscience*, 96(4), pp. 807–815. doi:10.1016/S0306-4522(99)00601-6.

Franco-Bocanegra *et al.* (2019) “Molecular Mechanisms of Microglial Motility: Changes in Ageing and Alzheimer’s Disease,” *Cells*, 8(6), p. 639. doi:10.3390/cells8060639.

Franco-Bocanegra, D.K. *et al.* (2021) “Microglial morphology in Alzheimer’s disease and after Aβ immunotherapy,” *Scientific Reports*, 11(1), p. 15955. doi:10.1038/s41598-021-95535-0.

Frankland, P.W. *et al.* (2004) “The Involvement of the Anterior Cingulate Cortex in Remote Contextual Fear Memory,” *Science*, 304(5672), pp. 881–883. doi:10.1126/science.1094804.

Frolov, Y.P. (1937) *Pavlov and his school: the theory of conditioned reflexes. [Trans. by C. P. Dutt.]*, *Pavlov and his school: the theory of conditioned reflexes.* Oxford, England: Oxford Univ. Press.

Frost, J.L. and Schafer, D.P. (2016) “Microglia: Architects of the Developing Nervous System,” *Trends in Cell Biology*, 26(8), pp. 587–597. doi:https://doi.org/10.1016/j.tcb.2016.02.006.

Fujimoto, T. *et al.* (2004) “Arc interacts with microtubules/microtubule-associated protein 2 and attenuates microtubule-associated protein 2 immunoreactivity in the dendrites.,” *Journal of neuroscience research*, 76(1), pp. 51–63. doi:10.1002/jnr.20056.

Gage, G.J., Kipke, D.R. and Shain, W. (2012) “Whole Animal Perfusion Fixation for Rodents,” *Journal of Visualized Experiments* [Preprint], (65). doi:10.3791/3564.

Gallo, F.T. *et al.* (2018) “Immediate Early Genes, Memory and Psychiatric Disorders: Focus on c-Fos, Egr1 and Arc,” *Frontiers in Behavioral Neuroscience*, 12. doi:10.3389/fnbeh.2018.00079.

Galloway, D.A. *et al.* (2019) “Phagocytosis in the Brain: Homeostasis and Disease,” *Frontiers in Immunology*, 10. doi:10.3389/fimmu.2019.00790.

García-Magro, N. *et al.* (2020) “Multiple Morphometric Assessment of Microglial Cells in Deafferented Spinal Trigeminal Nucleus,” *Frontiers in Neuroanatomy*, 13. doi:10.3389/fnana.2019.00103.

Garín-Aguilar, M.E. *et al.* (2012) “Extinction procedure induces pruning of dendritic spines in CA1 hippocampal field depending on strength of training in rats,” *Frontiers in Behavioral Neuroscience*, 6. doi:10.3389/fnbeh.2012.00012.

Gayral, P. *et al.* (2011) “Next-generation sequencing of transcriptomes: a guide to RNA isolation in nonmodel animals,” *Molecular Ecology Resources*, 11(4), pp. 650–661. doi:10.1111/j.1755-0998.2011.03010.x.

Gewirtz, Jonathan C, McNish, K.A. and Davis, M. (2000a) “Is the hippocampus necessary for contextual fear conditioning?,” *Behavioural Brain Research*, 110(1), pp. 83–95. doi:https://doi.org/10.1016/S0166-4328(99)00187-4.

Ghosh, A. *et al.* (1994) “Calcium regulation of gene expression in neuronal cells,” *Journal of Neurobiology*, 25(3), pp. 294–303. doi:10.1002/neu.480250309.

Gibney, S.M. *et al.* (2013) “Poly I:C-induced activation of the immune response is accompanied by depression and anxiety-like behaviours, kynurenine pathway activation and reduced BDNF expression,” *Brain, Behavior, and Immunity*, 28, pp. 170–181. doi:https://doi.org/10.1016/j.bbi.2012.11.010.

Gill, K.M., Miller, S.A. and Grace, A.A. (2018) “Impaired contextual fear-conditioning in MAM rodent model of schizophrenia,” *Schizophrenia Research*, 195, pp. 343–352. doi:10.1016/j.schres.2017.08.064.

Giordano, K.R. *et al.* (2021) “An update on the rod microglia variant in experimental and clinical brain injury and disease,” *Brain Communications*, 3(1). doi:10.1093/braincomms/fcaa227.

Giorgi, C. *et al.* (2007) “The EJC factor eIF4AIII modulates synaptic strength and neuronal protein expression.,” *Cell*, 130(1), pp. 179–91. doi:10.1016/j.cell.2007.05.028.

Giulian, D. and Baker, T.J. (1986) “Characterization of ameboid microglia isolated from developing mammalian brain.,” *The Journal of neuroscience : the official journal of the Society for Neuroscience*, 6(8), pp. 2163–78.

Giustino, T.F. and Maren, S. (2015) “The Role of the Medial Prefrontal Cortex in the Conditioning and Extinction of Fear,” *Frontiers in Behavioral Neuroscience*, 9. doi:10.3389/fnbeh.2015.00298.

Glenn, J.A. *et al.* (1992) “Characterisation of ramified microglial cells: detailed morphology, morphological plasticity and proliferative capability.,” *Journal of anatomy*, 180 (Pt 1), pp. 109–18.

Gold, J.M. (1997) “Auditory Working Memory and Wisconsin Card Sorting Test Performance in Schizophrenia,” *Archives of General Psychiatry*, 54(2), p. 159. doi:10.1001/archpsyc.1997.01830140071013.

Gorelik, A. *et al.* (2017) “Serping1/C1 Inhibitor Affects Cortical Development in a Cell Autonomous and Non-cell Autonomous Manner,” *Frontiers in Cellular Neuroscience*, 11. doi:10.3389/fncel.2017.00169.

Gorsuch, W.B. *et al.* (2012) “The complement system in ischemia–reperfusion injuries,” *Immunobiology*, 217(11), pp. 1026–1033.

Gottlieb, D.I. and Cowan, W.M. (1973) “Autoradiographic studies of the commissural and ipsilateral association connection of the hippocampus and detentate gyrus of the rat. I. The commissural connections.,” *The Journal of comparative neurology*, 149(4), pp. 393–422. doi:10.1002/cne.901490402.

Grabert, K. *et al.* (2016) “Microglial brain region− dependent diversity and selective regional sensitivities to aging,” *Nature neuroscience*, 19(3), pp. 504–516.

Graham, Bronwyn M and Milad, M.R. (2016) “Fear conditioning and extinction.,” in *Neurophenotypes: Advancing psychiatry and neuropsychology in the “OMICS” era.* New York, NY, US: Springer Science + Business Media (Innovations in cognitive neuroscience.), pp. 139–155. doi:10.1007/978-1-4614-3846-5_8.

Grahames, C.B.A. *et al.* (1999) “Pharmacological characterization of ATP- and LPS-induced IL-1β release in human monocytes,” *British Journal of Pharmacology*, 127(8), pp. 1915–1921. doi:10.1038/sj.bjp.0702732.

Gromski, P.S. *et al.* (2015) “The influence of scaling metabolomics data on model classification accuracy,” *Metabolomics*, 11(3), pp. 684–695. doi:10.1007/s11306-014-0738-7.

Gruart, A. *et al.* (2015) “Functional basis of associative learning and its relationships with long-term potentiation evoked in the involved neural circuits: Lessons from studies in behaving mammals,” *Neurobiology of Learning and Memory*, 124, pp. 3–18. doi:https://doi.org/10.1016/j.nlm.2015.04.006.

Guerrero, B.L. and Sicotte, N.L. (2020) “Microglia in Multiple Sclerosis: Friend or Foe?,” *Frontiers in Immunology*, 11. doi:10.3389/fimmu.2020.00374.

Gulati, S. *et al.* (2002) “Regulation of the Mannan-Binding Lectin Pathway of Complement on *Neisseria gonorrhoeae* by C1-Inhibitor and α_2-Macroglobulin,” *The Journal of Immunology*, 168(8), pp. 4078–4086. doi:10.4049/jimmunol.168.8.4078.

Guo, R.-F. and Ward, P.A. (2005) “Role of C5a in inflammatory responses.,” *Annual review of immunology*, 23, pp. 821–52. doi:10.1146/annurev.immunol.23.021704.115835.

Gupton, S.L. and Gertler, F.B. (2007) “Filopodia: The Fingers That Do the Walking,” *Science’s STKE*, 2007(400). doi:10.1126/stke.4002007re5.

Guzowski, J.F. *et al.* (1999) “Environment-specific expression of the immediate-early gene Arc in hippocampal neuronal ensembles.,” *Nature neuroscience*, 2(12), pp. 1120–4. doi:10.1038/16046.

Guzowski, J.F. *et al.* (2001) “Experience-Dependent Gene Expression in the Rat Hippocampus after Spatial Learning: A Comparison of the Immediate-Early Genes *Arc* , c- *fos* , and *zif268*,” *The Journal of Neuroscience*, 21(14), pp. 5089–5098. doi:10.1523/JNEUROSCI.21-14-05089.2001.

Györffy, B.A. *et al.* (2018) “Local apoptotic-like mechanisms underlie complement-mediated synaptic pruning,” *Proceedings of the National Academy of Sciences*, 115(24), pp. 6303–6308. doi:10.1073/pnas.1722613115.

Hajian-Tilaki, K. (2013) “Receiver Operating Characteristic (ROC) Curve Analysis for Medical Diagnostic Test Evaluation.,” *Caspian journal of internal medicine*, 4(2), pp. 627–35.

Hajishengallis, G. and Lambris, J.D. (2010) “Crosstalk pathways between Toll-like receptors and the complement system,” *Trends in Immunology*, 31(4), pp. 154–163. doi:https://doi.org/10.1016/j.it.2010.01.002.

Hall, J., Romaniuk, L., McIntosh, Andrew M, *et al.* (2009) “Associative learning and the genetics of schizophrenia,” *Trends in Neurosciences*, 32(6), pp. 359–365. doi:https://doi.org/10.1016/j.tins.2009.01.011.

Hall, J., Thomas, K.L. and Everitt, B.J. (2000) “Rapid and selective induction of BDNF expression in the hippocampus during contextual learning,” *Nature Neuroscience*, 3(6), pp. 533–535. doi:10.1038/75698.

Hall, J., Thomas, K.L. and Everitt, B.J. (2001) “Cellular Imaging of *zif268* Expression in the Hippocampus and Amygdala during Contextual and Cued Fear Memory Retrieval: Selective Activation of Hippocampal CA1 Neurons during the Recall of Contextual Memories,” *The Journal of Neuroscience*, 21(6), pp. 2186–2193. doi:10.1523/JNEUROSCI.21-06-02186.2001.

Hammad, A., Westacott, L. and Zaben, M. (2018) “The role of the complement system in traumatic brain injury: a review,” *Journal of neuroinflammation*, 15(1), pp. 1–15.

Han, S. *et al.* (2015) “Learning both weights and connections for efficient neural networks,” *arXiv preprint arXiv:1506.02626* [Preprint].

Hanisch, U.-K. and Kettenmann, H. (2007) “Microglia: active sensor and versatile effector cells in the normal and pathologic brain,” *Nature Neuroscience*, 10(11), pp. 1387–1394. doi:10.1038/nn1997.

Hansen, D. v., Hanson, J.E. and Sheng, M. (2018) “Microglia in Alzheimer’s disease,” *Journal of Cell Biology*, 217(2), pp. 459–472. doi:10.1083/jcb.201709069.

Hao, Y. *et al.* (2014) “Intra-amygdala microinfusion of IL-6 impairs the auditory fear conditioning of rats via JAK/STAT activation,” *Behavioural Brain Research*, 275, pp. 88–95. doi:10.1016/j.bbr.2014.08.052.

Harboe, M. *et al.* (2004) “The quantitative role of alternative pathway amplification in classical pathway induced terminal complement activation,” *Clinical and Experimental Immunology*, 138(3), pp. 439–446. doi:10.1111/j.1365-2249.2004.02627.x.

Hasan, M.R. *et al.* (2018) “Classification of cancer cells using computational analysis of dynamic morphology,” *Computer methods and programs in biomedicine*, 156, pp. 105–112.

Haubensak, W. *et al.* (2010) “Genetic dissection of an amygdala microcircuit that gates conditioned fear.,” *Nature*, 468(7321), pp. 270–6. doi:10.1038/nature09553.

Haubrich, J. *et al.* (2015) “Reconsolidation Allows Fear Memory to Be Updated to a Less Aversive Level through the Incorporation of Appetitive Information,” *Neuropsychopharmacology*, 40(2), pp. 315–326. doi:10.1038/npp.2014.174.

Heidbreder, C.A. and Groenewegen, H.J. (2003) “The medial prefrontal cortex in the rat: evidence for a dorso-ventral distinction based upon functional and anatomical characteristics.,” *Neuroscience and biobehavioral reviews*, 27(6), pp. 555–79. doi:10.1016/j.neubiorev.2003.09.003.

Heja, D. *et al.* (2012) “Revised mechanism of complement lectin-pathway activation revealing the role of serine protease MASP-1 as the exclusive activator of MASP-2,”

Proceedings of the National Academy of Sciences, 109(26), pp. 10498–10503. doi:10.1073/pnas.1202588109.

Heldt, S.A. and Ressler, K.J. (2007) “Training-induced changes in the expression of GABAA-associated genes in the amygdala after the acquisition and extinction of Pavlovian fear.,” *The European journal of neuroscience*, 26(12), pp. 3631–44. doi:10.1111/j.1460-9568.2007.05970.x.

Herry, C. and Mons, N. (2004) “Resistance to extinction is associated with impairedimmediate early gene induction in medial prefrontalcortex and amygdala,” *European Journal of Neuroscience*, 20, pp. 781-790.

Herdegen, T. and Leah, J.D. (1998) “Inducible and constitutive transcription factors in the mammalian nervous system: control of gene expression by Jun, Fos and Krox, and CREB/ATF proteins,” *Brain Research Reviews*, 28(3), pp. 370–490. doi:10.1016/S0165-0173(98)00018-6.

Herr, N., Bode, C. and Duerschmied, D. (2017) “The Effects of Serotonin in Immune Cells,” *Frontiers in Cardiovascular Medicine*, 4. doi:10.3389/fcvm.2017.00048.

Herrlich, P. (2001) “Cross-talk between glucocorticoid receptor and AP-1,” *Oncogene*, 20(19), pp. 2465–2475. doi:10.1038/sj.onc.1204388.

Hind, L.E., Vincent, W.J.B. and Huttenlocher, A. (2016) “Leading from the Back: The Role of the Uropod in Neutrophil Polarization and Migration,” *Developmental Cell*, 38(2), pp. 161–169. doi:10.1016/j.devcel.2016.06.031.

Hines, D.J. *et al.* (2013) “Prevention of LPS-induced microglia activation, cytokine production and sickness behavior with TLR4 receptor interfering peptides,” *PloS one*, 8(3), p. e60388.

Hofer, E. *et al.* (2001) “Impaired conditional discrimination learning in schizophrenia,” *Schizophrenia Research*, 51(2–3), pp. 127–136. doi:10.1016/S0920-9964(00)00118-3.

Hoffman, G.E., Smith, M.S. and Verbalis, J.G. (1993) “c-Fos and Related Immediate Early Gene Products as Markers of Activity in Neuroendocrine Systems,” *Frontiers in Neuroendocrinology*, 14(3), pp. 173–213. doi:https://doi.org/10.1006/frne.1993.1006.

Holers, V.M. (2000) “Phenotypes of complement knockouts,” *Immunopharmacology*, 49(1–2), pp. 125–131. doi:10.1016/S0162-3109(00)80298-2.

Holloway, O.G. *et al.* (2019) “Rod microglia and their role in neurological diseases,” *Seminars in Cell & Developmental Biology*, 94, pp. 96–103. doi:10.1016/j.semcdb.2019.02.005.

Holt, D.J. *et al.* (2009) “Extinction memory is impaired in schizophrenia,” *Biological psychiatry*, 65(6), pp. 455–463.

Holt, D.J. *et al.* (2012) “Failure of neural responses to safety cues in schizophrenia,” *Archives of general psychiatry*, 69(9), pp. 893–903.

Hoover, W.B. and Vertes, R.P. (2007) “Anatomical analysis of afferent projections to the medial prefrontal cortex in the rat.,” *Brain structure & function*, 212(2), pp. 149–79. doi:10.1007/s00429-007-0150-4.

Hovens, I., Nyakas, C. and Schoemaker, R. (2014) “A novel method for evaluating microglial activation using ionized calcium-binding adaptor protein-1 staining: cell body to cell size ratio,” *Neuroimmunology and Neuroinflammation*, 1(2), p. 82. doi:10.4103/2347-8659.139719.

Hovhannisyan, L.P. *et al.* (2010) “Alterations in the complement cascade in post-traumatic stress disorder,” *Allergy, Asthma & Clinical Immunology*, 6(1), pp. 1–5.

Hudgins, C. and Otto, T. (2019) “Hippocampal Arc protein expression and conditioned fear,” *Neurobiology of Learning and Memory*, 161, pp. 175–191. doi:https://doi.org/10.1016/j.nlm.2019.04.004.

Huerta, P.T. *et al.* (2000) “Formation of Temporal Memory Requires NMDA Receptors within CA1 Pyramidal Neurons,” *Neuron*, 25(2), pp. 473–480. doi:https://doi.org/10.1016/S0896-6273(00)80909-5.

Huff, N.C. *et al.* (2006) “Amygdala Regulation of Immediate-Early Gene Expression in the Hippocampus Induced by Contextual Fear Conditioning,” *The Journal of Neuroscience*, 26(5), pp. 1616–1623. doi:10.1523/JNEUROSCI.4964-05.2006.

Hughes, C.E. and Nibbs, R.J.B. (2018) “A guide to chemokines and their receptors.,” *The FEBS journal*, 285(16), pp. 2944–2971. doi:10.1111/febs.14466.

Hume, D. (1978) *Treatise of human nature*. Oxford University Press.

Humphries, C.L. *et al.* (2002) “Direct regulation of Arp2/3 complex activity and function by the actin binding protein coronin,” *Journal of Cell Biology*, 159(6), pp. 993–1004. doi:10.1083/jcb.200206113.

Husi, H. *et al.* (2000) “Proteomic analysis of NMDA receptor-adhesion protein signaling complexes.,” *Nature neuroscience*, 3(7), pp. 661–9. doi:10.1038/76615.

Idusogie, E.E. *et al.* (2000) “Mapping of the C1q binding site on rituxan, a chimeric antibody with a human IgG1 Fc.,” *Journal of immunology (Baltimore, Md. : 1950)*, 164(8), pp. 4178–84. doi:10.4049/jimmunol.164.8.4178.

Irie, Y. *et al.* (2000) “Molecular cloning and characterization of Amida, a novel protein which interacts with a neuron-specific immediate early gene product arc, contains novel nuclear localization signals, and causes cell death in cultured cells.,” *The Journal of biological chemistry*, 275(4), pp. 2647–53. doi:10.1074/jbc.275.4.2647.

Ito, D. *et al.* (2001) “Enhanced expression of Iba1, ionized calcium-binding adapter molecule 1, after transient focal cerebral ischemia in rat brain.,” *Stroke*, 32(5), pp. 1208–15. doi:10.1161/01.str.32.5.1208.

Izquierdo, I., Furini, C.R.G. and Myskiw, J.C. (2016) “Fear Memory,” *Physiological Reviews*, 96(2), pp. 695–750. doi:10.1152/physrev.00018.2015.

James, Conway and Morris (2005) “Genomic profiling of the neuronal target genes of the plasticity-related transcription factor - Zif268,” *Journal of Neurochemistry*, 95(3), pp. 796–810. doi:10.1111/j.1471-4159.2005.03400.x.

Jarrard, L.E. (1995a) “What does the hippocampus really do?,” *Behavioural Brain Research*, 71(1), pp. 1–10. doi:https://doi.org/10.1016/0166-4328(95)00034-8.

Jeffrey, M. (1987) “A Nerve Growth Factor-Induced Gene Encodes a Possible Transcriptional Regulatory Factor,” *Science*, 238(4828), pp. 797–799. doi:10.1126/science.3672127.

Jensen, R.K. *et al.* (2021) “Complement Receptor 3 Forms a Compact High-Affinity Complex with iC3b,” *The Journal of Immunology*, 206(12), pp. 3032–3042. doi:10.4049/jimmunol.2001208.

Jolliffe, I.T. and Cadima, J. (2016) “Principal component analysis: a review and recent developments,” *Philosophical Transactions of the Royal Society A: Mathematical, Physical and Engineering Sciences*, 374(2065), p. 20150202. doi:10.1098/rsta.2015.0202.

Joshi, J., Rubart, M. and Zhu, W. (2020) “Optogenetics: Background, Methodological Advances and Potential Applications for Cardiovascular Research and Medicine,” *Frontiers in Bioengineering and Biotechnology*, 7. doi:10.3389/fbioe.2019.00466.

Josselyn, S.A. and Tonegawa, S. (2020) “Memory engrams: Recalling the past and imagining the future,” *Science*, 367(6473). doi:10.1126/science.aaw4325.

Jurga, A.M., Paleczna, M. and Kuter, K.Z. (2020a) “Overview of General and Discriminating Markers of Differential Microglia Phenotypes,” *Frontiers in Cellular Neuroscience*, 14. doi:10.3389/fncel.2020.00198.

Kanai, Y., Dohmae, N. and Hirokawa, N. (2004) “Kinesin Transports RNA,” *Neuron*, 43(4), pp. 513–525. doi:10.1016/j.neuron.2004.07.022.

Karin, M. and Chang, L. (2001) “AP-1--glucocorticoid receptor crosstalk taken to a higher level,” *Journal of Endocrinology*, 169(3), pp. 447–451. doi:10.1677/joe.0.1690447.

Kawashima, T. *et al.* (2009) “Synaptic activity-responsive element in the Arc/Arg3.1 promoter essential for synapse-to-nucleus signaling in activated neurons.,”

Proceedings of the National Academy of Sciences of the United States of America, 106(1), pp. 316–21. doi:10.1073/pnas.0806518106.

Kee, N. *et al.* (2007) “Preferential incorporation of adult-generated granule cells into spatial memory networks in the dentate gyrus,” *Nature Neuroscience*, 10(3), pp. 355–362. doi:10.1038/nn1847.

Keifer, O.P. *et al.* (2015a) “The Physiology of Fear: Reconceptualizing the Role of the Central Amygdala in Fear Learning.,” *Physiology (Bethesda, Md.)*, 30(5), pp. 389–401. doi:10.1152/physiol.00058.2014.

Khalaf, O. *et al.* (2018) “Reactivation of recall-induced neurons contributes to remote fear memory attenuation,” *Science*, 360(6394), pp. 1239–1242. doi:10.1126/science.aas9875.

Kim, H.-S. *et al.* (2016) “Selective Control of Fear Expression by Optogenetic Manipulation of Infralimbic Cortex after Extinction,” *Neuropsychopharmacology*, 41(5), pp. 1261–1273. doi:10.1038/npp.2015.276.

Kim, J.J. and Jung, M.W. (2006) “Neural circuits and mechanisms involved in Pavlovian fear conditioning: a critical review.,” *Neuroscience and biobehavioral reviews*, 30(2), pp. 188–202. doi:10.1016/j.neubiorev.2005.06.005.

Kim, W. bin and Cho, J.-H. (2020) “Encoding of contextual fear memory in hippocampal–amygdala circuit,” *Nature Communications*, 11(1), p. 1382. doi:10.1038/s41467-020-15121-2.

Kim, W.G. *et al.* (2000) “Regional difference in susceptibility to lipopolysaccharide-induced neurotoxicity in the rat brain: role of microglia.,” *The Journal of*

neuroscience: the official journal of the Society for Neuroscience, 20(16), pp. 6309–16.

Kirtley, A. and Thomas, K.L. (2010) “The exclusive induction of extinction is gated by BDNF,” *Leaning & Memory*, 17, pp. 612-619.

Kitamura, T. *et al.* (2017) “Engrams and circuits crucial for systems consolidation of a memory,” *Science*, 356(6333), pp. 73–78. doi:10.1126/science.aam6808.

Kloss, C.U.A. *et al.* (2001) “Effect of Lipopolysaccharide on the Morphology and Integrin Immunoreactivity of Ramified Microglia in the Mouse Brain and in Cell Culture,” *Experimental Neurology*, 168(1), pp. 32–46. doi:https://doi.org/10.1006/exnr.2000.7575.

Knapska, E. *et al.* (2012) “Functional anatomy of neural circuits regulating fear and extinction,” *Proceedings of the National Academy of Sciences*, 109(42), pp. 17093–17098. doi:10.1073/pnas.1202087109.

Knapska, E. and Maren, S. (2009) “Reciprocal patterns of c-Fos expression in the medial prefrontal cortex and amygdala after extinction and renewal of conditioned fear,” *Learning & Memory*, 16(8), pp. 486–493. doi:10.1101/lm.1463909.

Knierim, J.J. (2015) “The hippocampus,” *Current Biology*, 25(23), pp. R1116–R1121. doi:https://doi.org/10.1016/j.cub.2015.10.049.

Knifton, L. and Quinn, N. (2008) “Media, Mental Health and Discrimination: A Frame of Reference for Understanding Reporting Trends,” *International Journal of Mental Health Promotion*, 10(1), pp. 23–31. doi:10.1080/14623730.2008.9721754.

Knobloch, H.S. *et al.* (2012) “Evoked Axonal Oxytocin Release in the Central Amygdala Attenuates Fear Response,” *Neuron*, 73(3), pp. 553–566. doi:https://doi.org/10.1016/j.neuron.2011.11.030.

Koeniger, T. and Kuerten, S. (2017) “Splitting the ‘Unsplittable’: Dissecting Resident and Infiltrating Macrophages in Experimental Autoimmune Encephalomyelitis,” *International Journal of Molecular Sciences*, 18(10), p. 2072. doi:10.3390/ijms18102072.

Koiliari, E. *et al.* (2014) “The CSMD1 genome-wide associated schizophrenia risk variant rs10503253 affects general cognitive ability and executive function in healthy males,” *Schizophrenia Research*, 154(1–3), pp. 42–47. doi:10.1016/j.schres.2014.02.017.

Kojouharova, M., Reid, K. and Gadjeva, M. (2010) “New insights into the molecular mechanisms of classical complement activation.,” *Molecular immunology*, 47(13), pp. 2154–60. doi:10.1016/j.molimm.2010.05.011.

Kongsui, R. *et al.* (2014) “Quantitative assessment of microglial morphology and density reveals remarkable consistency in the distribution and morphology of cells within the healthy prefrontal cortex of the rat,” *Journal of Neuroinflammation*, 11(1), p. 182. doi:10.1186/s12974-014-0182-7.

Korb, E. *et al.* (2013) “Arc in the nucleus regulates PML-dependent GluA1 transcription and homeostatic plasticity,” *Nature Neuroscience*, 16(7), pp. 874–883. doi:10.1038/nn.3429.

Kourou, K. *et al.* (2015) “Machine learning applications in cancer prognosis and prediction,” *Computational and Structural Biotechnology Journal*, 13, pp. 8–17. doi:https://doi.org/10.1016/j.csbj.2014.11.005.

Kozera, B. and Rapacz, M. (2013) “Reference genes in real-time PCR,” *Journal of Applied Genetics*, 54(4), pp. 391–406. doi:10.1007/s13353-013-0173-x.

Kraus, D.M. *et al.* (2006) “CSMD1 Is a Novel Multiple Domain Complement-Regulatory Protein Highly Expressed in the Central Nervous System and Epithelial Tissues,” *The Journal of Immunology*, 176(7), pp. 4419–4430. doi:10.4049/jimmunol.176.7.4419.

Kruijssen, D.L.H. and Wierenga, C.J. (2019) “Single Synapse LTP: A Matter of Context?,” *Frontiers in Cellular Neuroscience*, 13. doi:10.3389/fncel.2019.00496.

Kvitsiani, D. *et al.* (2013) “Distinct behavioural and network correlates of two interneuron types in prefrontal cortex.,” *Nature*, 498(7454), pp. 363–6. doi:10.1038/nature12176.

Lacagnina, A.F. *et al.* (2019) “Distinct hippocampal engrams control extinction and relapse of fear memory,” *Nature Neuroscience*, 22(5), pp. 753–761. doi:10.1038/s41593-019-0361-z.

Lai, C.S.W., Adler, A. and Gan, W.-B. (2018) “Fear extinction reverses dendritic spine formation induced by fear conditioning in the mouse auditory cortex,” *Proceedings of the National Academy of Sciences*, 115(37), pp. 9306–9311. doi:10.1073/pnas.1801504115.

Lai, C.S.W., Franke, T.F. and Gan, W.-B. (2012) “Opposite effects of fear conditioning and extinction on dendritic spine remodelling,” *Nature*, 483(7387), pp. 87–91. doi:10.1038/nature10792.

Lai, F.P. *et al.* (2008) “Arp2/3 complex interactions and actin network turnover in lamellipodia,” *The EMBO Journal*, 27(7), pp. 982–992. doi:10.1038/emboj.2008.34.

Lalkhen, A.G. and McCluskey, A. (2008) “Clinical tests: sensitivity and specificity,” *Continuing education in anaesthesia critical care & pain*, 8(6), pp. 221–223.

Lambert, H.K. and McLaughlin, K.A. (2019) “Impaired hippocampus-dependent associative learning as a mechanism underlying PTSD: A meta-analysis.,” *Neuroscience and biobehavioral reviews*, 107, pp. 729–749. doi:10.1016/j.neubiorev.2019.09.024.

Laursen, N.S. *et al.* (2020) “Functional and Structural Characterization of a Potent C1q Inhibitor Targeting the Classical Pathway of the Complement System,” *Frontiers in Immunology*, 11. doi:10.3389/fimmu.2020.01504.

Lawson, L.J. *et al.* (1990) “Heterogeneity in the distribution and morphology of microglia in the normal adult mouse brain,” *Neuroscience*, 39(1), pp. 151–170. doi:10.1016/0306-4522(90)90229-W.

LeDoux, J. *et al.* (1990) “The lateral amygdaloid nucleus: sensory interface of the amygdala in fear conditioning,” *The Journal of Neuroscience*, 10(4), pp. 1062–1069. doi:10.1523/JNEUROSCI.10-04-01062.1990.

LeDoux, J. (2003) “The emotional brain, fear, and the amygdala.,” *Cellular and molecular neurobiology*, 23(4–5), pp. 727–38. doi:10.1023/a:1025048802629.

Lee, H.J. *et al.* (2016) “Extinction and retrieval+ extinction of conditioned fear differentially activate medial prefrontal cortex and amygdala in rats,” *Frontiers in Behavioral Neuroscience*, 9, p. 369.

Lee, J. *et al.* (2019) “Heterogeneity of microglia and their differential roles in white matter pathology,” *CNS Neuroscience & Therapeutics*, 25(12), pp. 1290–1298. doi:10.1111/cns.13266.

Lee, J.D., Taylor, S.M. and Woodruff, T.M. (2020) “Is the C3a receptor antagonist SB290157 a useful pharmacological tool?,” *British Journal of Pharmacology*, 177(24), pp. 5677–5678. doi:10.1111/bph.15264.

Lee, J.L.C. (2009) “Reconsolidation: maintaining memory relevance,” *Trends in Neurosciences*, 32(8), pp. 413–420. doi:10.1016/j.tins.2009.05.002.

Lee, J.L.C., Everitt, B.J. and Thomas, K.L. (2004) “Independent Cellular Processes for Hippocampal Memory Consolidation and Reconsolidation,” *Science*, 304(5672), pp. 839–843. doi:10.1126/science.1095760.

Lee, J. L. C., Milton, A.L. and Everitt, B.J. (2006) “Reconsolidation and Extinction of Conditioned Fear: Inhibition and Potentiation,” *Journal of Neuroscience*, 26(39), pp. 10051–10056. doi:10.1523/JNEUROSCI.2466-06.2006.

Lee, K.Y. *et al.* (2017) “Age-related change of Iba-1 immunoreactivity in the adult and aged gerbil spinal cord,” *Anatomy & Cell Biology*, 50(2), p. 135. doi:10.5115/acb.2017.50.2.135.

Lee, K.Y. (2019) “M1 and M2 polarization of macrophages: a mini-review,” *Medical Biological Science and Engineering*, 2(1), pp. 1–5. doi:10.30579/mbse.2019.2.1.1.

Lee, L.-J. *et al.* (2009) “Neonatal whisker trimming causes long-lasting changes in structure and function of the somatosensory system,” *Experimental Neurology*, 219(2), pp. 524–532. doi:https://doi.org/10.1016/j.expneurol.2009.07.012.

Leng, F. and Edison, P. (2021) “Neuroinflammation and microglial activation in Alzheimer disease: where do we go from here?,” *Nature Reviews Neurology*, 17(3), pp. 157–172. doi:10.1038/s41582-020-00435-y.

Lenz, K.M. and Nelson, L.H. (2018) “Microglia and Beyond: Innate Immune Cells As Regulators of Brain Development and Behavioral Function,” *Frontiers in Immunology*, 9. doi:10.3389/fimmu.2018.00698.

Lerch, J.K. *et al.* (2014) “cJun promotes CNS axon growth,” *Molecular and Cellular Neuroscience*, 59, pp. 97–105. doi:10.1016/j.mcn.2014.02.002.

Leuner, B., Falduto, J. and Shors, T.J. (2003) “Associative Memory Formation Increases the Observation of Dendritic Spines in the Hippocampus,” *The Journal of Neuroscience*, 23(2), pp. 659–665. doi:10.1523/JNEUROSCI.23-02-00659.2003.

Levin, S.G. and Godukhin, O. v. (2017) “Modulating effect of cytokines on mechanisms of synaptic plasticity in the brain,” *Biochemistry (Moscow)*, 82(3), pp. 264–274. doi:10.1134/S000629791703004X.

Lévi-Strauss, M. and Mallat, M. (1987) “Primary cultures of murine astrocytes produce C3 and factor B, two components of the alternative pathway of complement activation.,” *Journal of immunology (Baltimore, Md. : 1950)*, 139(7), pp. 2361–6.

Levkovitz, Y. and Baraban, J.M. (2002) “A Dominant Negative Egr Inhibitor Blocks Nerve Growth Factor-Induced Neurite Outgrowth by Suppressing c-Jun Activation:

Role of an Egr/c-Jun Complex," *The Journal of Neuroscience*, 22(10), pp. 3845–3854. doi:10.1523/JNEUROSCI.22-10-03845.2002.

Lewitus, G.M. *et al.* (2014) "An adaptive role of TNFα in the regulation of striatal synapses.," *The Journal of neuroscience : the official journal of the Society for Neuroscience*, 34(18), pp. 6146–55. doi:10.1523/JNEUROSCI.3481-13.2014.

Leyh, J. *et al.* (2021) "Classification of Microglial Morphological Phenotypes Using Machine Learning," *Frontiers in Cellular Neuroscience*, 15. doi:10.3389/fncel.2021.701673.

Li, H. *et al.* (2018) "Cell dynamic morphology classification using deep convolutional neural networks," *Cytometry Part A*, 93(6), pp. 628–638. doi:10.1002/cyto.a.23490.

Li, L. *et al.* (2007) "The function of microglia, either neuroprotection or neurotoxicity, is determined by the equilibrium among factors released from activated microglia in vitro," *Brain Research*, 1159, pp. 8–17. doi:10.1016/j.brainres.2007.04.066.

Li, Q. and Barres, B.A. (2018) "Microglia and macrophages in brain homeostasis and disease," *Nature Reviews Immunology*, 18(4), pp. 225–242. doi:10.1038/nri.2017.125.

Lin, H.-C., Mao, S.-C. and Gean, P.-W. (2009) "Block of γ-Aminobutyric Acid-A Receptor Insertion in the Amygdala Impairs Extinction of Conditioned Fear," *Biological Psychiatry*, 66(7), pp. 665–673. doi:10.1016/j.biopsych.2009.04.003.

Liste, I. *et al.* (1995) "Cortical stimulation induces Fos expression in striatal neurons via NMDA glutamate and dopamine receptors," *Brain Research*, 700(1–2), pp. 1–12. doi:10.1016/0006-8993(95)00958-S.

Liu, I.Y.C. *et al.* (2004) “Brain-derived neurotrophic factor plays a critical role in contextual fear conditioning.,” *The Journal of neuroscience : the official journal of the Society for Neuroscience*, 24(36), pp. 7958–63. doi:10.1523/JNEUROSCI.1948-04.2004.

Liu, S.-L. *et al.* (2011) “Mechanism of a Concentration-dependent Switch between Activation and Inhibition of Arp2/3 Complex by Coronin,” *Journal of Biological Chemistry*, 286(19), pp. 17039–17046. doi:10.1074/jbc.M111.219964.

Liu, Y. *et al.* (2019) “Altered expression of the CSMD1 gene in the peripheral blood of schizophrenia patients,” *BMC Psychiatry*, 19(1), p. 113. doi:10.1186/s12888-019-2089-4.

Livak, K.J. and Schmittgen, T.D. (2001) “Analysis of Relative Gene Expression Data Using Real-Time Quantitative PCR and the 2−ΔΔCT Method,” *Methods*, 25(4), pp. 402–408. doi:10.1006/meth.2001.1262.

Loane, D.J. and Kumar, A. (2016) “Microglia in the TBI brain: The good, the bad, and the dysregulated,” *Experimental Neurology*, 275, pp. 316–327. doi:https://doi.org/10.1016/j.expneurol.2015.08.018.

Lobsiger, C.S., Boillée, S. and Cleveland, D.W. (2007) “Toxicity from different SOD1 mutants dysregulates the complement system and the neuronal regenerative response in ALS motor neurons,” *Proceedings of the National Academy of Sciences*, 104(18), pp. 7319–7326. doi:10.1073/pnas.0702230104.

Lu, B., Nagappan, G. and Lu, Y. (2014) “BDNF and Synaptic Plasticity, Cognitive Function, and Dysfunction,” in, pp. 223–250. doi:10.1007/978-3-642-45106-5_9.

Lucibello, F.C. *et al.* (1989) “Trans-repression of the mouse c-fos promoter: A novel mechanism of fos-mediated trans-regulation,” *Cell*, 59(6), pp. 999–1007. doi:10.1016/0092-8674(89)90756-3.

Luo, C. *et al.* (2017) “The role of microglia in multiple sclerosis,” *Neuropsychiatric disease and treatment*, 13, p. 1661.

Lyford, G.L. *et al.* (1995) “Arc, a growth factor and activity-regulated gene, encodes a novel cytoskeleton-associated protein that is enriched in neuronal dendrites.,” *Neuron*, 14(2), pp. 433–45. doi:10.1016/0896-6273(95)90299-6.

Lynch, M.A. (2004) “Long-Term Potentiation and Memory,” *Physiological Reviews*, 84(1), pp. 87–136. doi:10.1152/physrev.00014.2003.

Lynch, M.A. (2009) “The Multifaceted Profile of Activated Microglia,” *Molecular Neurobiology*, 40(2), pp. 139–156. doi:10.1007/s12035-009-8077-9.

Lyons, M.R. and West, A.E. (2011) “Mechanisms of specificity in neuronal activity-regulated gene transcription,” *Progress in Neurobiology*, 94(3), pp. 259–295. doi:10.1016/j.pneurobio.2011.05.003.

Lyra e Silva, N.M. *et al.* (2021) “Pro-inflammatory interleukin-6 signaling links cognitive impairments and peripheral metabolic alterations in Alzheimer’s disease,” *Translational Psychiatry*, 11(1), p. 251. doi:10.1038/s41398-021-01349-z.

Maes, M. *et al.* (2012) “Depression and sickness behavior are Janus-faced responses to shared inflammatory pathways,” *BMC Medicine*, 10(1), p. 66. doi:10.1186/1741-7015-10-66.

Magdalon, J. *et al.* (2020) “Complement System in Brain Architecture and Neurodevelopmental Disorders,” *Frontiers in Neuroscience*, 14. doi:10.3389/fnins.2020.00023.

Maggi, L. (2011) “CX3CR1 deficiency alters hippocampal-dependent plasticity phenomena blunting the effects of enriched environment,” *Frontiers in Cellular Neuroscience*, 5. doi:10.3389/fncel.2011.00022.

Mahesh, B. (2020) “Machine Learning Algorithms-A Review,” *International Journal of Science and Research (IJSR).[Internet]*, 9, pp. 381–386.

Maier, S.F. *et al.* (1993) “Interleukin-1 mediates the behavioral hyperalgesia produced by lithium chloride and endotoxin,” *Brain Research*, 623(2), pp. 321–324. doi:10.1016/0006-8993(93)91446-Y.

Malenka, R.C. and Nicoll, and R.A. (1999) “Long-Term Potentiation--A Decade of Progress?,” *Science*, 285(5435), pp. 1870–1874. doi:10.1126/science.285.5435.1870.

Mallya, A.P. *et al.* (2019) “Microglial Pruning of Synapses in the Prefrontal Cortex During Adolescence,” *Cerebral Cortex*, 29(4), pp. 1634–1643. doi:10.1093/cercor/bhy061.

Manocha, G.D. *et al.* (2016) “APP Regulates Microglial Phenotype in a Mouse Model of Alzheimer’s Disease,” *Journal of Neuroscience*, 36(32), pp. 8471–8486. doi:10.1523/JNEUROSCI.4654-15.2016.

Mao, S.-C., Hsiao, Y.-H. and Gean, P.-W. (2006) “Extinction training in conjunction with a partial agonist of the glycine site on the NMDA receptor erases memory

trace.,” *The Journal of neuroscience : the official journal of the Society for Neuroscience*, 26(35), pp. 8892–9. doi:10.1523/JNEUROSCI.0365-06.2006.

Marcoulides, K.M. and Raykov, T. (2019) “Evaluation of Variance Inflation Factors in Regression Models Using Latent Variable Modeling Methods,” *Educational and Psychological Measurement*, 79(5), pp. 874–882. doi:10.1177/0013164418817803.

Maren, S. (1999) “Neurotoxic Basolateral Amygdala Lesions Impair Learning and Memory But Not the Performance of Conditional Fear in Rats,” *The Journal of Neuroscience*, 19(19), pp. 8696–8703. doi:10.1523/JNEUROSCI.19-19-08696.1999.

Maren, S. (2001) “Neurobiology of Pavlovian Fear Conditioning,” *Annual Review of Neuroscience*, 24(1), pp. 897–931. doi:10.1146/annurev.neuro.24.1.897.

Maren, S. (2005) “Synaptic Mechanisms of Associative Memory in the Amygdala,” *Neuron*, 47(6), pp. 783–786. doi:https://doi.org/10.1016/j.neuron.2005.08.009.

Maren, S, Aharonov, G. and Fanselow, M.S. (1997) “Neurotoxic lesions of the dorsal hippocampus and Pavlovian fear conditioning in rats.,” *Behavioural brain research*, 88(2), pp. 261–74. doi:10.1016/s0166-4328(97)00088-0.

Maren, S., Phan, K.L. and Liberzon, I. (2013) “The contextual brain: implications for fear conditioning, extinction and psychopathology,” *Nature Reviews Neuroscience*, 14(6), pp. 417–428. doi:10.1038/nrn3492.

Marin, I. and Kipnis, J. (2013) “Learning and memory… and the immune system,” *Learning & memory*, 20(10), pp. 601–606.

Marker, D.F. *et al.* (2010) “A Thin-skull Window Technique for Chronic Two-photon In vivo Imaging of Murine Microglia in Models of

Neuroinflammation," *Journal of Visualized Experiments* [Preprint], (43). doi:10.3791/2059.

Markiewski, M.M. *et al.* (2007) "Complement and coagulation: strangers or partners in crime?," *Trends in immunology*, 28(4), pp. 184–92. doi:10.1016/j.it.2007.02.006.

Martinez, Fernando O. and Gordon, S. (2014) "The M1 and M2 paradigm of macrophage activation: time for reassessment," *F1000Prime Reports*, 6. doi:10.12703/P6-13.

Mathieu, M.-C. *et al.* (2005) "The C3a receptor antagonist SB 290157 has agonist activity," *Immunology Letters*, 100(2), pp. 139–145. doi:10.1016/j.imlet.2005.03.003.

Mathys, H. *et al.* (2019) "Single-cell transcriptomic analysis of Alzheimer's disease.," *Nature*, 570(7761), pp. 332–337. doi:10.1038/s41586-019-1195-2.

Mayilyan, K.R., Weinberger, D.R. and Sim, R.B. (2008) "The complement system in schizophrenia," *Drug news & perspectives*, 21(4), p. 200.

Mazzolini, J., Chia, K. and Sieger, D. (2018) "Isolation and RNA Extraction of Neurons, Macrophages and Microglia from Larval Zebrafish Brains," *Journal of Visualized Experiments* [Preprint], (134). doi:10.3791/57431.

McNally, K. (2013) "Dementia praecox revisited," *History of Psychiatry*, 24(4), pp. 507–509. doi:10.1177/0957154X13501454.

Mendez, P. *et al.* (2018) "Homeostatic Plasticity in the Hippocampus Facilitates Memory Extinction," *Cell Reports*, 22(6), pp. 1451–1461. doi:https://doi.org/10.1016/j.celrep.2018.01.025.

Merlini, M. *et al.* (2019) “Fibrinogen Induces Microglia-Mediated Spine Elimination and Cognitive Impairment in an Alzheimer’s Disease Model,” *Neuron*, 101(6), pp. 1099-1108.e6. doi:https://doi.org/10.1016/j.neuron.2019.01.014.

Michael Dougher (2004) “Clinical Behavior Analysis.”

Milad, M.R. *et al.* (2009) “Neurobiological Basis of Failure to Recall Extinction Memory in Posttraumatic Stress Disorder,” *Biological Psychiatry*, 66(12), pp. 1075–1082. doi:https://doi.org/10.1016/j.biopsych.2009.06.026.

Milad, M.R. and Quirk, G.J. (2002) “Neurons in medial prefrontal cortex signal memory for fear extinction.,” *Nature*, 420(6911), pp. 70–4. doi:10.1038/nature01138.

Milior, G. *et al.* (2016) “Fractalkine receptor deficiency impairs microglial and neuronal responsiveness to chronic stress,” *Brain, behavior, and immunity*, 55, pp. 114–125.

Miller, K.D., Pinto, D.J. and Simons, D.J. (2001) “Processing in layer 4 of the neocortical circuit: new insights from visual and somatosensory cortex.,” *Current opinion in neurobiology*, 11(4), pp. 488–97. doi:10.1016/s0959-4388(00)00239-7.

Minagar, A. and Alexander, J.S. (2003) “Blood-brain barrier disruption in multiple sclerosis,” *Multiple Sclerosis Journal*, 9(6), pp. 540–549. doi:10.1191/1352458503ms965oa.

Minatohara, K., Akiyoshi, M. and Okuno, H. (2016) “Role of Immediate-Early Genes in Synaptic Plasticity and Neuronal Ensembles Underlying the Memory Trace,” *Frontiers in Molecular Neuroscience*, 8. doi:10.3389/fnmol.2015.00078.

Miyamoto, A. *et al.* (2013) “Microglia and synapse interactions: fine tuning neural circuits and candidate molecules,” *Frontiers in Cellular Neuroscience*, 7. doi:10.3389/fncel.2013.00070.

Mody, M. *et al.* (2001) “Genome-wide gene expression profiles of the developing mouse hippocampus,” *Proceedings of the National Academy of Sciences*, 98(15), pp. 8862–8867. doi:10.1073/pnas.141244998.

Moga, D.E. *et al.* (2004) “Activity-regulated cytoskeletal-associated protein is localized to recently activated excitatory synapses.,” *Neuroscience*, 125(1), pp. 7–11. doi:10.1016/j.neuroscience.2004.02.004.

Moghaddam, B. (2004) “Targeting metabotropic glutamate receptors for treatment of the cognitive symptoms of schizophrenia,” *Psychopharmacology*, 174(1), pp. 39–44. doi:10.1007/s00213-004-1792-z.

Moreno-Jiménez, E.P. *et al.* (2019) “Adult hippocampal neurogenesis is abundant in neurologically healthy subjects and drops sharply in patients with Alzheimer’s disease,” *Nature Medicine*, 25(4), pp. 554–560. doi:10.1038/s41591-019-0375-9.

Morgan, B.P. and Harris, C.L. (2015) “Complement, a target for therapy in inflammatory and degenerative diseases,” *Nature Reviews Drug Discovery*, 14(12), pp. 857–877. doi:10.1038/nrd4657.

Morgan, J.I. and Curran, T. (1986) “Role of ion flux in the control of c-fos expression.,” *Nature*, 322(6079), pp. 552–5. doi:10.1038/322552a0.

Morgan, J.I. and Curran, T. (1991) “Stimulus-Transcription Coupling in the Nervous System: Involvement of the Inducible Proto-Oncogenes *fos* and *jun*,” *Annual Review of Neuroscience*, 14(1), pp. 421–451. doi:10.1146/annurev.ne.14.030191.002225.

Morimoto, K. and Nakajima, K. (2019) “Role of the Immune System in the Development of the Central Nervous System,” *Frontiers in Neuroscience*, 13. doi:10.3389/fnins.2019.00916.

Moriyama, M. *et al.* (2011) “Complement receptor 2 is expressed in neural progenitor cells and regulates adult hippocampal neurogenesis.,” *The Journal of neuroscience : the official journal of the Society for Neuroscience*, 31(11), pp. 3981–9. doi:10.1523/JNEUROSCI.3617-10.2011.

Morrison, H. *et al.* (2017b) “Quantitative microglia analyses reveal diverse morphologic responses in the rat cortex after diffuse brain injury,” *Scientific Reports*, 7(1), p. 13211. doi:10.1038/s41598-017-13581-z.

Mortensen, S.A. *et al.* (2017a) “Structure and activation of C1, the complex initiating the classical pathway of the complement cascade,” *Proceedings of the National Academy of Sciences*, 114(5), pp. 986–991. doi:10.1073/pnas.1616998114.

Moser, B. (2004) “Chemokines: role in inflammation and immune surveillance,” *Annals of the Rheumatic Diseases*, 63(suppl_2), pp. ii84–ii89. doi:10.1136/ard.2004.028316.

Moser, B. and Willimann, K. (2004) “Chemokines: role in inflammation and immune surveillance.,” *Annals of the rheumatic diseases*, 63 Suppl 2, pp. ii84–ii89. doi:10.1136/ard.2004.028316.

Mozzachiodi, R. and Byrne, J.H. (2010) “More than synaptic plasticity: role of nonsynaptic plasticity in learning and memory,” *Trends in Neurosciences*, 33(1), pp. 17–26. doi:https://doi.org/10.1016/j.tins.2009.10.001.

Müller-Eberhard, H.J. and Schreiber, R.D. (1980) “Molecular Biology and Chemistry of the Alternative Pathway of Complement” in Kunkel, H.G. and Dixon, F.J. (eds) *Advances in Immunology*. Academic Press, pp. 1–53. doi:https://doi.org/10.1016/S0065-2776(08)60042-5.

Mullins, R.D. (2000) “How WASP-family proteins and the Arp2/3 complex convert intracellular signals into cytoskeletal structures,” *Current Opinion in Cell Biology*, 12(1), pp. 91–96. doi:10.1016/S0955-0674(99)00061-7.

Muralidhar, S., Wang, Y. and Markram, H. (2014) “Synaptic and cellular organization of layer 1 of the developing rat somatosensory cortex,” *Frontiers in Neuroanatomy*, 7. doi:10.3389/fnana.2013.00052.

Murphy, T.H., Worley, P.F. and Baraban, J.M. (1991) “L-type voltage-sensitive calcium channels mediate synaptic activation of immediate early genes,” *Neuron*, 7(4), pp. 625–635. doi:10.1016/0896-6273(91)90375-A.

Myers, K.M. and Davis, M. (2007a) “Mechanisms of fear extinction,” *Molecular Psychiatry*, 12(2), pp. 120–150. doi:10.1038/sj.mp.4001939.

Myrum, C. *et al.* (2015) “Arc is a flexible modular protein capable of reversible self-oligomerization,” *Biochemical Journal*, 468(1), pp. 145–158. doi:10.1042/BJ20141446.

Nabavi, S. *et al.* (2014) “Engineering a memory with LTD and LTP,” *Nature*, 511(7509), pp. 348–352. doi:10.1038/nature13294.

Nakayama, D. *et al.* (2016) “Late Arc/Arg3.1 expression in the basolateral amygdala is essential for persistence of newly-acquired and reactivated contextual fear memories,” *Scientific Reports*, 6(1), p. 21007. doi:10.1038/srep21007.

Natekin, A. and Knoll, A. (2013) “Gradient boosting machines, a tutorial,” *Frontiers in Neurorobotics*, 7. doi:10.3389/fnbot.2013.00021.

Nelson, L.H. and Lenz, K.M. (2017) “Microglia depletion in early life programs persistent changes in social, mood-related, and locomotor behavior in male and female rats,” *Behavioural Brain Research*, 316, pp. 279–293. doi:10.1016/j.bbr.2016.09.006.

Nesargikar, P., Spiller, B. and Chavez, R. (2012) “The complement system: History, pathways, cascade and inhibitors,” *European Journal of Microbiology and Immunology*, 2(2), pp. 103–111. doi:10.1556/EuJMI.2.2012.2.2.

Nguyen, P.T. *et al.* (2020a) “Microglial Remodeling of the Extracellular Matrix Promotes Synapse Plasticity.,” *Cell*, 182(2), pp. 388-403.e15. doi:10.1016/j.cell.2020.05.050.

Niculescu, F. *et al.* (1993) “Generation of diacylglycerol and ceramide during homologous complement activation.,” *Journal of immunology (Baltimore, Md. : 1950)*, 150(1), pp. 214–24.

Niculescu, F. *et al.* (1997) “Activation of Ras and mitogen-activated protein kinase pathway by terminal complement complexes is G protein dependent.,” *Journal of immunology (Baltimore, Md. : 1950)*, 158(9), pp. 4405–12.

Niculescu, F. and Rus, H. (1999) “Complement activation and atherosclerosis,” *Molecular Immunology*, 36(13–14), pp. 949–955. doi:10.1016/S0161-5890(99)00117-0.

Nikolaev, A. *et al.* (2009) “APP binds DR6 to trigger axon pruning and neuron death via distinct caspases,” *Nature*, 457(7232), pp. 981–989. doi:10.1038/nature07767.

Nikolaienko, O. *et al.* (2018) “Arc protein: a flexible hub for synaptic plasticity and cognition,” *Seminars in Cell & Developmental Biology*, 77, pp. 33–42. doi:https://doi.org/10.1016/j.semcdb.2017.09.006.

Nimmerjahn, A. (2012) “Two-Photon Imaging of Microglia in the Mouse Cortex In Vivo,” *Cold Spring Harbor Protocols*, 2012(5), p. pdb.prot069294. doi:10.1101/pdb.prot069294.

Nimmerjahn, A., Kirchhoff, F. and Helmchen, F. (2005a) “Resting Microglial Cells Are Highly Dynamic Surveillants of Brain Parenchyma in Vivo,” *Science*, 308(5726), pp. 1314–1318. doi:10.1126/science.1110647.

Nonaka, M. and Yoshizaki, F. (2004) “Primitive complement system of invertebrates.,” *Immunological reviews*, 198, pp. 203–15. doi:10.1111/j.0105-2896.2004.00118.x.

Norden, D.M., Muccigrosso, M.M. and Godbout, J.P. (2015) “Microglial priming and enhanced reactivity to secondary insult in aging, and traumatic CNS injury, and

neurodegenerative disease," *Neuropharmacology*, 96, pp. 29–41. doi:https://doi.org/10.1016/j.neuropharm.2014.10.028.

Notter, T. (2021) "Astrocytes in schizophrenia," *Brain and Neuroscience Advances*, 5, p. 239821282110091. doi:10.1177/23982128211009148.

O'Barr, S.A. *et al.* (2001) "Neuronal expression of a functional receptor for the C5a complement activation fragment," *The Journal of Immunology*, 166(6), pp. 4154–4162.

Obuchowicz, E. *et al.* (2014) "Imipramine and fluoxetine inhibit LPS-induced activation and affect morphology of microglial cells in the rat glial culture," *Pharmacological Reports*, 66(1), pp. 34–43.

Ohm, D.T. *et al.* (2021) "Accumulation of neurofibrillary tangles and activated microglia is associated with lower neuron densities in the aphasic variant of Alzheimer's disease," *Brain Pathology*, 31(1), pp. 189–204. doi:10.1111/bpa.12902.

Ohsawa, K. *et al.* (2000) "Involvement of Iba1 in membrane ruffling and phagocytosis of macrophages/microglia.," *Journal of cell science*, 113 (Pt 17), pp. 3073–84.

Ohsawa, K. *et al.* (2004) "Microglia/macrophage-specific protein Iba1 binds to fimbrin and enhances its actin-bundling activity," *Journal of Neurochemistry*, 88(4), pp. 844–856. doi:10.1046/j.1471-4159.2003.02213.x.

O'Loughlin, E. *et al.* (2018) "Microglial Phenotypes and Functions in Multiple Sclerosis," *Cold Spring Harbor Perspectives in Medicine*, 8(2), p. a028993. doi:10.1101/cshperspect.a028993.

Olson, M. and Hergenhahn, B. (2011) *Introduction to Theories of Personality, An, 8th Edition*. 8th edn. Pearson.

Olson, M.H. and Ramirez, J.J. (2020) *An Introduction to Theories of Learning*. Routledge. doi:10.4324/9781003014447.

Orecchioni, M. *et al.* (2019) “Macrophage Polarization: Different Gene Signatures in M1(LPS+) vs. Classically and M2(LPS–) vs. Alternatively Activated Macrophages,” *Frontiers in Immunology*, 10. doi:10.3389/fimmu.2019.01084.

Orsini, C.A. and Maren, S. (2012) “Neural and cellular mechanisms of fear and extinction memory formation.,” *Neuroscience and biobehavioral reviews*, 36(7), pp. 1773–802. doi:10.1016/j.neubiorev.2011.12.014.

Owen, P.R. (2012) “Portrayals of schizophrenia by entertainment media: a content analysis of contemporary movies.,” *Psychiatric services (Washington, D.C.)*, 63(7), pp. 655–9. doi:10.1176/appi.ps.201100371.

Owens, T. *et al.* (2014) “Interferons in the central nervous system: a few instruments play many tunes.,” *Glia*, 62(3), pp. 339–55. doi:10.1002/glia.22608.

Paasila, P.J. *et al.* (2019) “The relationship between the morphological subtypes of microglia and Alzheimer’s disease neuropathology.,” *Brain pathology (Zurich, Switzerland)*, 29(6), pp. 726–740. doi:10.1111/bpa.12717.

Palkovits, M. (1973) “Isolated removal of hypothalamic or other brain nuclei of the rat,” *Brain Research*, 59, pp. 449–450. doi:10.1016/0006-8993(73)90290-4.

Pang, Y. *et al.* (2016) “Early Postnatal Lipopolysaccharide Exposure Leads to Enhanced Neurogenesis and Impaired Communicative Functions in Rats,” *PLOS ONE*, 11(10), p. e0164403. doi:10.1371/journal.pone.0164403.

Pangburn, M.K. and Müller-Eberhard, H.J. (1984) “The alternative pathway of complement,” *Springer Seminars in Immunopathology*, 7(2), pp. 163–192. doi:10.1007/BF01893019.

Paolicelli, Rosa C *et al.* (2011) “Synaptic pruning by microglia is necessary for normal brain development.,” *Science (New York, N.Y.)*, 333(6048), pp. 1456–8. doi:10.1126/science.1202529.

Paolicelli, Rosa C. *et al.* (2011) “Synaptic Pruning by Microglia Is Necessary for Normal Brain Development,” *Science*, 333(6048), pp. 1456–1458. doi:10.1126/science.1202529.

Paolicelli, R.C., Bisht, K. and Tremblay, M.-Ã. (2014) “Fractalkine regulation of microglial physiology and consequences on the brain and behavior,” *Frontiers in Cellular Neuroscience*, 8. doi:10.3389/fncel.2014.00129.

Papadimitriou, J.C. *et al.* (1994) “Ultrastructural studies of complement mediated cell death: a biological reaction model to plasma membrane injury,” *Virchows Archiv*, 424(6), pp. 677–685. doi:10.1007/BF00195784.

Papadimitriou, J.C., Carney, D.F. and Shin, M.L. (1991) “Inhibitors of membrane lipid metabolism enhance complement-mediated nucleated cell killing through distinct mechanisms.,” *Molecular immunology*, 28(8), pp. 803–9. doi:10.1016/0161-5890(91)90043-j.

Parakalan, R. *et al.* (2012) “Transcriptome analysis of amoeboid and ramified microglia isolated from the corpus callosum of rat brain,” *BMC Neuroscience*, 13(1), p. 64. doi:10.1186/1471-2202-13-64.

Park, J.-S. *et al.* (2021) “Blocking microglial activation of reactive astrocytes is neuroprotective in models of Alzheimer’s disease,” *Acta Neuropathologica Communications*, 9(1), p. 78. doi:10.1186/s40478-021-01180-z.

Park, K. *et al.* (2013) “Robust predictive model for evaluating breast cancer survivability,” *Engineering Applications of Artificial Intelligence*, 26(9), pp. 2194–2205. doi:https://doi.org/10.1016/j.engappai.2013.06.013.

Parkhurst, C.N. *et al.* (2013) “Microglia Promote Learning-Dependent Synapse Formation through Brain-Derived Neurotrophic Factor,” *Cell*, 155(7), pp. 1596–1609. doi:https://doi.org/10.1016/j.cell.2013.11.030.

Patel, K.R. *et al.* (2014) “Schizophrenia: overview and treatment options.,” *P & T : a peer-reviewed journal for formulary management*, 39(9), pp. 638–45.

Patro, I.K. *et al.* (2010) “Poly I:C induced microglial activation impairs motor activity in adult rats.,” *Indian journal of experimental biology*, 48(2), pp. 104–9.

Paul, S. *et al.* (no date) “Type I interferon response in the central nervous system.,” *Biochimie*, 89(6–7), pp. 770–8. doi:10.1016/j.biochi.2007.02.009.

Paxinos, G. and Watson, C. (2006) *The rat brain in stereotaxic coordinates: hard cover edition*. Elsevier.

Pedersen, E.D. *et al.* (2007) “CD59 Efficiently Protects Human NT2-N Neurons Against Complement-mediated Damage,” *Scandinavian Journal of Immunology*, 66(2–3), pp. 345–351. doi:10.1111/j.1365-3083.2007.01959.x.

Peebles, C.L. *et al.* (2010) “Arc regulates spine morphology and maintains network stability in vivo,” *Proceedings of the National Academy of Sciences*, 107(42), pp. 18173–18178. doi:10.1073/pnas.1006546107.

Peralta, V. and Cuesta, M.J. (2011) “Eugen Bleuler and the schizophrenias: 100 years after.,” *Schizophrenia bulletin*, 37(6), pp. 1118–20. doi:10.1093/schbul/sbr126.

Perez-Alcazar, M. *et al.* (2014) “Altered cognitive performance and synaptic function in the hippocampus of mice lacking C3,” *Experimental Neurology*, 253, pp. 154–164. doi:10.1016/j.expneurol.2013.12.013.

Pérez-Cadahía, B., Drobic, B. and Davie, J.R. (2011) “Activation and function of immediate-early genes in the nervous systemThis paper is one of a selection of papers in a Special Issue entitled 31st Annual International Asilomar Chromatin and Chromosomes Conference, and has undergone the Journal’s usual peer review process.,” *Biochemistry and Cell Biology*, 89(1), pp. 61–73. doi:10.1139/O10-138.

Perry, V.H., Hume, D.A. and Gordon, S. (1985) “Immunohistochemical localization of macrophages and microglia in the adult and developing mouse brain,” *Neuroscience*, 15(2), pp. 313–326. doi:10.1016/0306-4522(85)90215-5.

Phillips, R.G. and LeDoux, J.E. (1994) “Lesions of the dorsal hippocampal formation interfere with background but not foreground contextual fear conditioning.,” *Learning & Memory*, 1(1), pp. 34–44. doi:10.1101/lm.1.1.34.

Pintchovski, S.A. *et al.* (2009) “The serum response factor and a putative novel transcription factor regulate expression of the immediate-early gene Arc/Arg3.1 in neurons.,” *The Journal of neuroscience : the official journal of the Society for Neuroscience*, 29(5), pp. 1525–37. doi:10.1523/JNEUROSCI.5575-08.2009.

de Pittà, M., Brunel, N. and Volterra, A. (2016) “Astrocytes: Orchestrating synaptic plasticity?,” *Neuroscience*, 323, pp. 43–61. doi:https://doi.org/10.1016/j.neuroscience.2015.04.001.

Poirazi, P. and Mel, B.W. (2001) “Impact of Active Dendrites and Structural Plasticity on the Memory Capacity of Neural Tissue,” *Neuron*, 29(3), pp. 779–796. doi:https://doi.org/10.1016/S0896-6273(01)00252-5.

Posern, G. and Treisman, R. (2006) “Actin’ together: serum response factor, its cofactors and the link to signal transduction.,” *Trends in cell biology*, 16(11), pp. 588–96. doi:10.1016/j.tcb.2006.09.008.

Posillico, C.K. (2021) “Three’s Company: Neuroimmune activation, sex, and memory at the tripartite synapse,” *Brain, Behavior, & Immunity - Health*, 16, p. 100326. doi:https://doi.org/10.1016/j.bbih.2021.100326.

Pozo-Rodrigálvarez, A. *et al.* (2021) “Hyperactive Behavior and Altered Brain Morphology in Adult Complement C3a Receptor Deficient Mice,” *Frontiers in Immunology*, 12. doi:10.3389/fimmu.2021.604812.

Presumey, J., Bialas, A.R. and Carroll, M.C. (2017) “Complement System in Neural Synapse Elimination in Development and Disease,” in, pp. 53–79. doi:10.1016/bs.ai.2017.06.004.

Prieto, G.A. and Cotman, C.W. (2017) “Cytokines and cytokine networks target neurons to modulate long-term potentiation,” *Cytokine & Growth Factor Reviews*, 34, pp. 27–33. doi:10.1016/j.cytogfr.2017.03.005.

Pugh, C. (1999) “Role of interleukin-1 beta in impairment of contextual fear conditioning caused by social isolation,” *Behavioural Brain Research*, 106(1–2), pp. 109–118. doi:10.1016/S0166-4328(99)00098-4.

Pugh, C.R. *et al.* (1998) “Selective Effects of Peripheral Lipopolysaccharide Administration on Contextual and Auditory-Cue Fear Conditioning,” *Brain, Behavior, and Immunity*, 12(3), pp. 212–229. doi:10.1006/brbi.1998.0524.

Qin, L. *et al.* (2007) “Systemic LPS causes chronic neuroinflammation and progressive neurodegeneration,” *Glia*, 55(5), pp. 453–462. doi:10.1002/glia.20467.

Qin, L. *et al.* (2013) “NADPH oxidase and aging drive microglial activation, oxidative stress, and dopaminergic neurodegeneration following systemic LPS administration,” *Glia*, 61(6), pp. 855–868. doi:10.1002/glia.22479.

Raber, J. *et al.* (2019) “Current understanding of fear learning and memory in humans and animal models and the value of a linguistic approach for analyzing fear learning and memory in humans,” *Neuroscience & Biobehavioral Reviews*, 105, pp. 136–177. doi:https://doi.org/10.1016/j.neubiorev.2019.03.015.

Raetz, C.R.H. and Whitfield, C. (2002) “Lipopolysaccharide Endotoxins,” *Annual Review of Biochemistry*, 71(1), pp. 635–700. doi:10.1146/annurev.biochem.71.110601.135414.

Rahpeymai, Y. *et al.* (2006) “Complement: a novel factor in basal and ischemia-induced neurogenesis.,” *The EMBO journal*, 25(6), pp. 1364–74. doi:10.1038/sj.emboj.7601004.

Ramanathan, Karthik R. *et al.* (2018) “Nucleus Reuniens Is Required for Encoding and Retrieving Precise, Hippocampal-Dependent Contextual Fear Memories in Rats,” *The Journal of Neuroscience*, 38(46), pp. 9925–9933. doi:10.1523/JNEUROSCI.1429-18.2018.

Ramanathan, Karthik R *et al.* (2018) “Prefrontal projections to the thalamic nucleus reuniens mediate fear extinction,” *Nature Communications*, 9(1), p. 4527. doi:10.1038/s41467-018-06970-z.

Ramanathan, K.R. and Maren, S. (2019) “Nucleus reuniens mediates the extinction of contextual fear conditioning,” *Behavioural Brain Research*, 374, p. 112114. doi:https://doi.org/10.1016/j.bbr.2019.112114.

Ramírez-Amaya, V. *et al.* (2005) “Spatial exploration-induced Arc mRNA and protein expression: evidence for selective, network-specific reactivation.,” *The Journal of neuroscience : the official journal of the Society for Neuroscience*, 25(7), pp. 1761–8. doi:10.1523/JNEUROSCI.4342-04.2005.

Ramirez-Amaya, V. *et al.* (2013) “Sustained Transcription of the Immediate Early Gene Arc in the Dentate Gyrus after Spatial Exploration,” *Journal of Neuroscience*, 33(4), pp. 1631–1639. doi:10.1523/JNEUROSCI.2916-12.2013.

Ransohoff, R.M. (2016) “A polarizing question: do M1 and M2 microglia exist?,” *Nature Neuroscience*, 19(8), pp. 987–991. doi:10.1038/nn.4338.

Ransohoff, R.M. and Stevens, B. (2011) “How Many Cell Types Does It Take to Wire a Brain?,” *Science*, 333(6048), pp. 1391–1392. doi:10.1126/science.1212112.

Rao, V.R. *et al.* (2006) “AMPA receptors regulate transcription of the plasticity-related immediate-early gene Arc.,” *Nature neuroscience*, 9(7), pp. 887–95. doi:10.1038/nn1708.

Reif, A. *et al.* (2007) “Neurogenesis and schizophrenia: dividing neurons in a divided mind?,” *European Archives of Psychiatry and Clinical Neuroscience*, 257(5), pp. 290–299. doi:10.1007/s00406-007-0733-3.

Ren, W.-J. *et al.* (2011) “Peripheral Nerve Injury Leads to Working Memory Deficits and Dysfunction of the Hippocampus by Upregulation of TNF-α in Rodents,” *Neuropsychopharmacology*, 36(5), pp. 979–992. doi:10.1038/npp.2010.236.

Reshef, R. *et al.* (2017) “The role of microglia and their CX3CR1 signaling in adult neurogenesis in the olfactory bulb,” *Elife*, 6, p. e30809.

Restivo, L. *et al.* (2009) “The Formation of Recent and Remote Memory Is Associated with Time-Dependent Formation of Dendritic Spines in the Hippocampus and Anterior Cingulate Cortex,” *Journal of Neuroscience*, 29(25), pp. 8206–8214. doi:10.1523/JNEUROSCI.0966-09.2009.

Rial Verde, E.M. *et al.* (2006) “Increased Expression of the Immediate-Early Gene Arc/Arg3.1 Reduces AMPA Receptor-Mediated Synaptic Transmission,” *Neuron*, 52(3), pp. 461–474. doi:10.1016/j.neuron.2006.09.031.

Ricciotti, E. and FitzGerald, G.A. (2011) “Prostaglandins and Inflammation,” *Arteriosclerosis, Thrombosis, and Vascular Biology*, 31(5), pp. 986–1000. doi:10.1161/ATVBAHA.110.207449.

Ricklin, D. *et al.* (2010) “Complement: a key system for immune surveillance and homeostasis.,” *Nature immunology*, 11(9), pp. 785–97. doi:10.1038/ni.1923.

Ripke, S. (2011) “Genome-wide association study identifies five new schizophrenia loci,” *Nature Genetics*, 43(10), pp. 969–976. doi:10.1038/ng.940.

Ripke, S. *et al.* (2014) “Biological insights from 108 schizophrenia-associated genetic loci,” *Nature*, 511(7510), pp. 421–427. doi:10.1038/nature13595.

Rivest, S. (2009) “Regulation of innate immune responses in the brain.,” *Nature reviews. Immunology*, 9(6), pp. 429–39. doi:10.1038/nri2565.

Rizzo, F.R. *et al.* (2018) “Tumor Necrosis Factor and Interleukin-1 *β* Modulate Synaptic Plasticity during Neuroinflammation,” *Neural Plasticity*, 2018, pp. 1–12. doi:10.1155/2018/8430123.

Rodríguez, J.J. *et al.* (2005) “Long-term potentiation in the rat dentate gyrus is associated with enhanced Arc/Arg3.1 protein expression in spines, dendrites and glia.,” *The European journal of neuroscience*, 21(9), pp. 2384–96. doi:10.1111/j.1460-9568.2005.04068.x.

Rogers, J.T. *et al.* (2011) “CX3CR1 Deficiency Leads to Impairment of Hippocampal Cognitive Function and Synaptic Plasticity,” *Journal of Neuroscience*, 31(45), pp. 16241–16250. doi:10.1523/JNEUROSCI.3667-11.2011.

Rohan Walker, F., Nilsson, M. and Jones, K. (2013) “Acute and chronic stress-induced disturbances of microglial plasticity, phenotype and function,” *Current drug targets*, 14(11), pp. 1262–1276.

Roselli, F. *et al.* (2018) “Medusa’s Head: The Complement System in Traumatic Brain and Spinal Cord Injury,” *Journal of Neurotrauma*, 35(2), pp. 226–240. doi:10.1089/neu.2017.5168.

Rőszer, T. (2015) “Understanding the Mysterious M2 Macrophage through Activation Markers and Effector Mechanisms,” *Mediators of Inflammation*, 2015, pp. 1–16. doi:10.1155/2015/816460.

Rouiller, I. *et al.* (2008) “The structural basis of actin filament branching by the Arp2/3 complex.,” *The Journal of cell biology*, 180(5), pp. 887–95. doi:10.1083/jcb.200709092.

Ruiz-Martínez, J. *et al.* (2017) “Whole-exome sequencing associates novel *CSMD1* gene mutations with familial Parkinson disease,” *Neurology Genetics*, 3(5), p. e177. doi:10.1212/NXG.0000000000000177.

Sah, P. *et al.* (2003) “The amygdaloid complex: anatomy and physiology.,” *Physiological reviews*, 83(3), pp. 803–34. doi:10.1152/physrev.00002.2003.

Sakai, J. (2020) “Core Concept: How synaptic pruning shapes neural wiring during development and, possibly, in disease,” *Proceedings of the National Academy of Sciences*, 117(28), pp. 16096–16099. doi:10.1073/pnas.2010281117.

Salter, M.W. and Stevens, B. (2017) “Microglia emerge as central players in brain disease,” *Nature Medicine*, 23(9), pp. 1018–1027. doi:10.1038/nm.4397.

Sarma, J.V. and Ward, P.A. (2012) “New developments in C5a receptor signaling.,” *Cell health and cytoskeleton*, 4, pp. 73–82. doi:10.2147/CHC.S27233.

Sasaki, Y. *et al.* (2001) “Iba1 Is an Actin-Cross-Linking Protein in Macrophages/Microglia,” *Biochemical and Biophysical Research Communications*, 286(2), pp. 292–297. doi:10.1006/bbrc.2001.5388.

Savage, J.C., Carrier, M. and Tremblay, M.-È. (2019a) “Morphology of Microglia Across Contexts of Health and Disease,” in, pp. 13–26. doi:10.1007/978-1-4939-9658-2_2.

Schafer, D.P. *et al.* (2012) “Microglia sculpt postnatal neural circuits in an activity and complement-dependent manner.,” *Neuron*, 74(4), pp. 691–705. doi:10.1016/j.neuron.2012.03.026.

Schäfer, M.K.-H. *et al.* (2000) “Complement C1q Is Dramatically Up-Regulated in Brain Microglia in Response to Transient Global Cerebral Ischemia,” *The Journal of Immunology*, 164(10), pp. 5446–5452. doi:10.4049/jimmunol.164.10.5446.

Schartz, N.D. and Tenner, A.J. (2020) “The good, the bad, and the opportunities of the complement system in neurodegenerative disease,” *Journal of Neuroinflammation*, 17(1), p. 354. doi:10.1186/s12974-020-02024-8.

Scher, J.U. and Pillinger, M.H. (2009) “The Anti-Inflammatory Effects of Prostaglandins,” *Journal of Investigative Medicine*, 57(6), pp. 703–708. doi:10.2310/JIM.0b013e31819aaa76.

Schilling, M. *et al.* (2003) “Microglial activation precedes and predominates over macrophage infiltration in transient focal cerebral ischemia: a study in green

fluorescent protein transgenic bone marrow chimeric mice," *Experimental Neurology*, 183(1), pp. 25–33. doi:https://doi.org/10.1016/S0014-4886(03)00082-7.

Scholl, C., Rule, M.E. and Hennig, M.H. (2021) "The information theory of developmental pruning: Optimizing global network architectures using local synaptic rules," *PLOS Computational Biology*, 17(10), p. e1009458. doi:10.1371/journal.pcbi.1009458.

Scholz, B. *et al.* (2016) "The Regulation of Cytokine Networks in Hippocampal CA1 Differentiates Extinction from Those Required for the Maintenance of Contextual Fear Memory after Recall," *PLOS ONE*, 11(5), p. e0153102. doi:10.1371/journal.pone.0153102.

Schonthaler, H.B., Guinea-Viniegra, J. and Wagner, E.F. (2011) "Targeting inflammation by modulating the Jun/AP-1 pathway," *Annals of the Rheumatic Diseases*, 70(Suppl 1), p. i109. doi:10.1136/ard.2010.140533.

Schroeder, A. *et al.* (2006) "The RIN: an RNA integrity number for assigning integrity values to RNA measurements," *BMC Molecular Biology*, 7(1), p. 3. doi:10.1186/1471-2199-7-3.

Schulman, H. (2013) "Chapter 9 - Intracellular Signaling," in Squire, L.R. et al. (eds) *Fundamental Neuroscience (Fourth Edition)*. San Diego: Academic Press, pp. 189–209. doi:https://doi.org/10.1016/B978-0-12-385870-2.00009-3.

Segal, M.R. (2004) "Machine learning benchmarks and random forest regression."

Sekar, A. *et al.* (2016) "Schizophrenia risk from complex variation of complement component 4," *Nature*, 530(7589), pp. 177–183. doi:10.1038/nature16549.

Senn, V. *et al.* (2014) “Long-range connectivity defines behavioral specificity of amygdala neurons.,” *Neuron*, 81(2), pp. 428–37. doi:10.1016/j.neuron.2013.11.006.

Sevenich, L. (2018) “Brain-Resident Microglia and Blood-Borne Macrophages Orchestrate Central Nervous System Inflammation in Neurodegenerative Disorders and Brain Cancer,” *Frontiers in Immunology*, 9. doi:10.3389/fimmu.2018.00697.

Shakhar, K. and Shakhar, G. (2015) “Why Do We Feel Sick When Infected—Can Altruism Play a Role?,” *PLOS Biology*, 13(10), p. e1002276. doi:10.1371/journal.pbio.1002276.

Shen, Y. *et al.* (1997) “Neuronal expression of mRNAs for complement proteins of the classical pathway in Alzheimer brain,” *Brain Research*, 769(2), pp. 391–395. doi:10.1016/S0006-8993(97)00850-0.

Shepherd, J.D. *et al.* (2006) “Arc/Arg3.1 mediates homeostatic synaptic scaling of AMPA receptors.,” *Neuron*, 52(3), pp. 475–84. doi:10.1016/j.neuron.2006.08.034.

Shi, Q. *et al.* (2015) “Complement C3-Deficient Mice Fail to Display Age-Related Hippocampal Decline,” *Journal of Neuroscience*, 35(38), pp. 13029–13042. doi:10.1523/JNEUROSCI.1698-15.2015.

Shinjyo, N. *et al.* (2009) “Complement-Derived Anaphylatoxin C3a Regulates In Vitro Differentiation and Migration of Neural Progenitor Cells,” *Stem Cells*, 27(11), pp. 2824–2832. doi:10.1002/stem.225.

Sierra, A., Paolicelli, R.C. and Kettenmann, H. (2019) “Cien Años de Microglía: Milestones in a Century of Microglial Research,” *Trends in Neurosciences*, 42(11), pp. 778–792. doi:10.1016/j.tins.2019.09.004.

Silva, B.A., Burns, A.M. and Gräff, J. (2019) “A cFos activation map of remote fear memory attenuation,” *Psychopharmacology*, 236(1), pp. 369–381. doi:10.1007/s00213-018-5000-y.

Simon, D.W. *et al.* (2017) “The far-reaching scope of neuroinflammation after traumatic brain injury,” *Nature Reviews Neurology*, 13(3), pp. 171–191. doi:10.1038/nrneurol.2017.13.

Simonyan, K. and Zisserman, A. (2014) “Very deep convolutional networks for large-scale image recognition,” *arXiv preprint arXiv:1409.1556* [Preprint].

Sint, D., Raso, L. and Traugott, M. (2012) “Advances in multiplex PCR: balancing primer efficiencies and improving detection success,” *Methods in Ecology and Evolution*, 3(5), pp. 898–905. doi:10.1111/j.2041-210X.2012.00215.x.

Smith, K.L. *et al.* (2019) “Microglial cell hyper-ramification and neuronal dendritic spine loss in the hippocampus and medial prefrontal cortex in a mouse model of PTSD,” *Brain, Behavior, and Immunity*, 80, pp. 889–899. doi:10.1016/j.bbi.2019.05.042.

Soane, L. *et al.* (1999) “Inhibition of oligodendrocyte apoptosis by sublytic C5b-9 is associated with enhanced synthesis of bcl-2 and mediated by inhibition of caspase-3 activation.,” *Journal of immunology (Baltimore, Md. : 1950)*, 163(11), pp. 6132–8.

Soane, L. *et al.* (2001) “C5b-9 terminal complement complex protects oligodendrocytes from death by regulating Bad through phosphatidylinositol 3-kinase/Akt pathway.,” *Journal of immunology (Baltimore, Md. : 1950)*, 167(4), pp. 2305–11. doi:10.4049/jimmunol.167.4.2305.

Sofroniew, M. v. (2020) “Astrocyte Reactivity: Subtypes, States, and Functions in CNS Innate Immunity,” *Trends in Immunology*, 41(9), pp. 758–770. doi:10.1016/j.it.2020.07.004.

Sta, M. *et al.* (2011) “Innate and adaptive immunity in amyotrophic lateral sclerosis: Evidence of complement activation,” *Neurobiology of Disease*, 42(3), pp. 211–220. doi:10.1016/j.nbd.2011.01.002.

Steen, V.M. *et al.* (2013) “Neuropsychological Deficits in Mice Depleted of the Schizophrenia Susceptibility Gene CSMD1,” *PLoS ONE*, 8(11), p. e79501. doi:10.1371/journal.pone.0079501.

Stein, I.S. and Zito, K. (2019) “Dendritic Spine Elimination: Molecular Mechanisms and Implications,” *The Neuroscientist*, 25(1), pp. 27–47. doi:10.1177/1073858418769644.

Stellwagen, D. *et al.* (2005) “Differential regulation of AMPA receptor and GABA receptor trafficking by tumor necrosis factor-alpha.,” *The Journal of neuroscience : the official journal of the Society for Neuroscience*, 25(12), pp. 3219–28. doi:10.1523/JNEUROSCI.4486-04.2005.

Stellwagen, D. and Malenka, R.C. (2006) “Synaptic scaling mediated by glial TNF-alpha.,” *Nature*, 440(7087), pp. 1054–9. doi:10.1038/nature04671.

Stepan, J., Dine, J. and Eder, M. (2015) “Functional optical probing of the hippocampal trisynaptic circuit in vitro: network dynamics, filter properties, and polysynaptic induction of CA1 LTP.,” *Frontiers in neuroscience*, 9, p. 160. doi:10.3389/fnins.2015.00160.

Stephan, A.H. *et al.* (2013) “A Dramatic Increase of C1q Protein in the CNS during Normal Aging,” *Journal of Neuroscience*, 33(33), pp. 13460–13474. doi:10.1523/JNEUROSCI.1333-13.2013.

Stephan, Alexander H, Barres, B.A. and Stevens, B. (2012) “The Complement System: An Unexpected Role in Synaptic Pruning During Development and Disease,” *Annual Review of Neuroscience*, 35(1), pp. 369–389. doi:10.1146/annurev-neuro-061010-113810.

Stevens, B. *et al.* (2007) “The Classical Complement Cascade Mediates CNS Synapse Elimination,” *Cell*, 131(6), pp. 1164–1178. doi:https://doi.org/10.1016/j.cell.2007.10.036.

Steward, O. and Worley, P.F. (2001) “Selective targeting of newly synthesized Arc mRNA to active synapses requires NMDA receptor activation.,” *Neuron*, 30(1), pp. 227–40. doi:10.1016/s0896-6273(01)00275-6.

Stokes, M.G. (2015) “‘Activity-silent’ working memory in prefrontal cortex: a dynamic coding framework,” *Trends in Cognitive Sciences*, 19(7), pp. 394–405. doi:https://doi.org/10.1016/j.tics.2015.05.004.

Stokowska, A. *et al.* (2017) “Complement peptide C3a stimulates neural plasticity after experimental brain ischaemia,” *Brain*, 140(2), pp. 353–369. doi:10.1093/brain/aww314.

Stone, S.S.D. *et al.* (2011) “Functional convergence of developmentally and adult-generated granule cells in dentate gyrus circuits supporting hippocampus-dependent memory,” *Hippocampus*, 21(12), pp. 1348–1362. doi:10.1002/hipo.20845.

Storini, C. *et al.* (2005) “C1-inhibitor protects against brain ischemia–reperfusion injury via inhibition of cell recruitment and inflammation,” *Neurobiology of Disease*, 19(1–2), pp. 10–17. doi:10.1016/j.nbd.2004.11.001. doi:10.1034/j.1601-183X.2003.00001.x.

Strekalova, T., Zörner, B., Zacher, C., *et. al.* (2003) “Memory retrieval after contextual fear conditioning induces c-Fos and JunB expression in CA1 hippocampus,” *Genes, Brain and Behavior*, 2(1), pp. 2003.

Sugama, S. *et al.* (2019) “Stress-induced microglial activation occurs through β-adrenergic receptor: noradrenaline as a key neurotransmitter in microglial activation,” *Journal of Neuroinflammation*, 16(1), p. 266. doi:10.1186/s12974-019-1632-z.

Sugama, S. and Kakinuma, Y. (2020) “Stress and brain immunity: Microglial homeostasis through hypothalamus-pituitary-adrenal gland axis and sympathetic nervous system,” *Brain, Behavior, & Immunity - Health*, 7, p. 100111. doi:https://doi.org/10.1016/j.bbih.2020.100111.

Sun, R. *et al.* (2016) “Hippocampal activation of microglia may underlie the shared neurobiology of comorbid posttraumatic stress disorder and chronic pain,” *Molecular pain*, 12, p. 1744806916679166.

Swanson, L.W. (1981) “A direct projection from Ammon’s horn to prefrontal cortex in the rat.,” *Brain research*, 217(1), pp. 150–4. doi:10.1016/0006-8993(81)90192-x.

Taha, T.A. *et al.* (2006) “Loss of sphingosine kinase-1 activates the intrinsic pathway of programmed cell death: modulation of sphingolipid levels and the induction of

apoptosis.,” *FASEB journal : official publication of the Federation of American Societies for Experimental Biology*, 20(3), pp. 482–4. doi:10.1096/fj.05-4412fje.

Tan, Y.-L., Yuan, Y. and Tian, L. (2020) “Microglial regional heterogeneity and its role in the brain,” *Molecular Psychiatry*, 25(2), pp. 351–367. doi:10.1038/s41380-019-0609-8.

Tang, Y. and Le, W. (2016) “Differential Roles of M1 and M2 Microglia in Neurodegenerative Diseases,” *Molecular Neurobiology*, 53(2), pp. 1181–1194. doi:10.1007/s12035-014-9070-5.

Tarca, A.L. *et al.* (2007) “Machine Learning and Its Applications to Biology,” *PLoS Computational Biology*, 3(6), p. e116. doi:10.1371/journal.pcbi.0030116.

Tayler, K.K. *et al.* (2013) “Reactivation of Neural Ensembles during the Retrieval of Recent and Remote Memory,” *Current Biology*, 23(2), pp. 99–106. doi:https://doi.org/10.1016/j.cub.2012.11.019.

Taylor, S.E. *et al.* (2014) “Rod Microglia: A Morphological Definition,” *PLoS ONE*, 9(5), p. e97096. doi:10.1371/journal.pone.0097096.

Tchessalova, D., Posillico, C.K. and Tronson, N.C. (2018) “Neuroimmune Activation Drives Multiple Brain States,” *Frontiers in Systems Neuroscience*, 12. doi:10.3389/fnsys.2018.00039.

Teber, I. *et al.* (2004) “Muscarinic acetylcholine receptor stimulation induces expression of the activity-regulated cytoskeleton-associated gene (ARC).,” *Brain research. Molecular brain research*, 121(1–2), pp. 131–6. doi:10.1016/j.molbrainres.2003.11.017.

Tegla, C.A. *et al.* (2011) “Membrane attack by complement: the assembly and biology of terminal complement complexes,” *Immunologic Research*, 51(1), p. 45. doi:10.1007/s12026-011-8239-5.

Terzian, H. and Ore, G.D. (1955) “Syndrome of Klüver and Bucy; reproduced in man by bilateral removal of the temporal lobes.,” *Neurology*, 5(6), pp. 373–80. doi:10.1212/wnl.5.6.373.

Thameem Dheen, S., Kaur, C. and Ling, E.-A. (2007) “Microglial Activation and its Implications in the Brain Diseases,” *Current Medicinal Chemistry*, 14(11), pp. 1189–1197. doi:10.2174/092986707780597961.

Therien, A.G. (2005) “Agonist Activity of the Small Molecule C3aR Ligand SB 290157,” *The Journal of Immunology*, 174(12), pp. 7479–7480. doi:10.4049/jimmunol.174.12.7479.

Thion, M.S., Ginhoux, F. and Garel, S. (2018) “Microglia and early brain development: An intimate journey,” *Science*, 362(6411), pp. 185–189. doi:10.1126/science.aat0474.

Thomas, A. *et al.* (2000) “Expression of a complete and functional complement system by human neuronal cells in vitro,” *International Immunology*, 12(7), pp. 1015–1023. doi:10.1093/intimm/12.7.1015.

Thomas, K.L., Hall, J. and Everitt, B.J. (2002) “Cellular imaging with *zif268* expression in the rat nucleus accumbens and frontal cortex further dissociates the neural pathways activated following the retrieval of contextual and cued fear

memory,” *European Journal of Neuroscience*, 16(9), pp. 1789–1796. doi:10.1046/j.1460-9568.2002.02247.x.

Toda, T. *et al.* (2019a) “The role of adult hippocampal neurogenesis in brain health and disease,” *Molecular Psychiatry*, 24(1), pp. 67–87. doi:10.1038/s41380-018-0036-2.

Tonegawa, S., Morrissey, M.D. and Kitamura, T. (2018) “The role of engram cells in the systems consolidation of memory,” *Nature Reviews Neuroscience*, 19(8), pp. 485–498. doi:10.1038/s41583-018-0031-2.

Tong, L. *et al.* (2012) “Brain-Derived Neurotrophic Factor-Dependent Synaptic Plasticity Is Suppressed by Interleukin-1 via p38 Mitogen-Activated Protein Kinase,” *Journal of Neuroscience*, 32(49), pp. 17714–17724. doi:10.1523/JNEUROSCI.1253-12.2012.

Tovote, P., Fadok, J.P. and Lüthi, A. (2015a) “Neuronal circuits for fear and anxiety,” *Nature Reviews Neuroscience*, 16(6), pp. 317–331. doi:10.1038/nrn3945.

Tracey, M.D.K.J. and Cerami, Ph.D.A. (1994) “TUMOR NECROSIS FACTOR: A Pleiotropic Cytokine and Therapuetic Target,” *Annual Review of Medicine*, 45(1), pp. 491–503. doi:10.1146/annurev.med.45.1.491.

Tracy, J.A., Britton, G.B. and Steinmetz, J.E. (2001) “Comparison of single unit responses to tone, light, and compound conditioned stimuli during rabbit classical eyeblink conditioning.,” *Neurobiology of learning and memory*, 76(3), pp. 253–67. doi:10.1006/nlme.2001.4024.

Tremblay, M.-E. *et al.* (2011) “The Role of Microglia in the Healthy Brain,” *Journal of Neuroscience*, 31(45), pp. 16064–16069. doi:10.1523/JNEUROSCI.4158-11.2011.

Tremblay, M.-È., Lowery, R.L. and Majewska, A.K. (2010) “Microglial Interactions with Synapses Are Modulated by Visual Experience,” *PLoS Biology*, 8(11), p. e1000527. doi:10.1371/journal.pbio.1000527.

Trent, S. *et al.* (2015) “Rescue of long-term memory after reconsolidation blockade,” *Nature Communications*, 6(1), p. 7897. doi:10.1038/ncomms8897.

Trent, S. *et al.* (2017) “AMPA receptors control fear extinction through an Arc-dependent mechanism,” *Learning & Memory*, 24(8), pp. 375–380.

Treves, A. *et al.* (2008) “What is the mammalian dentate gyrus good for?,” *Neuroscience*, 154(4), pp. 1155–72. doi:10.1016/j.neuroscience.2008.04.073.

Tronel, S. and Sara, S.J. (2002) “Mapping of Olfactory Memory Circuits: Region-Specific c-fos Activation After Odor-Reward Associative Learning or After Its Retrieval,” *Learning & Memory*, 9(3), pp. 105–111. doi:10.1101/lm.47802.

Trouche, S. *et al.* (2009) “Recruitment of adult-generated neurons into functional hippocampal networks contributes to updating and strengthening of spatial memory,” *Proceedings of the National Academy of Sciences*, 106(14), pp. 5919–5924. doi:10.1073/pnas.0811054106.

Tsvetkov, E. *et al.* (2002) “Fear Conditioning Occludes LTP-Induced Presynaptic Enhancement of Synaptic Transmission in the Cortical Pathway to the Lateral Amygdala,” *Neuron*, 34(2), pp. 289–300. doi:https://doi.org/10.1016/S0896-6273(02)00645-1.

Tyler, C.M. and Boulanger, L.M. (2012) “Complement-Mediated Microglial Clearance of Developing Retinal Ganglion Cell Axons,” *Neuron*, 74(4), pp. 597–599. doi:10.1016/j.neuron.2012.05.002.

Tynan, R.J. *et al.* (2010) “Chronic stress alters the density and morphology of microglia in a subset of stress-responsive brain regions,” *Brain, Behavior, and Immunity*, 24(7), pp. 1058–1068. doi:https://doi.org/10.1016/j.bbi.2010.02.001.

VanRyzin, J.W. (2021) “Phagocytic microglia in development: Are they what they eat?,” *Brain, Behavior, & Immunity - Health*, 18, p. 100373. doi:https://doi.org/10.1016/j.bbih.2021.100373.

Vasek, M.J. *et al.* (2016) “A complement–microglial axis drives synapse loss during virus-induced memory impairment,” *Nature*, 534(7608), pp. 538–543. doi:10.1038/nature18283.

Vaverková, Z., Milton, A.L. and Merlo, E. (2020) “Retrieval-Dependent Mechanisms Affecting Emotional Memory Persistence: Reconsolidation, Extinction, and the Space in Between,” *Frontiers in Behavioral Neuroscience*, 14. doi:10.3389/fnbeh.2020.574358.

Veerhuis, R. *et al.* (1998) “Complement C1-inhibitor expression in Alzheimer’s disease.,” *Acta neuropathologica*, 96(3), pp. 287–96. doi:10.1007/s004010050896.

Veerhuis, Robert *et al.* (1999) “Cytokines Associated with Amyloid Plaques in Alzheimer’s Disease Brain Stimulate Human Glial and Neuronal Cell Cultures to Secrete Early Complement Proteins, But Not C1-Inhibitor,” *Experimental Neurology*, 160(1), pp. 289–299. doi:10.1006/exnr.1999.7199.

Veerhuis, R., Nielsen, H.M. and Tenner, A.J. (2011) “Complement in the brain,” *Molecular Immunology*, 48(14), pp. 1592–1603. doi:10.1016/j.molimm.2011.04.003.

Vereker, E., O’Donnell, E. and Lynch, M.A. (2000a) “The Inhibitory Effect of Interleukin-1β on Long-Term Potentiation Is Coupled with Increased Activity of Stress-Activated Protein Kinases,” *The Journal of Neuroscience*, 20(18), pp. 6811–6819. doi:10.1523/JNEUROSCI.20-18-06811.2000.

Vereker, E., O’Donnell, E. and Lynch, M.A. (2000b) “The Inhibitory Effect of Interleukin-1β on Long-Term Potentiation Is Coupled with Increased Activity of Stress-Activated Protein Kinases,” *The Journal of Neuroscience*, 20(18), pp. 6811–6819. doi:10.1523/JNEUROSCI.20-18-06811.2000.

Vetere, G. *et al.* (2011) “Spine growth in the anterior cingulate cortex is necessary for the consolidation of contextual fear memory,” *Proceedings of the National Academy of Sciences*, 108(20), pp. 8456–8460. doi:10.1073/pnas.1016275108.

Veyrac, A. *et al.* (2014) “Chapter Four - The Transcription Factor Zif268/Egr1, Brain Plasticity, and Memory,” in Khan, Z.U. and Muly, E.C. (eds) *Progress in Molecular Biology and Translational Science*. Academic Press, pp. 89–129. doi:https://doi.org/10.1016/B978-0-12-420170-5.00004-0.

Vezzani, A. *et al.* (1999) “Interleukin-1β Immunoreactivity and Microglia Are Enhanced in the Rat Hippocampus by Focal Kainate Application: Functional Evidence for Enhancement of Electrographic Seizures,” *The Journal of Neuroscience*, 19(12), pp. 5054–5065. doi:10.1523/JNEUROSCI.19-12-05054.1999.

Vidal-Gonzalez, I. *et al.* (no date) “Microstimulation reveals opposing influences of prelimbic and infralimbic cortex on the expression of conditioned fear.,” *Learning & memory (Cold Spring Harbor, N.Y.)*, 13(6), pp. 728–33. doi:10.1101/lm.306106.

Wadhwa, M. *et al.* (2019) “Complement activation sustains neuroinflammation and deteriorates adult neurogenesis and spatial memory impairment in rat hippocampus following sleep deprivation,” *Brain, Behavior, and Immunity*, 82, pp. 129–144. doi:10.1016/j.bbi.2019.08.004.

Wake, H. *et al.* (2009) “Resting Microglia Directly Monitor the Functional State of Synapses In Vivo and Determine the Fate of Ischemic Terminals,” *Journal of Neuroscience*, 29(13), pp. 3974–3980. doi:10.1523/JNEUROSCI.4363-08.2009.

Wake, H., Moorhouse, Andrew J, *et al.* (2013) “Microglia: actively surveying and shaping neuronal circuit structure and function,” *Trends in Neurosciences*, 36(4), pp. 209–217. doi:https://doi.org/10.1016/j.tins.2012.11.007.

Wang, A. *et al.* (2013) “Transcription factor complex AP-1 mediates inflammation initiated by *Chlamydia pneumoniae* infection,” *Cellular Microbiology*, 15(5), pp. 779–794. doi:10.1111/cmi.12071.

Wang, J.Q., Daunais, J.B. and McGinty, J.F. (1994) “Role of kainate/AMPA receptors in induction of striatal zif/268 and preprodynorphin mRNA by a single injection of amphetamine,” *Molecular Brain Research*, 27(1), pp. 118–126. doi:10.1016/0169-328X(94)90192-9.

Wang, M. *et al.* (2014) “Synaptic Modifications in the Medial Prefrontal Cortex in Susceptibility and Resilience to Stress,” *Journal of Neuroscience*, 34(22), pp. 7485–7492. doi:10.1523/JNEUROSCI.5294-13.2014.

Wang, W. *et al.* (2018) “Minocycline Attenuates Stress-Induced Behavioral Changes via Its Anti-inflammatory Effects in an Animal Model of Post-traumatic Stress Disorder,” *Frontiers in Psychiatry*, 9. doi:10.3389/fpsyt.2018.00558.

Wang, X. *et al.* (2008) “Extracellular proteolysis by matrix metalloproteinase-9 drives dendritic spine enlargement and long-term potentiation coordinately.,” *Proceedings of the National Academy of Sciences of the United States of America*, 105(49), pp. 19520–5. doi:10.1073/pnas.0807248105.

Wang, Y.-L. *et al.* (2018) “Microglial activation mediates chronic mild stress-induced depressive-and anxiety-like behavior in adult rats,” *Journal of Neuroinflammation*, 15(1), pp. 1–14.

Waung, M.W. *et al.* (2008) “Rapid translation of Arc/Arg3.1 selectively mediates mGluR-dependent LTD through persistent increases in AMPAR endocytosis rate.,” *Neuron*, 59(1), pp. 84–97. doi:10.1016/j.neuron.2008.05.014.

Wee, C.L. *et al.* (2014) “Nuclear Arc Interacts with the Histone Acetyltransferase Tip60 to Modify H4K12 Acetylation,” *eneuro*, 1(1), p. ENEURO.0019-14.2014. doi:10.1523/ENEURO.0019-14.2014.

Wegrzyn, D. *et al.* (2021) “Poly I:C Activated Microglia Disrupt Perineuronal Nets and Modulate Synaptic Balance in Primary Hippocampal Neurons in vitro,” *Frontiers in Synaptic Neuroscience*, 13. doi:10.3389/fnsyn.2021.637549.

Weinhard, L. *et al.* (2018) “Microglia remodel synapses by presynaptic trogocytosis and spine head filopodia induction,” *Nature Communications*, 9(1), p. 1228. doi:10.1038/s41467-018-03566-5.

Wessa, M. and Flor, H. (2007) “Failure of Extinction of Fear Responses in Posttraumatic Stress Disorder: Evidence From Second-Order Conditioning,” *American Journal of Psychiatry*, 164(11), pp. 1684–1692. doi:10.1176/appi.ajp.2007.07030525.

West, M.J. and Gundersen, H.J. (1990) “Unbiased stereological estimation of the number of neurons in the human hippocampus.,” *The Journal of comparative neurology*, 296(1), pp. 1–22. doi:10.1002/cne.902960102.

Westacott, L.J. *et al.* (2022) “Complement C3 and C3aR mediate different aspects of emotional behaviours; relevance to risk for psychiatric disorder,” *Brain, Behavior, and Immunity*, 99, pp. 70–82. doi:https://doi.org/10.1016/j.bbi.2021.09.005.

Wieland, G.D. *et al.* (2005) “Early growth response proteins EGR-4 and EGR-3 interact with immune inflammatory mediators NF-κB p50 and p65,” *Journal of Cell Science*, 118(14), pp. 3203–3212. doi:10.1242/jcs.02445.

Wilfinger, W.W., Mackey, K. and Chomczynski, P. (1997) “Effect of pH and Ionic Strength on the Spectrophotometric Assessment of Nucleic Acid Purity,” *BioTechniques*, 22(3), pp. 474–481. doi:10.2144/97223st01.

Williams, A.R. and Lattal, K.M. (2019) “Rapid reacquisition of contextual fear following extinction in mice: effects of amount of extinction, acute ethanol withdrawal,

and ethanol intoxication," *Psychopharmacology*, 236(1), pp. 491–506. doi:10.1007/s00213-018-5057-7.

Wilson, A., Brooks, D.C. and Bouton, M.E. (1995) "The role of the rat hippocampal system in several effects of context in extinction.," *Behavioral neuroscience*, 109(5), pp. 828–36. doi:10.1037//0735-7044.109.5.828.

Woo, J.J. *et al.* (2020) "The complement system in schizophrenia: where are we now and what's next?," *Molecular Psychiatry*, 25(1), pp. 114–130. doi:10.1038/s41380-019-0479-0.

Woodruff, T.M. *et al.* (2010) "The role of the complement system and the activation fragment C5a in the central nervous system.," *Neuromolecular medicine*, 12(2), pp. 179–92. doi:10.1007/s12017-009-8085-y.

Woodruff, T.M., Nandakumar, K.S. and Tedesco, F. (2011) "Inhibiting the C5–C5a receptor axis," *Molecular Immunology*, 48(14), pp. 1631–1642. doi:https://doi.org/10.1016/j.molimm.2011.04.014.

Wu, J. *et al.* (2011) "Arc/Arg3.1 Regulates an Endosomal Pathway Essential for Activity-Dependent β-Amyloid Generation," *Cell*, 147(3), pp. 615–628. doi:10.1016/j.cell.2011.09.036.

Wu, L.-J. and Zhuo, M. (2008) "Resting Microglial Motility Is Independent of Synaptic Plasticity in Mammalian Brain," *Journal of Neurophysiology*, 99(4), pp. 2026–2032. doi:10.1152/jn.01210.2007.

Wu, S.X. *et al.* (2018) “A Review of Distributed Algorithms for Principal Component Analysis,” *Proceedings of the IEEE*, 106(8), pp. 1321–1340. doi:10.1109/JPROC.2018.2846568.

Wu, Y. *et al.* (2015) “Microglia: Dynamic Mediators of Synapse Development and Plasticity,” *Trends in Immunology*, 36(10), pp. 605–613. doi:https://doi.org/10.1016/j.it.2015.08.008.

Xiao, J. *et al.* (2016) “Cerebral complement C1q activation in chronic Toxoplasma infection,” *Brain, Behavior, and Immunity*, 58, pp. 52–56. doi:https://doi.org/10.1016/j.bbi.2016.04.009.

Xu, H. *et al.* (2017) “The Polarization States of Microglia in TBI: A New Paradigm for Pharmacological Intervention,” *Neural Plasticity*, 2017, pp. 1–11. doi:10.1155/2017/5405104.

Xu, H. and Chen, M. (2016) “Targeting the complement system for the management of retinal inflammatory and degenerative diseases,” *European Journal of Pharmacology*, 787, pp. 94–104. doi:10.1016/j.ejphar.2016.03.001.

Xu, Z.-X. *et al.* (2019) “Caspase-2 promotes AMPA receptor internalization and cognitive flexibility via mTORC2-AKT-GSK3β signaling,” *Nature Communications*, 10(1), p. 3622. doi:10.1038/s41467-019-11575-1.

Xue, J. *et al.* (2014) “Transcriptome-Based Network Analysis Reveals a Spectrum Model of Human Macrophage Activation,” *Immunity*, 40(2), pp. 274–288. doi:10.1016/j.immuni.2014.01.006.

Yamada, D. *et al.* (2009) “Pharmacological Discrimination of Extinction and Reconsolidation of Contextual Fear Memory by a Potentiator of AMPA Receptors,” *Neuropsychopharmacology*, 34(12), pp. 2574–2584. doi:10.1038/npp.2009.86.

Yang, T. *et al.* (2020) “The Role of BDNF on Neural Plasticity in Depression,” *Frontiers in Cellular Neuroscience*, 14. doi:10.3389/fncel.2020.00082.

Yilmaz, M. *et al.* (2021) “Overexpression of schizophrenia susceptibility factor human complement C4A promotes excessive synaptic loss and behavioral changes in mice,” *Nature neuroscience*, 24(2), pp. 214–224.

Yin, Y., Edelman, G.M. and Vanderklish, P.W. (2002) “The brain-derived neurotrophic factor enhances synthesis of Arc in synaptoneurosomes.,” *Proceedings of the National Academy of Sciences of the United States of America*, 99(4), pp. 2368–73. doi:10.1073/pnas.042693699.

Ying, S.-W. *et al.* (2002) “Brain-derived neurotrophic factor induces long-term potentiation in intact adult hippocampus: requirement for ERK activation coupled to CREB and upregulation of Arc synthesis.,” *The Journal of neuroscience : the official journal of the Society for Neuroscience*, 22(5), pp. 1532–40.

Yirmiya, R. (2002) “Brain Interleukin-1 Is Involved in Spatial Memory and Passive Avoidance Conditioning,” *Neurobiology of Learning and Memory*, 78(2), pp. 379–389. doi:10.1006/nlme.2002.4072.

York, E.M. *et al.* (2018) “3DMorph Automatic Analysis of Microglial Morphology in Three Dimensions from *Ex Vivo* and *In Vivo* Imaging,” *eneuro*, 5(6), p. ENEURO.0266-18.2018. doi:10.1523/ENEURO.0266-18.2018.

Young, K.G., Yan, K. and Picketts, D.J. (2019) “C3aR signaling and gliosis in response to neurodevelopmental damage in the cerebellum,” *Journal of Neuroinflammation*, 16(1), p. 135. doi:10.1186/s12974-019-1530-4.

Yrjanheikki, J. *et al.* (1998) “Tetracyclines inhibit microglial activation and are neuroprotective in global brain ischemia,” *Proceedings of the National Academy of Sciences*, 95(26), pp. 15769–15774. doi:10.1073/pnas.95.26.15769.

Yu, Z. *et al.* (2017a) “Microglial production of TNF-alpha is a key element of sustained fear memory,” *Brain, Behavior, and Immunity*, 59, pp. 313–321. doi:10.1016/j.bbi.2016.08.011.

Yu, Z. *et al.* (2017b) “Microglial production of TNF-alpha is a key element of sustained fear memory,” *Brain, Behavior, and Immunity*, 59, pp. 313–321. doi:https://doi.org/10.1016/j.bbi.2016.08.011.

Zaben, M. *et al.* (2017) “Role of proinflammatory cytokines in the inhibition of hippocampal neurogenesis in mesial temporal lobe epilepsy,” *The Lancet*, 389, p. S105. doi:10.1016/S0140-6736(17)30501-9.

Zaromytidou, A.-I., Miralles, F. and Treisman, R. (2006) “MAL and ternary complex factor use different mechanisms to contact a common surface on the serum response factor DNA-binding domain.,” *Molecular and cellular biology*, 26(11), pp. 4134–48. doi:10.1128/MCB.01902-05.

Zenaro, E., Piacentino, G. and Constantin, G. (2017) “The blood-brain barrier in Alzheimer’s disease,” *Neurobiology of Disease*, 107, pp. 41–56. doi:10.1016/j.nbd.2016.07.007.

Zhan, Y. *et al.* (2014) “Deficient neuron-microglia signaling results in impaired functional brain connectivity and social behavior,” *Nature Neuroscience*, 17(3), pp. 400–406. doi:10.1038/nn.3641.

Zhang, C., Lam, T.T. and Tso, M.O.M. (2005) “Heterogeneous populations of microglia/macrophages in the retina and their activation after retinal ischemia and reperfusion injury,” *Experimental Eye Research*, 81(6), pp. 700–709. doi:https://doi.org/10.1016/j.exer.2005.04.008.

Zhang, H. and Bramham, C.R. (2021) “Arc/Arg3.1 function in long-term synaptic plasticity: Emerging mechanisms and unresolved issues,” *European Journal of Neuroscience*, 54(8), pp. 6696–6712. doi:10.1111/ejn.14958.

Zhang, S. (2019) “Microglial activation after ischaemic stroke,” *Stroke and Vascular Neurology*, 4(2), pp. 71–74. doi:10.1136/svn-2018-000196.

Zhang, W.-P., Guzowski, J.F. and Thomas, S.A. (2005) “Mapping neuronal activation and the influence of adrenergic signaling during contextual memory retrieval,” *Learning & Memory*, 12(3), pp. 239–247.

Zhou, B., Zuo, Y. and Jiang, R. (2019) “Astrocyte morphology: Diversity, plasticity, and role in neurological diseases,” *CNS Neuroscience & Therapeutics*, 25(6), pp. 665–673. doi:10.1111/cns.13123.

Zhu, Lei *et al.* (2018) “Memory reconsolidation and extinction of fear conditioning induced different Arc/Arg3.1 expression,” *NeuroReport*, 29(12), pp. 1036–1045. doi:10.1097/WNR.0000000000001069.

Ziebell, Jenna M *et al.* (2017) “Aging with a traumatic brain injury: Could behavioral morbidities and endocrine symptoms be influenced by microglial priming?,” *Brain, behavior, and immunity*, 59, pp. 1–7. doi:10.1016/j.bbi.2016.03.008.

Ziebell, J.M., Adelson, P.D. and Lifshitz, J. (2015) “Microglia: dismantling and rebuilding circuits after acute neurological injury,” *Metabolic Brain Disease*, 30(2), pp. 393–400. doi:10.1007/s11011-014-9539-y.

Ziebell, J.M. and Morganti-Kossmann, M.C. (2010) “Involvement of pro- and anti-inflammatory cytokines and chemokines in the pathophysiology of traumatic brain injury,” *Neurotherapeutics*, 7(1), pp. 22–30. doi:10.1016/j.nurt.2009.10.016.

Ziebell, J.M., Ray-Jones, H. and Lifshitz, J. (2017) “Nogo presence is inversely associated with shifts in cortical microglial morphology following experimental diffuse brain injury,” *Neuroscience*, 359, pp. 209–223. doi:https://doi.org/10.1016/j.neuroscience.2017.07.027.

Ziporen, L. *et al.* (2009) “Programmed necrotic cell death induced by complement involves a Bid-dependent pathway.,” *Journal of immunology (Baltimore, Md. : 1950)*, 182(1), pp. 515–21. doi:10.4049/jimmunol.182.1.515.

Appendices

Appendix 1: ImageJ/FIJI script for dividing tile scanned images

```
//open files in directory
	work_dir = "E:/RE_IBA1_Brains/";
//access all file in wording directory
	dir_list = getFileList(work_dir);
//creates a new file for the processed images to go into
	processed_output = "E:/Chopped_RE/";
//enable bigTiff plugin
	run("Bio-Formats Macro Extensions");
// loops over each file in the working directory
	for (j = 0; j < dir_list.length; j ++){
	file_name = work_dir + dir_list [j];


//takes the list name of the file to save later in a new directory
	to_save_file = dir_list [j];
// takes the to_save_file name and removes 4 characters from the end.
	file_length =  (lengthOf(to_save_file));
```

```
	new_name = file_length - 4;

	to_save_wo_tif = substring(to_save_file, 0 , new_name);

//print (to_save_file);

//uses a plugin to open big tiffs

	opened_image = Ext.openImagePlus(file_name);

//set the size of the square to use

	size_square = 500;

//values for the whole image

	width = getWidth();

	height = getHeight();

// takes the height and width calculated above and determines how many ROI's need to be aquired

	number_vert_samples = floor(height / size_square);

	print("There will be " + number_vert_samples + "vertical slices");

	number_horz_samples = floor(width / size_square);

	print("There will be " + number_horz_samples + "hoirzontal samples");

//loops will be nested. One loop which runs the vertical ROIs and a second loop to run the horizontal ROIs

//horizontal loop
```

```
	for (k = 0; k < number_horz_samples; k ++)
	{
//verticle loop
	for (i = 0; i < number_vert_samples; i ++)
	{
//creates a box with set dimensions and beginning at xy of 0 0 then increasing by the number assigned to size_square
	makeRectangle(size_square * k, size_square * i, size_square, size_square);
//crops the image
	run("Crop");
//changes file to 8bit so it can be seen and opened by matlab
	run("8-bit");
//saves the file as the list name (to_save_file) plus a suffix number then closes the file
	saveAs("Tiff", processed_output + to_save_wo_tif + "_" + k + "_" + i + ".tif");
//saveAs("Tiff", processed_output + to_save_file + "_" + k + "_" + i + ".tif");
	selectWindow(to_save_wo_tif + "_" + k + "_" + i + ".tif");
//selectWindow(to_save_file + "_" + k + "_" + i + ".tif");
	run("Close");
```

```
// opens the original file again
        Ext.openImagePlus(file_name);
        print ("completed vertical sample " + i);
        }
        print("completed horizonal sample " + k);
        }
//below needs changing if there are issues with the .tif naming format
//selectWindow(to_save_file);
//selectWindow(to_save_wo_tif);
        run("Close");
        }
```

Appendix 2: R csv complier

```
#!/usr/bin/Rscript

#merge_morph3d.R

#Merge cell and image data from multiple output files

#derived from Morph3D analysis

#Nick Clifton

#15th June 2021

#####################################

#### SET THE WORKING DIRECTORY ####

#####################################

# data location

setwd("C:/Users/jackr/Documents/3DMorph")

#####################################

################ RUN ################

#####################################

# load required packages

if(!require(dplyr)) {

  install.packages("dplyr")

  require(dplyr)
```

```
}
if(!require(data.table)) {
  install.packages("data.table")
  require(data.table)
}
all_filnames <- dir(path = ".")
# get all CellResults data filenames
all_cell_filenames <- all_filnames[grepl("Cell", all_filnames)]
# get all ImageResults data filenames
all_image_filenames <- all_filnames[grepl("Image", all_filnames)]
### Merge Cell Results in loop ###
# prime the output dataframe
cell_output <- cbind(data.frame(InputFile = character()),
read.csv(all_cell_filenames[1])[0,])
for (each_filename in all_cell_filenames) {
  # read each Cell Results file
  each_cell_data = read.csv(each_filename) %>%
    # append column with filename
    mutate(InputFile = each_filename) %>%
```

```
    # rearrange columns
    dplyr::select(InputFile, 1:(ncol(.)-1))
  # bind to output dataframe
  cell_output <- rbind(cell_output, each_cell_data)
}
### Merge Image Results in loop ###
# prime the output
image_output <- data.frame(InputFile = character(),
                           AvgCentroidDistance_um = double(),
                           TotMgTerritoryVol_um3 = double(),
                           TotUnoccupiedVol_um3 = double(),
                           PercentOccupiedVol_um3 = double())
for (each_filename in all_image_filenames) {
  # read each Image Results file
  each_image_data = read.csv(each_filename) %>%
    # select the Values column only
    dplyr::select(Value) %>%
    # transpose
    data.table::transpose() %>%
```

```
    # append filename column
    mutate(InputFile = each_filename) %>%
    dplyr::select(InputFile, 1:(ncol(.)-1))
  # re-assign variable names as colnames
  colnames(each_image_data) = c("InputFile", "AvgCentroidDistance_um",
"TotMgTerritoryVol_um3", "TotUnoccupiedVol_um3", "PercentOccupiedVol_um3")
  # bind to output dataframe
  image_output <- rbind(image_output, each_image_data)
}
### Write output files ###
write.table(cell_output, "CllResults_MERGED.csv", sep = ",", row.names = F,
col.names = T, quote = F)
write.table(image_output, "ImgResults_MERGED.csv", sep = ",", row.names = F,
col.names = T, quote = F)
```

Appendix 3: R random forest machine learning algorithm for predicting microglial activation status using microglial morphometrics

```
#load libaries caret for machine learning and pROC for analysis (esp AUC) of output

library(dplyr) # everything graphical and data wrangling

library(tidyverse)

library(tidyr)

library(reshape2)

library(caret) # ML modelling

library(mlr3)

library(pROC) # AUC assessment

library(DMwR) # for oversampling/undersampling as a solution to class imbalance.

library(ggplot2)

library(magrittr)

library(GGally)

library(car)

# ----------------------------------------------------

# reading and plotting data

#open datafile containing LPS/PBS with classes with classes set as 1 and 2. With 1 being LPS and 2 being PBS
```

```
#update location of PBS and LPS accordingly

working_dataset_with_zeros <-
read_csv("C:/Users/jackr/Documents/ML/LPS_PBS_ML_train_and_test.csv")


#remove any zero values from the dataset

#zero value represents a cell with no processes which would mean ameboid morph
which are not seen post LPS as theres no neuronal death

working_dataset <-
working_dataset_with_zeros[apply(working_dataset_with_zeros,1,function(z)
!any(z==0)),]


#somewhere in the script LPS and PBS is changed to 1 and 2 which doesnt work for
the below model so changed back here 1 is LPS and 0 is PBS

working_dataset$Class <- dplyr::recode(working_dataset$Class, "1" = "LPS", "2" =
"PBS")


#checking here that the presence of zero values is not influenced by group

#if means are roughly equal then there is no effect of treatment

working_dataset_zero_only <-
working_dataset_with_zeros[apply(working_dataset_with_zeros,1,function(z)
any(z==0)),]
```

```
paste('Mean outcome for rows with zeros: ',
mean(working_dataset_zero_only$Class), sep = '')

paste('Mean outcome for full dataset: ', mean(working_dataset_with_zeros$Class),
sep = '')


#setting up data

working_dataset$Class <- as.factor(working_dataset$Class)

working_dataset$Class <- dplyr::recode(working_dataset$Class, "1" = "LPS", "2" =
"PBS")


# both classes

working_dataset %>%

  tidyr::pivot_longer(cols=-Class, names_to='Predictor', values_to='Measurement')
%>%

  ggplot(aes(x=Measurement)) +

  geom_density(aes(group=Class, colour=Class, fill=Class), alpha=0.3) +

  facet_wrap(vars(Predictor), scales='free')

set.seed(107) # for reproducible splits in CV

inTrain <- createDataPartition(

  y = working_dataset$Class,
```

```
  p = .75,
  list = FALSE
)

#output is set of intergers for the row of the data set that have been asigned to the
the training set
str(inTrain)
#create serperate datasets
training <- working_dataset [ inTrain,]
testing  <- working_dataset [-inTrain,]
nrow(training)
nrow(testing)

# random forest
model_weights <-ifelse(training$Class == "LPS",
                       (1/table(training$Class)[1]) * 0.5,
                       (1/table(training$Class)[2]) * 0.5)
ctrl <- trainControl(
  method = "CV",
```

```
  number = 10,
  classProbs = TRUE,
  summaryFunction = twoClassSummary,
  search = 'random'
)
set.seed(107)
weighted_rf_mod = train(
  form = Class ~ .,
  data = training,
  trControl = ctrl,
  preProc = c("center", "scale"),
  weights = model_weights,
  method = "rf",
  tuneLength = 5,
  verbose = FALSE
)
weighted_rf_mod

# checking predicted probabilities as usual
```

```
rf_y_pred_train <- predict(weighted_rf_mod, training, type='prob') %>%
  as_tibble() %>%
  mutate(y_true = training$Class)

rf_y_pred_test <- predict(weighted_rf_mod, testing, type='prob') %>%
  as_tibble() %>%
  mutate(y_true = testing$Class)

#isolate only useful S/S values
#from this data table select threshold which provides best mix of S/S
auc.df <- tibble(
  auc_sens = auc$sensitivities,
  auc_spec = auc$specificities,
  thresholds = auc$thresholds)

#this helps narrow it down
#trying to isolate a good threshold level
auc.df[auc.df$auc_sens > 0.65 & auc.df$auc_spec > 0.6,]
```

```
#add in dataset to be predicted upon

experimental_data <-
read.csv("C:/Users/jackr/Documents/ML/CFC_cell_results_PL.csv",
fileEncoding="UTF-8-BOM")

experimental_data_wo_ID <-experimental_data %>%
  subset(select=c(-ID))


experimental_data_test <- predict(weighted_rf_mod, experimental_data, type='prob')
%>%
  as_tibble()


#adjust here with appropriate threshold determined from S/S
experimental_names <- experimental_data_test %>%
  mutate(classes=ifelse(experimental_data_test$LPS < 0.245 , "LPS","PBS")) %>%
  mutate(ID=experimental_data$ID)
```

Appendix 4: Freezing percentages separated by experimental group (Chapter 3)

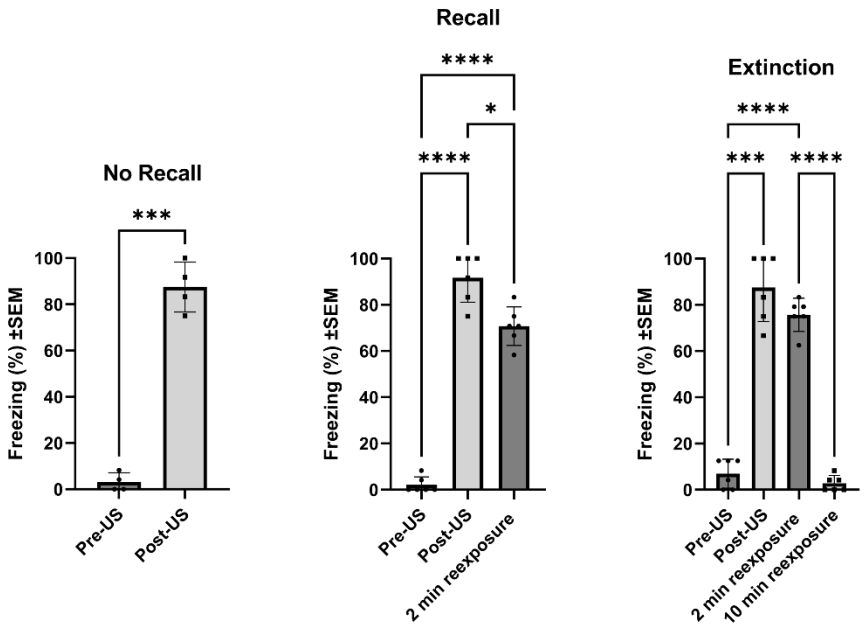

Appendix 4 – The retrieval and extinction of a contextual fear memories in rat. Subjects froze immediately following a single unconditioned shock in the context. 48 hours post-initial shock rats returned to the context froze initially. Freezing behaviour returned to pre-shock levels after 10 minutes re-exposure to the context. * denotes p <0.05, *** denotes p <0.001, **** denotes p <0.0001.

Appendix 5: Freezing percentages separated by experimental group (Chapter 4)

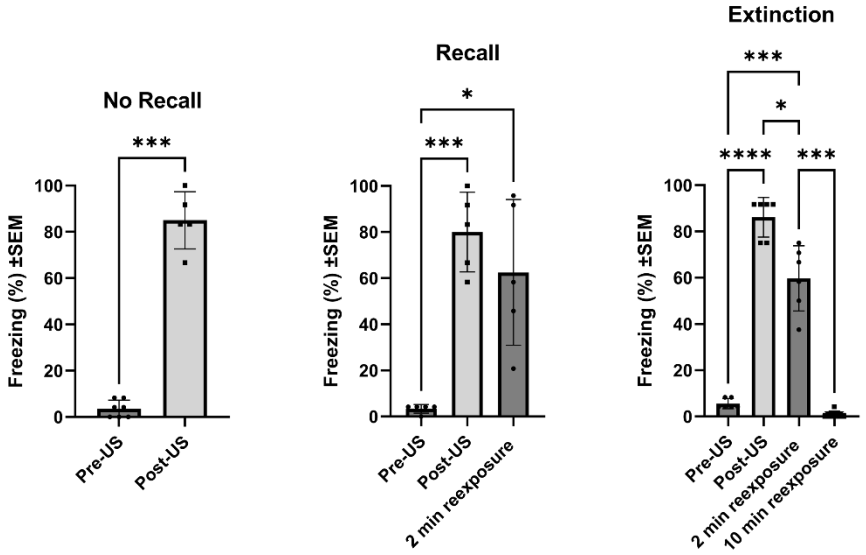

Appendix 5 – The retrieval and extinction of a contextual fear memories in rat. Subjects froze immediately following a single unconditioned shock in the context. 48 hours post-initial shock rats returned to the context froze initially. Freezing behaviour returned to pre-shock levels after 10 minutes re-exposure to the context. * denotes p <0.05, *** denotes p <0.001, **** denotes p <0.0001.

Appendix 6: Arc staining negative control

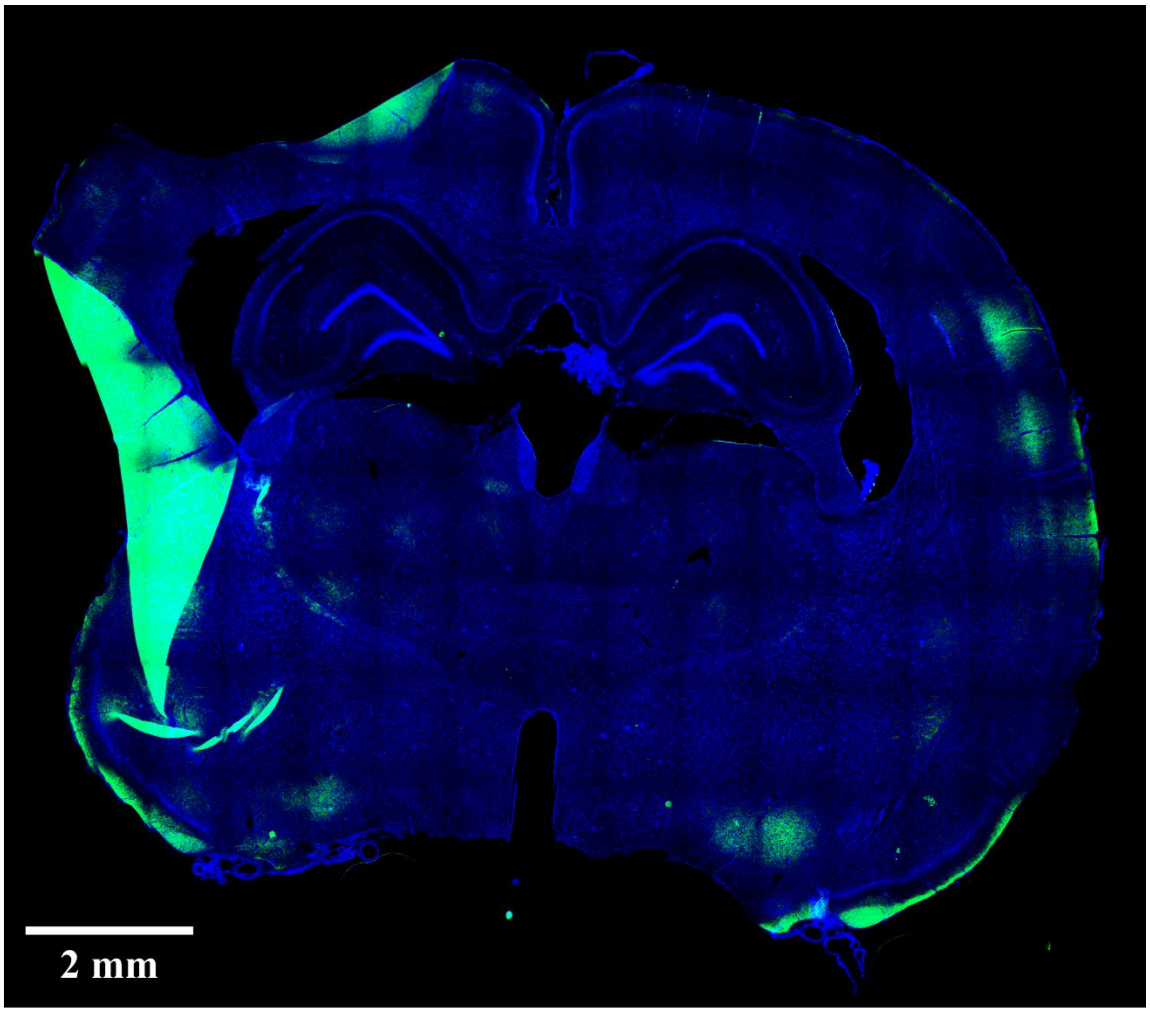

Appendix 6 – Negative control for Arc immunohistochemical staining.

Appendix 7: cFOS staining negative control

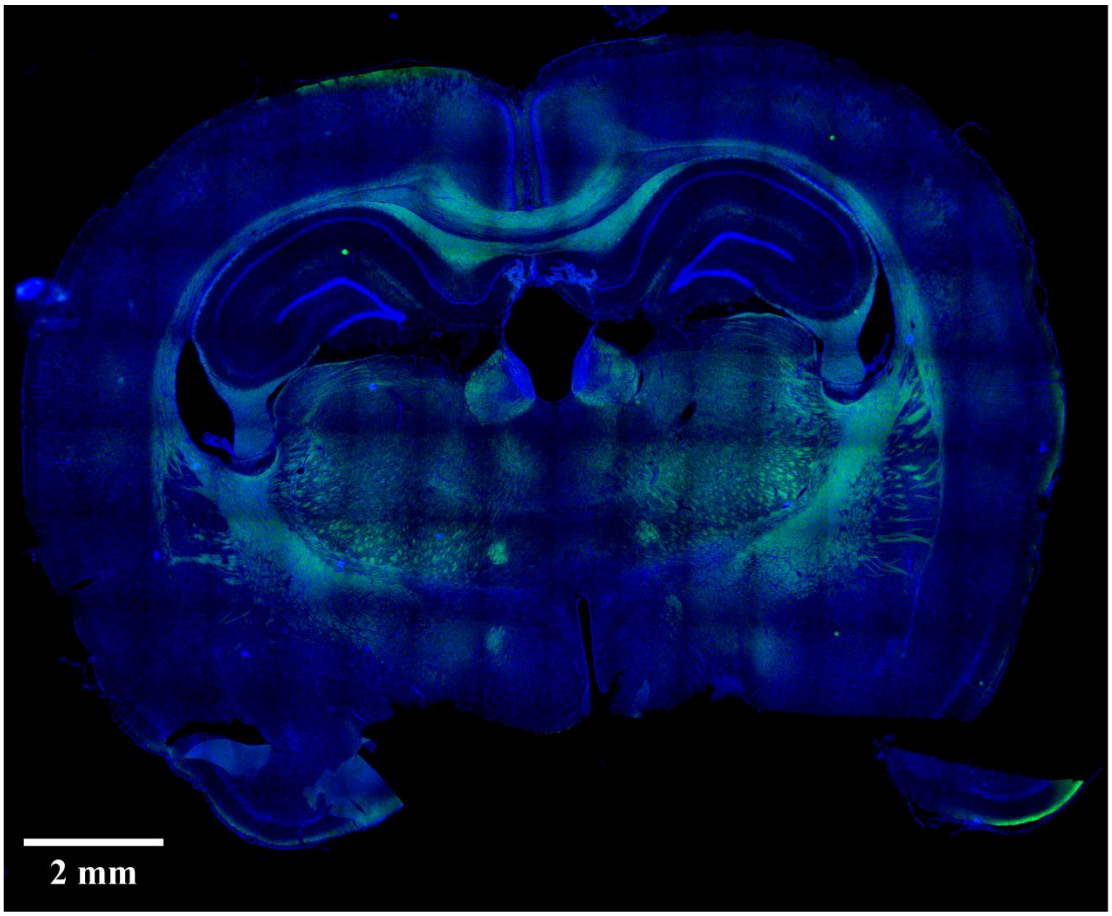

Appendix 7 – Negative control for cFOS immunohistochemical staining.

Appendix 8: zif268 staining negative control

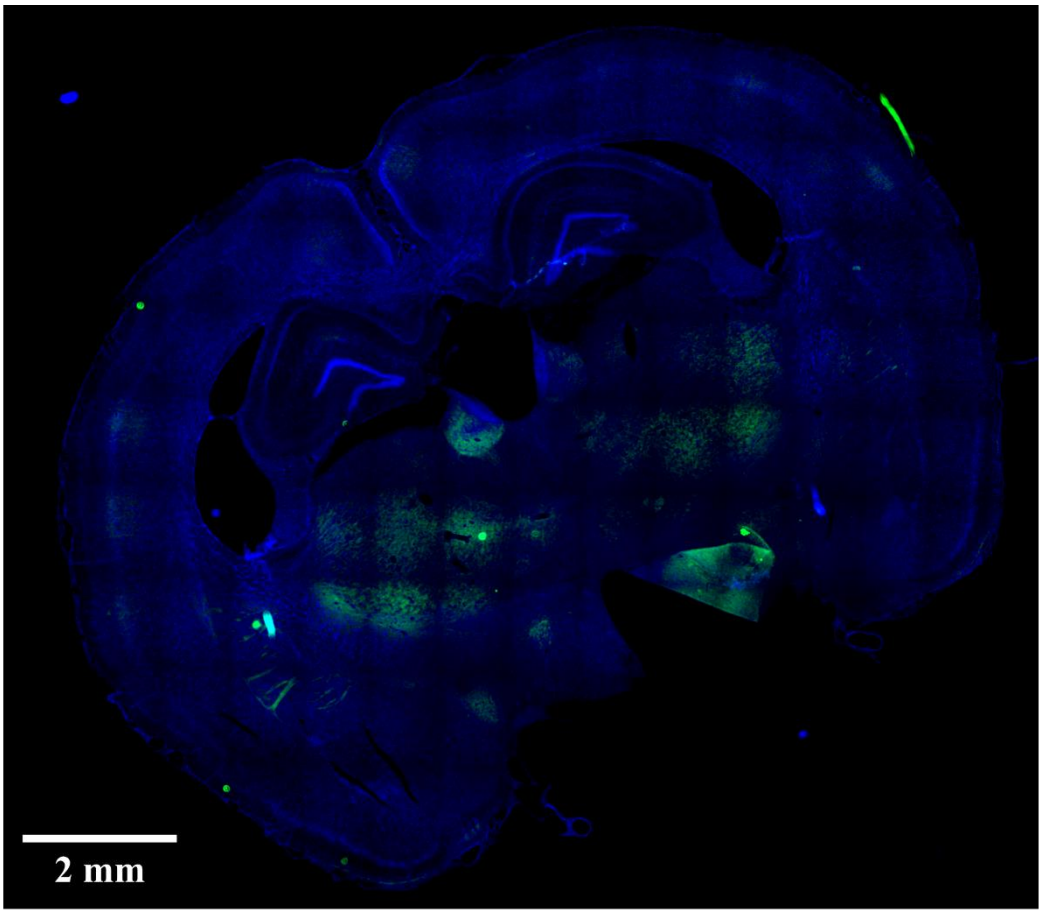

Appendix 8 – Negative control for zif268 immunohistochemical staining.

Appendix 9: IBA1 staining negative control

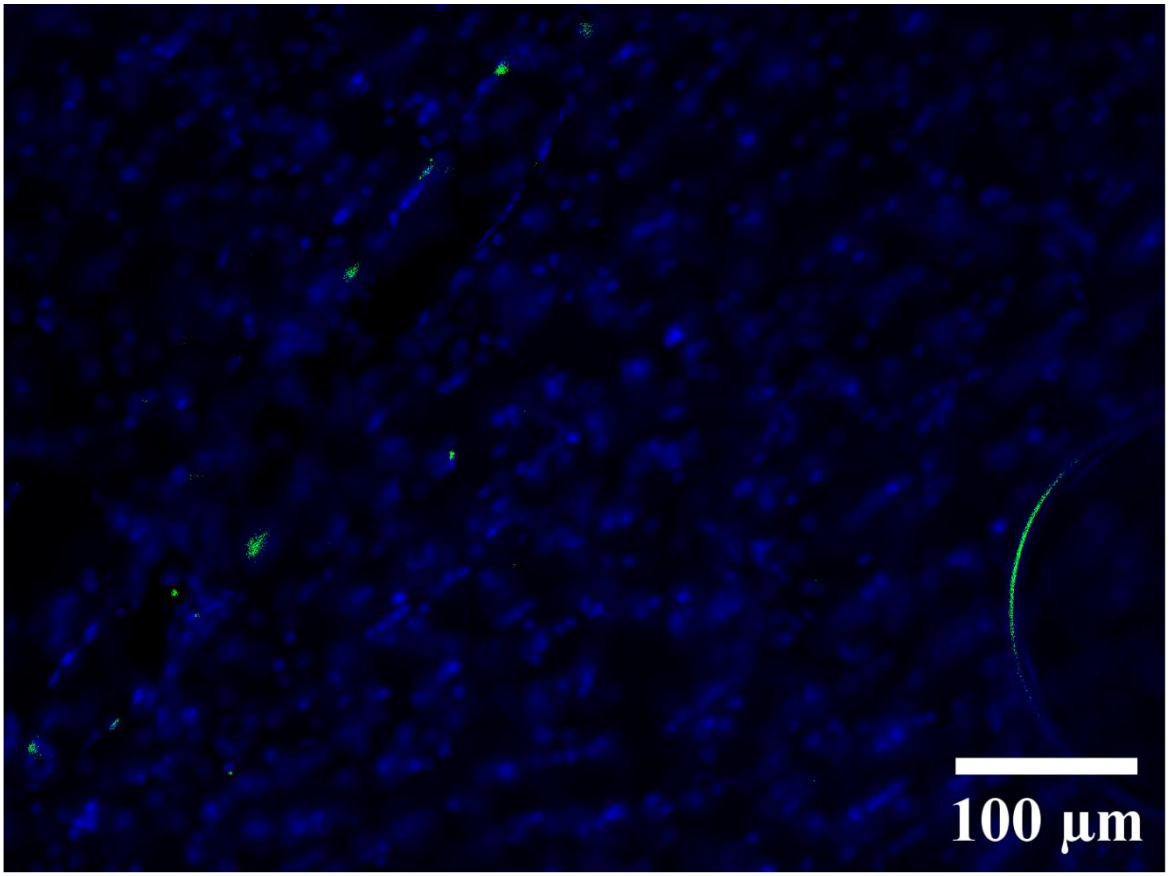

Appendix 9 – Negative control for IBA1 immunohistochemical staining.